GEORGIA INSTITUTE OF TECHNOLOGY — OFFICE OF CONTRACT ADMINISTRATION

PROJECT ADMINISTRATION DATA SHEET

[x] ORIGINAL [ ] REVISION NO. _____

Project No. E-19-622 GTRI/~~EES~~ DATE 6 / 25 / 84

Project Director: Dr. Jack Winnick School/~~ME~~ Chemical Engineering

Sponsor: U. S. Department of Energy
Pittsburg Energy Technology Center

Type Agreement: Grant No. DE-FG22-84PC73226

Award Period: From 6/4/84 To ~~6/3/86~~ 12/31/86 (Performance) ~~9/3/86~~ 3/31/87 (Reports)

Sponsor Amount:	This Change	Total to Date
Estimated:	$ 225,530	$ 225,530
Funded:	$ 80,000	$ 80,000 (through 12/31/84)

Cost Sharing Amount: $ _____ Cost Sharing No: _____

Title: Combined NO_x/SO_x Control From Flue Gas Using an Electrochemical Membrane Concentrator

ADMINISTRATIVE DATA OCA Contact Brian J. Lindberg x-4820

1) Sponsor Technical Contact:

~~Joseph P. Strakey~~ DR. R. J. WALKER
U. S. Department of Energy
Pittsburgh Energy Technology Center
P. O. Box 10940
Pittsburgh, PA. 15236
(412) 675-6125

2) Sponsor Admin/Contractual Matters:

DONA G. SHEEHAN
~~Kathryn M. Hurney~~
U. S. Department of Energy
Pittsburgh Energy Technology Center
P. O. Box 10940, MS 900-L
Pittsburgh, PA 15236
(412) 675-5913

Defense Priority Rating: N/A Military Security Classification: N/A
(or) Company/Industrial Proprietary: N/A

RESTRICTIONS

See Attached N/A Supplemental Information Sheet for Additional Requirements.

Travel: Foreign travel must have prior approval – Contact OCA in each case. Domestic travel requires sponsor approval where total will exceed greater of $500 or 125% of approved proposal budget category.

Equipment: Title vests with GIT

COMMENTS:

COPIES TO: I.D. #02.141.005.84.001

Project Director
Research Administrative Network
Research Property Management
Accounting
Procurement/EES Supply Services
Research Security Services
Reports Coordinator (OCA)
Research Communications (2)
GTRI
Library
Project File
Other I. Newton

FORM OCA 4:383

GEORGIA INSTITUTE OF TECHNOLOGY **OFFICE OF CONTRACT ADMINISTRATION**

SPONSORED PROJECT TERMINATION/CLOSEOUT SHEET

Date 5-7-87

Project No. E-19-622 School/~~XXX~~ ChE

Includes Subproject No.(s) N/A

Project Director(s) Dr. Jack Winnick GTRC /~~GIT~~

Sponsor U.S. Department of Energy- Pittsburg Energy Technology Center

Title Combined NO_x/SO_x Control From Flue Gas Using an Electrochemical Membrane Concentrator

Effective Completion Date: 12/31/86 (Performance) 3/31/87 (Reports)

Grant/Contract Closeout Actions Remaining:

- [ ] None
- [X] Final Invoice or Final Fiscal Report
- [ ] Closing Documents
- [X] Final Report of Inventions
- [X] Govt. Property Inventory & Related Certificate
- [ ] Classified Material Certificate
- [ ] Other

Continues Project No. Continued by Project No.

COPIES TO:

Project Director
Research Administrative Network
Research Property Management
Accounting
Procurement/GTRI Supply Services
Research Security Services
~~Reports Coordinator (OCA)~~
~~Legal Services~~

Library
GTRC
~~Research Communications~~
Project File
Other Duane H.
Angela DuBose
Russ Embry

FORM OCA 69.285

FORM DOE 538
(Rev. 10-80)

U.S. DEPARTMENT OF ENERGY

NOTICE OF ENERGY RD&D PROJECT

APPROVED FOR USE BY
SMITHSONIAN SCIENCE INFORMATION EXCHANGE

FORM APPROVED
OMB NO. 38 R-0180

1. Descriptive title of work
"Simultaneous SO_x/NO_x Removal from Flue Gas by Electrochemical Membrane Concenration"

2. Performing organization control number E-19-622
Work status ☒ New ☐ Continuing ☐ Terminated

3. Contract or grant number
DOE contract No. DE-FG22-84PC73226

4. Contractor's principal investigator/project manager and address where work is performed
A. Name (Last, First, MI) Winnick, Jack B. Phone: FTS- 404-894-2839
C. Research organization business address: Street School of Chemical Engineering Com.- Georgia Tech
City Atlanta, State Ga Zip 30332

5. A. Name of performing organization School of Chemical Engineering, Georgia Tech
(Organization) (Department)

B. Mailing address (If different from 4C)

C. Circle only one code for TYPE OF ORGANIZATION PERFORMING R&D (See instructions):
(CU) FF IN NP ST TA US XX EG

D. Location where the work is being performed
Georgia Institute of Technology

E. Country sponsoring research
U.S.A.

6. Supporting organization
A. Program division or office (Full name) Pittsburgh Energy Technology Center (PETC)

B. Technical monitor (Last, First, MI) Walker, Richard C. Phone: FTS-

D. Address (If different from DOE Hqs.) Coal Utilization Technology Division
P.E.T.C., Pittsburgh, Pa. 15236 Com.-

E. Administrative monitor (Last, First, MI) Strakey, Joseph P.

7. Project schedule
A. Start date June 4, 1984 (Month) (Year) B. Expected completion date June 3, 1986 (Month) (Year)

8. Funding in thousands of dollars (Funds represent budget obligations for operating and capital equipment)

	DIRECT COSTS ONLY: Funding organization(s)	Current FY 85	Next FY 86
A.	Personal Services	15,830.00	24,464.00
B.	Non-Personal Services	1,956.00	1,964.00
C.	Equipment	7,097.00	4,235.00

D. For DOE projects, enter budgeting and reporting classification code
E. Interagency agreement (Specify funding agency)
F. Agency in-house effort (Check if applicable) ☐
G. EPA "pass-thru" funding (Check if applicable) ☐

Note: Funding Section utilization is optional on Federal Financial Assistance Programs: grants, direct payments, cooperative agreements, loan guarantees, and other related programs.

9. Descriptive summary of work (Limit to 200 words. Include objective, approach, results to date and their significance, and expected product. Quantify where possible).

An electrochemical membrane technique has been shown effective for removal and concentration of SO_x from flue gases at temperatures above 550c. For commercial application, it is necessary to achieve lower temperature operation at 200-300c. Further, simultaneous removal and/or concentration of NO_x is desirable.

This type of removal system is superior to others since it is a one-step, low-power, no-waste process. Further, it concentrates the contaminants into a salable product. No reagents, other than electricity are needed, at least for the SO_x step.

A laboratory study is underway to ascertain the reactions and their rates at lower temperatures (200-300c). New electrolytes, mixtures of bisulfates, pyrosulfates and vanadia are being tested in glassware. Rates of NO_x removal or concentration will be determined. This will be followed by cell tests with the candidate electrolytes held in suitable ceramic or fibrous membranes. Electrodes will be of conductive perovskite-type oxides developed in this laboratory.

Results of these tests will verify the commercial potential of this system. A preliminary design will be possible, based on the thermodynamic and kinetic information determined. Levels of NO_x and SO_x achievable will be demonstrated.

10. List the five most descriptive publications in the last year that are available to the public which have resulted from the project (Please give a complete bibliographic citation. Use additional sheets if necessary).

None in the last twelve months.

11. General technology categories (Enter applicable code of codes from instructions).

A 1 | | | | | | | | | | | | |

12. Type of research activity (Check applicable activities)

- A. [X] Basic research
- B. [X] Applied research
- C. [X] Laboratory scale R&D
- D. [X] Technology development
- E. [ ] Field study
- F. [ ] Pilot plant scale R&D
- G. [ ] Full scale demonstration
- H. [ ] Mathematical model development
- I. [ ] Data analysis/assessments
- J. [ ] Information systems management
- K. [ ] Policy analysis
- L. [ ] Socioeconomic
- M. [ ] Other (Specify)_____
- N. [ ] Not applicable

13. keywords (Please list 5 keywords).

SO_x , NO_x , Membrane, Electrochemistry, Hot-Gas

14. Is this research project solely an ANALYTICAL/PAPER STUDY? (Non-experimental, paper and pencil, computer analysis, etc.). YES _____ NO X

15. Respondent's Name: Dr. Jack Winnick Phone No.: 404-894-2839 Date: January 4, 1985

Street: 778 Atlantic Dr. - Bunger-Henry Bldg.

Chemical Engineering Department, Georgia Institute of Technology

City: Atlanta, State: Ga. Zip: 30332

☆U.S. G.P.O. 1980-720-050/4816

COMBINED NO_x/SO_x CONTROL FROM FLUE GAS USING AN ELECTROCHEMICAL MEMBRANE CONCENTRATOR

Six Month Progress Report

D.O.E./P.E.T.C.

Grant Number: DE-FG22-84PC73226

B & R Number: AA0505

B & R Class: Flue Gas Cleanup

T.P.O.: Richard Walker

Principal Investigator: J. Winnick

February 1985

INTRODUCTION

In the United States, flue gas treatment is used primarily to control sulfur dioxide and particulate emissions. Concern over increased emissions of oxides of nitrogen from the increased use of coal as a fuel in both the utility and industrial sectors has prompted new interest in processes for the simultaneous removal of NO_x and SO_x from flue gas. Use of commercially available equipment for the removal of NO_x, SO_x and particulates is not necessarily optimized as a combined process and generally the processes (1) require excessive land area, (2) require huge quantities of chemicals and (3) produce large volumes of troublesome waste products. In addition, it is not certain that this equipment can meet the anticipated requirements of 90% reduction in both NO_x and SO_x levels with high sulfur (3.5%) coal as a fuel.

An electrochemical membrane cell stack can be a simple, cost-effective means of combined NO_x-SO_x control in flue gas. A laboratory-scale device has proven the SO_x control process. The SO_2 in simulated flue gas has been reduced to less than 100 ppm while a concentrated by-product stream of oleum is continuously manufactured. The projected economics of this device are highly favorable. No reagents are required, no waste stream produced and flue gas reheat is avoided. However, it has been demonstrated only at high temperatures (> 500C).

Several possibilities exist for lowering the temperature of operation. These include changes in the electrolyte as well as incorporation of a low-melting, non-reactive solvent. The

temperature of operation can likely be reduced to 250C and perhaps below 200C.

The geometry and materials of the SO_2 membrane cell offer the promise of simultaneous NO_x removal. Cathodic reduction to elemental nitrogen (and oxide ion), membrane transport as nitrate or selective catalytic reduction are all possible. If successful, none would require major capital or operating cost increase over costs for the SO_x control.

The purpose of this project is to develop a simple combined NO_x-SO_x control device. In this report the proposed research plan will be shown and the results of the first six months work presented.

THEORY

The electrochemical membrane concentration cell is, in principle, very simple. An applied electrical field produces an electrochemical potential which drives the most acidic component in the cathode stream across the memberane. A small voltage provides the driving force to overcome a large chemical potential gradient. Thus a concentrated anodic stream can be produced.

Several matters of rather basic nature must be addressed at this point. These deal with selectivity with regard to SO_x, temperature limits, rates of transfer, and electrode materials. Clearly these are somewhat interrelated.

RESEARCH PLAN

ACTIVITY	6 MONTHS	YEAR	18 MONTHS	2 YEARS
BISULFATE	Stability Free electrolyte tests V_2O_5 addition	Best Option Chosen	Full Cell Test	
PYROSULFATE	Stability Free electrolyte test V_2O_5 addition			
ELECTRODES	Gold	Molybdates Cobaltates	Porous Perovskite	
MEMBRANE	-------	Tile Fabrication MgO, Al_2O_3, $SrTiO_3$		
NO REDUCTION (Electrochem.)	Free electrolyte ($S_2O_7^{2-}$, NO_3^-)			
NO REDUCTION	-------	V_2O_5 + TiO_2 Tests	Full Cell Test	
NO CONC'N. (Nitrate)	Free electrolyte Gold			
Simultaneous NO/SO_2	-------	-------	Free electrolyte Gold	Full Cell Tests

Selectivity

The alkali sulfate melt is very stable with respect to the components of flue gas other than SO_2, SO_3, and O_2. The reaction with CO_2

$$M_2SO_4 + CO_2 \rightarrow M_2CO_3 + SO_3 \qquad (1)$$

has an equilibrium constant of less than 10^{-5}, so that even if CO_2 is present at concentrations over 100 times that of the SO_x, little carbonate formation will occur. The presence of water in flue gas presents the possibility of the formation of sulfuric acid:

$$SO_3 + H_2O \rightarrow H_2SO_4 \qquad (2)$$

which has an equilibrium constant of 10^{-2}. Therefore, very little sulfuric acid formation is expected.

Temperature Limit

The minimum temperature for operation with the sulfate electrolyte-membrane is 512C. This is well above that of typical flue gases. Application would thus require boiler modification with the flue gas treatment upstream from the economizer. This problem stimulated the search for lower-melting electrolytes.

The alkali metal pyrosulfates are especially attractive. As suggested by Shores [1], the pyrosulfate ion is probably involved in the cathode sulfate reaction. If pyrosulfate mixtures are

used, the temperature of operation can be reduced to 250 - 350C. This is in the range of gas effluent from the economizer.

The reactions involved with pyrosulfate are perhaps similar to those with sulfate:

$$2\ SO_2 + 3/2 + 2e \rightarrow S_2O_7^{2-} \qquad (3)$$

at the cathode, and

$$S_2O_7^{2-} \rightarrow 2\ SO_3 + 1/2\ O_2 + 2e \qquad (4)$$

at the anode.

Some additional advantages are accrued from the lower temperatures. A lower volumetric gas flow needs to be treated, which decreases the size estimate. Also, the particulate removal system is less costly. Furthermore, reactions (3) and(4) involve only one electron per mole of SO_2, doubling the theoretical current efficiency from that with sulfate, and thus decreasing the potential operating costs.

Even lower temperatures are possible using the bisulfates (150 - 200°C). The corresponding electrochemical reactions at the cathode and anode are:

at the cathode,

$$H_2O + 2SO_2 + 3/2\ O_2 + 2e^- \rightarrow 2HSO_4^- \qquad (5)$$

and at the anode,

$$2HSO_4^- \rightarrow 2SO_3 + 1/2\ O_2 + H_2O + 2e^-. \qquad (6)$$

In the bisulfate configuration, some of the SO_3 at the lower temperatures will combine with water to form pyrosulfuric acid ($H_2S_2O_7$) which is a desired product for the anode stream.

The stability of the bisulfate electrolyte in the EC cell has not been tested (the sulfate electrolyte has). A significant portion of the work proposed here is to complete fundamental electrochemical experiments with the bisulfate electrolyte. If the bisulfate proves acceptable, it also will reduce (1) the electrical current required for the SO_x removal by about 50% (since the bisulfate ion is monovalent while the sulfate ion is divalent) and (2) the operating temperature of the EC cell from, say, 550°C to 200°C or less.

A recent study [2] has shown that the eutectic Na-K nitrate melt may be an effective low-temperature solvent for sulfate or pyrosulfate. This system may be usable as low as 175C. The precise limit will depend upon the amount of sulfate species at steady-state as increased amounts will raise the melting points.

An interesting serendipity occurs with this solvent when NO_x is present in the flue gas. The NO_x can be electronated with vanadia as a catalyst:

$$NO_2 + 1/2\ O_2 + e \rightarrow NO_3^- \qquad (7)$$

$$NO + O_2 + e \rightarrow NO_3^- \qquad (8)$$

This will maintain a certain amount of nitrate within the electrolyte. Preliminary testing in free electrolyte will reveal what fraction nitrate, and hence what melting point, can be maintained with typical flue gas levels of NO_x along with the SO_x.

A complication arises in that concentrated NO_2 will be emitted along with the concentrated SO_3 at the anode. However, there is a use for the mixed, strong acid in fertilizer manufacture [3].

Transfer Rates

Several processes must occur in sequence in the electrochemical membrane concentrator. The component(s) in question must diffuse from the bulk gas stream to the electrode-electrolyte interface, electrochemical and chemical reactions must proceed, the products must migrate (due to the applied field) to the anode and there be oxidized. These anodic products, concentrated gases must diffuse away into the anode gas.

The rates of the first and last steps are easily calculated. With a dilute gas, such as we are treating, the first will be rate-limiting (11) as long as the active areas and reaction rates are maximized. The active area of the electrodes can be enhanced, over the superficial area, by a factor of 300 or so [4] using porous electrodes manufactured from powders. The reaction rates are measured using standard electrochemical techniques in the free electrolyte.

BISULFATE ELECTROLYTE TESTING

A potassium-sodium (46.5 - 53.5 mole %) bisulfate eutectic was tested in a pyrex glass cell with a removable top containing gas inlet and outlet lines. Flat gold foils (1.95 cm^2) were used as the working and counter electrodes. The reference electrode was composed of 0.010 inch gold wire in a pyrex tube made into a Luggen-Haber capillary tip. The electrodes were immersed directly in the electrolyte melt.

The object of these experiments was to determine the electrochemical kinetic behavior of the bisulfate eutectic, and its suitability for use as an electrolyte in the sulfur dioxide concentrator cell.

The principle technique employed here was chronoamperometry [5]. Potential steps are applied to the working electrode, and the current decay data recorded.

Przansnyski [6] and Hagy [7] have presented the following equation which accounts for the charge time delay, t_2:

$$i = (W/t_2\lambda^2 \{\exp(\lambda^2 t)\operatorname{erfc}(\lambda t^{1/2}) + 2\lambda(t/\pi)^{1/2} - \exp[\lambda^2(t - t_2)]\operatorname{erfc}[\lambda(t - t_2)^{1/2}] - 2\lambda[(t - t_2)/\pi]^{1/2}\} \quad (\text{for } t > t_2) \tag{9}$$

where $W = \dfrac{V}{R_s + R_r}$

V is the applied potential step

R_s is the solution resistance per unit electrode area

$$R_r = \frac{r \nu RT}{nFI_o} \tag{11}$$

r is the number of working electrodes

ν is stoichiomnetric number of the reaction mechanism

$$\lambda = \frac{i_o}{\nu nF} \cdot \frac{R_r}{R_s + R_r} \quad \frac{1}{D_O^{1/2} C_O} + \frac{1}{D_R^{1/2} C_R} \tag{12}$$

Non-linear fitting techniques were used to calculate the parameters w and λ.

Bisulfate Procedure

Twenty-two chronoamperometric runs were made using various working electrode gas compositions and flow rates. All experiments were conducted at 205°C. The concentration of SO_2 in the working electrode gas ranged from 0.0% to 3.063% and O_2 concentration ranged from 0.0% to 32.82%. Water vapor concentration varied from 4.40% to 13.94%. The reference gas used was always 0.338% SO_2, 2.81% O_2 and 4.40% H_2O. Bubbling of pure N_2 at the counter electrode did not cause any apparent change in the melt behavior and was not done in any of the experiments.

Potential steps were made roughly every 50 mV for overpotentials from 0 to ± 200 mV. The resulting current decay traces were recorded on the storage oscilloscope and

photographed.

Bisulfate Data Analysis

The large amount of data accumulated required most of the data analysis to be done by computer. Equation (9), which accounts for the charging delay, was found to fit the data well. The resistance, R_u, was measured with an AC impedance bridge to be approximately 43 ohms. The capacitance, C_d, has been found to be about 60 $\mu F/cm^2$ for this melt at this temperature, but on Pt [8]. It was assumed the same here, giving an estimated '1% accuracy' delay time of 10 ms. However, smaller delay times can be used if 10-15% accuracy is sufficient [9]. We thus used, typically, 5 or 6 ms, with the advantage of incorporating more highly-kinetic data.

Bisulfate Equilibrim Potentials

The equilibrium potential between the working and reference electrodes with different working-gas compositions can be used to attempt to define the overall reaction.

Reactions (13) and (14) are possible anodic reactions:

$$SO_4^{2-} = SO_3 + 1/2\ O_2 + 2e \qquad (13)$$

$$S_2O_7^{2-} = 2SO_3 + 1/2\ O_2 + 2e \qquad (14)$$

For reaction [13] the change in OCV with gas composition is:

$$\Delta E = \frac{RT}{2F} \ln \frac{a_{SO_3} \cdot a_{O_2}^{1/2}}{a_{SO_4}^{2-}}_2 - \ln \frac{a_{SO_3} \cdot a_{O_2}^{1/2}}{a_{SO_4}^{2-}}_1 \quad (15)$$

where the SO_3 is dependent on the inlet SO_2 and O_2, though not in total equilibrium:

$$SO_3 = SO_2 + 1/2\ O_2 \quad (14)$$

The change in OCV for reaction [14] is

$$\Delta E = \frac{RT}{2F} \ln \frac{a_{SO_3} \cdot a_{O_2}^{1/2}}{a_{S_2O_7}^{2-}}_2 - \ln \frac{a_{SO_3}^{2} \cdot a_{O_2}^{1/2}}{a_{S_2O_7}^{2-}}_1 \quad (16)$$

If we assume the sulfate and pyrosulfate at the working electrode do not change greatly with the incoming gas, rough estimates can be made and compared with experiment. The results in Table 1 show that neither reaction (13) nor (14) characterizes the changes in OCV with gas composition. In fact, there is no apparent effect on the OCV of the inlet oxygen level; the response is only to the SO_2. These results suggest a reaction with an available oxygen species in solution or on the electrode:

$$SO_2 + X + 2e \rightarrow SO_3^{2-} \text{ or } SO_4^{2-} \quad (17)$$

or

$$2SP_2 + Y + 2e \rightarrow S_2O_7^{2-} \quad (18)$$

Reaction (18), as seen in Table 1, is the most likely on the basis of these OCV data. The likely species Y is discussed later.

Bisulfate Cyclic Voltammetry

Cyclic voltammograms were run over a five-fold range in scan rates for one gas composition. Two representative plots are shown as Figures 1 and 2. The one discernible peak in the cathodic sweep clearly shows a kinetically controlled electron transfer. The peak voltage (IR-corrected) varies linearly with the logarithm of the scan rate. From the slope of this line the cathodic transfer coefficient can be roughly calculated to be 0.4.

The second cathodic peak may be the result of a reversible charge tranfer followed by a fast irreversible chemical reaction [19]. In this situation, a limiting current is seen which is invariant with scan rate, as seen here. This will be discussed later.

Exchange Current Densities

The exchange current densities found from regression of equation (9) ranged from 0.035 to 0.67 mA/cm^2. They are displayed in Figures 3 (cathodic) and 4 (anodic). Both cathodic and anodic i_o increase with increasing SO_2 concentration in the working gas. Values for the mass-transfer parameter, λ, ranged from 2 to 17 sec^{-1} with no obvious dependence on gas composition.

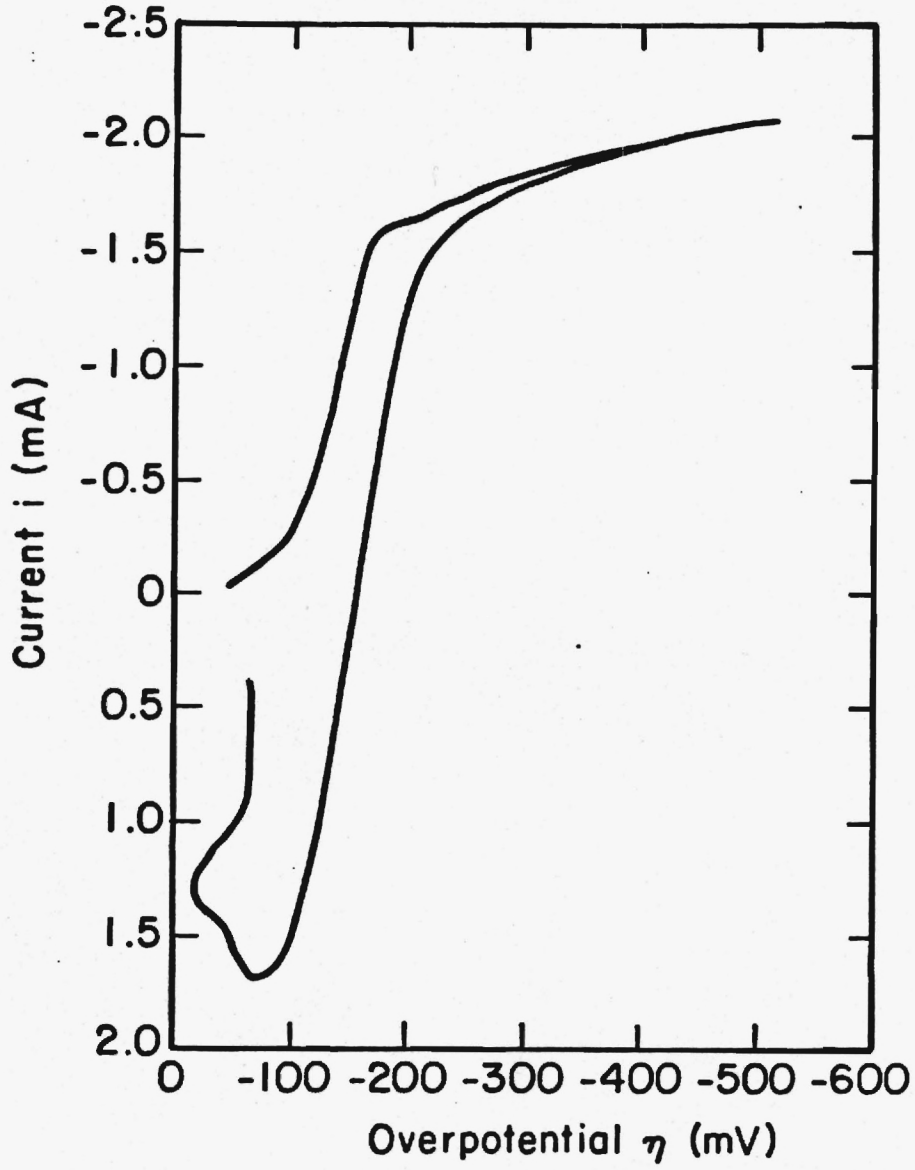

Figure 1. Cyclic Voltammogram at 160 mV/s

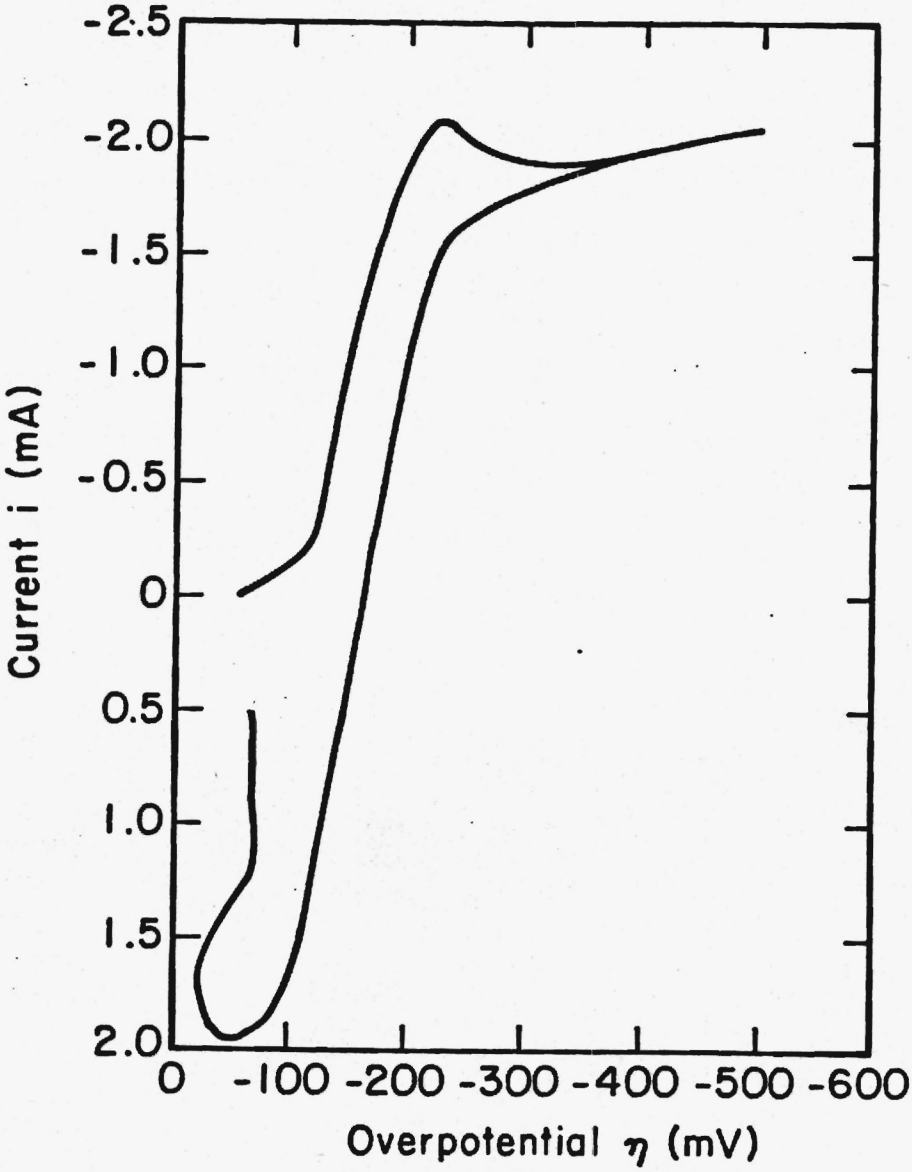

Figure 2. Cyclic Voltammogram at 320 mV/s

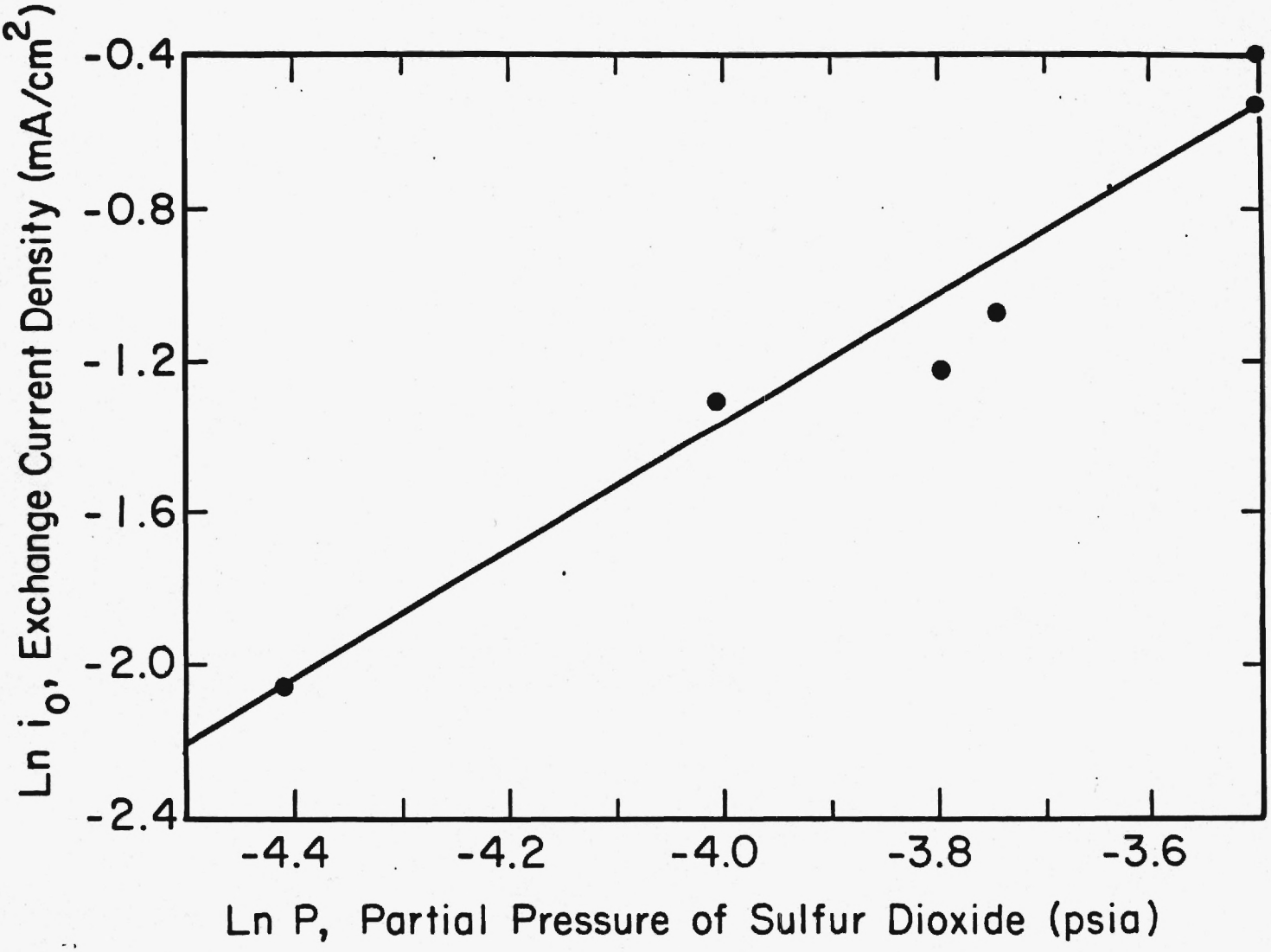

Figure 3. Effect of SO_2 on Observed Cathodic Exchange Currents

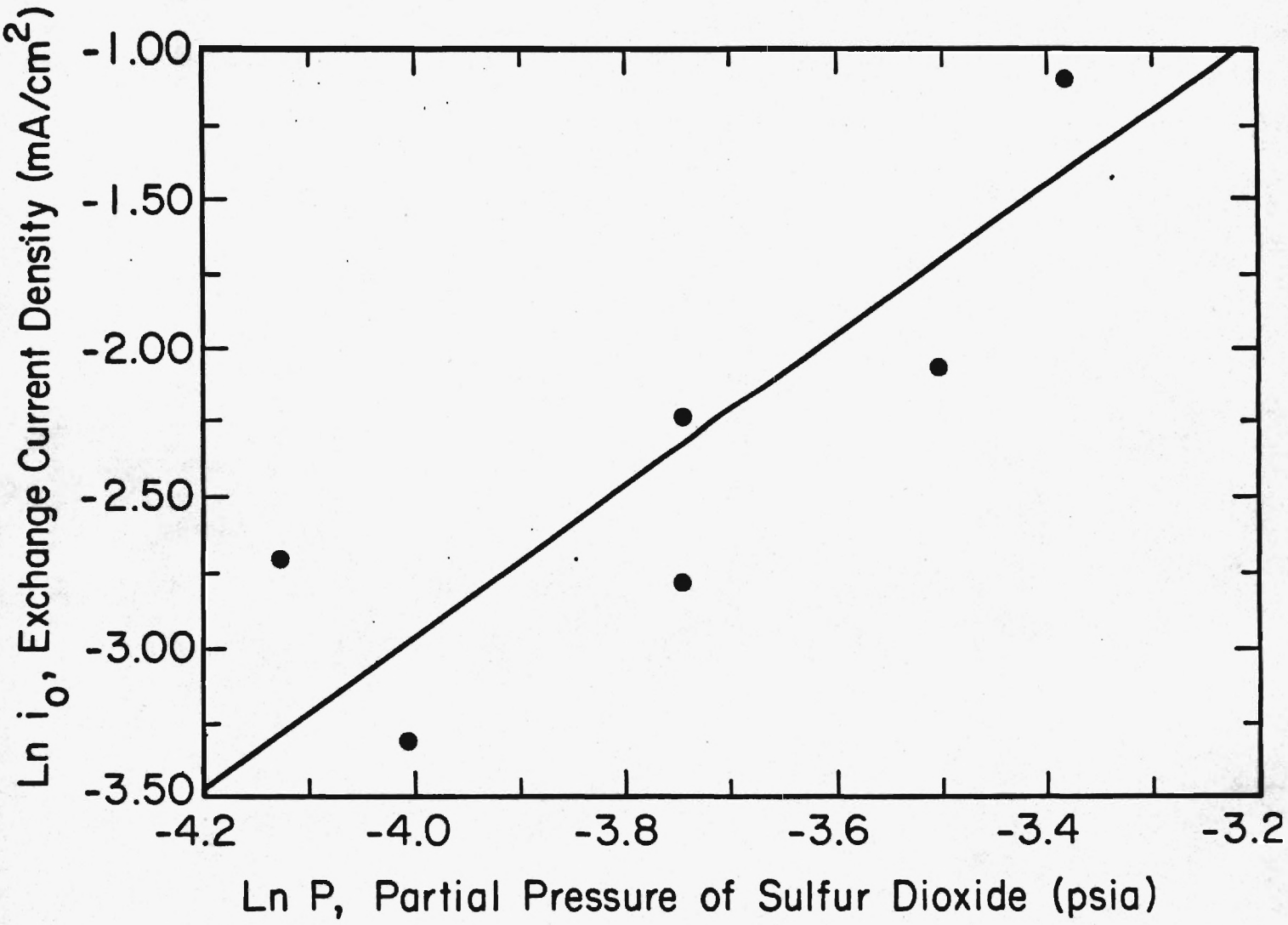

Figure 4. Effect of SO_2 on Observed Anodic Exchange Currents

Table 1
Change in OCV with Gas Composition

Point	Inlet Gas, psia x 10^2		$\Delta E_{expt.}$	$\Delta E_{[13]}$	$\Delta E_{[4]}$	$\Delta E_{[17]}$	$\Delta E_{[18]}$
	SO_2	O_2			millivolts		
1	3.38	28.14					
			-20.5	42.8	60.5	-7.5	-15.0
2	2.35	323.8					
1	26.17	257.5					
			10.4	-40.5	-58.	5.6	11.1
2	34.28	27.48					
1	3.38	28.14					
			- 4.0	- 6.0	-12.1	-6.4	-12.8
2	2.48	28.73					
1	3.38	28.14					
			-26.0	42.8	60.5	-7.5	-15.0
2	2.35	323.3					

These results have been compared with 'applicability' criteria arrived at by Nagy [7] from comparison with numerical solution of a more exact treatment. They fall in the optimum region for accurate determination of the parameters. A check was also made as to the loss of accuracy due to the electro-kinetic linearization assumption involved in equation (9) [10]. Over the range of pulses used, with $\frac{\alpha}{n} = 0.4$, an accuracy in exchange currents of 10-15% is expected.

The reaction is under mixed control. These values of i_o and λ show charge-transfer is responsible for 30-90% of the total IR-free overpotential during the time duration of the data ($\sim$ 5-25 ms).

A number of runs were done using N_2 as the working gas. In these runs the current decayed very rapidly to below the detection limits of the equipment. For times after about 5 ms, the faradaic current was essentially the small steady-state current. The small amount of SO_2 that was dissolved in the melt was probably quickly consumed by the electrochemical reactions and no further reactions occurred. This is precisely the behavior noted by Arvia [8] under these conditions.

Delahay [11] notes that different anodic and cathodic exchange current densities, for potential steps under the same conditions, indicate that the cathodic and anodic reaction mechanisms are different.

Reaction Orders

The exchange currents showed no discernible trend with the changes in gas-phase oxygen or water vapor in keeping with the OCV results. There was, however, a distinct effect of SO_x content, as shown in Figures 3 and 4. The reaction order for SO_x may be calculated to be 2.0 ± 0.2 in both cathodic and anodic directions.

Residual Potential

After the application of a cathodic overpotential step, when the cell is at rest, there is a large residual potential that remains between the working electrode and the reference electrode. This residual potential appeared only for cases where the applied potential was cathodic and more than -150 mV. Arvia has noted similar behavior at this same potential [8]. The working electrode to counter electrode potential difference, W/C, differed from the working electrode to reference potential difference, W/R, by less than 10 mV. This indicates that all of the residual overpotential is caused by some changes that occurred on the working electrode when cathodic overpotential was applied. The residual potential remained steady for about ten minutes, after which it slowly decayed. The resumption of reference gas bubbling did not affect the residual potential. The composition of the working gas bubbled did not influence the rate of potential decay. However, larger flow rates of working gas tended to hasten the process.

Limiting Currents

Limiting currents were found during both cathodic and anodic chronamperometric studies. The cathodic were 2.2 ± 0.2 mA and the anodic 1.7 ± 0.1 mA. Both were independent of gas concentrations.

Bisulfate Discussion

The results point clearly to a cathodic reaction scheme involving pyrosulfate as the electroactive species. The effect of SO_x is unequivocal. The current densities seen here are some three orders of magnitude larger than those found by Arvia [8] under nearly identical conditions, with gas-phase oxygen but no SO_2.

In a sulfate melt at 900°C, Shores [1] and Fang [12] noted a similar effect of SO_3 with only small participation in the cathodic current of the dissolved oxygen. A reaction scheme in the bisulfate melt is suggested which involves a surface oxide formed on the electrode in these melts [13]:

$$2SO_2 + \text{Surface gold oxide} + 2e \rightarrow S_2O_7^{2-} \qquad (17)$$

The residual potentials offer large (> -150 mV) excursions were probably due to renewal of the oxide film reduced by the cathodic pulse. This is precisely as observed by Arvia [14] with oxygen present.

The anodic oxidation was presumed by Arvia [8] to involve sulfate ions. However, here, with pyrosulfate present, it is

more likely the active species,

$$S_2O_7^{2-} = 2(SO_3^-)_{ads} + (O) \quad (19)$$

$$2(SO_3^- = SO_3 + e) \quad (20)$$

The effect of dissolved SO_3 would be seen in the pyrosulfate concentration, as under cathodic polarization. A reaction order more near unity, however, would be expected, rather than the order of 2 which was observed.

Pyrosulfate Electrolyte Testing

Potassium pyrosulfate, and potassium pyrosulfate containing small quantities of V_2O_5, were tested in pyrex glass cells of various design depending on the experiments being conducted. Flat gold foils were used as the working and counter electrodes. The reference consisted of a silver wire immersed in a mixture of KNO_3 and $AgNO_3$ contained in a small closed pyrex tube.

Pyrosulfate Procedure

The experiments could be broken into 3 main categories.

Thin Film Exponents

Polarization experiments were carried out in thin films of electrolyte. The thickness of the salt was determined from the geometry of the cell, the weight of salt added and the density of the salt at operating temperatures. The environment above the melt could be controlled by altering the composition of the gas

sent to the cell at a flow rate of 50 cc/minute. Whenever the gas composition was changed the cell was allowed to stand for two hours so that there were no residual effects of the previous gas.

Pyrosulfate Chronamperometry

The PAR potentiostat/galvanostat operating in the potentiostatic mode was used to supply an overpotential while the HP function generator was used to supply the equilibrium potential. Before each experiment all gas flows are stopped to allow the electrolyte to become quiescent. This prevented convection effects interfering with the development of the concentration profile. With the system at equilibrium, an overpotential step function was applied by closing the fast-acting potentiostat switch. The resulting current jump and decay versus time were recorded on a storage oscilloscope and photographed with an oscilloscope camera. Gas bubbling was then resumed and the cell allowed to stand until the original equilibrium conditions were again obtained (i.e., until the electrode potential is returned to their original values). The above procedure was repeated for potential steps ranging from 0 to 300 mV.

Pyrosulfate Effluent Analysis Experiments

The purpose of these experiments is to measure the concentration of sulfur species in the gas streams to and from the working electrode compartment. Ten ml samples were withdrawn by a gas-tight syringe from sample ports in each line. The

syringe was flushed several times in the gas stream to ensure that a representative sample is obtained. The sample was then immediately injected into the gas chromatograph operating in the flame photometric detector mode. At least three samples were analyzed under each set of experimental conditions so that an average reading could be calculated. Frequent instrument calibrations were performed by injecting known volumes of primary grade analyzed gases containing known concentrations of SO_2. Each time the G.C. flame was re-lit calibration was especially important.

Pyrosulfate Thin Film Experiments

Polarization data were taken for a system consisting of planar gold electrodes covered by a molten electrolyte film of variable thickness exposed to an atmosphere of variable gas composition. The results showed that the limiting current was not significantly influenced by either a change in environment or a change in film thickness. This strongly suggests that no reactants of the electrochemical reactions taking place are supplied by the gaseous phase. In other words, the predominant electrode reactions involve direct oxidation and reduction of a species originally in the liquid phase, and the current is probably limited by diffusion of the products away from the electrodes.

Similar experiments by Shores and Fang [1] with a Na_2SO_4 melt show a ten-fold increase in limiting current with a corresponding ten-fold decrease in film thikcness, and a marked

effect of gas composition on the limiting current. These authors eliminate a number of reduction reaction possibilities by showing that an unreasonable value of the diffusion coefficient, D (calculated by assuming a stagnant film: $D = i_L \delta/nFC$) would be required for the experimental data to be consistent. In the present work, certain reactions can also be eliminated by showing that unrealistic values of the diffusion coefficient would be required. The solubilities of K_2SO_3, K_2O_2, and KO_2 were calculated from thermodynamic stability data assuming ideal solution behavior [15]. Then values of D, required if any of these species were the active ones, were calculated for the case of a 2.6 mm film of $K_2S_2O_7$ electrolyte with a 10% SO_2, 20% O_2, 70% N_2 gas environment. The results are shown in Table 2. The calculated diffusivities are clearly unreasonably large, eliminating the indicated reactions. On the other hand, if the active species is assumed to be the potassium pyrosulfate, and the diffusion distance is taken to be the electrode separation (6 cm), a required diffusivity of 1.9×10^{-5} can be calculated. This is quite feasible and suggests that the pyrosulfate may be the electroactive species.

Pyrosulfate Chronoamperometry

As in the bisulfate testing phase of this work, the exchange current density was found by regression of equation (9).

The value of t_2 for this system was taken to be 10 msec which, according to the criteria presented by Nagy [7], should cause less than 1% error.

Table 2

Diffusiviities Calculated from Limiting Reduction Current Densitiies in $K_2S_2O_7$ in 10% SO_2, 20% O_2, 70% N_2.

Possible Reaction	Concentration of Active Species mol/m^3	Diffusivity Required cm^2/sec
$SO_3^{2-} + 6e = S^{2-} + 3O^{2-}$	1×10^{-12}	3×10^{3}
$O_2^{2-} + 2e = 2O^{2-}$	$\sim 10^{-20}$	9×10^{11}
$O_{\overline{2}} + 3e = 2O^{2-}$	$\sim 10^{-21}$	6×10^{12}

The parameters W and λ were determined for cathodic potential steps of 25, 50, 75, 100, 150, 200, 250, and 300 mV. An example of a calculated curve and experimental data for a 50 mV step is shown in Figure 5.

The exchange current density, i_o, may be calculated by rearranging Equation (10). The value of the solution resistance, R_s, was found by an independent AC technique to be approximately 1.5 ohms. Table 3 summarizes the values of W and λ obtained from each cathodic potential step. It also shows the value of i_o and $\frac{1}{D_O^{1/2}C_O} + \frac{1}{D_R^{1/2}C_R}$ calculated from Equations (10) and (12). The average value of the cathodic exchange current density is 0.029 ± 0.005 A/cm^2. The average value of the concentration and diffusion term is $2.4 \times 10^7 \pm 0.8 \times 10^7$ $S^{1/2}cm^2/mol$. From the thin film results presented earlier, the species being reduced is potassium pyrosulfate and C_o = 0.01 $mole/cm^3$. By substituting reasonable values for the diffusivities (2×10^{-5} cm^2/sec), C_R can be estimated to be 9×10^{-6} $mole/cm^3$. The concentration of sulfate ion in the melt may be calculated by considering the equilibrium reaction

$$K_2S_2O_7 = K_2SO_4 + SO_3 \qquad (21)$$

The equilibrium constant at 340°C may be calculated using thermodynamic data to be 2.78×10^{-6}. If approximately 10% of the entering SO_2 is oxidized to SO_3 (as may be estimated from kinetic data [16]) the concentration of K_2SO_4 is equal to 28×10^{-6} $mole/cm^3$. This value is the same order of magnitude as that

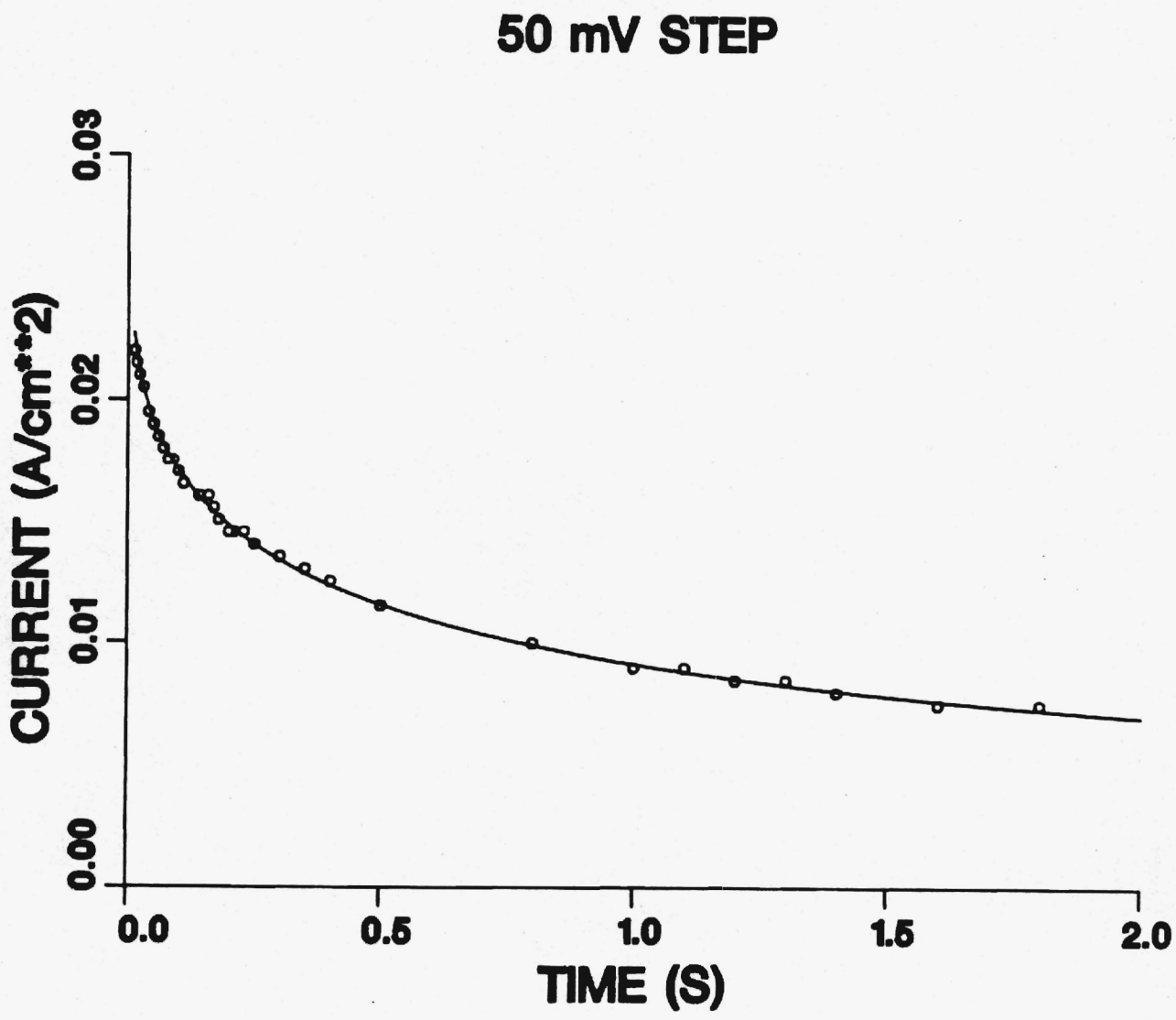

Figure 5. Cathodic Current Decay After 50 mV Cathodic Step

Table 3

Parameters Obtained by Fitting Cathodic Potential Step Data in 1% V_2O_5 - 99% $K_2S_2O_7$ at 340C.

Potential Step	W (A/cm^2)	($s^{-1/2}$)	i_o (A/cm^2)	$\frac{1}{D_o^{1/2}C_o} + \frac{1}{D_R^{1/2}C_R}$ $\frac{s^{1/2}cm^2}{mole}$
0.025	0.0099	1.718	0.0264	3.09×10^7
0.050	0.0209	1.240	0.0300	2.23×10^7
0.075	0.0290	1.092	0.0249	1.96×10^7
0.100	0.0392	2.365	0.0262	4.25×10^7
0.150	0.0567	1.120	0.0236	2.01×10^7
0.200	0.081	1.093	0.0279	1.97×10^7
0.250	0.110	1.172	0.0349	2.11×10^7
0.300	0.139	1.074	0.0391	1.92×10^7

determined for C_R, and may indicate that pyrosulfate is being reduced to form sulfate in the first electrochemical step.

Effluent Analysis

More insight can be gained on the reactions taking place by analyzing the gases leaving the cell. The sulfur content of the exit gas streams are examined, using a flame photometric detector, for relations between sulfur concentration, electrolyte composition and applied current. Table 4 shows the results for the following electrolyte compositions: pure $K_2S_2O_7$, 25 weight percent K_2SO_4 in $K_2S_2O_7$, and 40% K_2SO_4 in $K_2S_2O_7$. The operating temperature employed (340°C) sets a limit on the maximum sulfate concentration (40%) which can be tested.

In this set of experiments nitrogen is the working gas and is bubbled into the system at a flow rate of 40 cc/minute. Several observations can be made. First, at the cathode, the exit sulfur concentration increases with increasing current. This effect is most dramatic in pure $K_2S_2O_7$, where the exit concentration ranges from 23 ppm at open circuit to 910 ppm at 30 mA. Over a time period of several hours these results remained constant but they obviously cannot represent the true steady state values since more sulfur is leaving the system than is entering. The increased sulfur effluent with current indicates that an electrochemical reaction takes place at the cathode which produces either SO_2 directly or an intermediate product which then reacts to form SO_2. Proposed reaction schemes will be presented later.

Table 4

Effluent Gas Analysis. Gas to Cell is N_2.

I	[Pure $K_2S_2O_7$]		[25% K_2SO_4, 75% $K_2S_2O_7$]		[40% K_2SO_4, 60% $K_2S_2O_7$]	
	Cathode	Anode	Cathode	Anode	Cathode	Anode
(mA)	Exit	Exit	Exit	Exit	Exit	Exit
	(Concentrations in parts per million sulfur oxide)					
0	23	23	23	23	20	20
5	92	44	83		81	
10	282	156	184	376	208	510
15	486	136				
20	618	214	432	475	390	677
30	910	290				

At the anode, increased sulfur oxide concentration is also observed at higher currents, suggesting tha the pyrosulfate is being reduced to form SO_2 or SO_3. Higher K_2SO_4 concentrations in the electrolyte cause a substantial rise in the exit sulfur concentration.

Table 5 shows the results of a similar set of experiments with a working gas of 0.3% SO_2, 3% O_2, 15% CO_2 and the balance N_2. Similar trends in exit sulfur oxide concentration are noticeable. At open circuit there is significant sulfur dioxide absorption. The inlet gas stream contains 3000 ppm SO_2. With no applied current the exit concentration in pure $K_2S_2O_7$ is 2660 ppm. The open circuit SO_2 removal is slightly greater at higher sulfate concentrations which indicate that more SO_2 is adsorbed into molten sulfate than into pyrosulfate.

The gas analysis results examined to this point showed no reduction in the cathode SO_2 exit concentration when current is applied. Next the effect of adding V_2O_5 to the electrolyte will be reported. Table 6 shows the results for the following electrolyte compositions: pure $K_2S_2O_7$, 0.1% V_2O_5 in $K_2S_2O_7$, and 1% V_2O_5 in $K_2S_2O_7$. The working gas is 1% SO_2, 10% O_2 and the balance N_2, again the flow rate is 40 cc/minute, and the operating temperature is 340°C. At open circuit in pure $K_2S_2O_7$, 10% of the entering SO_2 is adsorbed, and the exit SO_2 concentration is 9000 ppm. As the percentage of V_2O_5 is increased the open circuit adsorption of SO_2 is slightly enhanced. This is in agreement with other work in a V_2O_5 - $K_2S_2O_7$ melt [17]. Consistent with the data of Tables 4 and 5,

Table 5

Effluent Analysis. 0.3 SO_2, 3% O_2, 15% CO_2, Balance N_2 to Cell.

I	[Pure $K_2S_2O_7$]		[25% K_2SO_4, 75% $K_2S_2O_7$]		[40% K_2SO_4, 60% $K_2S_2O_7$]	
	Cathode	Anode	Cathode	Anode	Cathode	Anode
(mA)	Exit	Exit	Exit	Exit	Exit	Exit
	(Concentrations in parts per million sulfur oxide)					
0	2660	2660	2500	2570	2410	2330
5			3620	2850	2260	3290
10	7040	4400	5260	3120	3300	4000
20	15210	5090	11800	5470		

Table 6

Effluent Analysis. 1% SO_2, 10% O_2, 89% N_2 to Cell.

I	[Pure $K_2S_2O_7$]		[0.1% V_2O_5, 99.9% $K_2S_2O_2$]		[1% V_2O_5, 99% $K_2S_2O_7$]	
(mA)	Cathode Exit	Anode Exit	Cathode Exit	Anode Exit	Cathode Exit	Anode Exit
	(Concentrations in parts per million sulfur oxide)					
0	9020	8980	8980	9000	8770	8790
5			9400		8580	8960
10	14000	11290	9810		8000	9820
20	17100	12400	11930		7940	10440
30	19170	14500			7940	

the cathode and anode exit SO_2 concentration in pure $K_2S_2O_7$ increases with higher currents. Again, at the anode pyrosulfate is being reduced to form SO_2.

A significant difference at the cathode is observed when the electrolyte is 1% V_2O_5 in $K_2S_2O_7$. The exit SO_2 concentration is measured at 8770, 8580, 7940, and 7940 ppm at 0, 5, 10, 20 and 30 mA, respectively. A limit of 9.5% sulfur removal with application of current is observed. Calculations show that this limit may be due either to mass transfer limitations or kinetic limitations induced in the oxidation of SO_2 to SO_3.

Pyrosulfate Reaction Scheme

A cathodic reaction mechanism will now be presented with evidence supporting the postulated reactions:

$$S_2O_3^{2-} + e = SO_4^{2-} + SO_3^- \qquad (22)$$

The thin film experiments indicate that the electrochemical reduction reaction involves direct pyrosulfate reduction because there is no dependence of limiting current on the gas phase. Examination of experimental open-circuit working versus reference potentials shows that as the sulfate concentration in the electrolyte is increased, the potential of the working electrode becomes less positive, which is exactly the response predicted by the Nernst equation written for Reaction (22).

$$SO_3^- + e = SO_3^{2-} \qquad (23)$$

This reaction occurs at a similar potential to Reaction (22) and has been independently proposed in a reaction mechanism in a Na_2SO_4 melt [12]. The species SO_3^{2-} is unstable under the experimental conditions and further chemical reaction will take place.

$$SO_3^{2-} = SO_2 + O^{2-} \tag{24}$$

This reaction explains the increased SO_2 concentration at the cathode. Higher currents result in higher concentrations of SO_3^{2-} and thus higher levels of sulfur dioxide in the cathode gas effluent.

$$3SO_2 + \frac{3}{2} O_2 = 3SO_3 \tag{25}$$

This equilibrium reaction must be taken into account since both SO_2 and O_2 are present in the feed stream to the cathode. The equilibrium constant may be calculated using free energy of formation data at 600°K [15]:

$$K = \frac{P_{SO_3}}{P_{SO_2}(P_{O_2})^{1/2}} = 4.4 \times 10^3 \tag{26}$$

Thermodynamically, then, the conversion to SO_3 would be expected to be nearly complete, but without a catalyst the kinetics of this reaction are extremely slow and in a melt with

no vanadium pentoxide the formation of SO_3 is negligible. With V_2O_5 added, conversion is significant as calculated earlier. The following three-step redox reaction mechanism of this SO_2 oxidation over V_2O_5 in unsupported $K_2S_2O_7$ has been proposed [18, 19]:

$$V_2O_5 \cdot SO_3 + SO_2 = (VOSO_4)_2 \tag{27}$$

$$(VOSO_4)_2 = V_2O_4 \cdot SO_3 + SO_3 \tag{28}$$

$$\frac{V_2O_4\ SO_3\ \frac{1}{2}\ O_2 = V_2O_5\ SO_3}{SO_2 + \frac{1}{2}\ O_2 = SO_3} \tag{29}$$

$$SO_3 + O^{2-} = SO_4^{2-} \tag{30}$$

This reaction provides a means of removing SO_3 at the cathode. The reaction will occur faster when V_2O_5 is present in the melt because reaction (25) will be enhanced. The SO_3 then combines with sulfate ions:

$$2SO_3 + 2SO_4^{2-} = 2S_2O_7^{2-} \tag{31}$$

This reaction also allows SO_3 removal at the cathode. It was observed that adding SO_4^{2-} to the melt increased the absorption rate of SO_3 which is also consistent with this reaction. Formation of $S2O7^{2-}$ maintains a low electrolyte

melting point.

The overall cathodic reaction is

$$2SO_2 + \frac{3}{2} O_2 + 2e = S_2O_7^{2-} \quad . \qquad (32)$$

CONCLUSIONS

The electrochemical reactions have been studied in (Kn/Na) HSO_4 and $K_2S_2O_7$ with gas phase oxygen, sulfur oxides, and water vapor. In the bisulfate system the results show a marked effect of SO_x content, with exchange currents three orders of magnitude greater than those in its absence. In the pyrosulfate melt, addition of 1% V_2O_5 was found to enhance SO_2 removal with applied current.

Reaction schemes have been presented which are mostly consistent with these and other results. The schemes are not considered firm; there remain some inconsistencies and uncertainties.

The kinetic parameters obtained are in keeping with those required for economic performance in a commercial electrochemical device [1]. The composite size of the kinetic currents and the relative stability indicate that potassium pyrosulfate with 1% vanadia is the electrolyte of choice.

REFERENCES

1. Shores, D. A. and Fang, W. C., J. Electrochem. Soc., 128, 346 (1981).

2. Abdel-Salem, O. E. and Kou, A. L., Electrochimica Acta (1983).

3. Davis, W. L., et. al., Chem. Eng. Prog., 64, 75 (1968).

4. IGT, Project 898A, Final Report 1978.

5. Bard, A. J., Faulkner, C. R., "Electrochemical Methods", John Wiley (1980).

6. Przasnyski, M., J. Electroanal. Chem., 107, 419 (1980).

7. Nagy, Z., J. Electrochem. Soc., 129, 1943 (1982).

8. Arvia, A. J., et al., Electrochim. Acta., 13, 167 (1968).

9. Nagy, Z., Personal Communications (1984).

10. Nagy, Z., J. Electrochem. Soc., submitted (1984).

11. Delahay, P., "Double-layer and Electrode Kinetics", New York, Wiley-Interscience (1965).

12. Fang, W. C., Rapp, R. A., J. Electrochem. Soc., 130, 2335 (1983).

13. Calandra, H. J., de Tacconi, N. R., Arvia, A. R., J. Electroanal. Chem. 49, 145 (1974).

14. Ferro, C. M., Calandra, A. J., Arvia, A. J., Electroanal. Chem., 55, 291 (1974).

15. Barin, I. and Knacke, O., "Thermochemical Properties of Inorganic Substances", Springer Verlag, Berlin (1973).

16. Davidson, B. and Thodos, G., AIChE J., 10, 568 (1964).

17. Sundheim, E., "Fused Salts", McGraw Hill (1964).

18. Holroyd, F. P. B., Kenney, C. N., Chem. Eng. Sci., 26, 1971 (1971).

19. Glueck, A. R., Kenney, C. N., Chem. Eng. Sci., 23, 1257 (1968).

COMBINED NO NO_x/SO_x

USING AN ELECTROCHEMICAL MEMBRANE CONCENTRATOR

Six Month Progress Report No.
DOE/PC/73226-2

DOE/PETC

Grant No: DE - FG22 - 84PC73226

B & R No: AA0505

B & R Class: Flue Gas Cleanup

TPO: Richard Walker

P.I.: J. Winnick

GEORGIA INSTITUTE OF TECHNOLOGY

August 1985

COMBINED NO NO_x/SO_x

USING AN ELECTROCHEMICAL MEMBRANE CONCENTRATOR

Six Month Progress Report No.
DOE/PC/73226-2

DOE/PETC

Grant No: DE - FG22 - 84PC73226

B & R No: AA0505

B & R Class: Flue Gas Cleanup

TPO: Richard Walker

P.I.: J. Winnick

GEORGIA INSTITUTE OF TECHNOLOGY

August 1985

INTRODUCTION

Results in the previous period showed that pyrosulfate, with 1% vanadia, was the electrolyte of choice for the membrane. The operating temperature range with this electrolyte is 300-400C, well within the range of economizer exit-gas values.

Work has proceeded on two fronts: free-electrolyte testing with gold and perovskite electrodes, comparing polarization and contaminant (SO_x/NO_x) removal; and full-cell tests with ceramic matrices permeated with the electrolyte, using perovskite electrodes only. The results to date are presented separately.

I. FREE ELECTROLYTE

Introduction:

A major part in simultaneous SO_x/NO_x removal process involves fundamental testing in a cell environment in order to get some indication of actual performance in a full cell/pilot plant set-up. Some of the fundamental testing involves the development of adequate electrode and electrolyte compositions which meet the necessary established criteria. Once possible candidates are selected, tests such as cyclic voltammetry, SEM analysis, steady-state polarization and effluent analysis can give helpful information to choose the best possible electrode and/or electrolyte and hopefully to predict performance in an actual full cell set-up.

Cell Design:

The basic cell used for the fundamental testing is made of pyrex and was built in the Georgia Tech Chemistry Department Glass Blowing Laboratory. This cell, showed in Figure A, provides gas-tight, separate working and counter compartments for effluent analysis studies. In all cases, the counter electrodes were flat gold foils of known area with mechanical support by attached gold wires. The reference electrodes consisted of 0.1M $AgNO_3$ in 1000g KNO_3 contained in 1/4" diameter pyrex tubing.

The pyrex tubing was blown at a high temperature to form a thin-walled bulb at one end to allow the transport of potassium ions. The electrolyte was then added in a powder form, heated to melting, a silver wire attached to platinum wire dipped into the melt, and the temperature lowered to freeze everything in place. The open end of the pyrex was then heated and then pinched closed to form a small, completely sealed reference electrode.

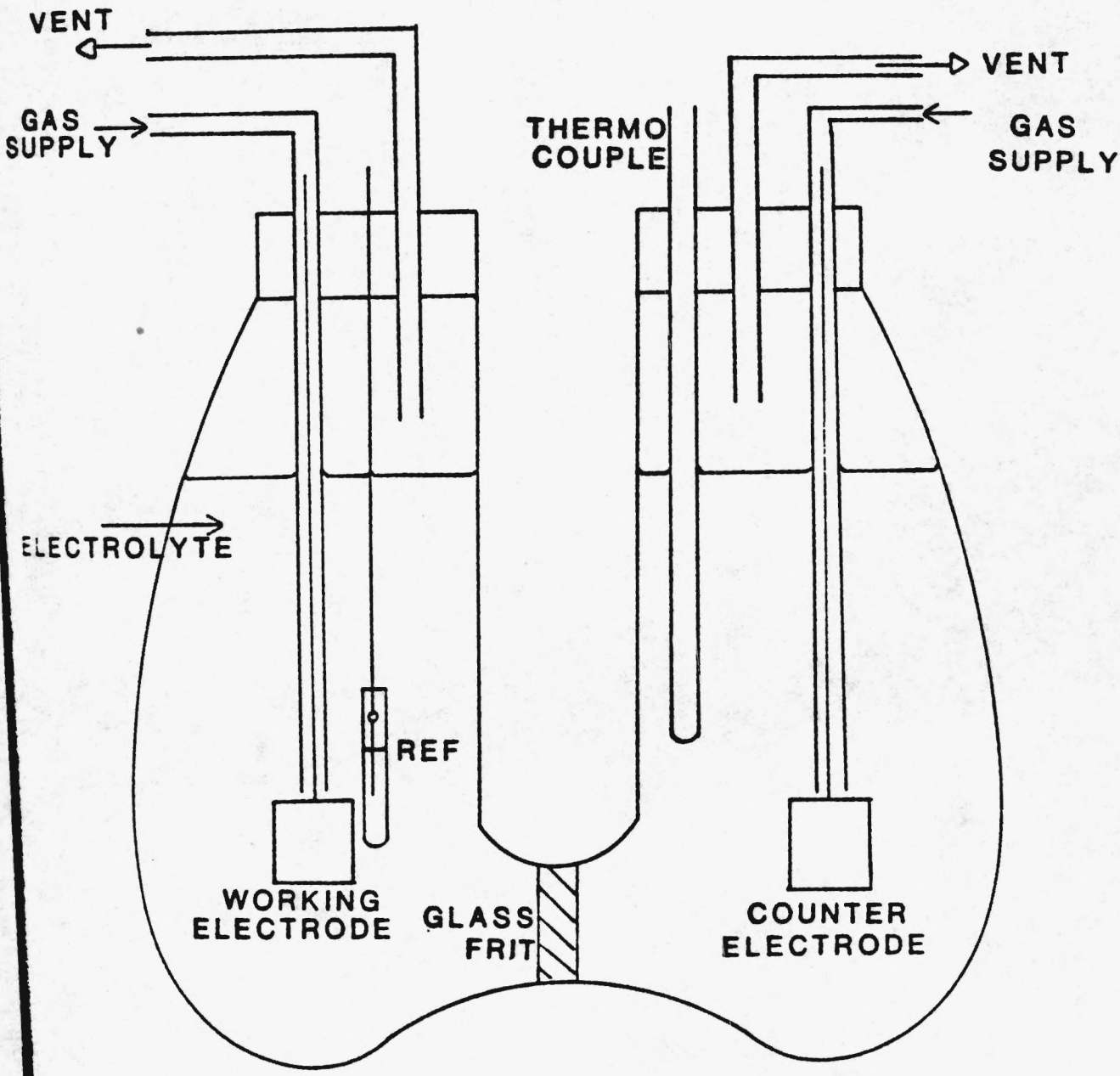

Figure A. Gas Tight Cell for Effluent Analysis.

Effluent Analysis:

Insight into the actual cell reactions can be obtained by analyzing the gases entering and exiting the test cell. Tests have been completed with the addition of N_2 gas containing concentrations of NO with the NO concentrations being determined by a Model 10AR Thermo Electron Chemiluminescent NO/NO_x Analyzer. Runs have been made with N_2 and NO gas, with and without the addition of dry in-house air, being bubbled into pure $K_2S_2O_7$ electrolyte at both the working and counter ports at a temperature of 340°C.

Results show that the addition of pure N_2 gas with NO into the electrolyte at a flow rate of 40 cc/min produced a significant decrease in NO concentration, as shown in Table 1. However, this gas mixture also produced stability problems with the potentials between the working and counter electrodes, which were both gold in this case. In order to eliminate this problem, in-house air was mixed with the gas mixture to give a total entering flow of 70cc/min. The introduction of this new mixture to both the counter and working ports also resulted in a noticeable decrease in NO concentration but without any serious effect to the cell potentials.

The application of current to the cell produced no significant change in the exiting NO concentrations at either the working or counter side. Generation of a small amount of NO_2 gas was noticed however, during the current application. It is believed that the addition of the NO gas and the resulting

decrease in NO concentration is due to the oxidation of NO to NO_2 which is absorbed into the electrolyte. It is hoped that analysis of the electrolyte after the completion of testing will bring some more insight into this theory.

Thus, the application of current seems to have produced more NO_2 production which was detected in the exit stream. Further studies will include various electrolyte compositions, simultaneous flue gas - NO/N_2 gas mixtures, and perovskite instead of gold as the working electrode.

Table 1

Effluent Analysis Results

Condition-Gas	NO Conc. In	NO Conc. Out	NO_2 Conc. In	NO_2 Conc. Out
N_2 with NO	830ppm	220ppm	2ppm	2ppm
N_2-NO with Air	650ppm	255ppm	2ppm	3ppm
N_2-NO with Air and with applied current	650ppm	240ppm	2ppm	11ppm

Steady State Polarizations:

Results were obtained by applying current to the cell set-up and recording the steady state potentials obtained during the current application; the currents were generated by a PAR 271 Galvanostat/Potentiostat in the Galvanostat mode. Data has been collected using both gold and perovskite as the working electrode in pure $K_2S_2O_7$ at various temperatures.

A comparison of data taken at 340°C for both perovskite and gold as the working electrode is shown in Table 2 and plotted in Figures 1 and 2. These data are very similar and also symmetric with respect to polarity. During actual testing, however, more stability in potential was found with the perovskite electrodes than with the gold. Table 3 shows polarization data for the cell system under the influence of gas flow. This data compares favorably with the data without flow and also shows that the presence of NO has no significant effect on the polarization.

Figures 3 and 4 show Tafel plots concerning the linearity of the data for N_2 and N_2/NO flow. These graphs indicate the accuracy of the data and again show the addition of NO has no effect on steady-state potentials. Further testing using perovskite electrodes under gas flow and with various electrolytes are currently being conducted.

Table 2

Steady State Polarization Data- No Gas Flow

Current	Ec-a-Perovskite	Ec-a-Gold
100 μ A	-	0.43V
500 μ A	-	0.56V
1mA	0.65V	0.59V
5mA	0.76V	0.79V
10mA	0.95V	0.96V
20mA	1.08V	-
25mA	1.13V	-

Table 3

Steady State Polarization Data - with Gas Flow & Gold Electrode

Current	Ec-a (N_2 Flow)	Ec-a (N_2/NO Flow)
10 μ A	-0.13V	-0.34V
50 μ A	-0.41V	-0.45V
100 μ A	-0.45V	-0.49V
500 μ A	-0.54V	-0.57V
1mA	-0.59V	-0.64V
5mA	-0.75V	-0.81V
10mA	-0.92V	-1.01V

Figure 1 Current-Potential Relationships for Perovskite Electrode Without Flow

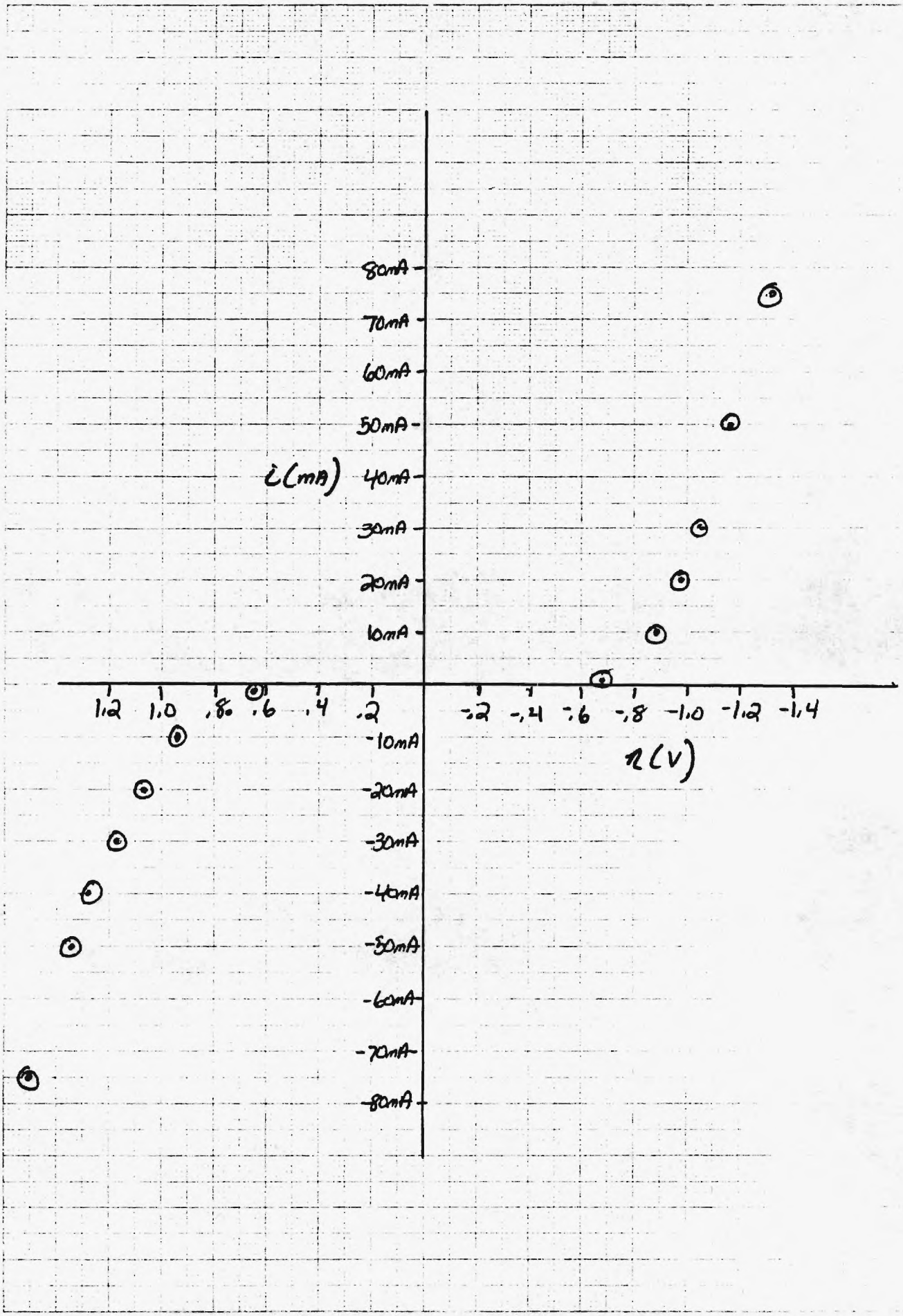

Figure 2 Current-Potential Relationships For Gold Electrode Without Flow

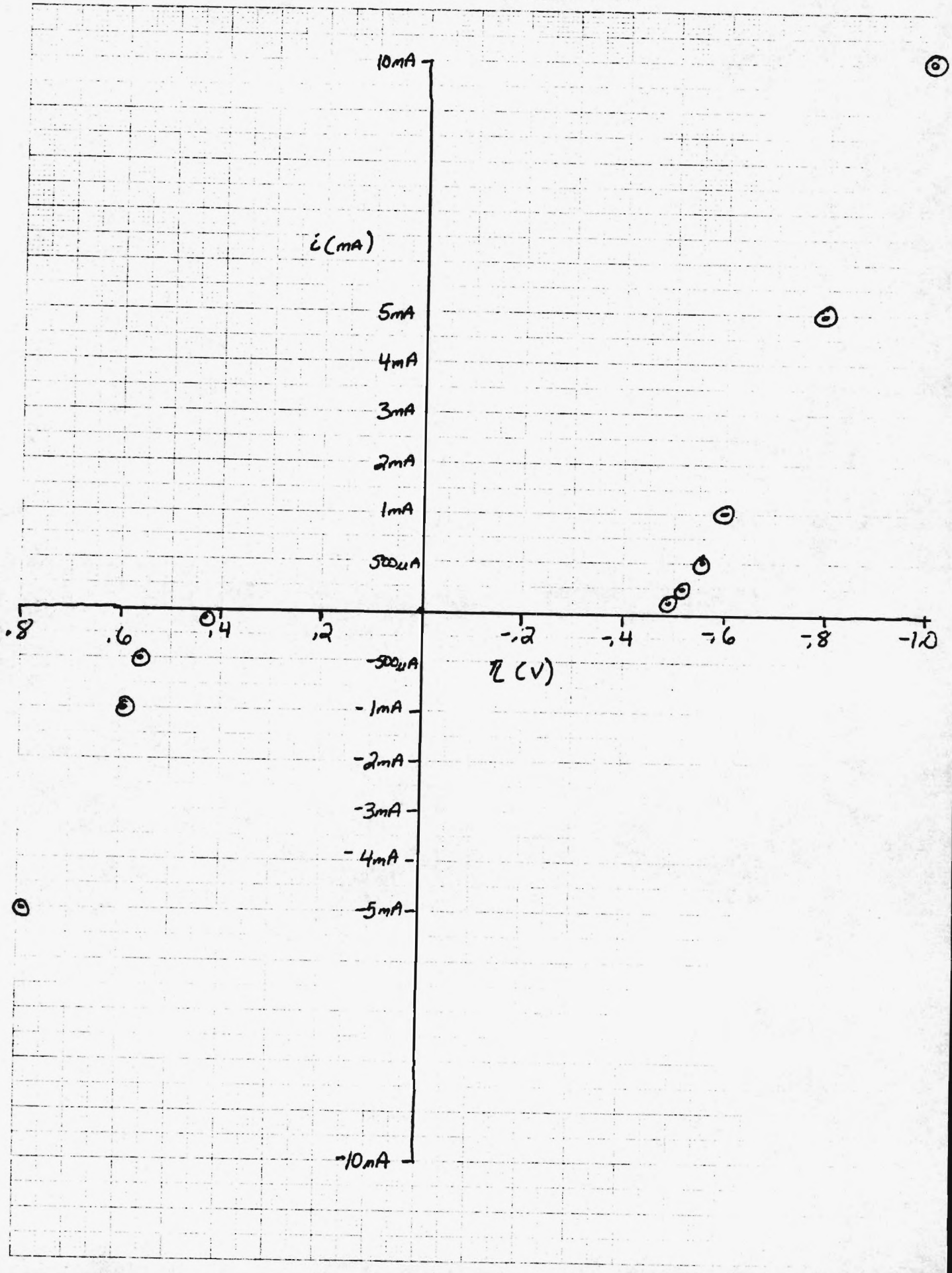

FIGURE 3: Polarization Results: Gold Electrode

No Flow

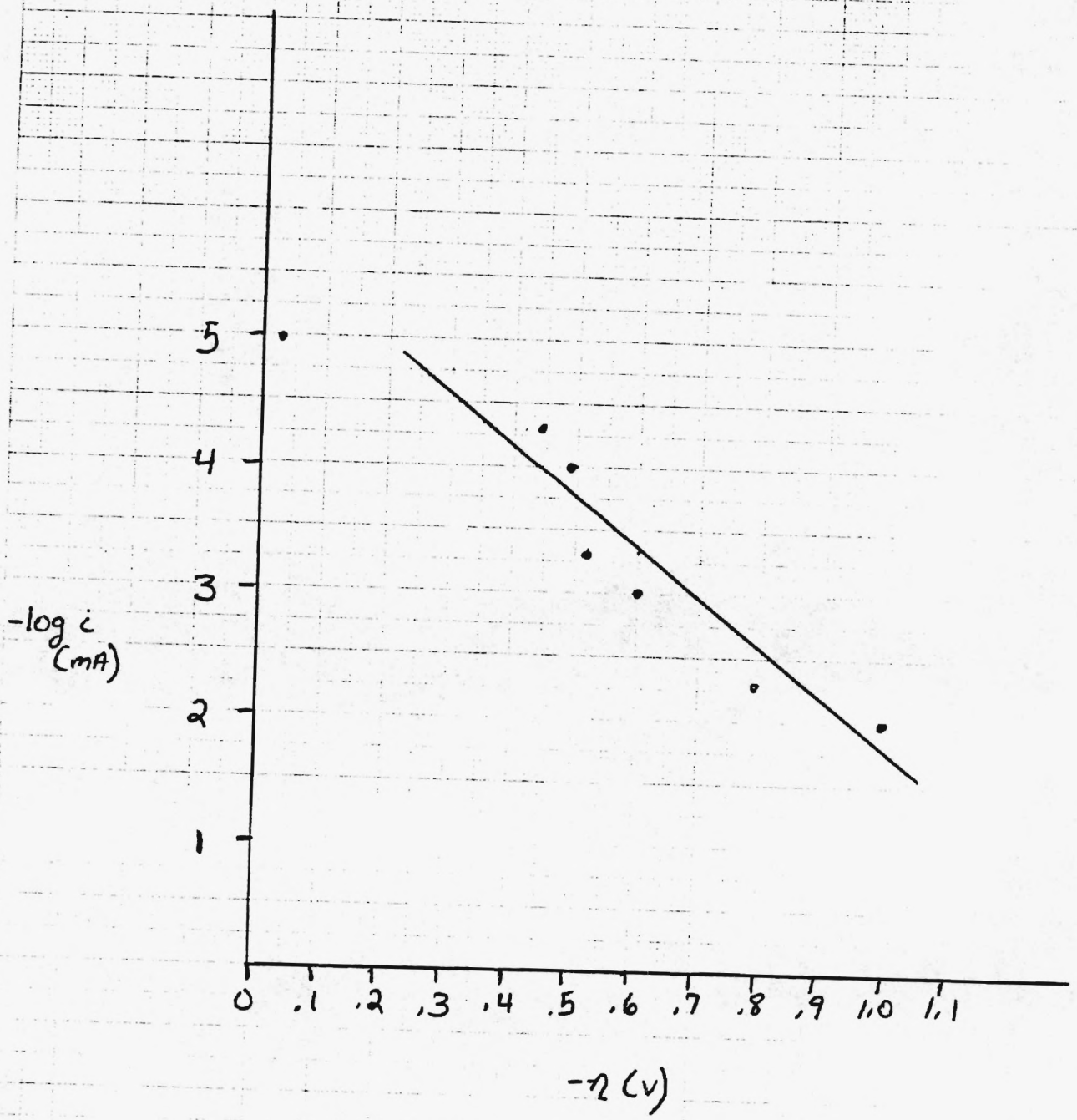

FIGURE 4 Polarization Results - Gold Electrode

N_2 Gas Flow

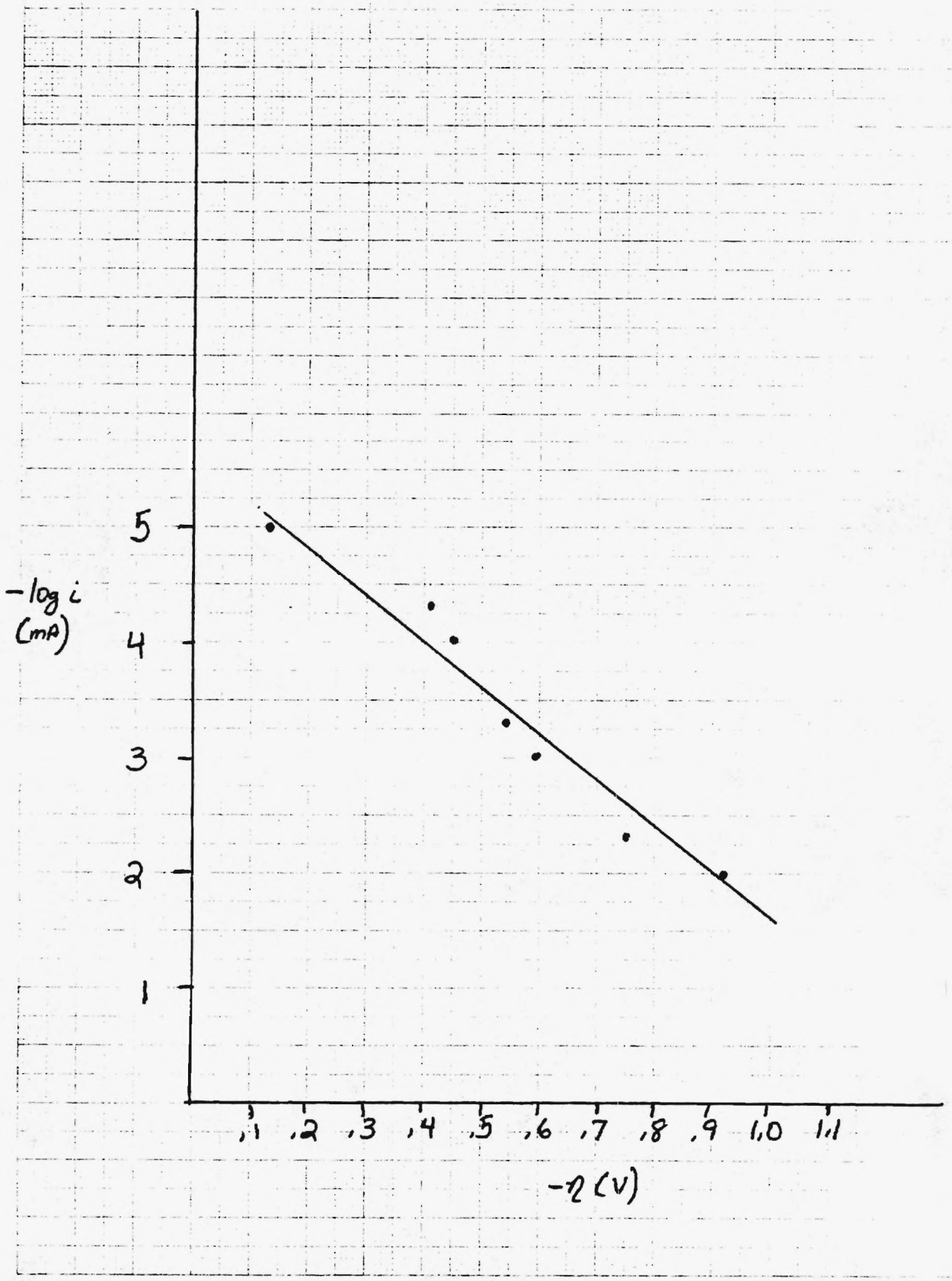

Perovskite Preparation:

The standard cathode used previously in molten carbonate fuel cells is porous NiO formed from sintered Ni powder and reinforced with Ni screen. Many problems with NiO including long-time stability problems have caused the search for alternative electrode materials. New materials must meet several general criteria such as:

1) Extended stability in the cell environment.

2) Electronically conductive at operating temperatures.

3) Low cost and sample preparation times.

In our work, we have looked at the perovskite type compounds $Ln_{(1-x)}M_xM'O_3$ (Ln = lanthanoid element, M = alkaline earth element, M' = transition metal element) which have been found to be satisfactory in both polarization characteristics and stability testing under actual working conditions as oxygen electrode materials.

Most of the work has been concentrated on the material $La._8Sr._2CoO_3$ due to its stability and ease in preparation. However, some recent testing has been completed with varying La and Sr compositions along with the substitution of Nd for La.

The preparation of the perovskite electrodes was modified from procedures developed by Kudo and Yoshiba. After obtaining the desired molar ratios of the various acetates containing the desired products, the acetates were dry mixed by rolling for a period of 6-8 hours and then heated slowly at temperatures below 300°C until decomposition (a period of 3-4 hours).

The decomposed product was then ground into a fine powder, and this powder sintered at 1100°C for twenty-four hours. After this period of time, 5% methyl cellulose (by weight) was added to the powder and mixed thoroughly. The powder was then cold-pressed into 1/4" diameter pellets at pressures between 8,000 and 10,000 psig. The samples were then re-sintered at 1100°C for twenty-four hours and then used for testing in the cell environment.

Preliminary testing has found the perovskite samples to hold up quite well during addition to the cell environment with no serious problems encountered. Steady-state polarization testing has found the perovskite to withstand more current than planar gold electrode used previously in the cell environment.

In order to study the perovskite structure in more detail, pictures of various samples were taken with a Scanning Electron Microscope (SEM). These pictures showed no real noticeable structural differences between perovskites with varying compositions of La, but did show the importance of sintering the samples containing methyl cellulose. The sintering process was effective in obtaining needed sample porosity and also to smooth the internal structure leading to more effective use as a possible electrode. Included are pictures of sintered and unsintered samples taken at the same magnification.

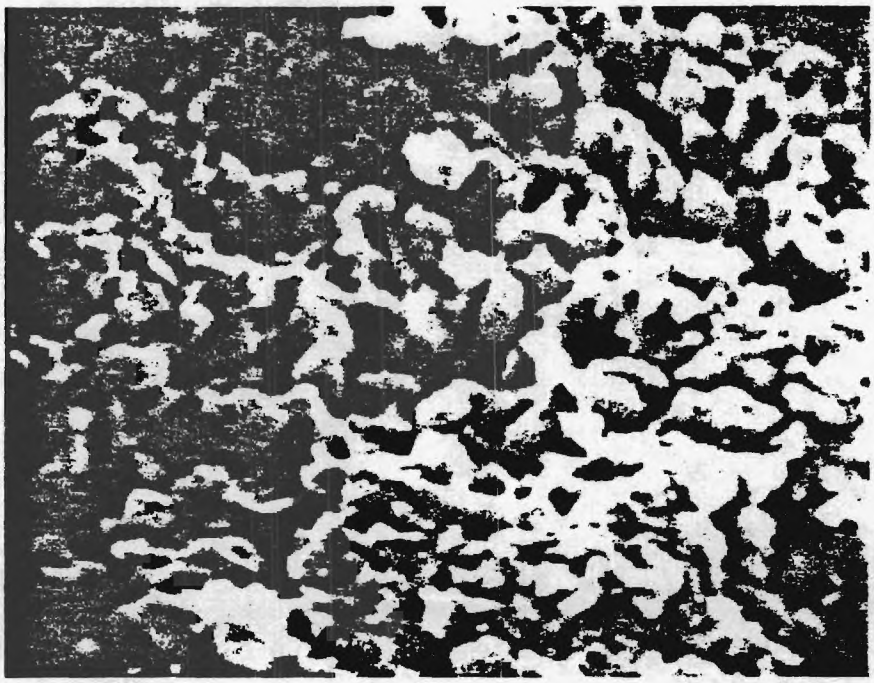

FIGURE # 5 $La_{.7}\ Sr_{.3}\ CoO_3$ - (UNSINTERED) 45° 10,000 X
+ 5% Methyl Cellulose

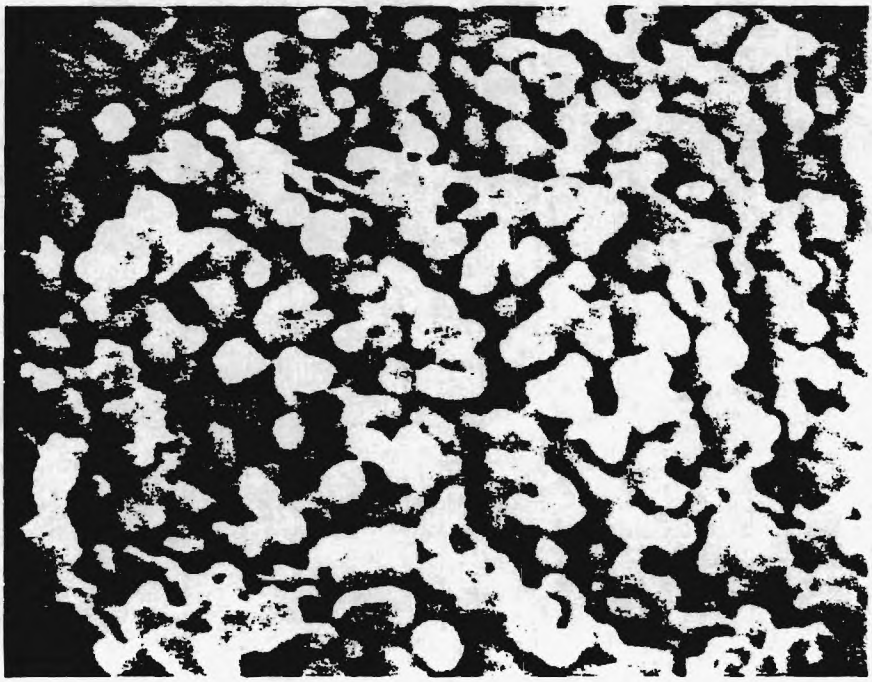

FIGURE # 6 $La_{.7}\ Sr_{.3}\ CoO_3$ - (SINTERED) 45°, 10,000 X

Cyclic Voltammetry:

Cyclic voltammetry is a process in which the potential is swept with time and the resultant current recorded on a storage oscilloscope. Earlier testing in this manner had produced some interesting results but encountered some major problem thought to be due to uncompensated solution resistance. The acquisition of a new PAR 273 Potentiostat/Galvanostat has eliminated this problem with its capability to provide IR compensation. In fact, testing has shown that uncompensated solution resistance can affect both the magnitude and location of the major peak current.

Table 4 and Figure 7 show some data taken with the new instrument in pure $K_2S_2O_7$ at 340°C with no gas flow and with gas at the working electrode. These data, particularly the peak voltages, are quite different from earlier data taken with uncompensated solution resistance. The actual amount of solution resistance was determined from current interruption. This value has been found to be approximately 1.5 Ω , a value well within operational limits of the potentiostat.

Figure 8 contains a plot of the current function, $i_p/\sqrt{\nu}$, for the anodic current versus the scan rate. On the basis of these results and the amount of shift in potential with scan rate, it appears that an irreversible charge transfer occurs within the electrolyte during the potential sweep. This conclusion is based upon results presented by Nicholson and Shain and also upon equations from Bard and Faulkner.

Figure 9 shows actual oscilloscope outputs as taken with a Polaroid camera. Due to the nature of the signal this is the most accurate means of measuring current output.

Work is continuing with different electrodes and various electrolytes to check the validity of the results obtained thus far and to help choose the best possible candidate materials. It is hoped that more work will help determine whether or not there is irreversible charge transfer taking place during the potential sweep.

Table 4

Cyclic Voltammetry Data

Pure $K_2S_2O_7$ - Anoidic Direction First

ν(V/s)	ν1/2(V/s)	Epa(V)	Ipa(MA)
0.1	0.316	0.06	55
0.2	0.447	0.10	60
0.25	0.5	0.14	65
0.5	0.707	0.21	80
0.75	0.866	0.29	100
1.0	1.00	0.37	120

Figure 7 : Dependence of Current with Scan Rate

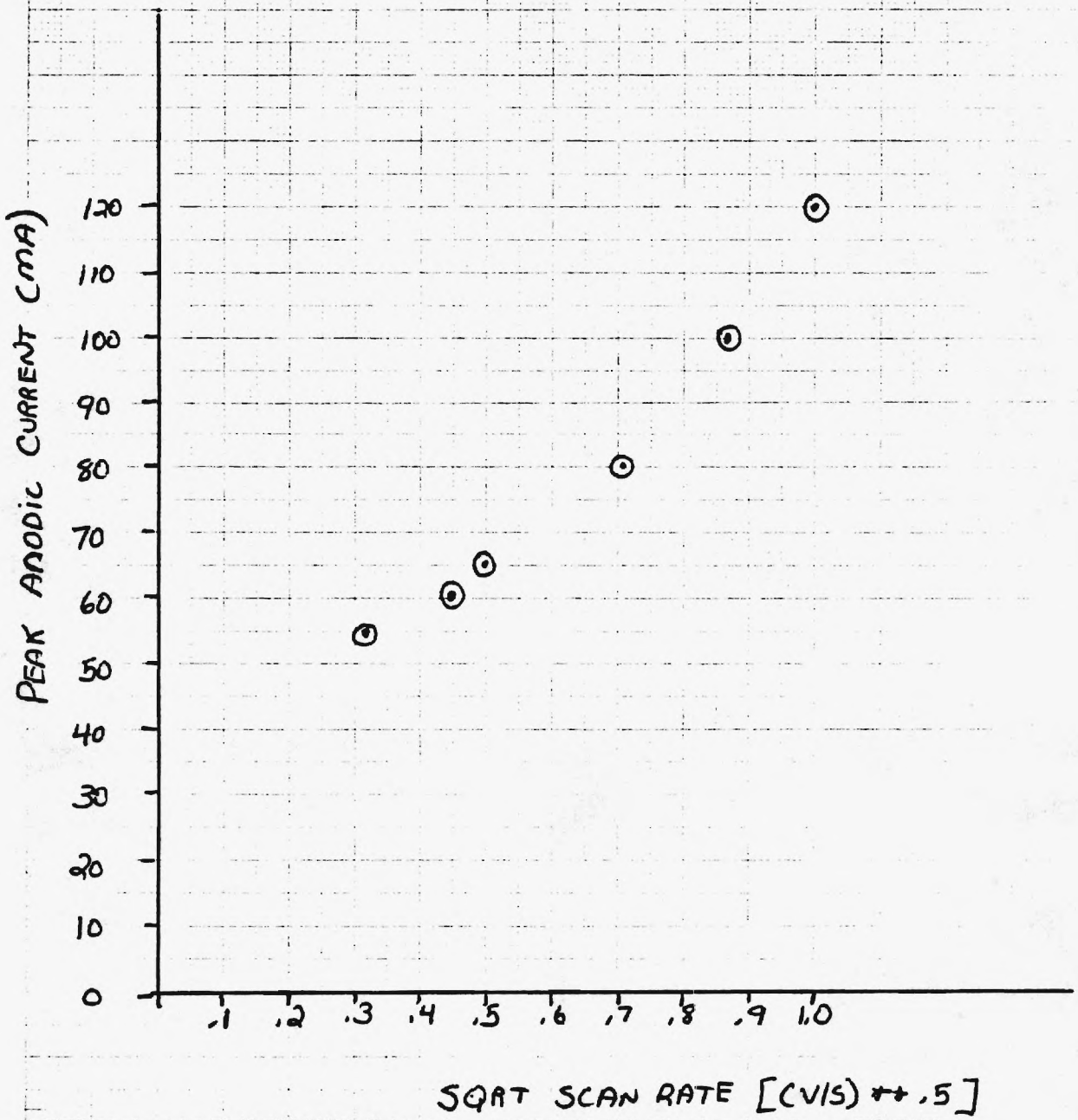

FIGURE 8 DETERMINATION of System Behavior Using Current Funct

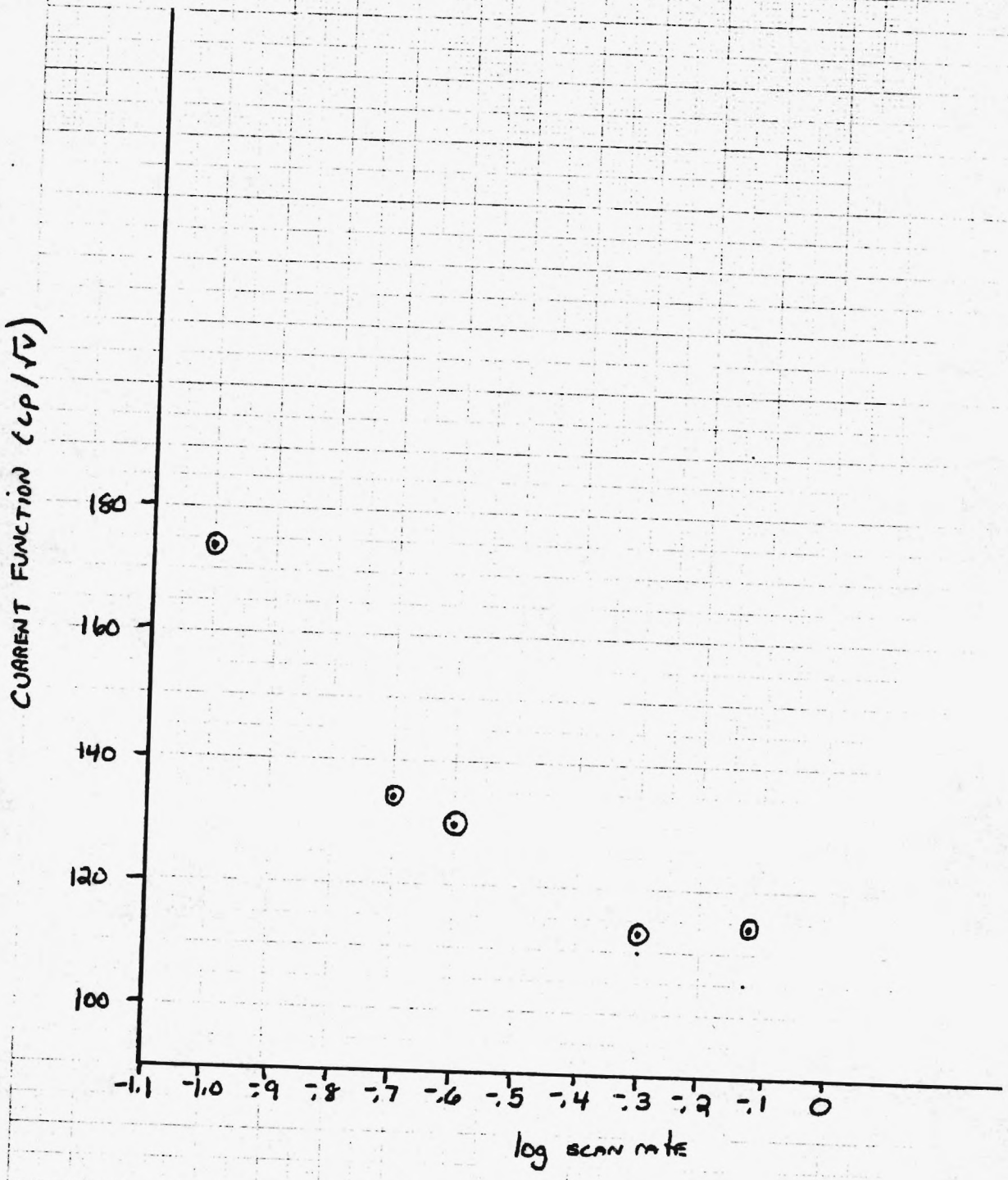

Figure 9 : Cyclic Voltammograms at Varying Scan Rate

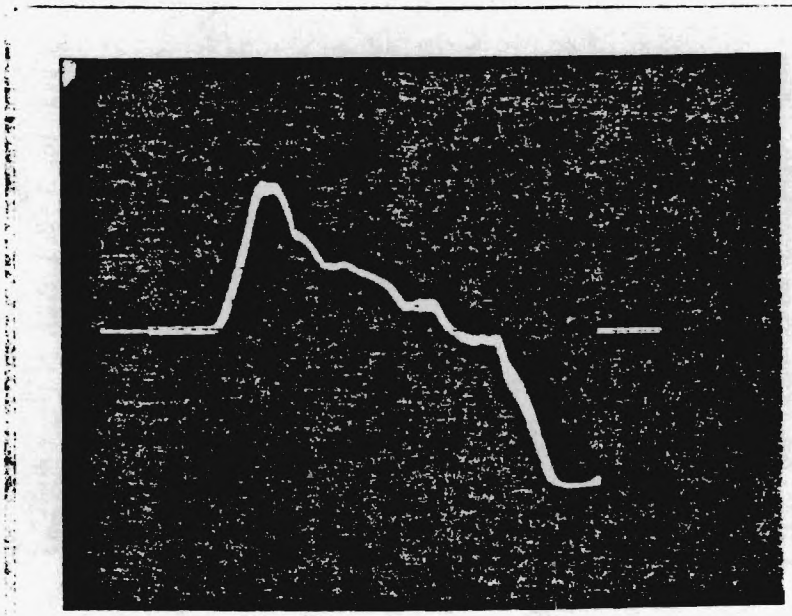

← Current Vs Time

Scan Rate : 1 V/sec
.5 V/Div
(y-axis)

Eq = 1.1 V

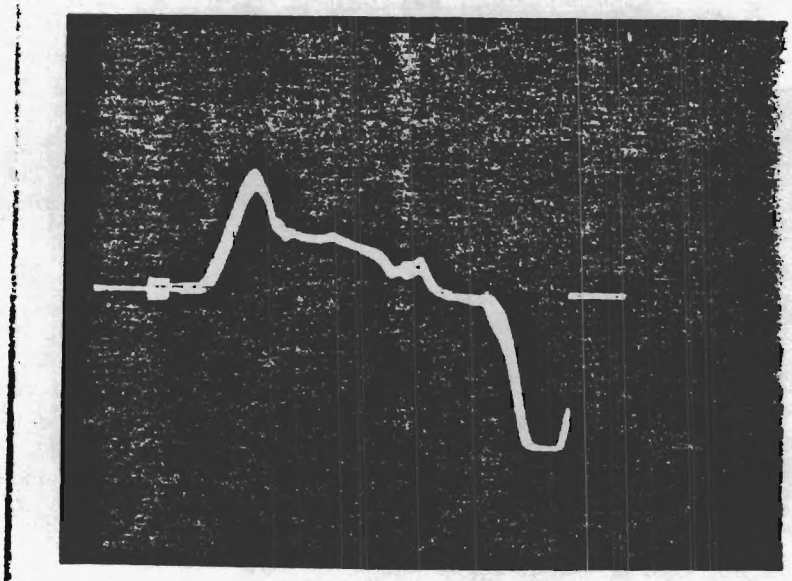

Scan Rate : .5 V/sec
.5 V/Div

Eq = 1.2 V

II. FULL CELL

Apparatus:

The bench-scale model of the flue gas desulfurization apparatus has been built. The apparatus basically consists of cylinders of simulated flue gas, anode gas (N_2), and various diluting gases, a Matheson multichannel gas-flow controller, and rotameters to monitor the inlet and outlet flow rates of the anode and cathode. Ports on the panel are provided for gas sampling.

The electronic instrumentation consists of a PAR model 371 Potentiostat/Galvanostat, Hewlett Packard 3310B function generator, Tektronix Model 5111 Storage Oscilloscope and Simpson Model 460 multimeters. All connections to the cell are made through the electronic board on the main panel.

The furnace is custom made with Lindbergh ceramic heating plates and fiber glass insulation. A pneumatic cylinder provides the force (~5psi) to hold the cell housings together within the furnace.

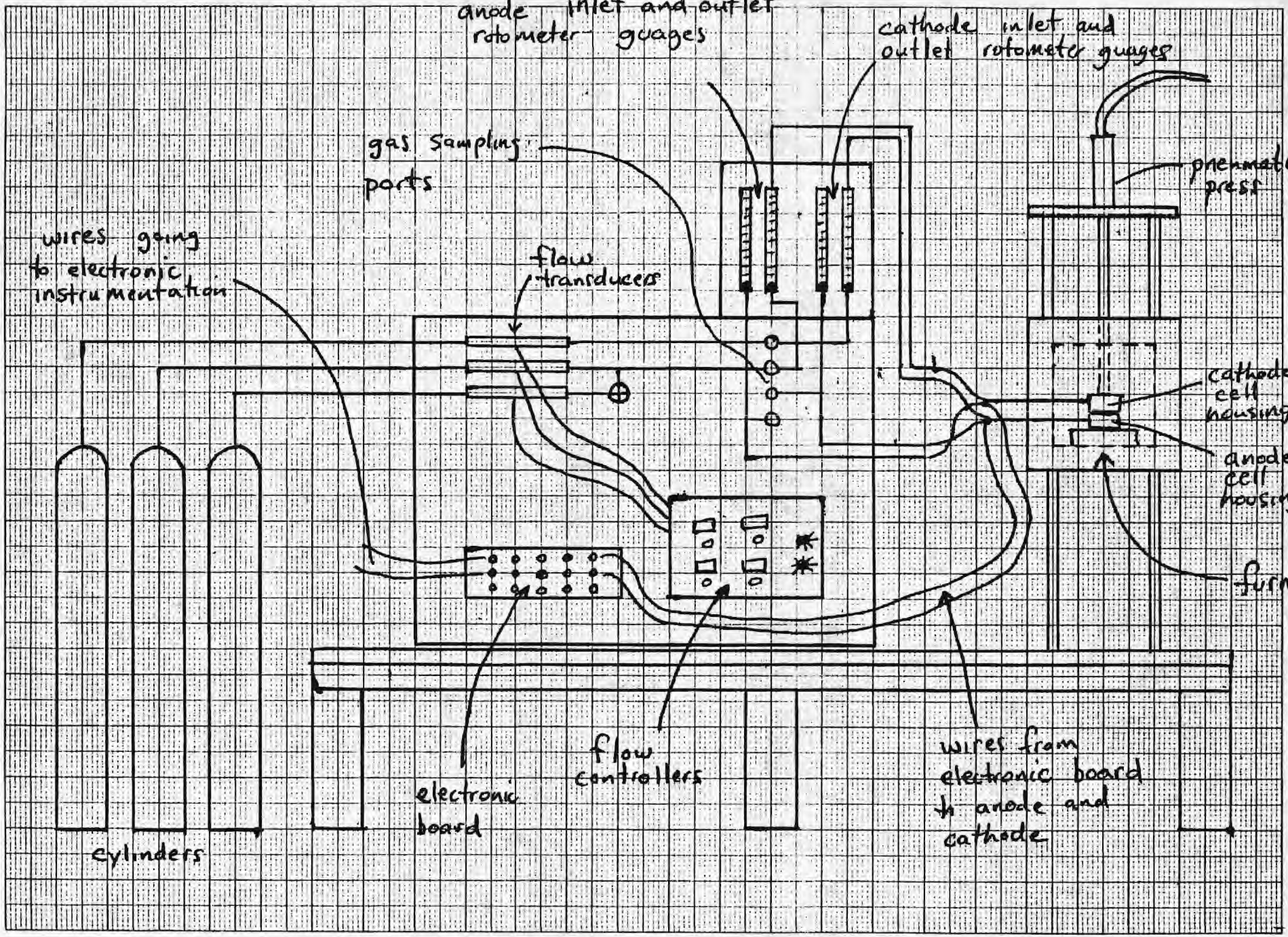

Electrodes:

The electrodes used thus far have been of the perovskite type ($La._8Sr._2CoO_3$). These electrodes have performed quite well. Their stability under the operating conditions is very good and their conductivity remains high after operation. The method used to produce the perovskite is as follows:

1. Weigh out stoichiometric quantities of lanthanum strontium and cobalt acetates.
2. Mix on tumbler for at least 2 hours.
3. Bake at 150°C for 1 hour.
4. Bake at 200°C for 1 hour.
5. Bake at 240°C for 1 hour.
6. Bake at 275°C for 1 hour.
7. Cool slowly.
8. Grind with mortar and pestal to a fine powder.
9. Sinter at 1100°C overnight.
10. Cool slowly.
11. Grind with mortar and pestle.
12. Add 5.0 weight % methyl cellulose.
13. Ball mill for 10 hours.
14. Place 2.8g of perovskite in electrode die (this gives ~1mm thick electrode).
15. Press at 10,000 lb pressure in die.
16. Sinter at 500°C for 1 hour.
17. Sinter at 800°C for 1 hour.
18. Sinter at 1100°C for overnight.
19. Cool slowly.

Electrolyte Membrane:

1.Zirconia felt as matrix

The high thermal stability (>2200^{o}C) and the ability of the zirconia felt to absorb high quantities of liquid made this material a candidate for the matrix material. A number of electrolyte impregnation procedures were tested on the felt but none were successful.

The major problems encountered with the zirconia felt stemmed from insufficient capillary forces to hold the electrolyte in the matrix. When the membrane was incorporated into the cell this led to electrode flooding and a partial drying of membrane which led to low conductivities.

A more dense zirconia felt, one with a higher density of zirconia fibers would help to enhance the capillary forces and perform better; but even under these circumstances zirconia felt may not be capable of performing its required duties.

2. Silicon carbide as matrix

Silicon carbide is both thermally and chemically stable and has been used previously as a matrix material for electrolyte membranes. The major problem encountered with the silicon carbide matrix was similar to the zirconia felt above, in that the capillary forces exerted by the silicon carbide on the $K_2S_2O_7$ with 1% V_2O_5 electrolyte were insufficient to hold the electrolyte in place. The result was problems with partial drying of the membrane and flooding of the electrodes.

The reason the silicon carbide matrix was unable to exert adequate capillary forces appears to be due to the particle size. Approximately 200 mesh silicon carbide was used in the experiments and the results indicate a smaller particle size is required. As the mesh size increases (particle size decreases), the surface area to volume ratio increases drastically. Since it is the surface forces between the matrix and electrolyte which hold the electrolyte stationary, as the mesh size increases so will the capillary forces.

Future experimentation will examine and evaluate electrolyte membrane manufacture utilizing silicon carbide of much higher mesh sizes. The silicon carbide should be of particle size of at least 1000 mesh.

3. Strontium titanate as matrix

Strontium titanate has also been used as the matrix in the production of commercial tiles and shows promise for the matrix material in this work.

The strontium titanate used is of an extremely small particle size. Various methods of manufacturing the membrane were used and are listed below:

a) mixing a 50-50 weight percent mixture of the powders (electrolyte and matrix) and cold pressing at 10,000 psi.

b) mixing a 50-50 weight percent powder mixture and hot pressing at 320^{o}C (M.p. ~ 280^{o}C).

c) pressing matrix only at various pressures and sintering, then impregnating with electrolyte.

Matrix (c) worked poorly due to a very fragile matrix structure and difficulty in dispersing the electrolyte evenly through the strontium titanate matrix. Method (a) and (b) both gave similar results; neither has been successful as of yet but both have promise. The major problem encountered with the hot and cold pressing procedures is a low membrane conductivity in the cell. Density analyses have revealed the membranes have been in the neighborhood of 40% porosity, and this is the root of the problem. The porosity comes from very small air pockets dispersed throughout the membrane. In order for the membrane to be effective during cell operation, the electrolyte must provide a continuous pathway for the current-promoted diffusion of sulfur anions from the cathode to the anode. Microscopic air pockets dispersed within the membrane break up the continuous pathway and what is observed is a very high resistance across the cell.

At this time we are in the process of building a vacuum chamber which can be incorporated into the hydraulic press. The membrane die will then be under a vacuum during the pressing (either hot or cold pressing) of the electrolyte - matrix mixture. This should greatly improve the membrane density and reduce the amount of microscopic air pockets within the ceramic membrane.

X-ray diffraction studies have been performed on the membrane and its components under various conditions to determine whether the strontium titianate matrix is reacting with the electrolyte. Pattern #1 shows the diffraction trace of pure

strontium titanate and #2 shows the diffraction pattern of potassium pyrosulfate with 1% vanadia. The third pattern is simply a 50-50 weight percent mixture of strontium titanate and potassium pyrosulfate with 1% vanadia. The diffraction pattern of the mixture is virtually identical to the combination of the two separate component diffraction patterns. The fourth diffraction pattern is again a 50-50 weight percent mixture of matrix and electrolyte but this time it was pressed under 10,000 pounds of pressure and baked at 350°C for 3 hours, then pulverized to a fine powder after cooling. This pattern is very different from #3 suggesting a reaction between the components. Trace #4 again shows all the strontium titanate peaks as in #3 but they are all approximately 30% smaller than in #3.

In diffraction trace #4 the unknown peaks arriving from the apparent reaction between the matrix and electrolyte are at 26.5°C, 27.0°C and 28.6°C tilt angles and smaller peaks arose at 20.6°C, 42.0°C and 47.7°C tilt. Although these new peaks did not clearly indicate what was being formed, it is likely a potassium strontium sulfate is the main product.

The last diffraction pattern is of the electrolyte, as in pattern #2, but this time was melted at 325°C and then pulverized. This pattern is identical to pattern #2 and assures us that no reaction is taking place between the electrolyte components.

Although the x-ray diffraction results indicate strontium titanate may be an inappropriate matrix material because of the reaction, commercial membranes are produced which have the same

problems between the matrix and electrolyte. In these processes a "new" matrix material, the reaction product of the original matrix and electrolyte, is used. Currently, we are experimenting with this idea. Initially we start with the previous 50-50 weight percent mixture, press it and bake it overnight at 325°C. This membrane is then pulverized and a small sample is withdrawn for experimentation. The rest is then mixed with a small quantity of additional electrolyte (99% $K_2S_2O_7$, 1% V_2O_5), 10-20 weight percent, mixed thoroughly, repressed and sintered at 325°C overnight. This process is continued until a stable material (the reaction product of the matrix and electrolyte) is observed by x-ray diffraction. At a point, these small additions of electrolyte will no longer react and a mixture of the "new" matrix and electrolyte will be the final product.

SO_2 Removal:

Open circuit removal rates using silicon carbide as the electrolyte-tile matrix have been found to be:

gas analyzed	ppm SO_2
cathode in	3000
cathode out	2840
anode in	0
anode out	160

All flow rates were approximately 60ml/min and the overall removal from the above numbers at steady state was approximately 5% of the entering SO_2. The gas analysis was done on an HP 5840 gas chromatagraph with a flame photometric detector.

electrodes: perovskite

electrolyte: $K_2S_2O_7$ with 1% V_2O_5

matrix: SiC (200 mesh)

No current was able to be passed due to the high membrane resistance.

COMBINED NO_x/SO_x CONTROL FROM FLUE GAS USING AN ELECTROCHEMICAL MEMBRANE CONCENTRATOR

Six Month Progress Report for Grant DE-FG22-84PC73226

B&R No.: AA0505

B&R Class: Flue Gas Cleanup

T.P.O.: Richard Walker

Principal Investigator: J. Winnick

Georgia Institute of Technology

February 1986

Report No. PC-73226-3

LIST OF FIGURES

SUMMARY

During the last forty years, the increased use of coal as the prime source of energy has dramatically increased the emissions of SO_2 and NO_x into the atmosphere. These gases are often absorbed into the atmosphere resulting in the formation of acids which are deposited onto the earth by the process known as acid rain. The majority of the acid is created from the SO_2/NO_x emissions from power plants. Unfortunately, the major methods used for the removal of these harmful contaminant gases are not always cost-effective or result in the production of troublesome waste sludges. The current investigation examines an alternative process in which the contaminant gases are removed and concentrated in one continuous step without the production of any waste sludge. This method utilizes a molten-salt electrochemical cell which requires electricity instead of chemical reagents.

Previous work utilizing the principles of such a device has been found to successfully remove sulfur dioxide from flue gas but at an operating temperature too high ($T > 500^{o}$ C) for practical industrial application. Other work was conducted on the finding of candidate electrolyte materials suitable for lower temperature operation. In the present work, these electrolytes along with other potential candidates were tested for cell operation to remove not only SO_2 but also nitrogen oxide gases from simulated flue

CHAPTER I

INTRODUCTION

Throughout the development of our society, coal has been used as a prime source of energy in both industrial and home type of environments. Although coal has been an abundant, inexpensive solution to many of our nation's energy problems, the burning of coal produces the emission of gases such as sulfur dioxide and nitrogen oxide into the atmosphere. These emissions often result in considerable damage to the land environment and pose a serious threat to the health and safety of human life.

In the past fifty years, the steadily increasing use of fossil fuels as an energy source has dramatically increased the emissions of sulfur dioxides and nitrogen oxides. These gases are converted into acids upon absorption into cloud water and raindrops, and then deposited in significant quantities on land and water surfaces. One end result is that average pH values of 4 to 5 are now seen in many lakes and streams in parts of Canada and the eastern half of the United States [1]. This phenomena, known as acid rain, has been shown to have many damaging characteristics such as damage to reproductive and feeding habits of fresh water fish, resulting in potential

harm to the natural food chain [2]. There have also been reports concerning the corrosion and leaching of many land areas severely curtailing the productivity of the soil.

Recent figures indicate that sixty to seventy percent of the acidity present in the atmosphere is caused by sulfuric acid with the balance coming from nitric acid [2]. Major sources for both NO_x and SO_2 pollution include coal and oil combustion with mobile sources such as car exhausts contributing more heavily to the nitrogen oxide emissions. The actual emmision concentrations can depend on the type of coal being burnt with a typical flue analysis of 0.3% SO_2, 3% O_2, 10% H_2O, 15% CO_2, and a nitrogen balance being produced from the combustion of 3.5% sulfur coal. In addition, the nitrogen oxide emissions from the steam boiler of a power plant can reach 500 to 1000 ppm, with ninety percent or more being NO and the balance NO_2 [1]. Since the effects of acid rain are irreversible, the emissions must be controlled at the source. Although coal desulfurization is important, SO_2 and NO_x control is needed to help stop the long-range dispersion of these dangerous gases.

It has been popular in the past to confront the problems of sulfur dioxide and nitrogen oxide contol on an individual basis. Due to the increasing costs of the removal techniques, the emphasis today is being shifted to combine the separate removal technologies in an effort to

the sulfur dioxide concentrations are much larger, making the isolation and removal of the NO_x gases very difficult. There are also major waste disposal problems when adsorption or absorption techniques are used. Methods such as catalytic reduction, catalytic decomposition, and absorption may provide some limited means for the reduction of the flue gas NO_x emissions. The limited reactivity of nitrogen oxides and the large quantities of gas to be treated, however, places tough restrictions on the overall flue-gas cleaning process [1].

Studies on simultaneous NO_x/SO_2 removal have been conducted since the early 1970's by many different groups. Shell has demonstrated simultaneous removal using CuO on Al_2O_3 with ammonia as a reductant. In this process, the CuO is converted to sulfate and must be regenerated with hydrogen [4]. Some recent work has produced a design where the sulfur dioxide is first treated by dry FGD and the nitrogen oxides subsequently removed by a downstream Electron beam (E-beam process). This method has produced high efficiency 90% SO_x removal and 90% NO_x removal for high sulfur fuels but is hampered by projected capital costs of over $260/kw [5].

Electrochemical technology for gas separation has been used to remove trace amounts of contaminant gases and to concentrate them into a by-product stream. An electrochemical driving force produces a net-transfer of

capabilities by cell stacking, and favorable economic comparsions to existing processes. It is also believed that this device can be adapted for both NO_x removal and simultaneous NO_x/SO_x removal without any major operational changes. The cell will be described in some detail later in this thesis and it will be shown that a reduction in operating temperature is crucial for future commercialization. Previous work [8] has produced candidate electrolyte and electrode materials which may be suitable for the operation of a lower temperature device. The emphasis of this investigation is to conduct fundamental bench-scale tests on these and other candidate materials to determine their capacity for simultaneous NO_x/SO_x removal and the feasibility of operation for the proposed device.

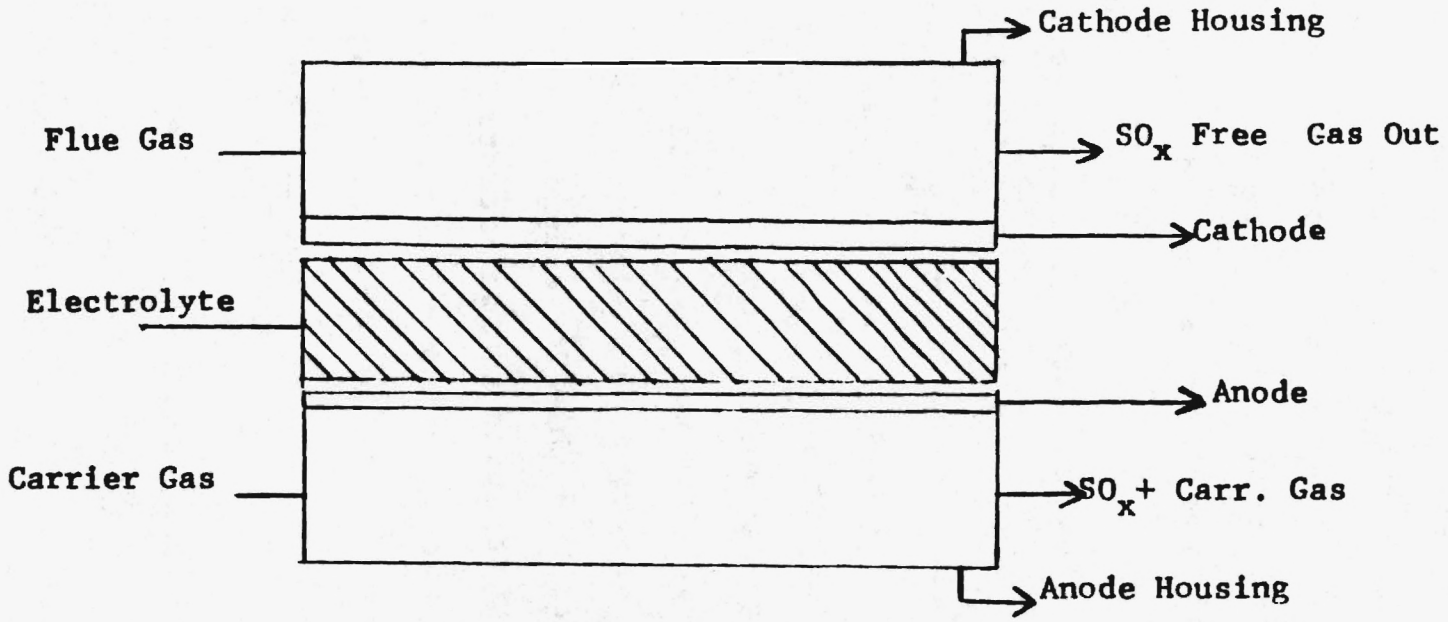

Figure 2.1. Flue Gas Desulfurization Device Schematic

was accomplished, the melting point of the sulfate eutectic sets a lower limit on the posible operating temperature at 512 ^{o}C. The high operating temperature is incompatable with direct application to conventional power plants. The effluent from a traditional power plant leaves the economizer at 250-330^{o}C [13]. The use of this sulfate eutectic would require the use of a preheater to heat the exiting gases. The cost of such a preheater and the potential damage to cell components in terms of corrosion hastened the search for a new electrolyte with melting point between the exiting temperature range.

Scott [14] examined the kinetics of sulfur dioxide reactions in a molten potassium pyrosulfate eutectic (m.p. = 320-350^{o}). The overall cathodic reaction was found to be

$$2S_2O_7^{2-} + 2e = 2SO_4^{2-} + 2SO_2 + O_2^{2-} \qquad (2.1)$$

This reaction provided the means of sulfur dioxide removal at the cathode. Without a catalyst, however, the conversion of SO_2 to SO_3 though thermodynamically favored is extremely slow. Upon the addition of a catalyst, vanadium pentoxide, in small volume quantities, removal of incoming SO_2 and any generated SO_2 was observed. The presence of the catalyst produces an overall net reaction

Scott [8] also examined the perovskite type compounds, $Ln_{1-x}M_xM'O_3$ (Ln=Lanthanoid element, M=Alkaline Earth element, M'=Transition Metal element), as candidate electrode materials. The perovskite materials appear to be viable candidates since they are inexpensive, easy to prepare, and exhibit many of the characteristics needed for electrodes in the proposed device. Perovskites have high electrical conductivity and possess a high electrocatalytic activity rivaling that of platinum [16]. Perovskites are also chemically inert and thermally stable under varying temperature conditions [17]. Finally, the perovskites have shown to be satisfactory in both polarization and stability studies under actual working conditions as electode materials [18].

The use of perovskites as electrodes has not been studied in a molten salt environment as would be present in the proposed device, therefore this investigation will look at fundamental parameters of perovskites under simulated cell conditions. The behavior of the electrodes in SO_2, NO, and NO_x/SO_x removal studies will be monitored and evaluated in comparison to other inert planar electrodes such as gold foil.

Fundamental test cell experiments are necessary to further test the feasibility of the proposed electrolyte candidates. It is also important to study the possibility

CHAPTER III

THEORY

In this chapter, the theory behind each major type of experiment used in this study will be examined. The first part will describe the basic electrochemical cell and outline its detail by showing electrical circuit elements. Next, the theory involved in steady-state polarization techniques for obtaining limiting current data used to give information about the electrode and electrolyte activity will be discussed. The third section will detail cyclic voltammetry in which the current is monitored during potential scans giving rise to possible kinetic and mechanism information concerning the electrolyte and the gases under investigation. The last section will discuss the effluent analysis studies in which open-circuit and steady state conditons were examined in order to determine possible current/removal relationships for the contaminant gases under investigation.

Electrochemical Cell

During the course of this investigation, a standard three-electrode cell (Figure 3.1) was employed. The working electrode, either the anode or cathode, is the electrode at which the actual reactions are occuring. The reference

electrode is an electrode that approaches an ideal nonpolarizable electrode of known potential. The reference electrode may not always be a true thermodynamic electrode but provides a stable known potential. The third electrode known as the auxiliary or counter electrode is a source or sink for electrons so that current can pass through the cell. The counter can be virtually any desired electrode because its electrochemical properites do not affect the behavior of the electrode of interest.

Whenever the potential of an electrode of interest is measured against a nonpolarizable reference electrode during the passage of current, a voltage drop equal to iR_s will always be included in the measured potenial. The term R_s refers to the solution resistance between the electrodes which behaves as an ideal resistance over a varying range of conditions. This total resistance has two major components: the compensated resistance R_c and the uncompensated resistance R_u. By positioning the reference electrode close to the working electrode surface, the effect of the uncompensated resistance can be lessened but at any position other than exactly at the electrode surface this resistance can create possible errors in any potential measurements.

In the event of substantial current flow, even small values of R_u, such as one to ten ohms, can cause a large control error. This fact explains why large-scale

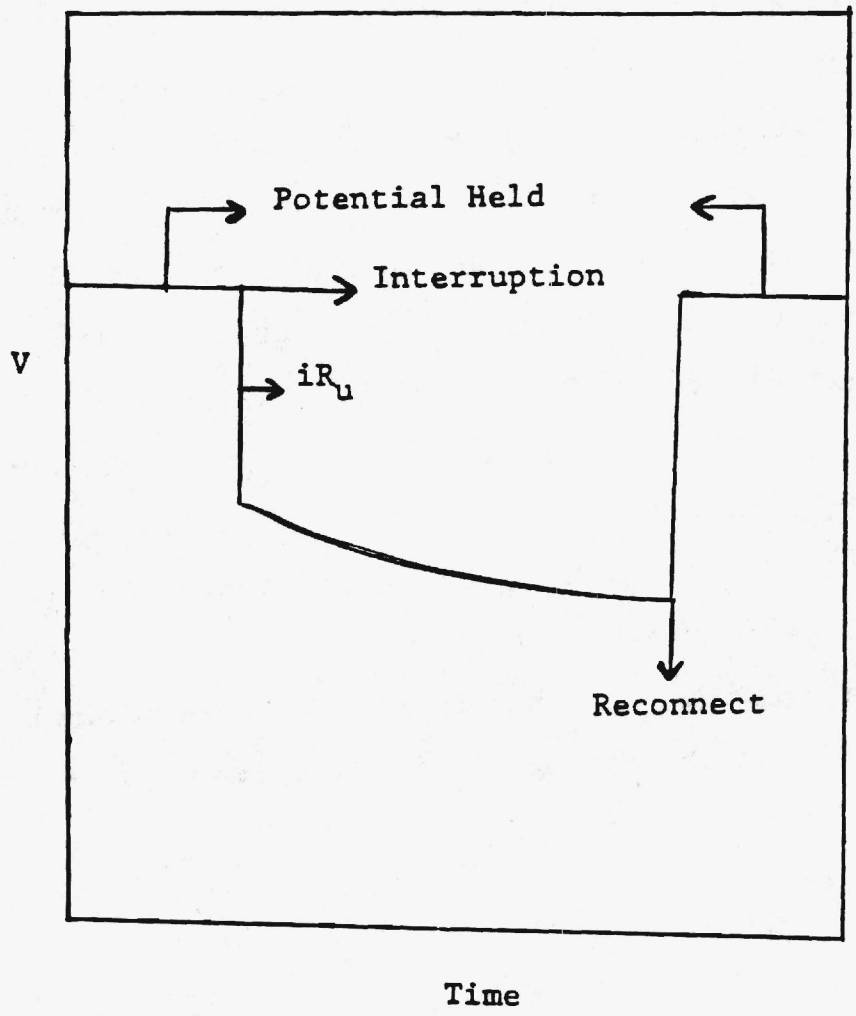

Figure 3.2. Current Interrupt Waveform

E, from the equilibrium value, E_{eq} :

$$\eta = E - E_{eq} \qquad (3.1)$$

The overpotential in an SO_2 concentrator cell contains contributions from mass transfer and the kinetics of the chemical and charge transfer reactions occuring inside the cell.

In basic electrochemical cells, the limiting current or current density can be estimated by monitoring current versus potential data. The limiting current is the largest current value realized despite the application of increasing potentials. This current limitation is usually a result of mass transfer limiations placed upon the system by cell design or the physical limitations of the electrodes. When the limiting current is flowing, the electrode process is occuring at the maximum possible rate for a given set of mass transfer conditions. This results from the oxidizing agent being reduced as quickly as it is being brought to the electrode surface [19].

In the course of steady-state polarization studies, it is often necessary to introduce various gas and electrolyte environments in order to look at the resulting limiting current values. Significant changes in the resulting current values can give indications of the species involved in the reaction schemes. For example, if

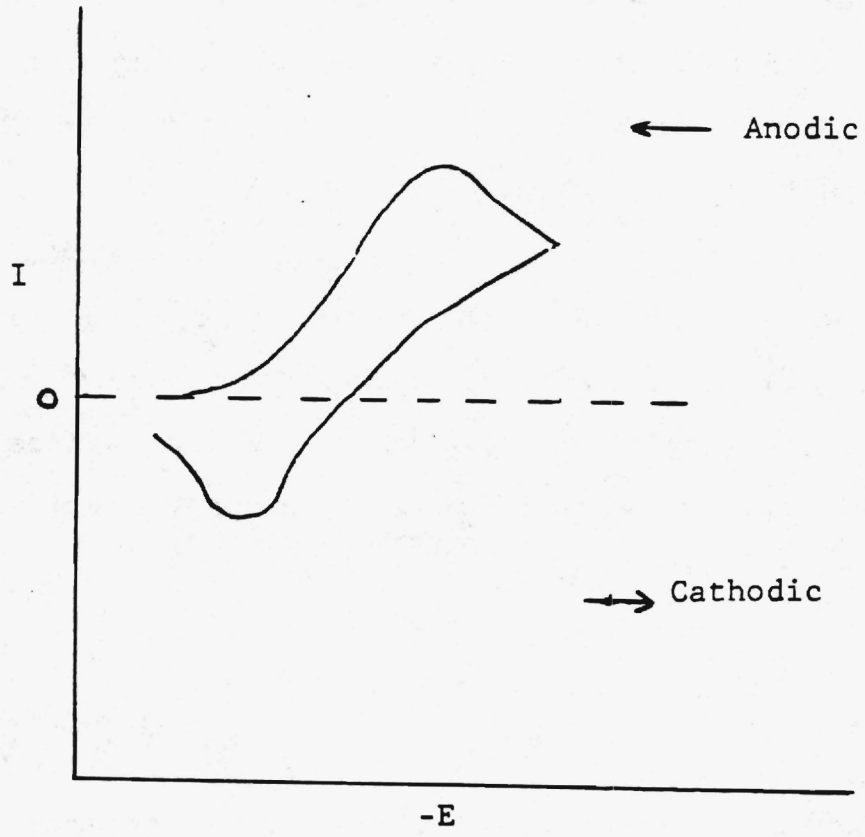

Figure 3.3. Cyclic Voltammetry Response

occuring in the liquid phase. By plotting a value known as the current function, which is approximately equal to the peak current divided by the square root of the scan rate and comparing the resulting curves to those found in the literature, a good estimation of the type of charge transfer taking place can be obtained. This information can then be used to help determine possible reaction schemes for the electrolyte system under investigation.

In all cyclic voltammetry experimentation, it is important to measure the faradaic current from a baseline of charging current. Also, if the solution resistance is uncompensated, severe errors in the voltammetric data will occur limiting its usefulness. In this case, for increasing voltage and current the amount of error due to the uncompensated solution resistance will also increase. This is a major reason for the necessity of some type of IR compensation such as positive feedback in all potential/current measurements.

Effluent Analysis

The basic premise behind the effluent analysis experiments is to measure the amount of species production or removal in the effluent gas streams in order to help determine the mechanisms and species responsible for the activity. One measure resulting from effluent analysis is

CHAPTER IV

EQUIPMENT AND INSTRUMENTATION

In this chapter, the equipment and instrumentation used for this investigation will be detailed. For clarity, it is broken into three sections: electrochemical cells and furnaces, electrical equipment, and gas handling and analysis. A simple schematic of the entire apparatus is pictured in Figure 4.1

Electrochemical Cells and Furnace Cell Housings

For purposes of this investigation, a simple pyrex cell housing was used. This cell was designed in-house and built in the Georgia Tech. Chemistry Department Glass Blowing Laboratory. This cell, pictured in Figure 4.2, was used for all experimentation providing a gas-tight separate anode and cathode compartments for the effluent analysis experiments.

Working and Counter Electrodes for Electrolyte Testing

In all cases, the working counter electrodes were flat surfaces of known area. Planar gold foil, porous perovskite, and porous carbon were used as candidate working electrodes. The gold and perovskite were also used as the counter electrodes. For each case, support and

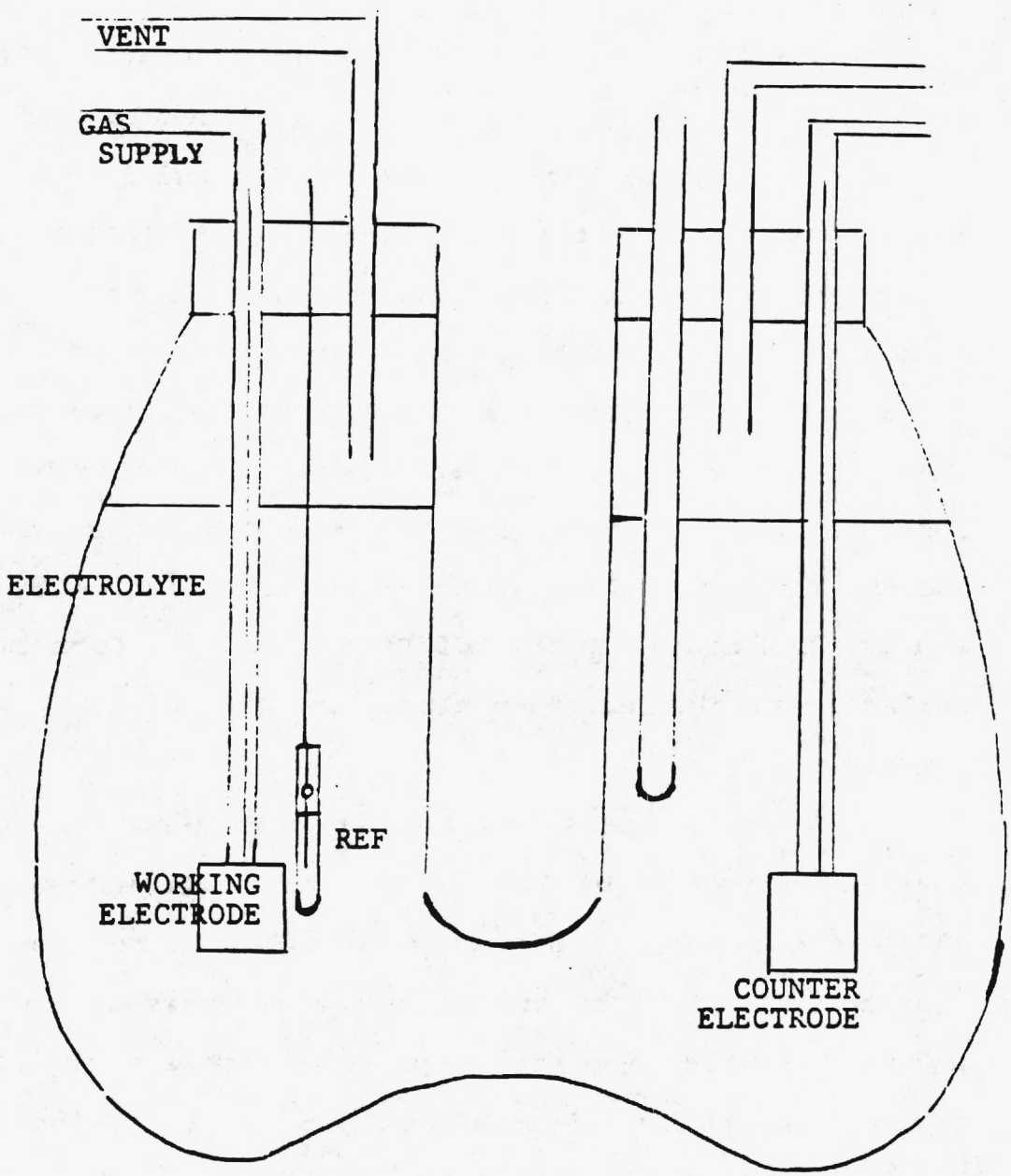

Figure 4.2 Gas Tight Cell for Effluent Analysis

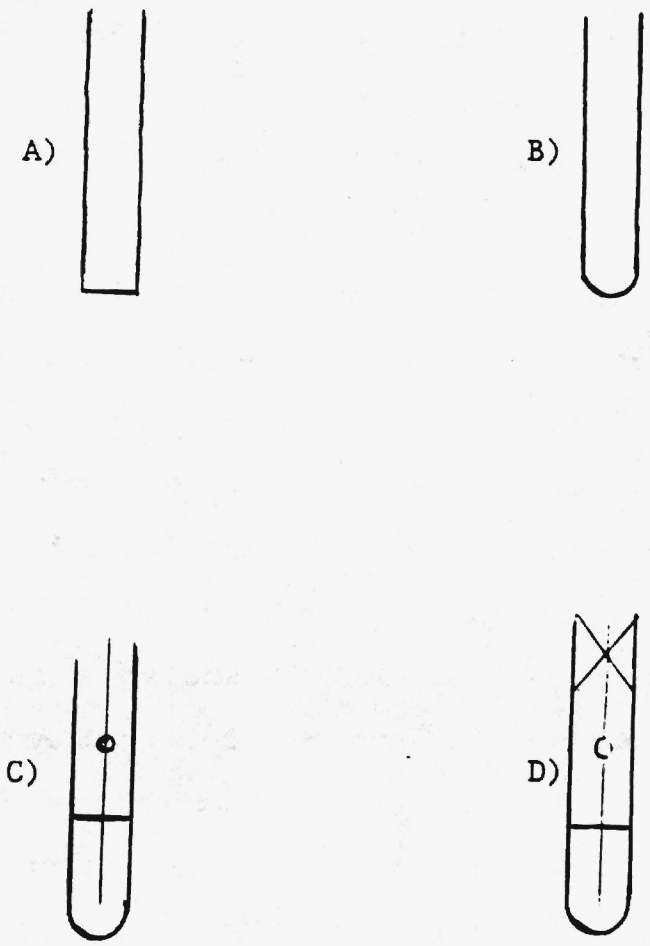

Figure 4.3. Reference Electrode. A) Pyrex closed at one end; B) Formation of thin walled bulb C) Silver wire frozen in refence electrolyte D) End sealed to form final electrode

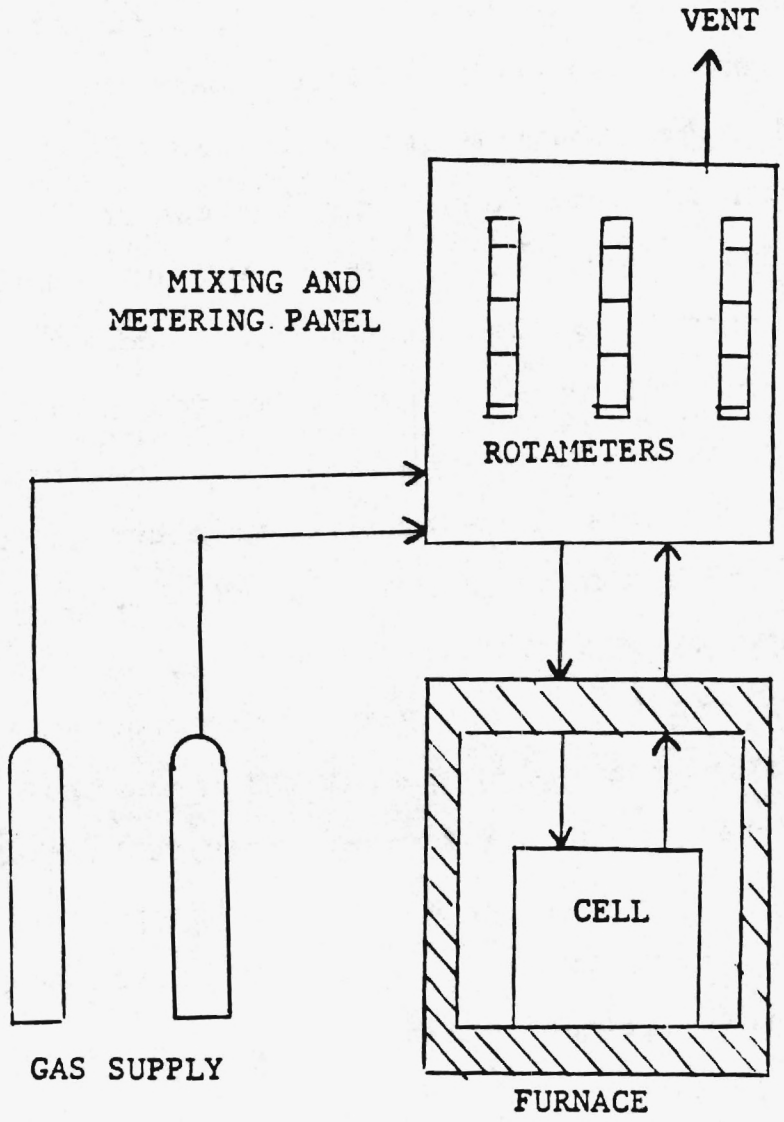

Figure 4.4 Gas Flow Schematic

To monitor and store cell response during experimentation, a Tektronix 5111 Storage Oscilloscope was used in conjucntion with a 5B10N time amplifier and 5A19N differential amplifier. Photographs of stored data could be taken and kept with an accompanying Tektronix C-5C Oscilloscope Camera using high-speed Polaroid Type 107 film.

X-Y Recorder

Using external leads from the PAR 273, traces could also be recorded on a Hewlett Packard Model 7015B X-Y plotter. These plotter are of particular value for sweep rates slower than 500 mV per second.

5) Sinter powder at 1100°C for 24 hours.

6) Add 5% methyl cellulose and mix thoroughly.

7) Cold-press at pressures between 8000 and 10000 psig into 1/4" diameter discs 1.5 mm thick.

8) Sinter in air at 1100°C for 24 hours.

The prepared discs were then cooled in air and readied for use as both working and counter electrodes in a molten electrolyte in bench-scale testing.

Electrode/Electrolyte Testing

There were many tests involving the use of the prepared electrodes and the various electrolytes which were to be examined. In all cases, the electrolyte to be tested was prepared by weighing out the required portions of each component and ballmilling to a fine homogeneous mixture. All electrolyte powders were provided by the J.T. Baker Company. The different types of experiments used in this investigation will now be examined in some detail.

Steady-State Polarizations

Polarization studies were carried out in the full cell environment. The procedure used in these experiments was generally begun by monitoring the working to reference steady-state potential on a voltmeter. Using the PAR 273 in the potentiostat mode, this potential was driven to values both anodic and cathodic from the rest potential. Upon the application of these potentials, the currents generated

was measured by sending the gas directly to the analyzer outside the cell. This value was then used as a comparison to the results obtained after the gas passage through the molten electrolyte.

In the sulfur dioxide analysis, 0.1 liter samples were drawn by a gas-tight syringe from the exiting and entering gas lines. After ensuring that representative samples were taken, the samples were injected into the Gas Chromatograph operating in the flame photometric detector mode. At least five samples were analyzed under each set of experimental conditions in order to obtain an average calculated result. The G.C. was calibrated frequently with gases having known SO_2 values to obtain a standard curve.

During the course of this investigation, it was essential that the experimental cell was sealed satisfactory to ensure that no major gas losses occured inside the furnace. This task was usually accomplished with the help of strong clamps which were tightened before each experimental run. Some gas losses were observed by monitoring both the incoming and exiting flows, but these were considered insignificant to the obtained results. Many different gas compositions were analyzed during these studies and were mixed outside the test cell for the purposes for examining simultaneous NO_x/SO_2 removal in the various electrolytes.

For all types of experimentation,the cell temperatures were kept slightly above the melting point of the molten salt electrolyte. This temperature usually fell between the range of 330-350^{o}C. The electrolyte was often checked to ensure that it remained molten by passing large gas flows through both the cathode and anode compartments. To help keep the salt from creeping up the glassware and clogging the exit ports, a dilute acid solution was placed in an Erlenmeyer flask and inserted in the entering gas streams. To prevent the possible decomposition of the electrolyte, the cell temperature was kept below 400^{o}C. The assembly of the apparatus took place in parts, the first of which was the melting of the free electrolyte. Next the anode and cathode compartments were put in place separately and clamped tightly. Insulation was then used to prevent the tygon connectors from melting and to reduce the loss of thermal energy.

composition powder. Photographs were then taken of both sintered and unsintered (still containing the methyl cellulose) electrodes. Representative pictures are shown in Figures 6.1., 6.2., and 6.3. These pictures, all taken at the same angle and magnification, show the effect of sintering as evidenced by the presence of smooth rounded edges on the sintered samples. The inclusion of the methyl cellulose binder can also be detected through the porosity found in the sintered samples.

Upon examination of the SEM photographs, it can be concluded that no major structual differences exist between the three sample electrodes for the purposes of this investigation. The inclusion of a binder such as methyl cellulose and the resintering of the perovskite containing this binder to acquire sample porosity does produce significant differences in the electrode structure. On the basis of these findings, the $La_{.8}Sr_{.2}CoO_3$ electrodes were used throughout this investigation in order to provide a consistent basis on which to examine the results.

Steady-State Polarizations

Polarization data was taken for various electrolyte compositions using the perovskite electrodes as both the working and counter electrodes. These electrodes were exposed to both gaseous and non-gaseous atmospheres. A representative data set is shown in Figure 6.4., with a

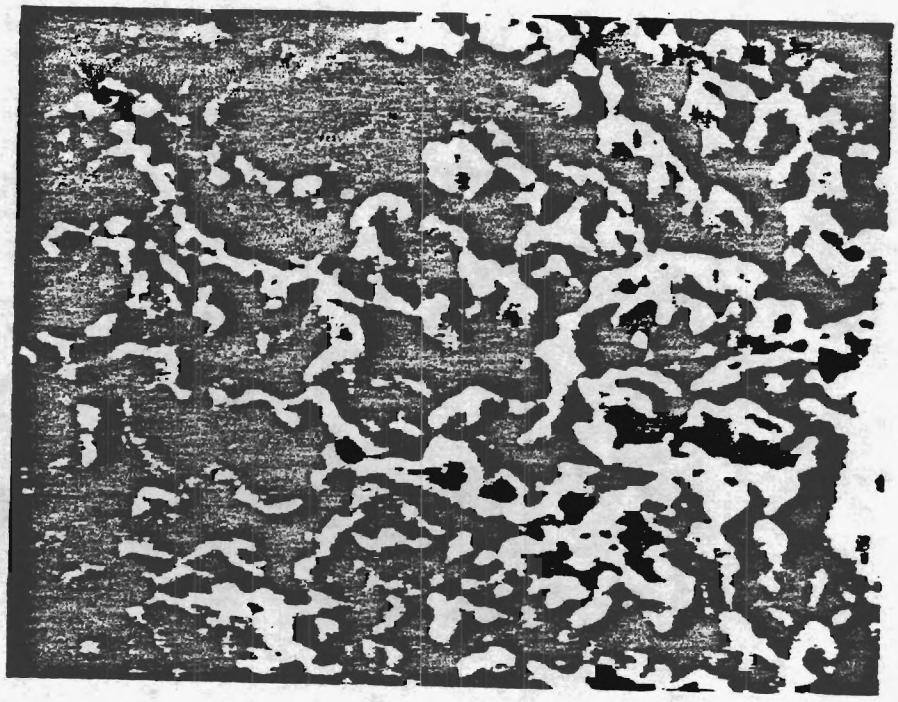

Figure 6.2. SEM Picture of $La_{.8}Sr_{.2}CoO_3$

at 10,000x and 45°
(unsintered)

complete set of data appearing in the appendix.

Using these data, an estimation for the limiting current values for a given set of experimental conditions can be obtained. Table 6.1. shows the limiting current values for each electrolyte and corresponding gas environment. Examining the data, it is clear that the limiting current is not significantly affected by changes in the gas environment. The data also shows that the introduction of potassium sulfate to the electrolyte mixture has very little effect on the limiting current values. On the average, the experimental limiting current values were around 6 ma/cm^2. In potential-step experiments conducted in similar electrolytes [8], current values of 30 ma/cm^2 were obtained. The potential-step measurements, which were taken rapidly, represent a maximum amount of current which can be obtained. The current values obtained from these polarization experiments are limited by a surface build-up of material, probably sulfate, blocking any further electrochemical reactions.

Cyclic Voltammetry

This section presents the results of experiments in which the potential was swept with time with the resultant current being recorded on a storage oscilloscope. The main pupose of this type of experimentation is to obtain data regarding possible reaction mechanisms. The current

Table 6.1. Limiting Currents From Polarization Data

Electrolyte	Gas Environment	i_l (a/cm^2)
$K_2S_2O_7$	Air	0.0048
$K_2S_2O_7$	Nitrogen	0.0059
1% V_2O_5- $K_2S_2O_7$	Air	0.0036
1% V_2O_5- $K_2S_2O_7$	Flue Gas	0.0044
1% V_2O_5- 10% K_2SO_4- 89% $K_2S_2O_7$	Air	0.0031
1% V_2O_5- 10% K_2SO_4- 89% $K_2S_2O_7$	Flue Gas	0.0035
1% V_2O_5- 25% K_2SO_4- 74% $K_2S_2O_7$	Air	0.0040
1% V_2O_5- 25% K_2SO_4- 74% $K_2S_2O_7$	Flue Gas	0.0043

* Flue Gas contains .3% SO_2, 3% O_2, 15% CO_2, bal N_2

Table 6.2. Cyclic Voltammetry Data:Pure $K_2S_2O_7$

V (V)	$V^{.5}$ ($V^{.5}$)	E_{pc} (V)	i_{pc} (A/cm^2)	E_{pa} (V)	i_{pa} (A/cm^2)	i_{pa}/i_{pc}
.1	.316	-.25	.0069	.9	.0075	1.09
.25	.500	-.31	.0081	.93	.010	1.23
.50	.707	-.35	.0100	.95	.0125	1.25
.75	.866	-.38	.0127	.96	.0148	1.17
1.00	1.00	-.40	.0150	1.01	.0163	1.09

Equilibrium Potential : .65 V

Table 6.4. Cyclic Voltammetry Data: 1% V_2O_5- 10% K_2SO_4- 89% $K_2S_2O_7$

V (V/s)	$V^{.5}$ $(V/s)^{.5}$	E_{pc} (V)	i_{pc} (A/cm^2)	E_{pa} (V)	i_{pa} (A/cm^2)	i_{pa}/i_{pc}
.100	.316	-.500	.0069	.65	.010	1.45
.25	.500	-.525	.0094	.68	.0150	1.60
.50	.707	-.610	.0106	.71	.0188	1.77
.75	.866	-.660	.0125	.75	.0223	1.78
1.0	1.0	-.760	.0188	.80	.0263	1.49

Equilbrium Potential : .37

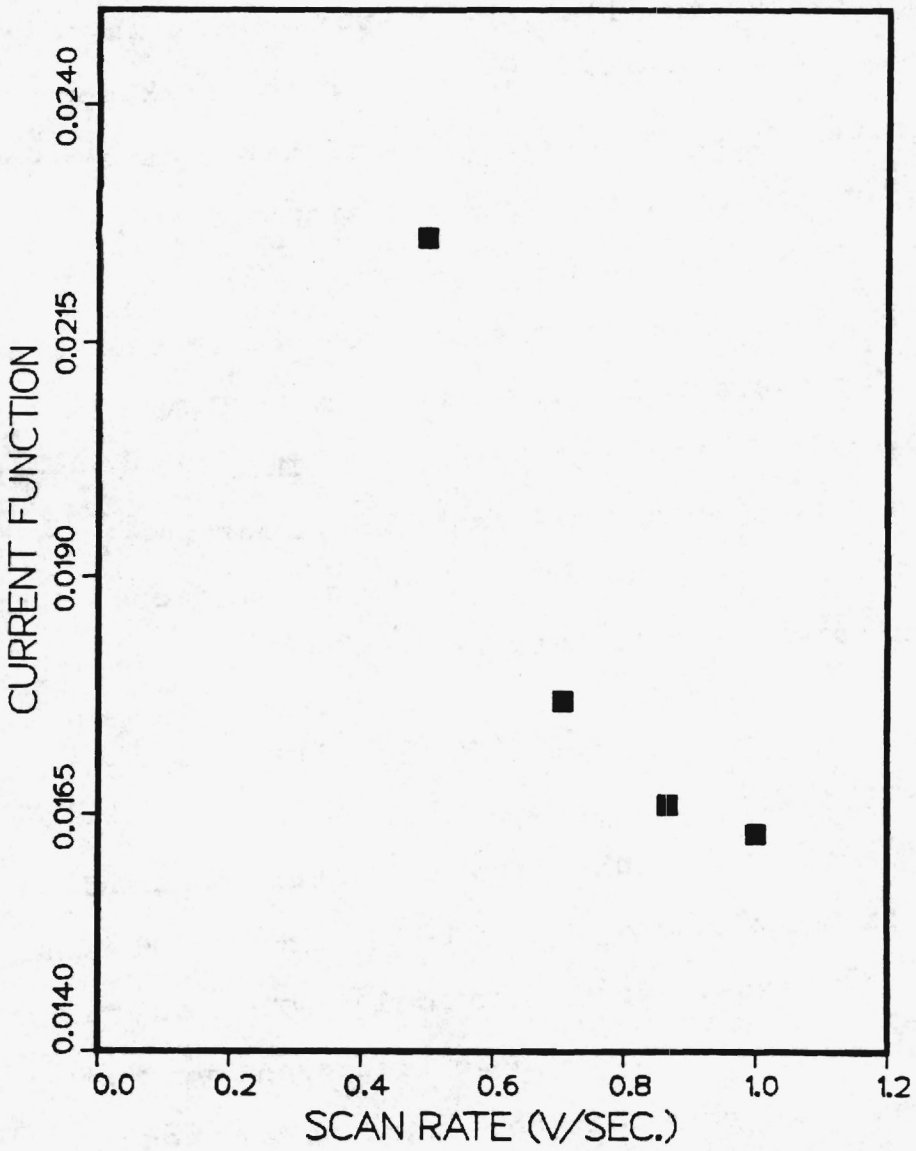

Figure 6.5. Current Function Data for a 25% Sulfate Electrolyte.

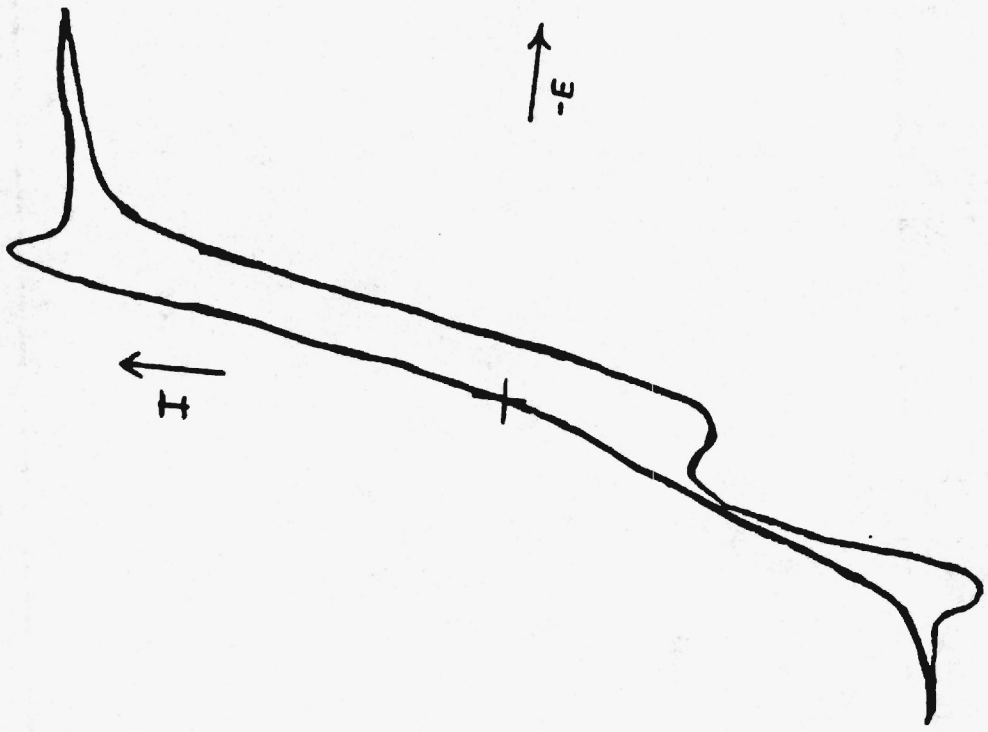

Figure 6.6. Cyclic Voltammogram in $K_2S_2O_7$ (Cathodic Direction First)

and 6.9. show results obtained for all tested electrolytes at an operating temperature of 340°C. These results represent average removal efficiencies taken during separate runs. In this experimentation, the working gas had a composition of 0.3% SO_2, 3% O_2, 15% CO_2, and balance Nitrogen at a flow rate of 30 cc/min.

In all electrolytes the exiting cathodic SO_2 concentrations decrease with increasing current. The addition of sulfate was found to significantly increase the amount of open-circuit SO_2 removal with removal efficiencies as high as 20% being obtained. Contrary to earlier findings [8], a decrease in SO_2 concentration was noticed at open-circuit and with the application of current.

The effect of V_2O_5 as a catalyzing reactant to the overall removal process can be seen by comparison between the pure pyrosulfate and 1% V_2O_5-pyrosulfate electrolytes. At the same current densities, the amount of SO_2 being removed in the vanadia mixture was doubled as compared to the pure pyrosulfate melt. Looking at the data found in Figure 6.9., the addition of sulfate does not play as important a role in the overall removal process as compared to the presence of vanadia. At the highest applied currents, the 1% V_2O_5-99% $K_2S_2O_7$ electrolyte produced the largest removal efficiencies. In all cases, the amount of SO_2 removal (compared to open-circuit values) levels off at

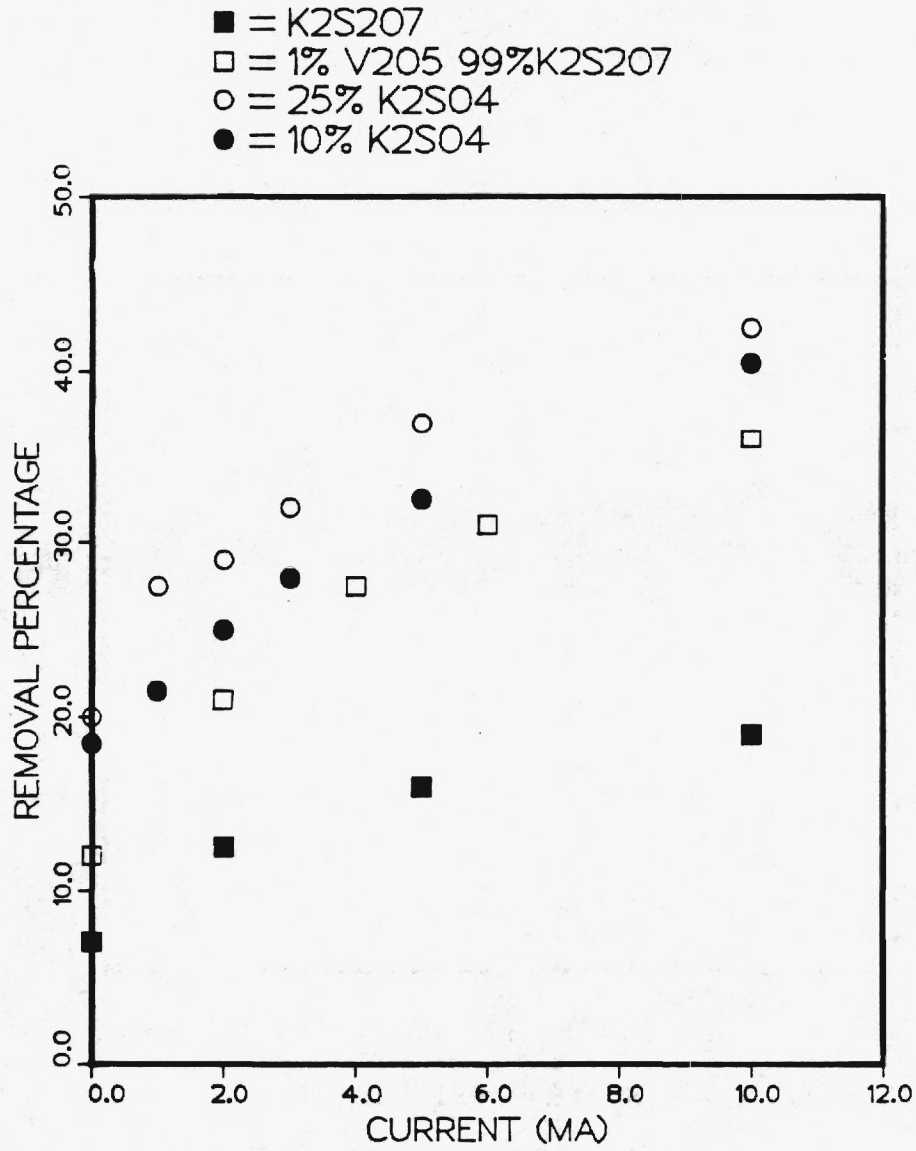

Figure 6.8. SO_2 Removal Data (Compared to Inlet).

values between 25 and 30%.

NO Removal

The removal of NO was examined in all electrolytes containing vanadia. Initial tests were made in a 1% V_2O_5-99% $K_2S_2O_7$ melt with NO removals ranging from 30 to 60%. This removal did not change with the application of current nor did the NO_x concentrations change during the course of the experimentation. The amount of removal did depend upon the flow rate of the working gas with the highest removals occuring at the lowest flow rates. The working gas in these experiments contained 900 ppm NO and bal nitrogen.

More extensive studies were then conducted in the sulfate-containing electrolytes. Figure 6.10. shows the results of these experiments, detailing the dependence of NO removal with flow rate. At optimum flow rates of 30-40 cc/min, NO removals up to 50% were realized. The application of current did not change the removal rate in these electrolytes. The addition of sulfate, however, raised the NO removal values by an average of six to ten percent as compared to the removals seen in the vanadia-pyrosulfate melts. It is important to note that even at extremely high gas flow rates, a significant amount of NO was removed.

NO/SO_2 Removal

The passage of gases containing both SO_2 and NO through the test electrolytes revealed some additional

insight into the contaminant gas removal process. Tests were conducted in the two sulfate-containing electrolytes with equi-volume and other volume concentrations of the separate working gases being used.

In these experiments, the amounts of NO removal were similar to the values obtained for the pure removal studies. The amounts of NO removal, ranging from 25 to 58%, were dependent on the total gas flow rate, not necessarily the flow rate of the NO_x gas mix. However, SO_2 removal versus applied current is enhanced as shown in Figure 6.11. for a 30 cc SO_2/ 10cc NO gas mixture. For this and other flow rates, the SO_2 removal efficiencies were on average five to ten percent higher than the corresponding values obtained in the pure SO_2 removal studies. As noted earlier the total amounts of SO_2 removal were again limited at values between 40 and 45%.

CHAPTER VII

DISCUSSION

This chapter will detail the discussion of the results obtained in this investigation. The discussion is broken down into three main sections with the first section describing the results from the polarization experiments. The second section will examine the data obtained from the cyclic voltammetry experimentation. The last section will discuss the reaction mechanisms involved in the contaminant species removal found by effluent analysis.

Steady-State Polarizations

The observation that changes in the gas environment do not change the limiting current values in the test elctrolyte correlates with earlier findings by Scott [8]. This suggests that no reactants of the electrochemical reations are being supplied by the gaseous phase. The electrode reations involve the direct oxidation and reduction of a species originally in the liquid phase. These results along with the data showing that sulfate addition had little or no effect on the limiting current values indicates that the pyrosulfate is the electroactive species, and the only species in large enough concentration to affect the limiting current values.

thin film experimentation [8]. The Thin Film experiments produced molar concentrations on the order of 10^{-2} moles/cm^3. This difference in concentrations indicates a blockage on the electrode surface as noticed during the polarization studies. It is believed that the voltammetry results are affected by the formation of oxide layers on the electrode surface. These oxide layers produce interferences making the species concentrations inconsistent with those produced by other experimental techniques [25]. This interference makes the acquisition of useful kinetic data from these experiments unfeasible.

Problems developed after the peak current and potential data for the gold electrodes were obtained. The potentiostat used for the voltammetric scans did not allow a full series of sweeps possible, forcing the use of an oscilloscope to record the ouput currents. The oscilloscope presented problems with high signal to noise ratios limiting the accuracy of any acquired data. Attempts to use the perovskite electrodes in place of the gold electrodes in hopes of eliminating the surface oxidation problems were hampered by structual problems associated with the test cell and the connections to the electrodes.

Effluent Analysis

SO_2 Removal

The removal of sulfur dioxide in a pure pyrosulfate

removed per two Faradays termed a n=2 case, involves the formation of sulfur trioxide in the presence of vanadia :

$$2SO_2 + O_2 = 2SO_3 \qquad (7.3)$$

The sulfur dioxide from the flue gas can react to form sulfate ions [26] :

$$SO_2 + O_2^{2-} = SO_4^{2-} \qquad (7.4)$$

The sulfate ions will then react with the sulfur trioxide to generate pyrosulfate ions

$$2SO_3 + 2SO_4^{2-} = 2S_2O_7^{2-} \qquad (7.5)$$

This series of reactions leaves an overall net reaction

$$O_2 + SO_2 + 2e = SO_4^{2-} \qquad (7.6)$$

These reactions show the importance of vanadia and the oxygen from the flue gas to the overall removal process. The end result is a build-up of excess sulfate ions, which explains the lowering of the equilibrium cell potentials observed during the experimentation, and a regeneration of the starting pyrosulfate supply.

Another possible reaction path exists in which one

These reaction schemes indicate that a means of removing both SO_2 and SO_3 exists with the aid of a catalyst and the formation of ions in equilibrium with the starting product. Figures 7.1. thru 7.3. show the experimental removal efficiency curves to inlet presented with theoretical curves based on the n=2 case. These curves show that the experimental data closely responds to the n=2 case at the lower currents. This is supported by the drop in equilibrium potentials noticed during the experiment.

For the case of the observed open circuit removals, the breakdown of the pyrosulfate ions into SO_3 and sulfate ions allow for the proposed reaction scheme to take place. Without the presence of vanadia, however, these reactions are very slow [27]. The effect of the additional sulfate ions is to reduce the net SO_2 evolution. This might occur through dithionate formation [28]

$$SO_2 + SO_4^{2-} = S_2O_6^{2-} \qquad (7.12)$$

The dithionate will then undergo subsequent disproportionation

$$S_2O_6^{2-} = SO_3 + SO_3^{2-} \qquad (7.13)$$

$$SO_3 + SO_4^{2-} = S_2O_7^{2-} \qquad (7.14)$$

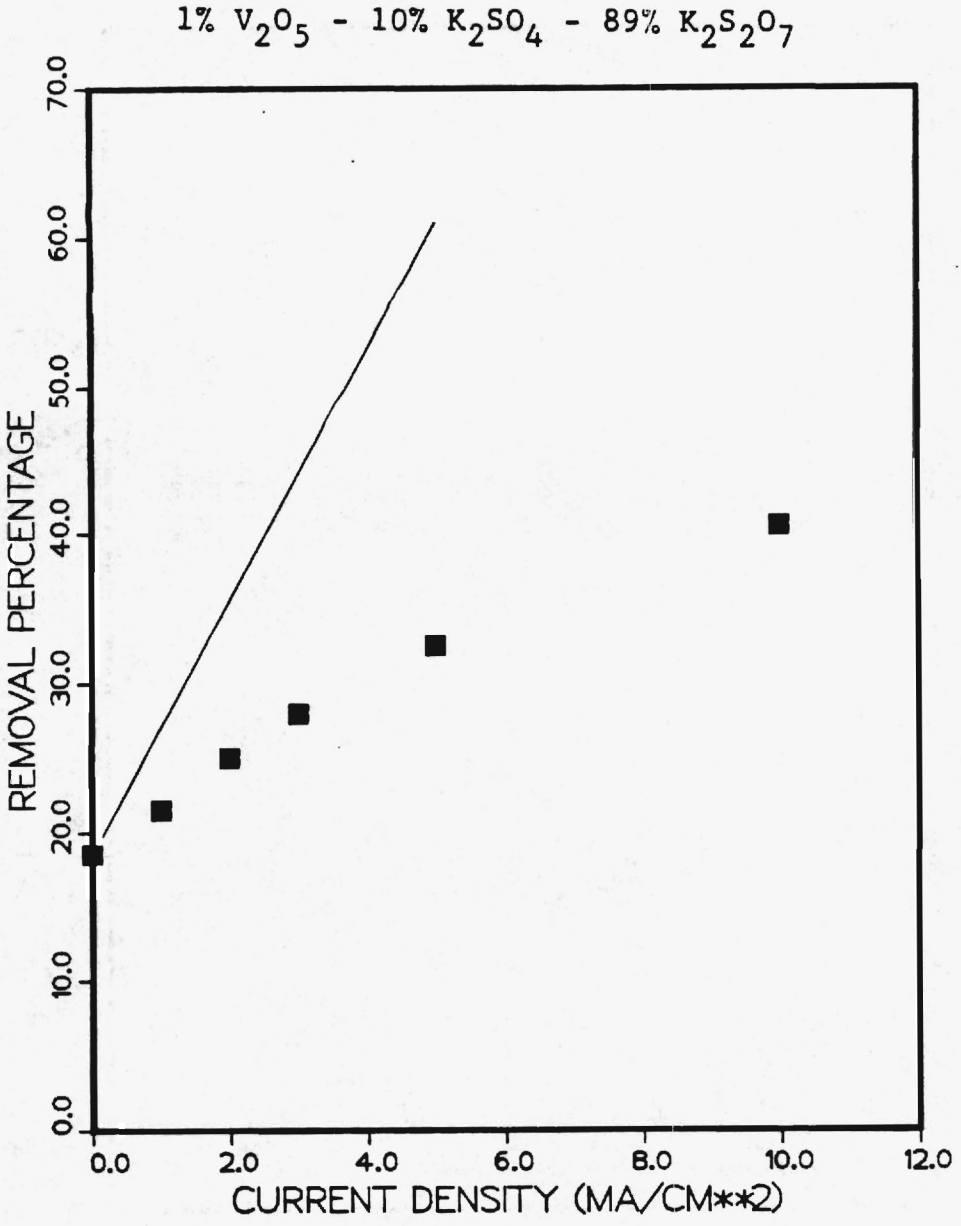

Figure 7.2. SO_2 Removal Curve Compared to Theoretical Case.

The net result is the formation of pyrosulfate ions to replenish the starting supply.

The experimental removal results are limited by mass transfer at values between 40 and 45%. The mass transfer limitation is from the rate of SO_2 transfer from the flue gas bubbles to the electrolyte. At the higher currents, the sulfate produced in the electrochemical step has insufficient opportunity to react with the gas. In a device with immobilized electrolyte in contact with gas-diffusion electrodes, this limitation can be avoided. Detailed calculations shown in the appendix show this limitation to range from 19 to 51% for this system which is consistent with the experimental data.

NO-NO/SO_2 Removal

A definite reaction scheme detailing the actual NO removal process has not yet been determined. It had been hoped that a definite relationship between current application and NO removal would exist giving rise to a number of possible reaction schemes. Analysis of an electrolyte sample after experimentation could only reveal that possible NO_3^- concentration was less than 0.05%. The experimental results suggest that the NO is being removed by chemical reaction in the electrolyte melt.

The increase in the amount of SO_2 removal in the simultaneous NO/SO_x studies has also been noticed in

CHAPTER VIII

CONCLUSIONS

This chapter will discuss the conclusions reached on the basis of the experimental results obtained from this investigation. This work was focused on the testing of electrolyte and electrode candidates for use in a flue-gas desulfurization device operating at a temperature of 340°C. These materials were also tested to determine the capacity for NO and NO/SO_2 removal in the proposed device.

Perovskite electrodes were prepared in house and their stability performance evaluated under simulated cell conditions. Tests were also conducted for the basis of comparing the performance of the perovskites to that of planar gold electrodes used in earlier experimentation. These tests reveal that the perovskites would be satisfactory electrode materials in a full-cell device.

Four candidate electrolytes, pure $K_2S_2O_7$, potassium pyrosulfate with 1% V_2O_5, this electrolyte with 10% potassium sulfate, and the pyrosulfate/vanadia melt with 25% sulfate, were prepared and used as candidate electrolyte materials. Preliminary testing excluded the pure pyrosulfate melt as a viable electrolyte candidate and showed the importance of the vanadia as a catalyst to

sulfur dioxide with applied current was seen in all four electrolytes, but the addition of the vanadia catalyst to the pure pyrosulfate melt doubled the amount of SO_2 being removed. The addition of potassium sulfate to the electrolyte increased the amount of open circuit removal but did not change the effect of applied current to the overall removal process. In all electrolytes containing vanadia, the amount of sulfur dioxide removal increased with increasing current until the process was limited by the rate of SO_2 transfer from the flue gas bubbles. A possible reaction scheme was proposed which is consistent with experimental data, and results in the catalytic regeneration of pyrosulfate with a net production of sulfate which lowers the equilibrium cell potential.

Effluent analysis with gas streams containing nitrogen oxide was also conducted in the melts containing vanadia. All of these electrolytes exhibited NO removal capacity and did not produce the generation of harmful NO_2 gases as by-products. The removal rate was not enhanced by the application of current but was dependent upon the flow rate of the NO gas stream into the test cell.

Finally, simultaneous NO/SO_2 studies were conducted in the test electrolyes. These studies revealed that the amount of nitrogen oxide removal did not change but the rate of sulfur dioxide removal with applied current was

CHAPTER IX

RECOMMENDATIONS

Based on the results of this investigation, a number of recommendations can be given for possible work in this area. Eventually, full-cell tests should be run with the electrolyte held in a porous matrix in contact with porous electrodes. I believe that some more testing in the bulk electrolyte should be carried out.

The acquistion of a digital oscilloscope or another data recording device for use in the cyclic voltammetry studies might aid in outputting the data more efficiently. Tests should also be run using the perovskite electrodes in place of the planar gold ones in order to prevent oxide formation on the electrode surface. Further work should also be done on the NO studies with hopes of determining the actual reaction schemes. More work could also be done in the simultaneous removal studies such as preparing different gas mixtures to examine along with using various flow rates. The addition of even more potassium sulfate to the electrolyte melt might be attempted in order to study the effect on open circuit gas removal.

Improvements could also made to the existing test cell design in order to lessen the effects of the mass

APPENDIX A

MASS TRANSFER CALCULATIONS

To help understand the data from the effluent analysis experiments, the rate of mass transfer from the SO_2-containing flue gas bubbles to the electrolyte must be calculated. A liquid phase mass transfer coefficient, k_l (cm/sec.), for the free rise of single bubbles may be determined [30]:

$$k_l = \left(\frac{\mu}{\rho D_l}\right)^{-.5} \times .42 \left(\frac{\Delta\rho\mu g}{\rho}\right)^{.33} \qquad (A.1)$$

where D_l is the diffusivity of the SO_2 in the electrolyte, μ is the electrolyte viscosity, ρ is the electrolyte density, $\Delta\rho$ is the density difference between gas and liquid, and g is the acceleration due to gravity.

Using values of D_l equal to 2×10^{-5} [31], μ equal to .1g/cm-sec [32], and an experimental density value of $2.5 g/cm^3$ results in a k_l value of 3.19×10^{-2} cm/sec for the experimental system.

The transfer of sulfur dioxide from each bubble to the liquid phase can be found from the integrated equation [8]:

The experimental values were then used in equation (A.2) along with the calculated mass transfer coefficient term, which was assumed to remain constant for this system, to calculate the mass-transfer limits. These values, ranging from 20% to 80% proportional to the flow rate, were consistent with the experimental results.

t	rise time
v	scan rate
η	deviation from equilbrium potential
ρ	density of liquid
$\Delta\rho$	density difference between liquid and gas
μ	viscosity of liquid

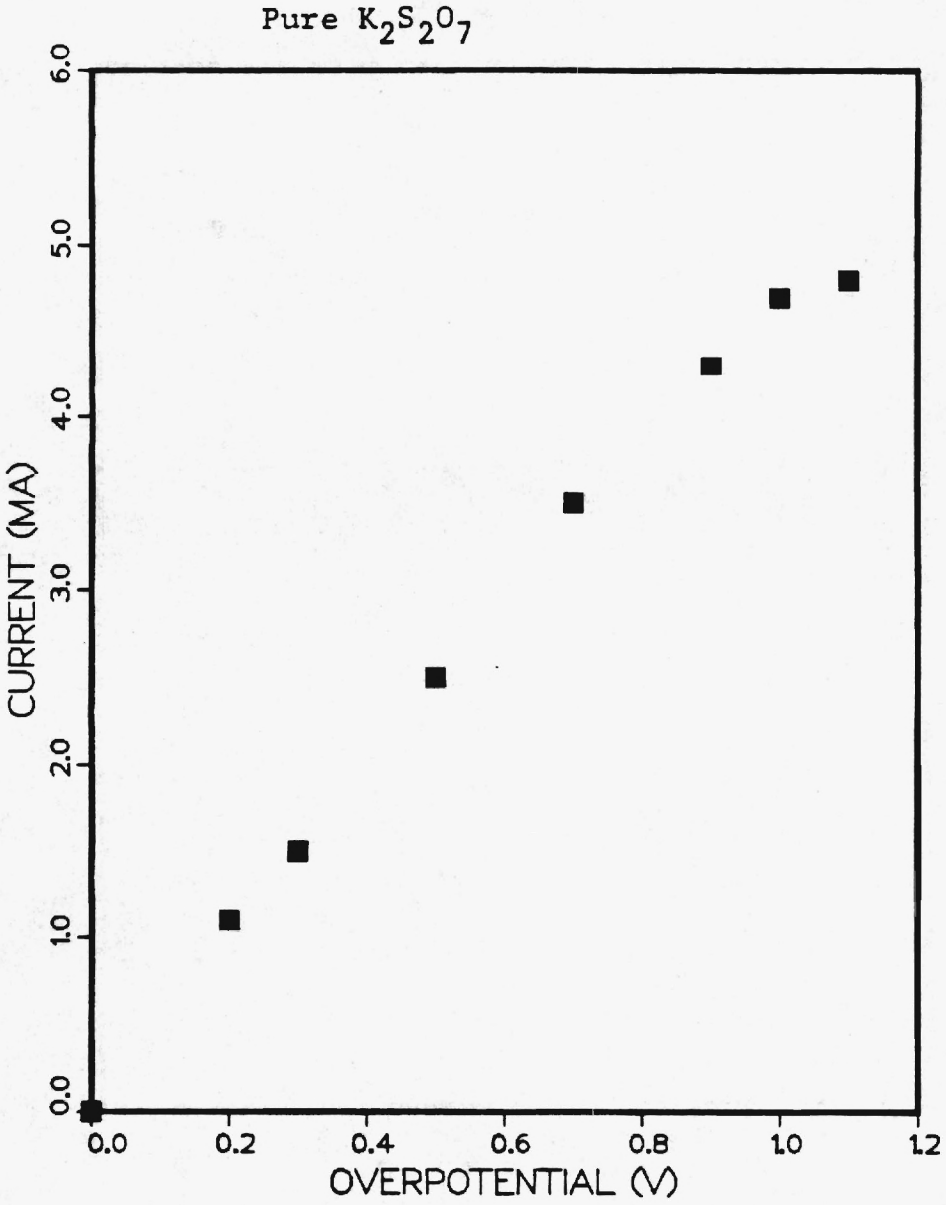

Figure C.1. Polarization Data Under Air Environment.

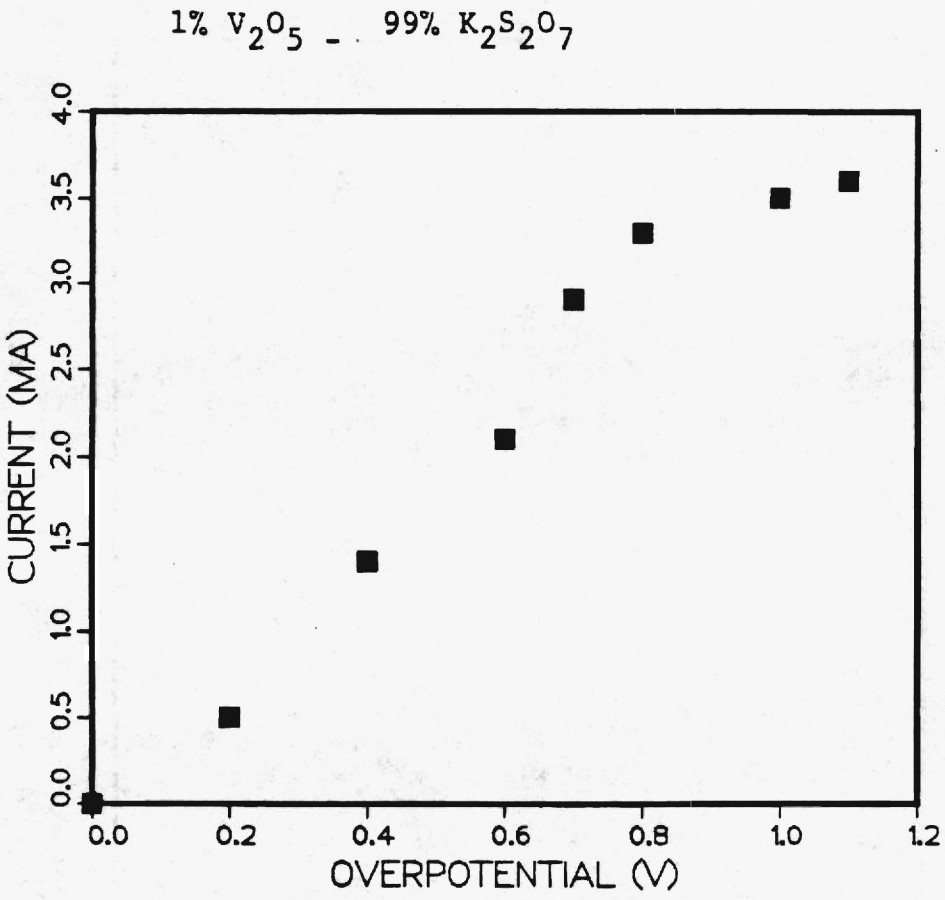

Figure C.3. Polarization Data Under Air Environment.

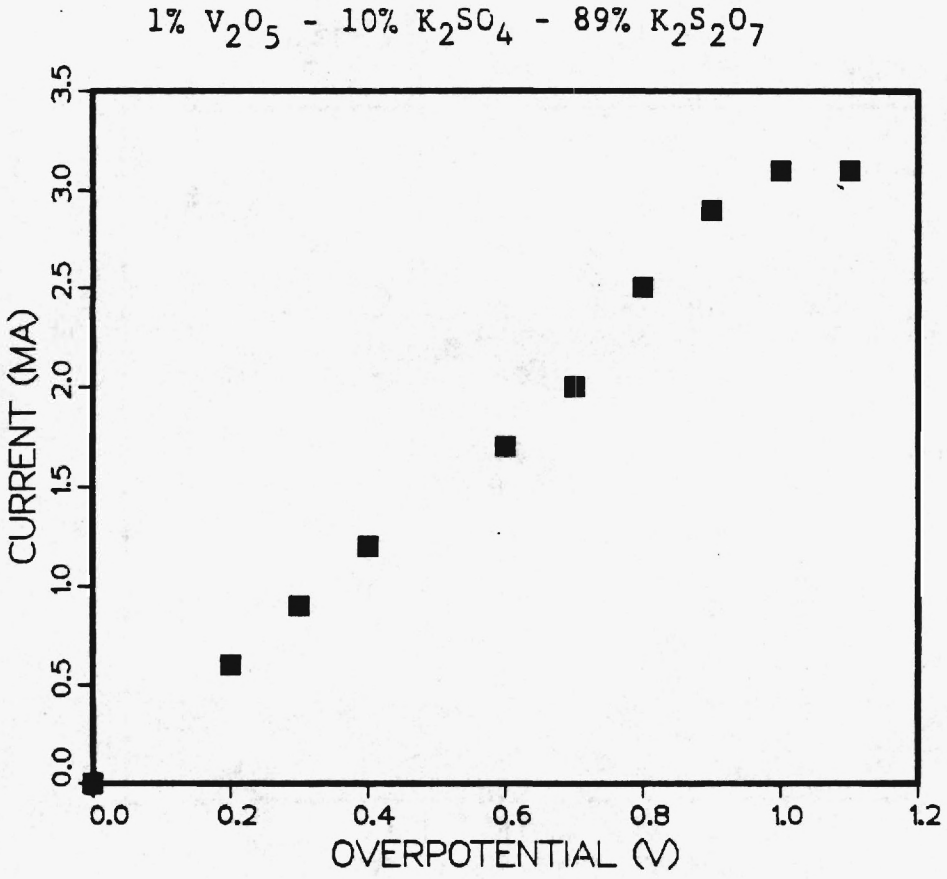

Figure C.5. Polarization Data Under Flue Gas Environment.

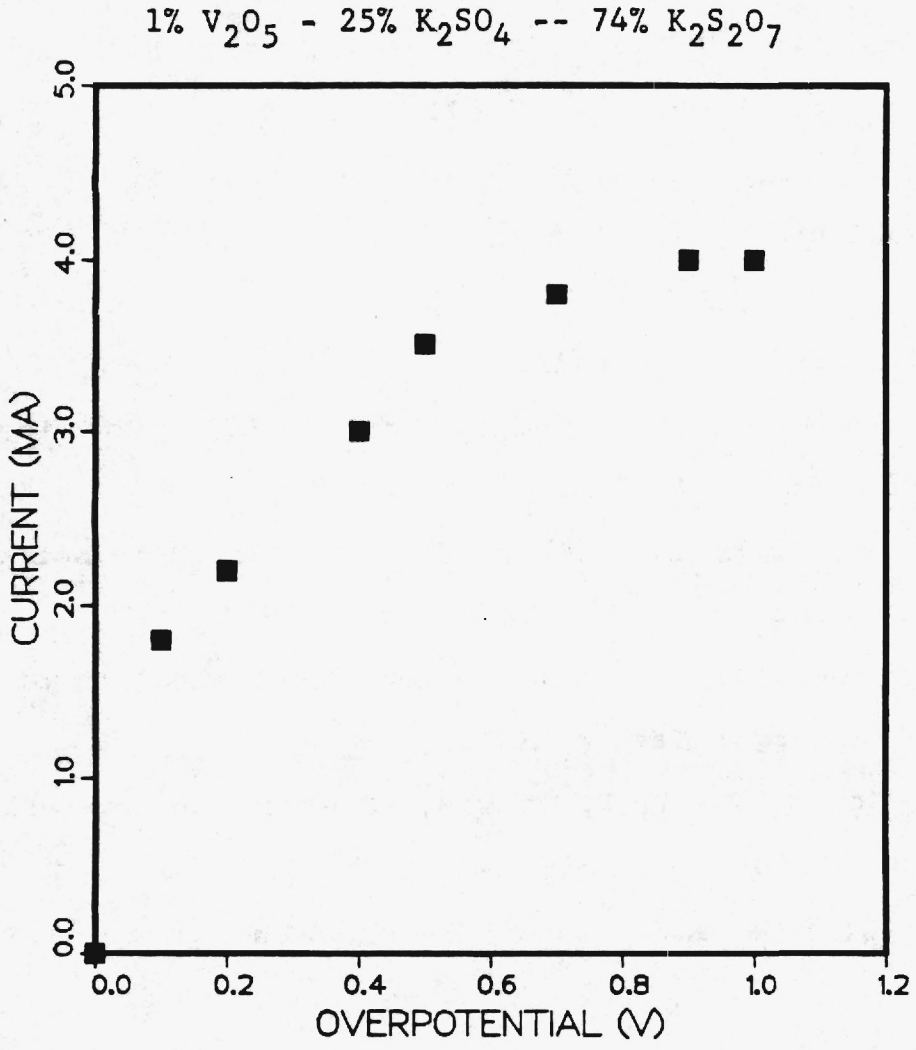

Figure C.7. Polarization Data Under Air Environment.

12. Johnson, K.E., and Lastiner, H.A., J. of Electrochem. Soc., 110, 314 (1963).

13. Potter, P.J., "Power Plant Theory and Design," The Ronald Press Company, New York (1959).

14. Scott, K., Fannon, T., and Winnick, J., submitted to J. of Electrochem. Soc., (1986).

15. Koutsoukos, E.P., et. al., EPA-650 / 2-75-001-A, 1975.

16. Kudo, T., Ohayashi, H., and Yoshiba, M., J. of Electrochem. Soc., 122, 159 (1975).

17. Tedmon, C.S., J. of Electrochem. Soc., 116, 1618 (1969).

18. Kudo, T., Ohayashi, H., and Yoshiba, M., J. of Electrochem. Soc., 124, 321 (1977).

19. Bard, A.J., and Faulkner, L.R., "Electrochemical Methods," John Wiley and Sons, 1980.

20. Nicholson, R.S., and Shain, I., Anal. Chem., 36, 706 (1964).

21. Nicholson, R.S., and Shain, I., Anal. Chem., 37, 178 (1965).

22. Nicholson, R.S., and Shain, I., Anal. Chem., 37, 190 (1965).

23. Plambeck, J.A., "Electroanalytical Chemistry," John Wiley and Sons, New York (1982).

24. Kudo, T., Ohayashi, H., and Geio, T., Japanese

DOE/PC/73226-4

COMBINED SO_x/NO_x REMOVAL AND CONCENTRATION FROM FLUE GAS THROUGH AN ELECTROCHEMICAL MEMBRANE

Progress Report for the Period June, 1984-January, 1987

By
Jack Winnick

April 14,1987

Work Performed Under Contract No. DE-FG22-84PC73226

Georgia Institute of Technology
Atlanta, Georgia 30332-0100

DOE/PC/73226-4

COMBINED SO_x/NO_x REMOVAL AND CONCENTRATION FROM FLUE GAS THROUGH AN ELECTROCHEMICAL MEMBRANE

Progress Report for Period
June, 1984 to January, 1987

By
Jack Winnick

April 14, 1987

Work Performed Under Contract No. DE-FG22-84PC73226

B&R Code AA0505

Prepared for
U.S. Department of Energy
Assistant Secretary for Nuclear Energy

Prepared by
Georgia Institute of Technology
Department of Chemical Engineering
Atlanta, Georgia 30332-0100

INDEX

INTRODUCTION

As the United States strives to become energy independent, coal, because of its domestic abundance, is becoming an increasingly important source of energy. A major drawback associated with coal is the resulting emissions of SO_2 and NO_x to the atmosphere. These pollutants must be removed from the flue gas in order to adhere to environmental regulations. Presently, commercial processes for achieving emission standards are unattractive because they generally require excessive land area, huge volumes of chemicals, and produce large volumes of troublesome waste products. Current flue gas clean-up (FGC) research emphasizes the development of reliable, less costly processes which produce useful by-products instead of wastes.

A novel approach to FGC is one which utilizes an electrochemical membrane concentrator (EMC). The research within this report was conducted under DOE grant number DE-FG22-84PC73226.

BACKGROUND

As early as 1964, EMCs were used to remove dilute components from gas streams and concentrate them in by-product streams [1]. The alkaline aqueous CO_2 concentrator was selected by NASA to control the level of CO_2 in cabin air during manned space missions [2]. In this EMC, an asbestos matrix filled with the electrolyte separates the cathode and anode chambers. At the cathode, cabin air containing 1% CO_2 or less dissolves in the alkaline electrolyte and in the presence of excess base (produced from oxygen at the cathode, equation (3)) forms the carbonate ion:

$$CO_2 + OH^- \rightarrow HCO_3^- \quad (1)$$

$$HCO_3^- + OH^- \rightarrow CO_3^{2-} + H_2O \quad (2)$$

$$1/2\ O_2 + H_2O + 2e^- \rightarrow 2OH^- \quad (3)$$

At the anode, hydrogen is supplied and CO_2 is released from the resulting weakly acidic solution, i.e.,

$$H_2 + CO_3^{2-} \rightarrow H_2O + CO_2 + 2e^- \quad (4)$$

A natural pH gradient is established in the electrochemical cell: alkaline at the cathode and near neutral at the anode. The CO_2 is thus evolved at high concentration into the hydrogen anode

stream. This stream then undergoes further processing to recover the oxygen and hydrogen.

The success of the molten carbonate fuel cell promoted application of this concept to CO_2 concentration [3, 4]. This technique appears to be an improvement over the aqueous cell in several respects. Because the electrolyte is non-aqueous, humidity control is not required. Flooding and drying-out of the asbestos matrix is a concern in the aqueous cell. The more rapid kinetics at the higher temperature of the molten carbonate cell (ca. 500°C) allow operation at much higher current densities, lowering the size requirement for given duty. Further, noble electrodes, necessary in the aqueous cell, are replaced with nickel. Finally, the molten carbonate cell permits operation as a true concentrator in an alternative mode:

cathode,

$$CO_2 + 1/2\ O_2 + 2e^- \rightarrow CO_3^{2-} \qquad (5)$$

anode,

$$CO_3^{2-} \rightarrow CO_2 + 1/2\ O_2 + 2e^- \qquad (6)$$

Beginning in 1977, work under ERDA and DOE sponsorship was initiated to examine the feasibility of an SO_x concentrator cell. The electrode was the ternary eutectic (0.79 Li, 0.12 K, 0.09 Na)$_2SO_4$. This mixture melts at 512°C and is stable with low SO_2 and SO_3 vapor pressures [5]. Investigation of the cathodic reaction in a sulfate melt [6] under an atmosphere of SO_2 and O_2

shows that the electrode potential does not respond to the SO_2 directly but rather to the SO_3 resulting from the oxidation of SO_2.

$$SO_2 + 1/2\ O_2 = SO_3 \qquad (7)$$

$$SO_3 + 1/2\ O_2 + 2e = SO_4^{2-} \qquad (8)$$

This sequence gives an overall reaction of

$$SO_2 + O_2 + 2e = SO_4^{2-} \qquad (9)$$

This reaction provides the basis for SO_2 removal at the cathode. The anodic reaction has been shown to be [7, 8]:

$$SO_4^{2-} = SO_3 + \frac{1}{2}\ O_2 + 2e \qquad (10)$$

The exact mechanisms are unknown though a number of possibilities have been postulated [8-10].

The cathode gas, premixed simulated flue gas contains 0.3% SO_2, 3.0% O_2, 15.0% CO_2, 9% H_2O and the balance N_2. This is the approximate composition of flue gas when the coal contains 3.5% sulfur. The cell is insensitive to carbon dioxide as it is inhibited from reaction due to the equilibrium between sulfate and carbonate which lies far to the right ($K \approx 10^{23}$):

$$CO_3^{2-} + SO_2 + \frac{1}{2}\ O_2 + SO_4^{2-} + CO_2 \qquad (11)$$

Water vapor will not affect performance as any alkali metal bisulfates formed at these temperatures will decompose according to the reaction:

$$2HSO_4^- = SO_4^{2-} + SO_2 + H_2O + \frac{1}{2} O_2 \qquad (12)$$

Though up to 90% SO_2 removal can be accomplished, there is a major flaw with industrializing this device: The melting point of the sulfate (512^oC) sets a lower limit on the possible operating temperature. Retrofitting this high temperature device to existing power plants is unattractive. The effluent from the economizer is typically at $250-400^oC$ [11]. Increased costs would be incurred due to the need for a regenerative heat exchange section to heat the gases to 600^oC. In addition, an electrostatic precipitator is required upstream of the electrochemical device, and a precipitator operating at 600^oC must be built of extremely expensive materials. The high temperature is also detrimental to any metal components of the cell housing due to rapid corrosion in the harsh environment.

It would be desirable to design an electrochemical flue gas desulfurization device to operate in the vicinity of 300^oC. This lower temperature provides little problem as far as membrane material selection is concerned. The membranes employed at 600^oC (e.g., $LiAlO_2$, MgO, Al_2O_3, $SrTiO_3$, and SiC) should be quite suitable for cooler operation due to increased stability. Alternative lower melting electrolytes must be identified for possible use in the lower temperature electrochemical

desulfurization device. It is also necessary to find an electrode material which is sufficiently inexpensive, stable, and active at the lower temperatures. In addition, capability for NO_x destruction or removal must be ascertained.

STATEMENT OF WORK

In the previous section it was shown that an electrochemical membrane concentrator could be an attractive alternative to flue gas clean-up process in place today. Here, we outline the research activities and procedures which were planned to develop the electrochemical process. The activities are broken down into five tasks, corresponding to the tasks outlined in the statement of work in the contract, exhibit 1.

1. Free Electrolyte:

The first objective was to identify an electrolyte which could be used in the temperature range of interest, described earlier to be near 300^{o}C. Alkali metal bisulfates, pyrosulfates and sulfates were examined as base electrolytes on the basis of melting point and stability. The effect of additives, such as vanadia, a well known oxidation catalyst, were also examined. The best electrolyte combinations were investigated by standard electrochemical tests to characterize the electrode reaction mechanisms and removal processes. The type of tests utilized included thin film experiments, chronoamperometry effluent analysis, x-ray diffraction, cyclic voltammetry, and equilibrium potentials. A reaction mechanism is proposed following the effluent analysis results and is then further substantiated and built upon in the results which follow.

2. Electrode Development

The second task deals with the development of porous electrodes. Perovskite type materials, $Ln_{1-x}\ M_x\ M'O_3$ (Ln = lanthanoid element, M = alkaline earth element, M' = transition metal element) appear to be satisfactory and were examined in some detail. First, perovskite was compared to commercial NiO electrodes in a molten carbonate CO_2 concentrator. Commercially produced carbonate membranes were used in these tests so that changes in performance were due solely to be electrodes. The polarization characteristics and stability of each electrode was examined and compared. Polarizations were examined for perovskite electrodes in contact with the electrolyte identified in Task 1.

3. Ceramic Membrane Development

Various types of matrix materials were combined with the electrolyte identified in Task 1 to produce ceramic membranes. The types of matrix materials investigated include zirconia felt, pyrex frits, SiC, $SrTiO_3$ and MgO. Three types of fabrication procedures were examined. The first type, used with the prefabricated zirconia felt matrix, involved electrolyte impregnation at high temperature. The second type involved impregnation of matrix structures which were cold pressed and partially sintered. The third kind of membrane was produced by hot-pressing a homogeneous mixture of the matrix and electrolyte powders near the electrolyte melting point. The membranes were first evaluated on the basis of density, strength, and

conductivity. X-ray diffraction was then used to assess the structures. Membranes which appeared to meet the requirements were then utilized in full-cell tests, Task V.

4. NO_x Removal

Here tests were done to explore NO_x removal in free electrolyte. The gas consisted of NO_x, N_2 and O_2 with concentration of NO similar to that in flue gas. The gas was bubbled through the electrolyte past the working electrode. The effluent gas was monitored for NO_x content as a function of the applied current and the gas flow rate. Finally, tests were conducted using a gas containing NO_x and N_2, and in addition SO_2, CO_2 and O_2 in concentrations consistent with flue gas. The effluent gas was monitored for both NO_x and SO_2 removal as a function of applied current and gas flow rate.

5. Full-Cell Testing

Full-cell tests were performed using machined Macor housings with membranes as identified in Task 3. The electrodes identified in Task 2 had not been fully developed so in addition to these semi-developed perovskite electrodes, other materials were utilized. Alternate electrodes included porous carbon, porous nickel, and gold screen. The full-cell tests generally consisted of steady-state polarization and SO_2 removal efficiency as a function of the applied current.

EXHIBIT 1

STATEMENT OF WORK

Five tasks are to be performed toward assessing the system capabilities for removing and concentrating sulfur oxides and nitrogen oxides from flue gases.

1. The first task will define the best electrolyte for sulfur oxide removal. Tests shall be performed regarding thermal stability, ionic conductivity and cathodic and anodic reaction rates for sulfur oxide removal. These electrolytes shall consist of pure and mixed alkali bisulfates and pyrosulfates. Additivies to promote reaction rates and stability shall be tested. These include well-known oxidation catalysts as vanadia.

   These tests shall be conducted in free electrolyte housed in pyrex, gas-tight, two-component cells. Planar gold working electrodes of known area shall be used in these tests. A silver/silver ion reference electrode shall be provided. Gases shall be bubbled past the working electrode and provision made for sampling by a gas chromatograph. These gases shall contain known concentrations of O_2, SO_2, CO_2 and N_2.

   Results shall include data on steady-state polarization, ohmic loss, chronoamperometry, linear sweep voltammetry, cyclic foltammetry, and sulfur oxide removal efficiency as a function of applied current.

2. The second task will define inexpensive porous electrodes. perovskite-type materials including the molybdates and cobaltates will be tested. The electrodes shall be constructed by known techniques from available starting materials. Surface area shall be characterized by standard methods, as BET analysis. The performance of these electrodes shall be compared with that of the gold in Task 1, in free electrolyte. These tests shall be performed in the same pyrex cells as defined in Task 1.

3. Three types of membranes for use in the full cell tests of Task 5 shall be constructed. The first type shall be flexible and constructed from mat material, as zirconia felt. The second shall be rigid, cold pressed, partially sintered membranes constructed from materials such as alumina. These first two type of membrane shall be infiltrated with electrolyte. The third kine of membrane shall be hot-pressed membrane/electrolyte structures produced from mixed powders.

4. The capacity for NO_x removal shall be tested in the free electrolyte identified in Task 1. Gas consisting of NO_x, N_2 and O_2 with concentrations similar to that in flue gas shall be bubbled past the working electrode in the electrolyte. The effluent gas, in both anodic and cathodic polarization, shall be tested for NO_x content. The first tests shall be on gold electrodes. Further tests shall be on the electrodes identified in Task 2. Finally, tests shall be performed using gas containing, in addition, sulfur dioxides and CO_2 consistent with flue gas. Measurement shall be made of simultaneous NO_x and SO_x removal as a function of applied current.

5. Full-cell tests shall be performed using machined Macor housings with membranes as identified in Task 3, impregnated with electrolyte defined in Task 1, contacted with electrodes as produced in Task 2. First tests of the full-cell shall be of steady state polarization and SO_2 removal performance as a function of applied current. The gases used in these tests shall be simulated flue gas without NO_x or fly ash. The final testing shall be performed using simulated flue gas, with SO_2 and NO_x, but without fly ash.

EXPERIMENTAL

The electrochemical cells, equipment, and experimental procedures used in the investigations are described in this section. Subsections correspond to the Tasks outlined in the Statement of Work.

1. Free Electrolyte:

A schematic of the overall system is shown in figure 1. The system can be broken down into three basic catagories, electronic equipment, gas handling and analysis, and the furnace/electrochemical cell.

A PAR-371 Potentiostat/Galvanostat with a model 178 electrometer probe was used in most experiments to control the overall cell potential, the potential of either electrode with respect to the reference electrode, or the cell current. For studies of transient cell behavior a Hewlett Packard model 3310B function generator was utilized. In cyclic voltammetry experiments a PAR 273 poentiostat with automatic IR compensation was employed. All potentials of interest were monitored with Simpson model 460 digital multimeters. During transient experiments, the cell behavior was monitored and recorded by either a Hewlett Packard #7015B x-y plotter or a Tektronix model 5111 storage oscilloscope with a 5BION time amplifier and a 5A19N differential amplifier.

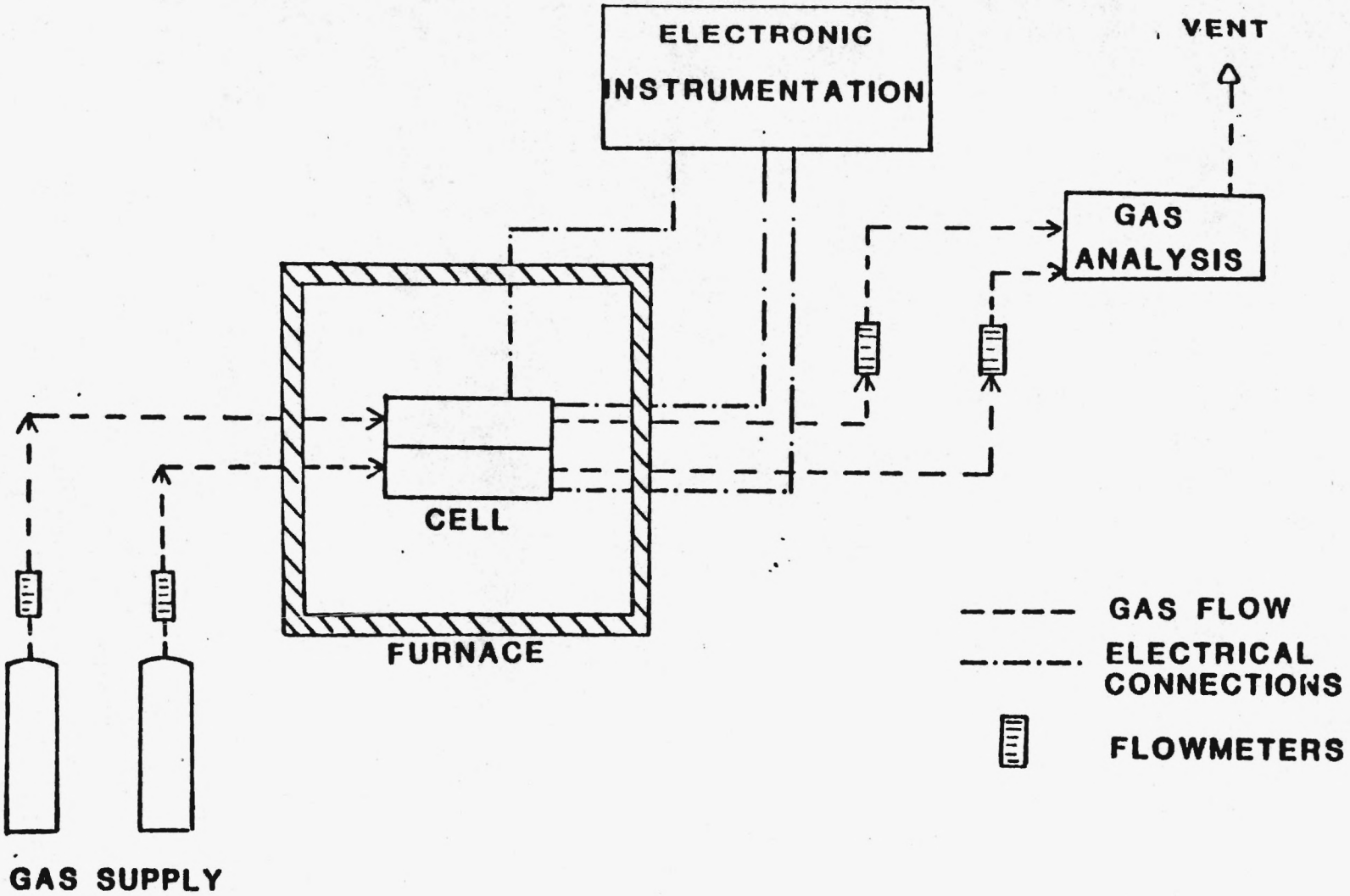

Figure 1. Schematic of Experimental Apparatus

Gases were all premixed primary standard grades supplied by Matheson. From the cylinders the gases flowed to a metering panel, then to the cell, back to the metering panel and finally to a fume hood. The connections were all made of 1/4 inch stainless steel and Tygon tubing. The flows were controlled by either Matheson 600 series flowmeters or a Matheson model 8259 electronic flow controller with model 8141 flow transducers. Sample ports were provided on the inlet and outlet lines to allow syringe removal of samples for gas analysis. A Hewlett Packard model 5840A programmable gas chromatograph with a thermal conductivity detector and a flame photometric detector was used to analyze the gases.

The furnace was custom built, with temperatures controlled to within $\pm 5^{o}C$ by a double-pole solenoid relay connected to a Barber Coleman #122-B temperature controller. All electrodes within the cells were planar gold foils of known area with exception to the thermodynamic reference. The thermodynamic reference was always a silver wire immersed in a $AgNO_3/KNO_3$ melt contained in a sealed pyrex capsule. The cell housings, described in the proceeding paragraphs, were all built in the Georgia Tech Chemistry Department Glass Blowing Shop. The electrolytes consisted of Baker standard laboratory grade reagents.

Figure 2 shows the cell configuration used in the thin-film experiments. It consists of a beaker-like pyrex container with a lid designed to allow gas flow into the environment above the melt. The cell used in the chronoamprometry experiments is

depicted in figure 3. This cell is similar to the previous one except a different lid, designed to hold the electrodes in bulk molten electroyte, with provisions for gas bubbling into the melt, was used. Figure 4 displays the cell employed for effluent analysis tests. This cell emphasizes gas-tight compartments for both the anode and cathode gases. Gases are bubbled through the electrolyte past the working and counter electrodes. A glass frit separates the compartments but allows ions to migrate. Figure 5 shows the cell used in the cyclic voltammetry experiments. The housing is a large test-tube like vessel. A four electrode arrangement, including a quasi-reference made of gold foil, was employed to allow the ohmic resistance to be easily measured. The pyrex capsule has a high impedance, so the thermodynamic reference alone made measurement of the ohmic resistance difficult.

2. Electrode Development

The perovskite material is made by the following procedure:

1. Mix stoichiometric quantities of the metal acetates.
2. Ball-mill for 8 to 10 hours.
3. Bake for one hour at each of the 5 consecutive temperatures; 140^{o}C, 180^{o}C, 210^{o}C 240^{o}C and 275^{o}C (in air).
4. Let cool slowly.
5. Ball-mill for one hour.
6. Sinter at 1100^{o}C overnight.
7. Cool slowly and then grind to obtain the final perovskite powder.

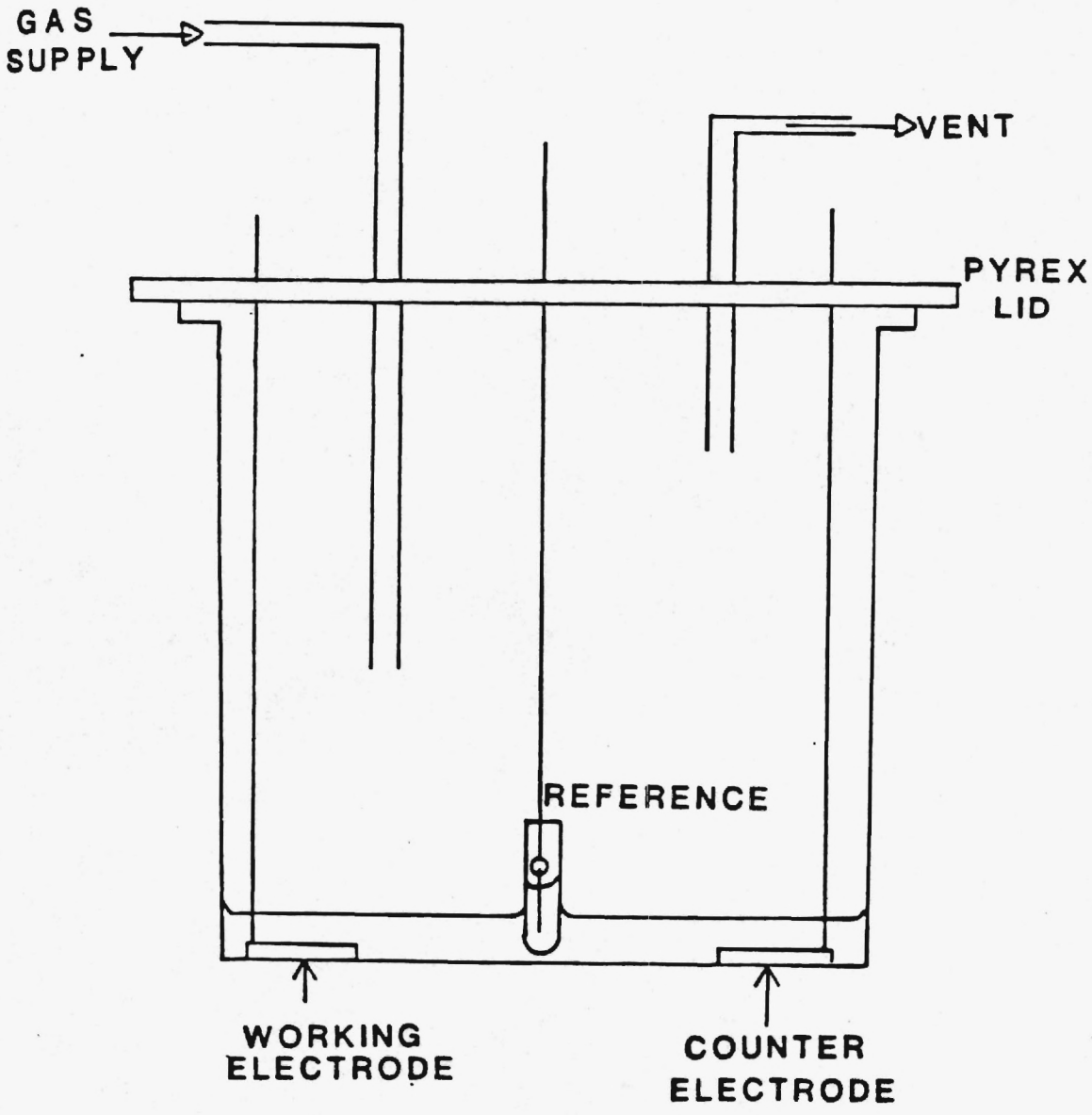

Figure 2. Cell For Thin Electrolyte Film Experiments

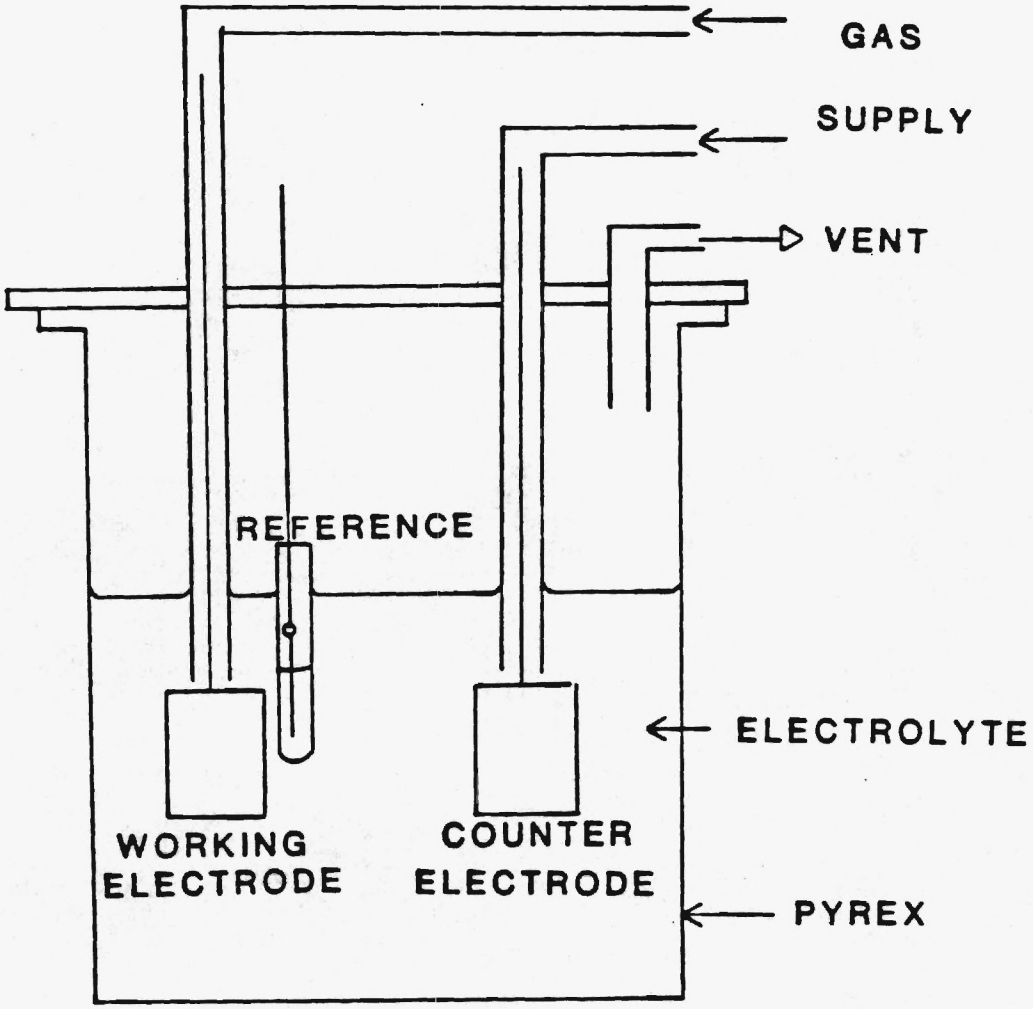

Figure 3. Cell for Potential Step and Cyclic Voltammetry Experiments

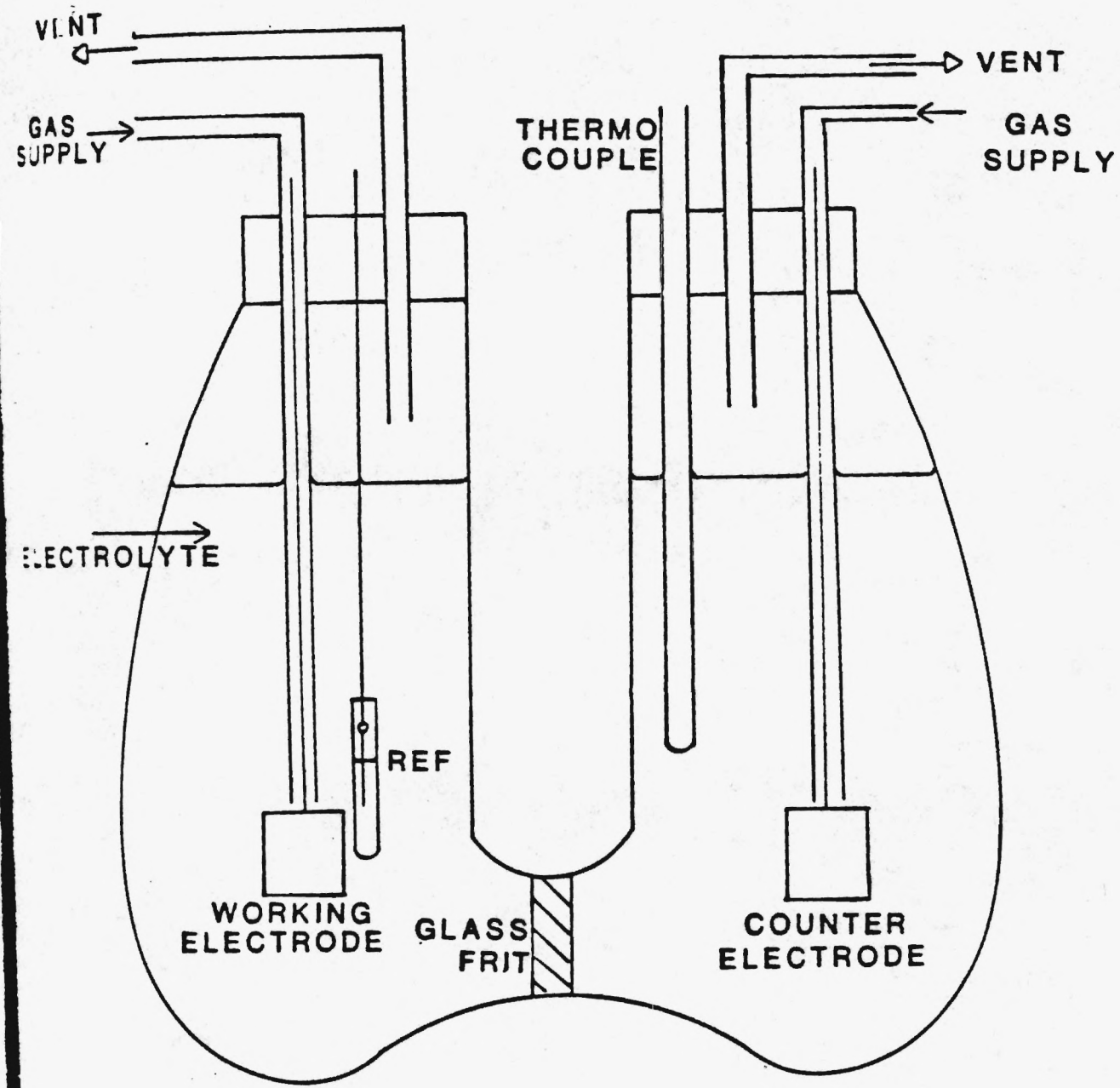

Figure 4. Gas-Tight Cell For Effluent Analysis

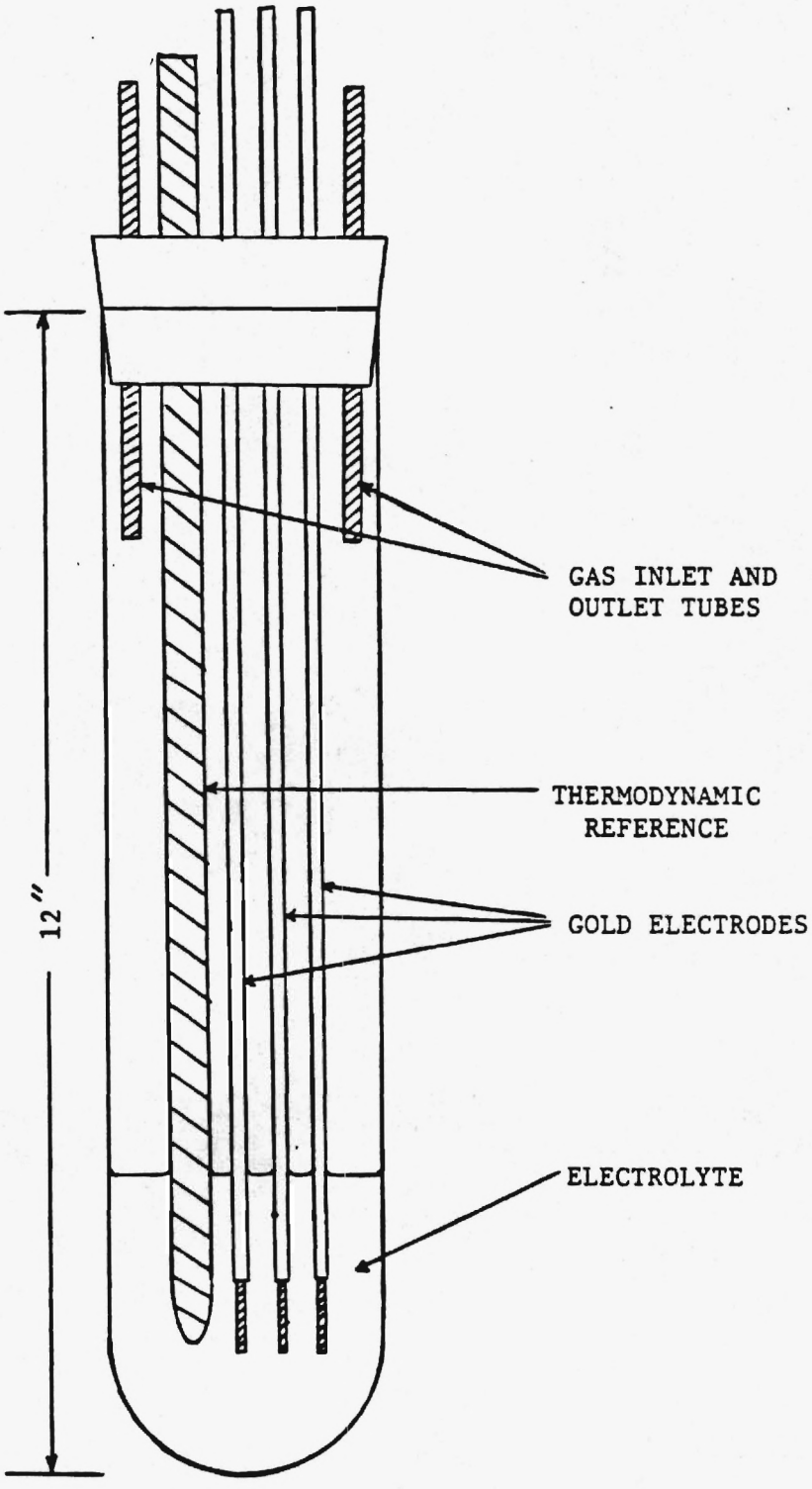

Figure 5. Cell used in Cyclic Voltammetry

3. Ceramic Membrane Development

The ceramic membrane is a homogeneous mixture of electrolyte and matrix materials, the matrix holding the electrolyte within by capillarity. These procedures were followed in fabricating the membranes.

a. Impregnation of Commercial "Matrices"

In this procedure materials made commercially, such as zirconia felt or fritted pyrex discs, are impregnated with electrolyte. The matrix is contacted with a reservior of electrolyte, drawing it into the matrix by capillary forces.

b. Impregnation of Constructed Matrices

This method is quite similar to (a) except that the matrix is constructed here. A ceramic material, such as SiC, $SrTiO_3$ or MgO is pressed in a die under high pressure and then partially sintered to form a porous matrix. Fillers, such as methylcellulose, are added to the ceramic prior to sintering to enhance porosity. Then, as above, the matrix is impregnated with electrolyte to form the ceramic membrane.

c. Hot Pressing

Here, a mixture of electrolyte and matrix powders are thoroughly mixed by ball-milling. The mixture is measured into a die and heated to 200^{o}C for one hour to drive off any adsorbed water. The die is then pressed under 10,000 lb

pressure, placed in an oven and heated to within 2°C of the electrolyte melting point, then repressed under high pressure to produce the final membrane.

The fabricated membranes were initially assessed on the basis of strength and density. Membranes which satisfied these criteria were tested for conductivity at elevated temperature and also examined by x-ray diffraction to discern whether the matrix was stable in contact with the electrolyte. Finally, membranes which met all requirements were stored for use in full cell tests.

4. NO_x Removal

The procedures followed in these experiments mirrored the effluent analysis experiments described earlier. The cell employed is shown in figure 4. The NO_x-containing gas was bubbled through the electrolyte past the cathode. The concentration of NO_x in the inlet and outlet streams were monitored with a Thermo Electron Model 10 Chemiluminescent NO_x analyzer as a function of gas flowrate and applied current.

5. Full Cell Tests

A schematic of the assembled cell is shown in figure 6. The ceramic membranes used in full cell test were fabricated according to task 3. Various electrode materials were tested, in addition to perovskite (task 2), porous carbon, porous nickel, and gold screen were all used in full cell experiments. During

operation the concentration of SO_2 in all streams was monitored s a function of the applied current. Post mortem tests included x-ray diffraction of cell components and visual observation concerning electrolyte drainage from the membrane and pore flooding in the electrodes.

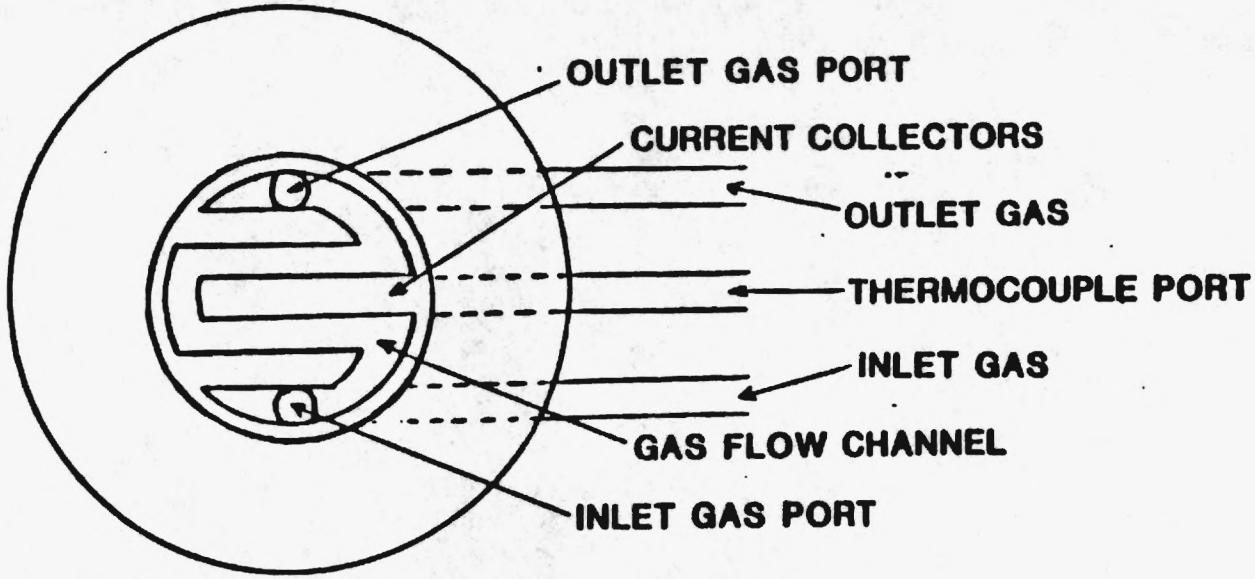

ASSEMBLED CELL

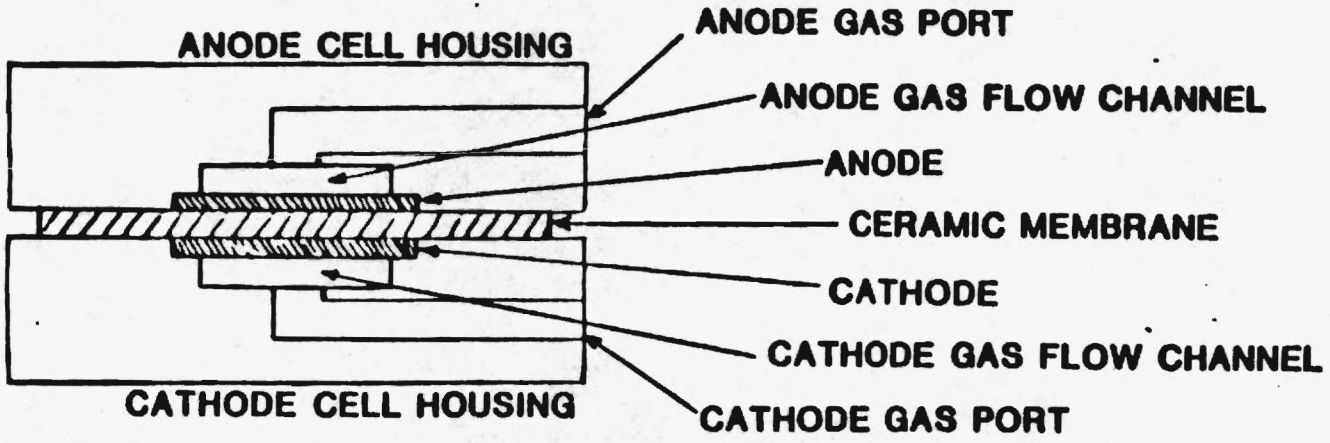

Figure 6. Schematic Of Cell Used In Full Cell Tests

RESULTS/DISCUSSION

The results are broken down into section corresponding to the Tasks outlined earlier. The first section examines the results of free electrolyte testing. The second and third sections are devoted to results which examine the development of the electrodes and ceramic membrane respectively. In section four the results of NO_x removal is free electrolyte are reported. The final section deals with full-cell testing results.

TASK 1 FREE ELECTROLYTE TESTING

a. Stability and Melting Point

Several electrolyte composition were tested for melting point and stability. The results were summarized in Table 1. Previous work by Townley [12] and Cheng [13] utilized sulfate and bisulfate melts respectively; the melting points and stability limits were re-examined, and are presented here for the sake of completeness. The data show that the alkali pyrosulfates ($M_2S_2O_7$) represent an intermediate-melting group of compounds whose stability increases in the order: lithium-, sodium-, potassium-pyrosulfate. According to Spitsyn [14] this is because the polarizing effects of the cation upon the anion progressively diminishes as the ionic radius of the cation increases.

Table 1. Melting Point and Stability Analysis of Candidate Electrolytes

Electrolyte	Melting Point (°C)	Stability
$K_2S_2O_8$	100	Decomposition begins <100°C
50% $KHSO_4$, 50% $NAHSO_4$	125	Decomposition begins 180°C
$NaHSO_4$	180	Decomposition begins 180°C
$KHSO_4$	210	Decomposition begins 200°C
$Li_2S_2O_7$	210	Decomposition begins near m.p.
85% $K_2S_2O_7$, 15% $Na_2S_2O_7$	260	Decomposition begins 300°C
10% V_2O_5, 90% $K_2S_2O_7$	280	Decomposition begins 380°C
1% V_2O_5, 99% $K_2S_2O_7$	290	Decomposition begins 380°C
$K_2S_2O_7$	310	Decomposition begins 360°C
75% $K_2S_2O_7$, 40% K_2SO_4	320	Decomposition begins 370°C
60% $K_2S_2O_7$, 40% K_2SO_4	330	Decomposition begins 370°C
$Na_2S_2O_7$	410	Decomposition begins 300°C
17% K_2SO_4, 11% Na_2SO_4, 72% Li_2SO_4	510	stable*
37% $K_2S_2O_7$, 63% Li_2SO_4	530	Decomposition begins 320°C
Li_2SO_4	830	stable*
Na_2SO_4	860	stable*
K_2SO_4	1000	stable*

* Stable to 1000°C

As discussed earlier, the flue gas leaving the economizer in a power plant is at approximately 300°C, making this the optimal operating temperature. On the basis of the information in Table 1, pure potassium pyrosulfate and mixtures of potassium pyrosulfate with vanadium pentoxide are most attractive. Vanadium pentoxide was chosen as an additive because of its catalytic properties in the oxidation of SO_2. It also lowers the melting point of the electrolyte mixture. In addition to suitable melting and stability characteristics, potassium pyrosulfate is also widely available and relatively inexpensive.

b. Thin Film Experiments

Polarization data were taken for a system consisting of planar gold electrodes covered by a molten electrolyte film of variable thickness exposed to an atmosphere of variable gas composition. Figure 7 shows a representative set of these data. The abscissa shows the potential of the working electrode with respect to the reference electrode.

Using this information the limiting current for a given set of conditions can be estimated. Table 2 shows the relationship found between the limiting current density, type of electrolyte, and film thickness. It is clear that the limiting current is not significantly influenced by either a change in environment or a change in film thickness. This strongly suggests that no reactants of the electrochemical reactions taking place are supplied by the gaseous phase. In other words, the predominant electrode reactions involve direct oxidation and reduction of a

species originally in the liquid phase, and the current is probably limited by diffusion of the products away from the electrodes.

Similar experiments by Shores and Fang [15] with a Na_2SO_4 melt show a tenfold increase in limiting current with a corresponding tenfold decrease in film thickness, and a market effect of gs composition on the limiting current. These authors eliminate a number of reduction reaction possibilities by showing that an unreasonable value of the diffusion coefficient, D (calculated by assuming a stagnant film: $D = i_L \delta/nFC$) would be required for the experimental data to be consistent. In the present work, certain reactions can also be eliminated by showing that unrealistic values of the diffusion coefficient would be required. The solubilities of K_2SO_3, K_2O_2, and KO_2 were calculated from thermodynamic stability data assuming ideal solution behavior [16]. Then values of D, required if any of these species were the active ones, were calculated for the case of a 2.6 m film of $K_2S_2O_7$ electrolyte with a 10% SO_2, 20% O_2, 70% N_2 gas environment. The results are shown in Table 3. The calculated diffusivities are clearly unreasonably large, eliminating the indicated reactions. On the other hand, if the active species is assumed to be the potassium pyrosulfate, and the diffusion distance is taken to be the electrode separation (6 cm), a required diffusivity of 1.9×10^{-5} can be calculated. This is quite feasible and suggests that the pyrosulfate may be the electroactive species.

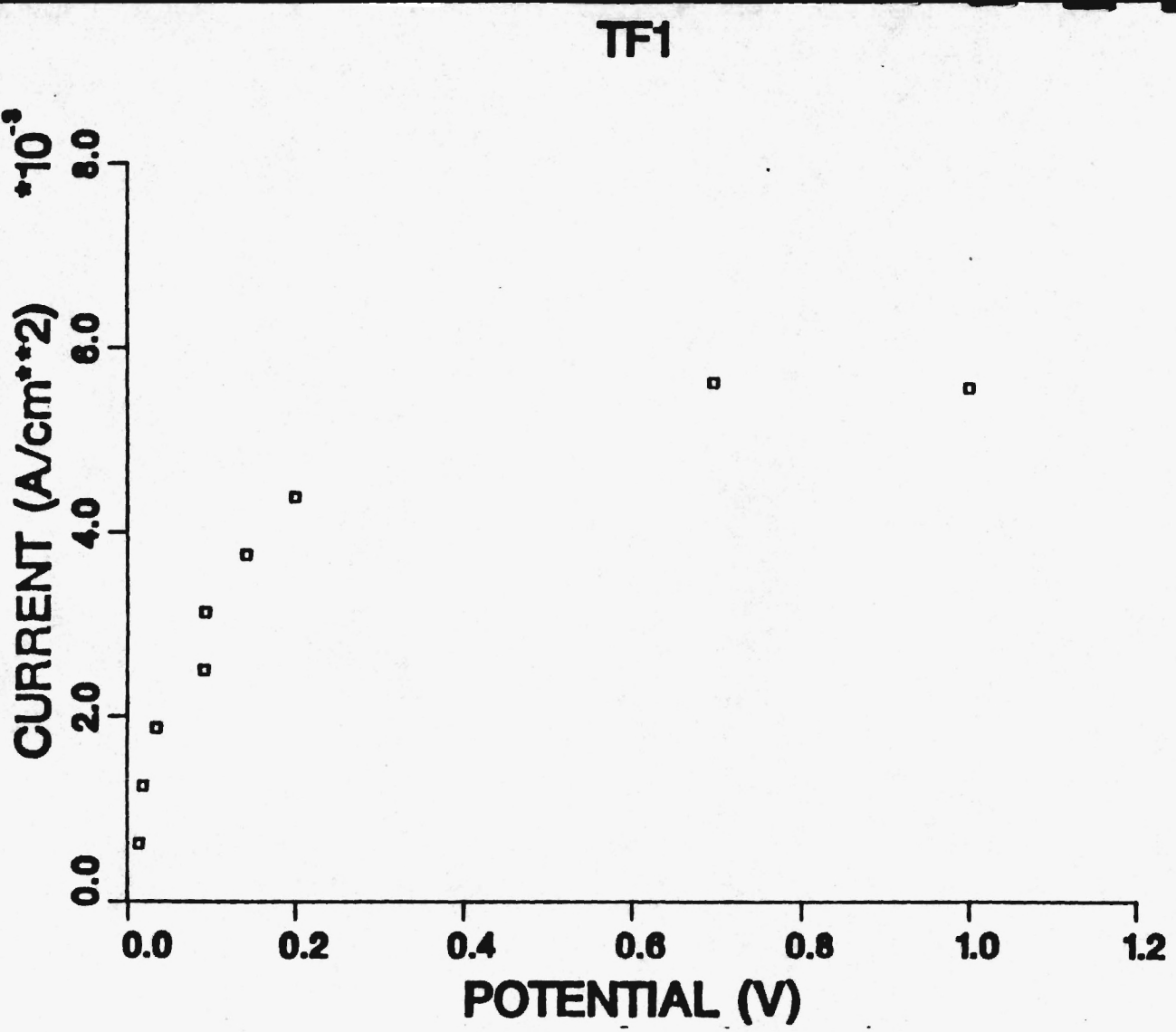

Figure 7. Polarization Data for a 1.1 mm Film of $K_2S_2O_7$ in Air.

Table 2. Limiting Currents from Thin Film Polarization Data

Electrolyte*	Film Thickness (mm)	Gas Environment**	i_L (A/cm^2)
$K_2S_2O_7$	1.1	Air	0.00575
$K_2S_2O_7$	1.3	Air	0.00688
$K_2S_2O_7$	1.3	10% SO_2, 20% O_2 70%N_2	0.00813
$K_2S_2O_7$	2.6	N_2	0.00538
$K_2S_2O_7$	2.6	Air	0.00525
$K_2S_2O_7$	2.6	10% SO_2, 20% O_2, 70% N_2	0.00688
10% V_2O_5, 90% $K_2S_2O_7$	1.1	Air	0.00813
10% V_2O_5, 90% $K_2S_2O_7$	1.3	N_2	0.00625
10% V_2O_5, 90% $K_2S_2O_7$	1.3	10% SO_2, 20% O_2, 70% N_2	0.00613

*Electrolyte compositions in weight percent

**Environment compositions in volume percent

c. Chronoamperometry

Figure 8 shows an example of the original oscilloscope photographs recording the current decay after an applied cathodic and anodic overpotential step. Current versus time data is taken by hand from these oscilloscope photographs. Non-linear computer regression is then used to fit the data to Equation (13).

$$i = (w/t_2\lambda^2)\{\exp(\lambda^2 t)\mathrm{erfc}(\lambda t^{\frac{1}{2}}) + 2\lambda(t/\pi)^{\frac{1}{2}} - \exp[\lambda^2(t-t_2)]\mathrm{erfc}[\lambda(t-t_2)^{\frac{1}{2}}] - 2\lambda[t-t_2)/\pi]^{\frac{1}{2}}\} \quad (\text{for } t > t_2) \qquad (13)$$

The value of t_2 was taken to be 10 msec which, according to the criteria presented by Nagy [17], eliminates more than 99% of the error associated with the assumption of no capactive current required to obtain Equation (13).

The parameters W and λ were determined for cathodic potential steps of 25, 50, 75, 100, 150, 200, 250 and 300 mV. The calculated curves and experimental data are shown in Figures 9 to 16. The quality of the fit decreases as the potential step is increased. This is to be expected because for the larger potential step experiments the assumption of a linear relationship between the faradaic current density and the overpotential becomes less accurate.

Table 3. Diffusivities Calculated from Limiting Reduction Current Densities in $K_2S_2O_7$ in 10% SO_2, 20% O_2, 70% N_2

Possible Reaction	Concentration of Active Species	Diffusivity Required
	mol/cm^3	cm^2/sec
$SO_3^{2-} + 6e = S^{2-} + 3O^{2-}$	1×10^{-12}	3×10^{3}
$O_2^{2-} + 2e = 2O^{2-}$	$\sim 10^{-20}$	9×10^{11}
$O_2^{-} + 3e = 2O^{2-}$	$\sim 10^{-21}$	6×10^{12}

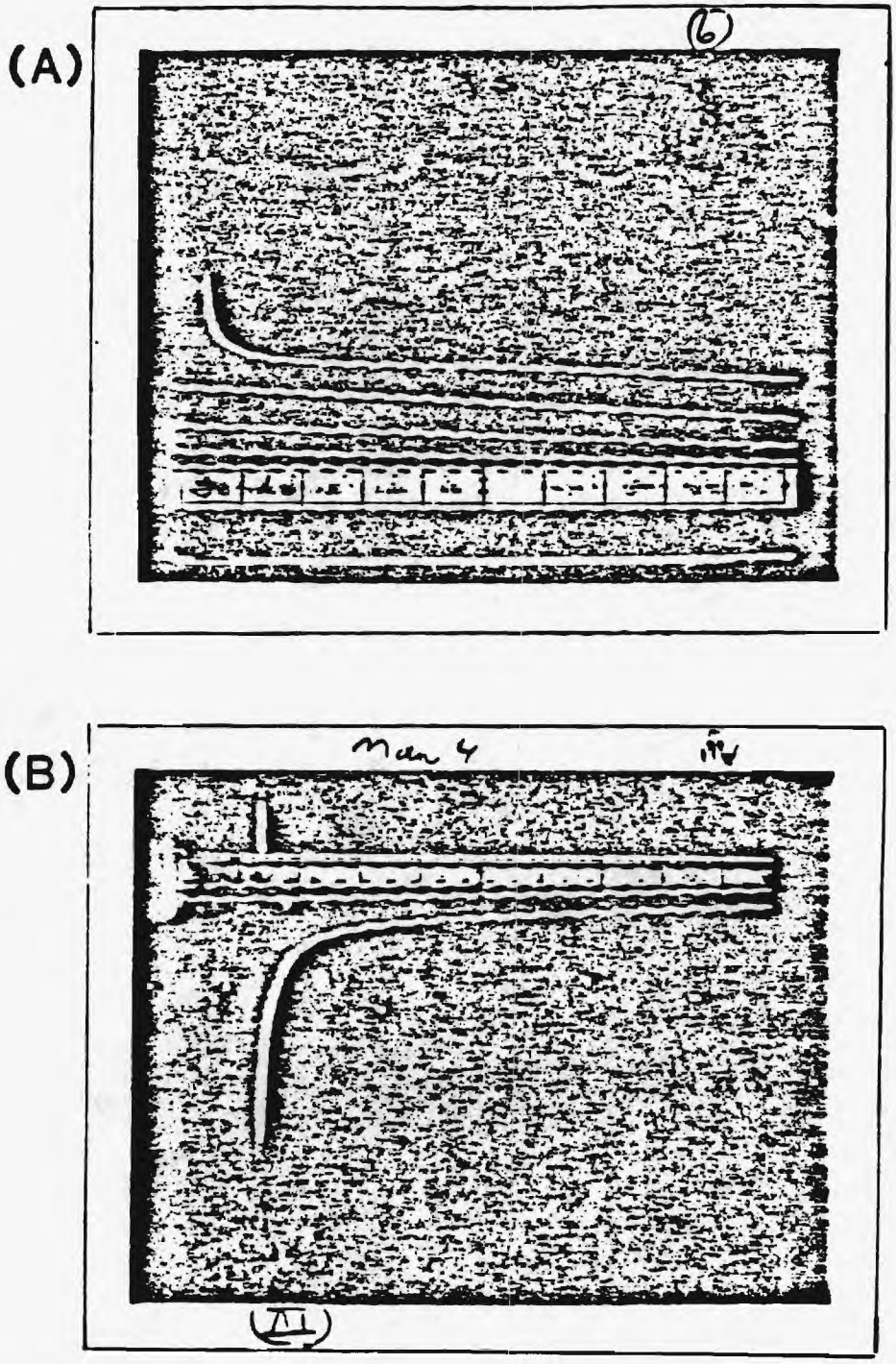

Figure 8. Examples of Original Oscillographs After Applied Cathodic (A) and Anodic (B) Over-potential Step.

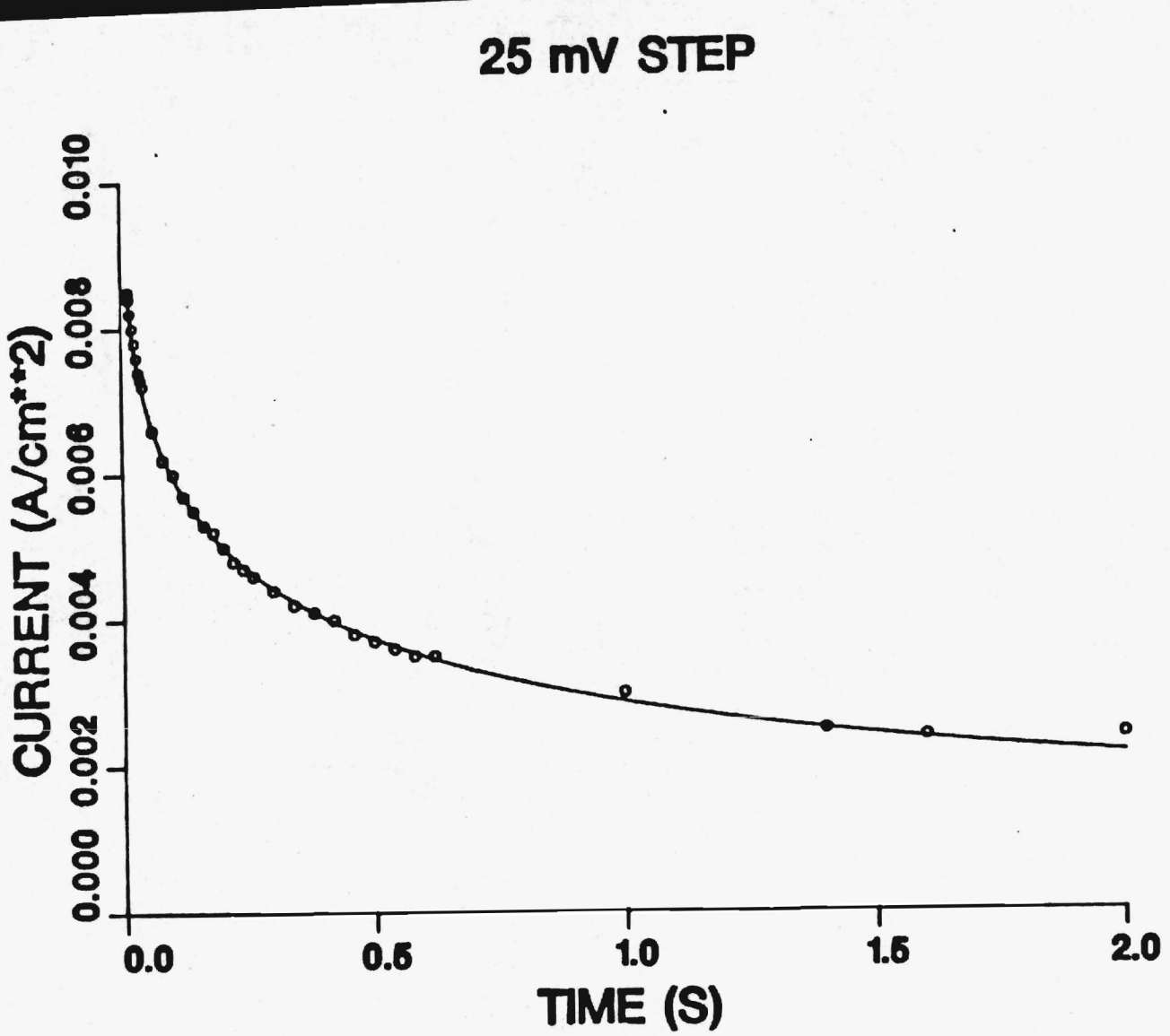

Figure 9. Cathodic Current Decay After 25 mV Cathodic Step.

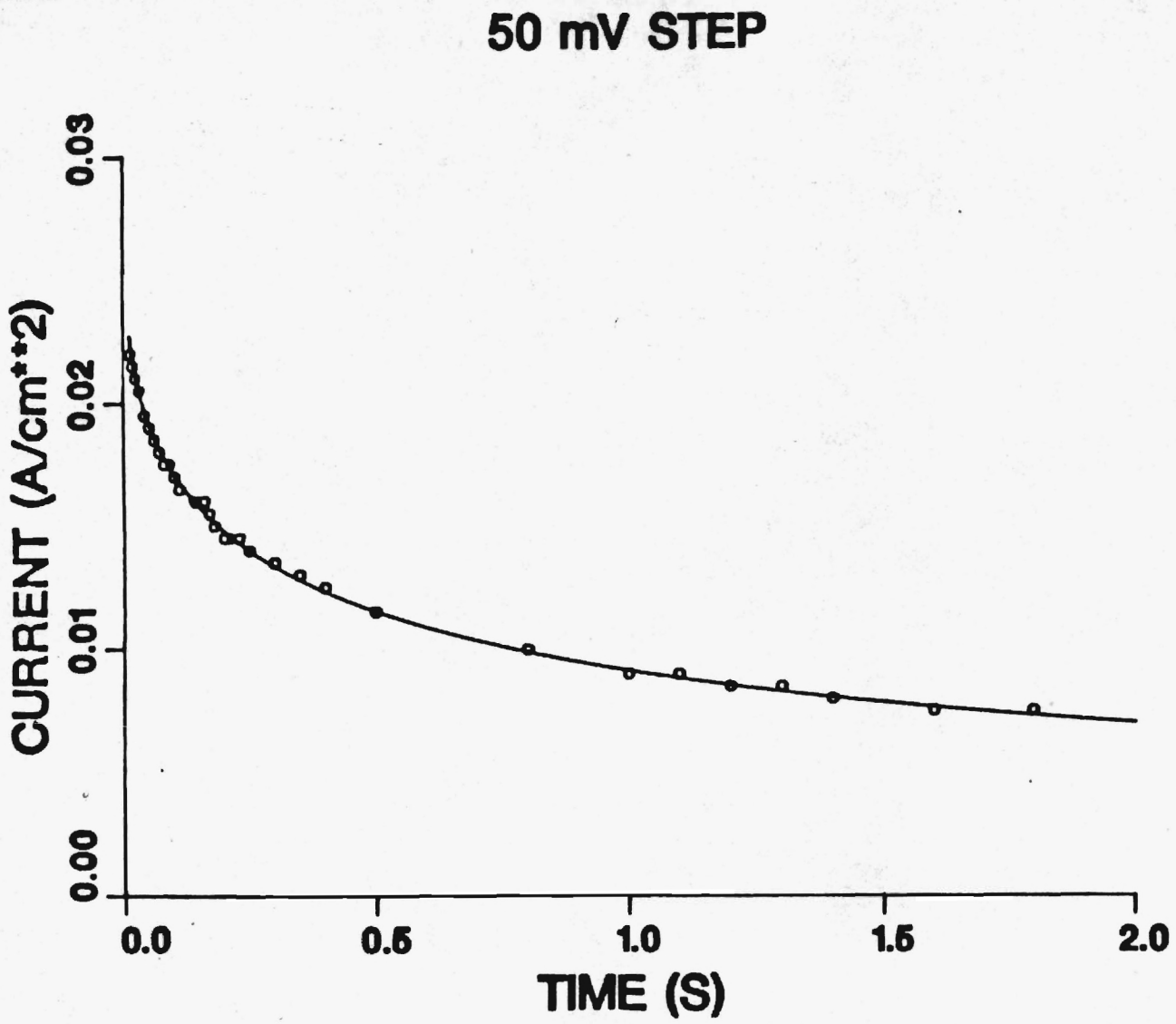

Figure 10. Cathodic Current Decay After 40 mV Cathodic Step.

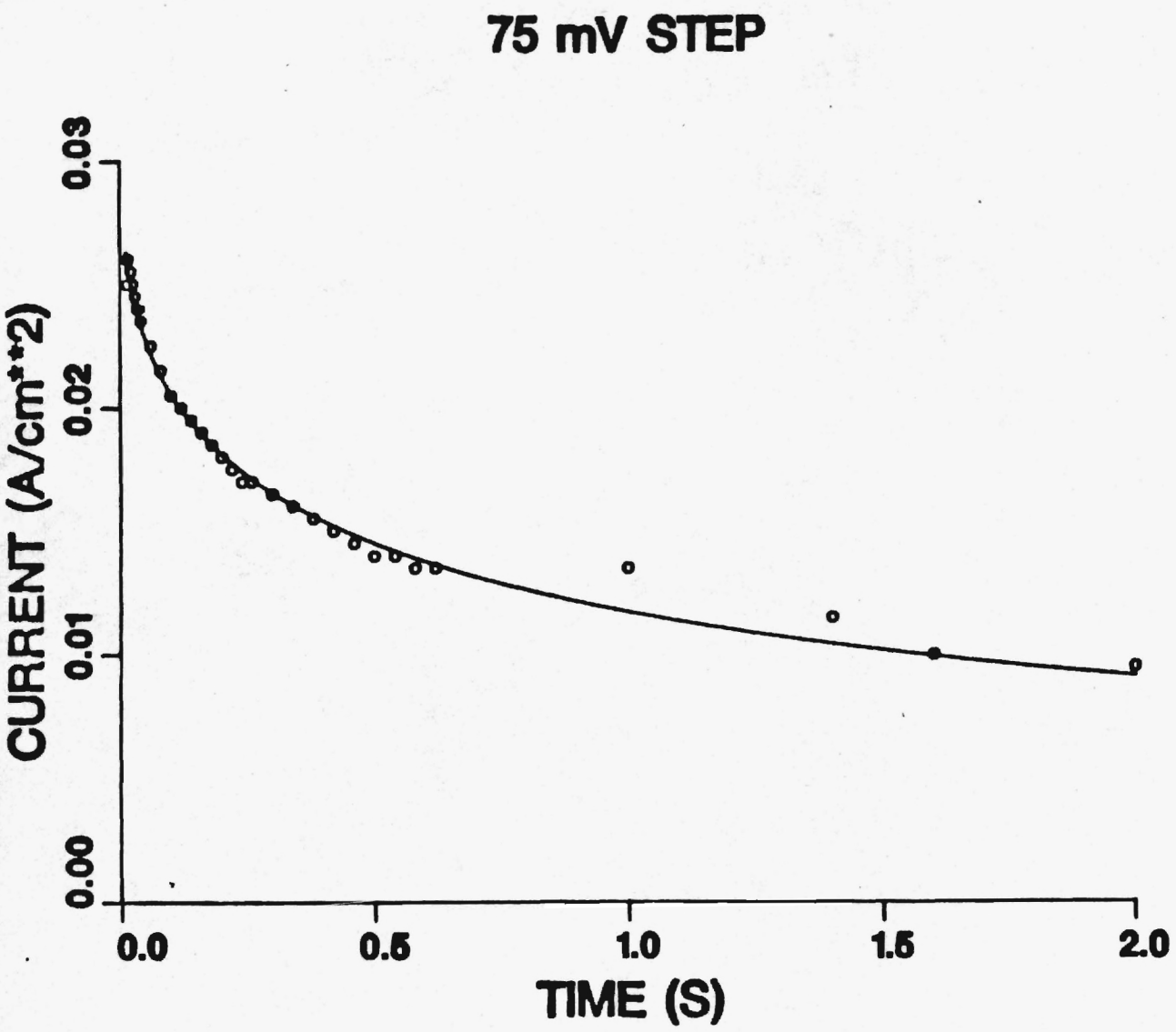

Figure 11. Cathodic Current Decay After 75 mV Cathodic Step.

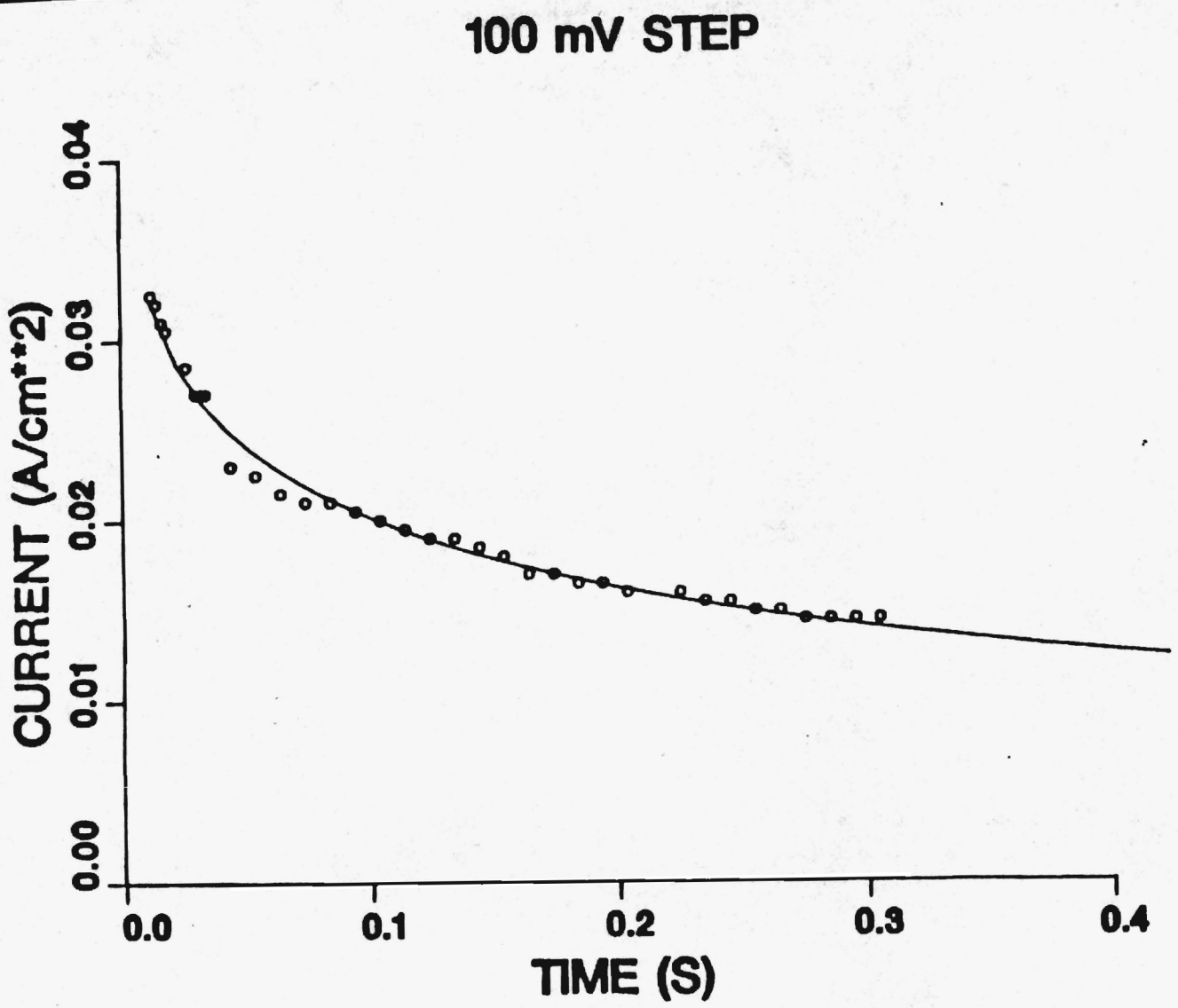

Figure 12. Cathodic Current Decay After 100 mV Cathodic Step.

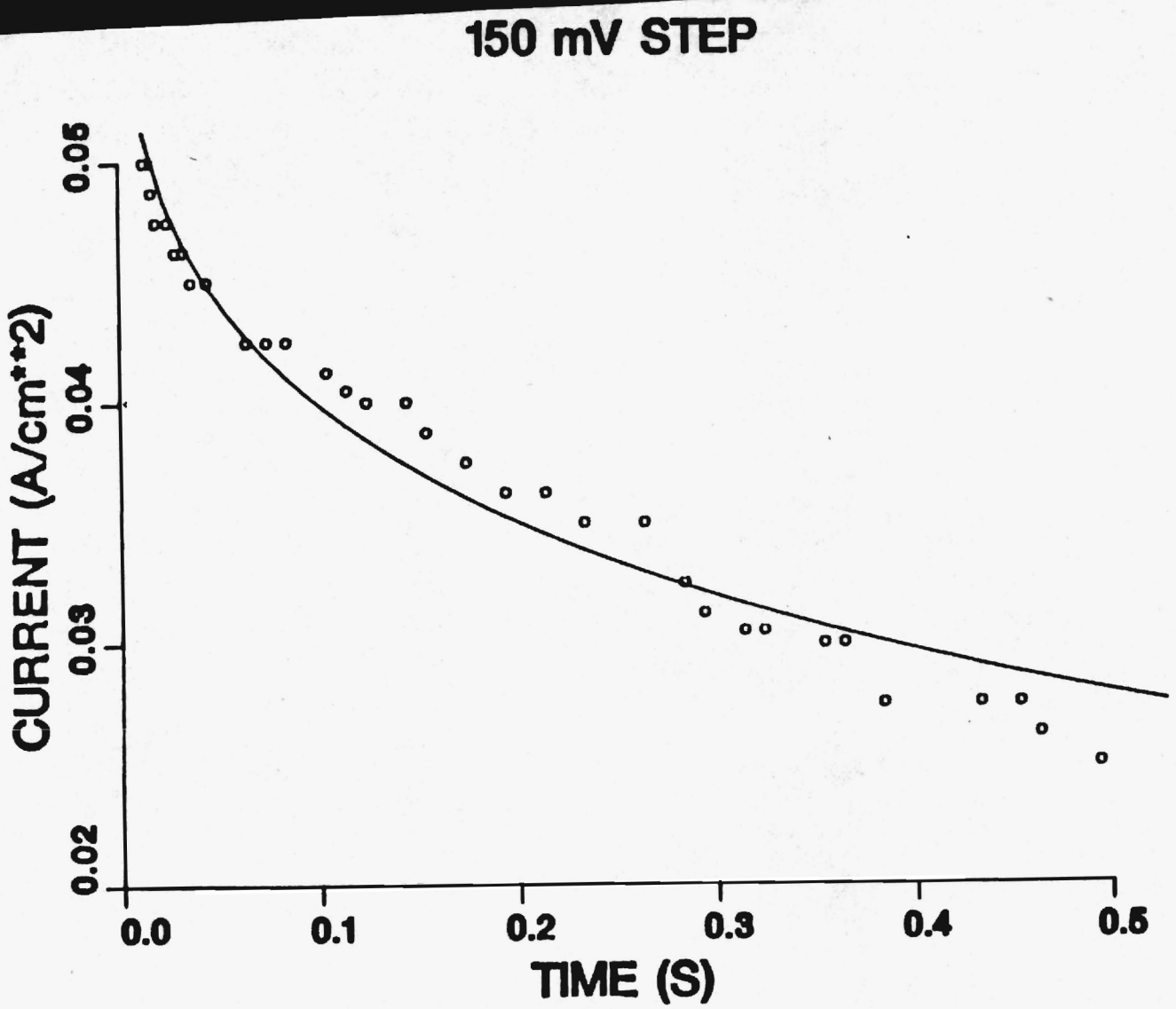

Figure 13. Cathodic Current Decay After 150 mV Cathodic Step.

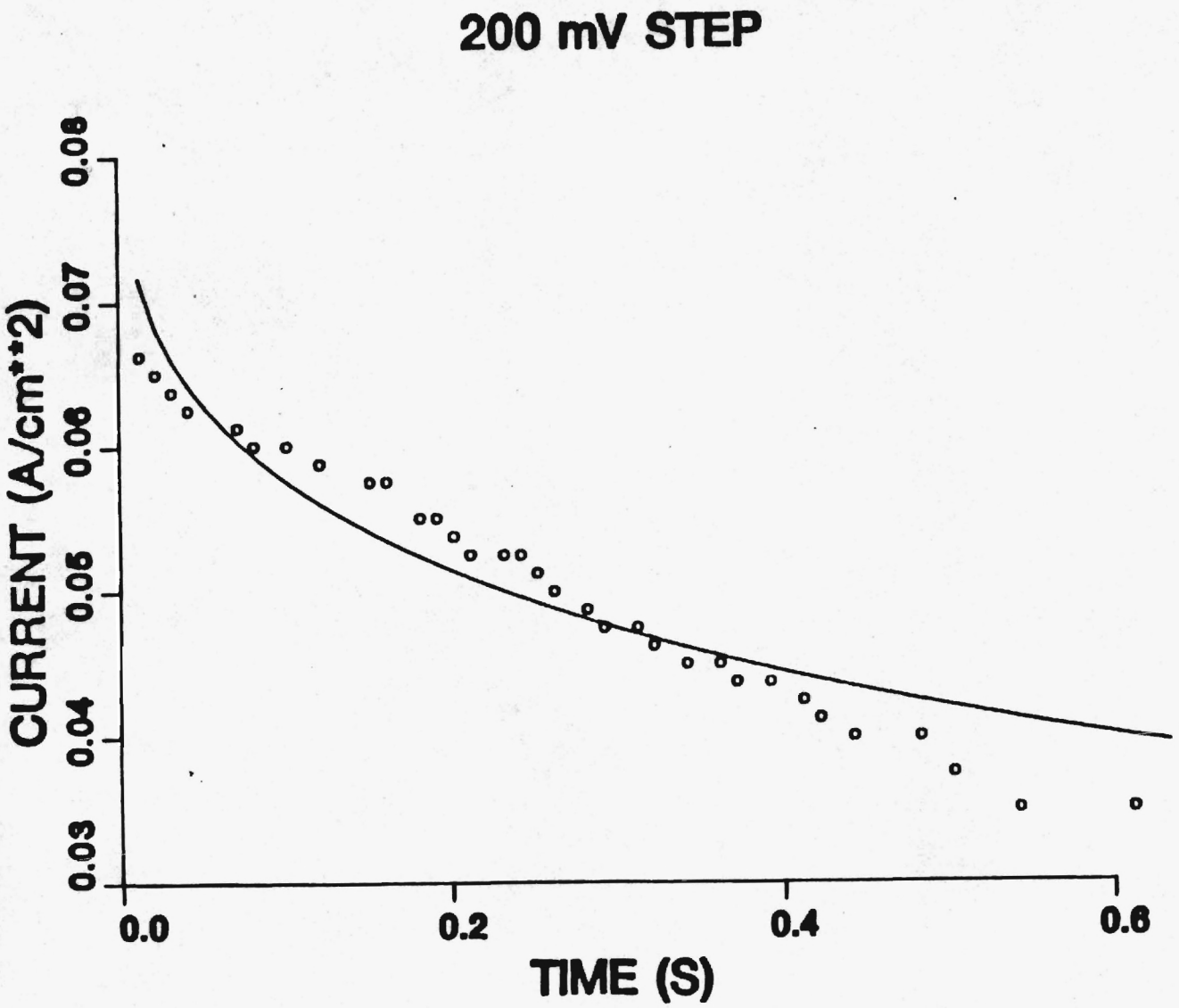

Figure 14. Cathodic Current Decay After 200 mV Cathodic Step.

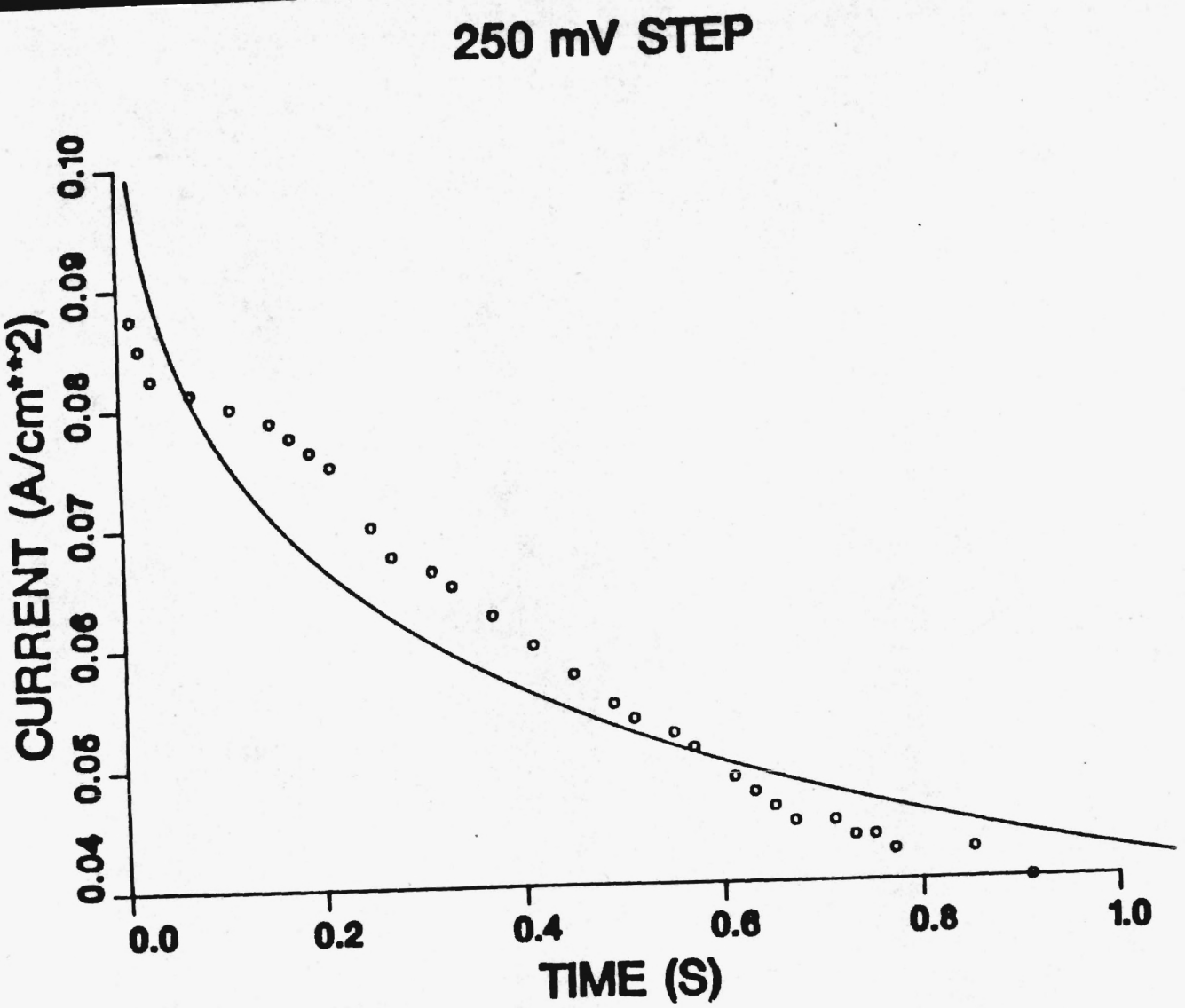

Figure 15. Cathodic Current Decay After 250 mV Cathodic Step.

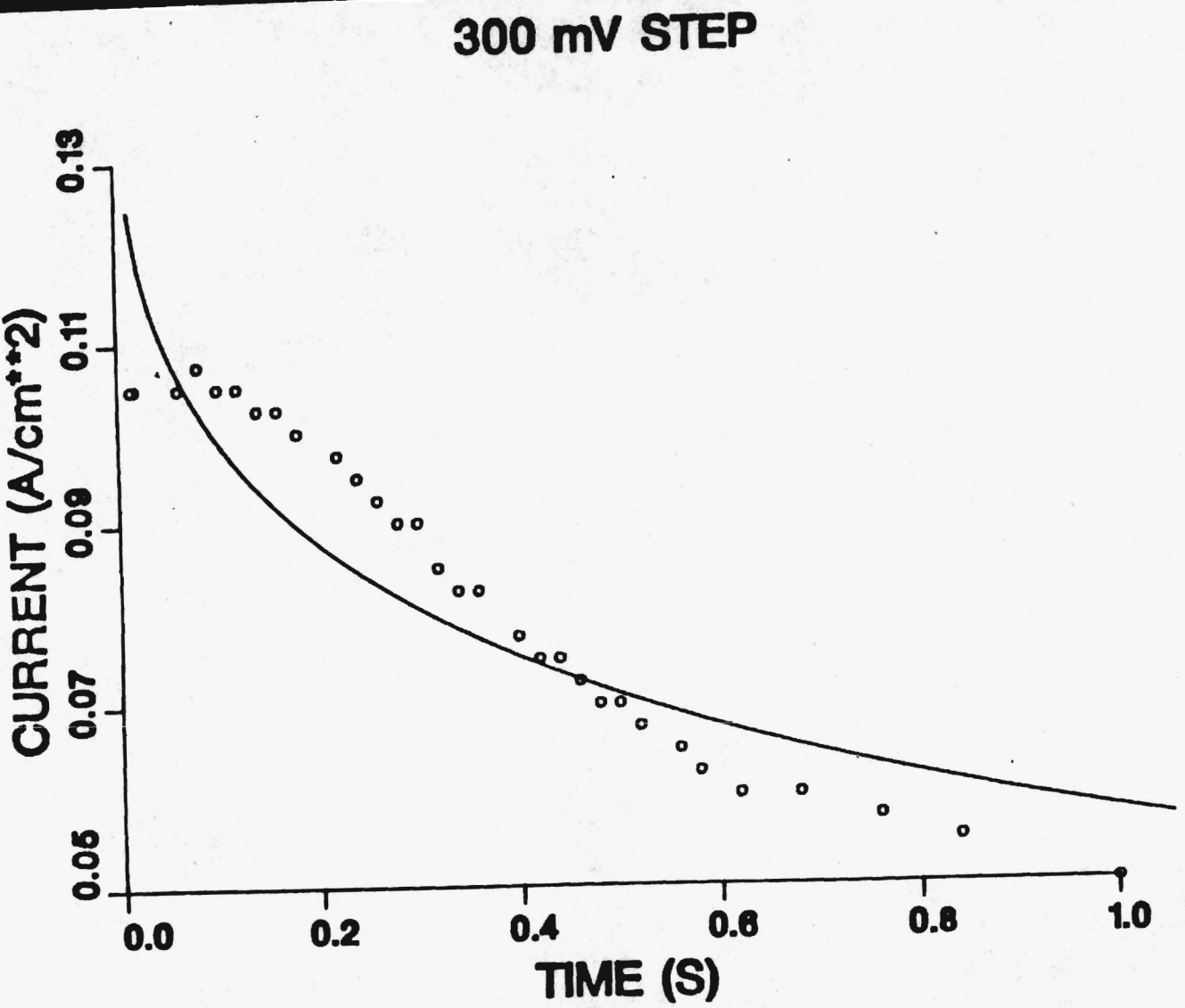

Figure 16. Cathodic Current Decay After 300 mV Cathodic Step.

Table 4. Parameters Obtained by Fitting Cathodic Potential Step Data in 1% V_2O_5 - 99% $K_2S_2O_7$ at 340°C

Potential Step (V)	W (A/cm^2)	($S^{-1/2}$)	i_o (A/cm^2)	$\left(\frac{1}{D_O^{1/2}C_O} + \frac{1}{D_R^{1/2}C_R}\right)$ $\left(\frac{S^{1/2}cm^2}{mole}\right)$
0.025	0.0099	1.718	0.0264	3.09×10^7
0.050	0.0209	1.240	0.0300	2.23×10^7
0.075	0.0290	1.092	0.0249	1.96×10^7
0.100	0.0392	2.365	0.0262	4.25×10^7
0.150	0.0567	1.120	0.0236	2.01×10^7
0.200	0.081	1.093	0.0279	1.97×10^7
0.250	0.110	1.172	0.0349	2.11×10^7
0.300	0.139	1.074	0.0391	1.93×10^7

The exchange current density, i_o, may be calculated. The value of the solution resistance, R_s, was found by an independent AC technique to be approximately 1.5 ohms. Table 4 summarizes the values of W and λ obtained from each cathodic potential step. It also shows the value of i_o and $\frac{1}{D_O^{\frac{1}{2}} C_O} + \frac{1}{D_R^{\frac{1}{2}} C_R}$. The average value of the cathodic exchange current density is 0.029 + 0.005 A/cm^2. The average value of the concentration and diffusion term is $2.4 \times 10^7 \pm 0.8 \times 10^7$ $S^{\frac{1}{2}}$ cm^2/mol. From the thin film results presented earlier, the species being reduced is potassium pyrosulfate and C_o = 0.01 $mole/cm^3$. By substituting reasonable values for the diffusivities (2×10^{-5} cm^2/sec), C_R can be estimated to be 9×10^{-6} $mole/cm^3$. The concentration of sulfate ion in the melt may be calculated by considering the equilibrium reaction

$$K_2S_2O_7 = K_2SO_4 + SO_3 \qquad (14)$$

The equilibrium constant at 340°C may be calculated using thermodynamic data to be 2.78×10^{-6}. If approximately 10% of the entering SO_2 is oxidized to SO_3 (as is shown later), the concentration of K_2SO_4 is equal to 28×10^{-6} $mole/cm^3$. This value is the same order of magnitude as that determined for C_R, and indicates that pyrosulfate is being reduced to form sulfate in the first electrochemical step.

d. Effluent Analysis

More insight can be gained on the reactions taking place by analyzing the gases leaving the cell. The sulfur content of the exit gas streams are examined, using a flame photometric detector, for relations between sulfur concentration, electrolyte composition and applied current. Table 5 shows the results for the following electrolyte compositions: pure $K_2S_2O_7$, 25 weight percent K_2SO_4 in $K_2S_2O_7$, and 40% K_2SO_4 in $K_2S_2O_7$. The operating temperature employed (340°C) sets a limit on the maximum sulfate concentration (40%) which can be tested.

In this set of experiments nitrogen is the working gas and is bubbled into the system at a flow rate of 40 cc/minute. Several observations can be made. First, at the cathode, the exit sulfur concentration increases with increasing current. This effect is most dramatic in pure $K_2S_2O_7$, where the exit concentration ranges from 23 ppm at open circuit to 910 ppm at 30 mA. Over a time period of several hours these results remained constant but they obviously cannot represent the true steady state values since more sulfur is leaving the system than is entering. The increased sulfur effluent with current indicates that an electrochemical reaction takes place at the cathode which produces either SO_2 directly or an intermediate product which then reacts to form SO_2. Similar results are seen in the full-cell tests, described later. Proposed reaction schemes are presented later.

Table 5. Effluent Gas Analysis. Gas to Cell is N_2.

I (mA)	[Pure $K_2S_2O_7$] Cathode Exit	[Pure $K_2S_2O_7$] Anode Exit	[25% K_2SO_4, 75% $K_2S_2O_7$] Cathode Exit	[25% K_2SO_4, 75% $K_2S_2O_7$] Anode Exit	[40% K_2SO_4, 60% $K_2S_2O_7$] Cathode Exit	[40% K_2SO_4, 60% $K_2S_2O_7$] Anode Exit
0	300 (23)	300 (23)	300 (23)	300 (23)	200 (20)	200 (20)
5	6800 (92)	1400 (44)	5700 (83)		5500 (81)	
10	32100 (282)	19000 (156)	23200 (184)	41800 (376)	25600 (208)	77200 (510)
15	74500 (486)	14800 (136)				
20	84000 (618)	26500 (214)	52100 (432)	72600 (475)	42900 (390)	94000 (677)
30	161000 (910)	32700 (290)				

At the anode, increased sulfur oxide concentration is also observed at higher currents, suggesting that the pyrosulfate is being reduced to form SO_2 or SO_3. Higher K_2SO_4 concentrations in the electrolyte cause a substantial rise in the exit sulfur concentration.

Table 6 shows the results of a similar set of experiments with a working gas of 0.3% SO_2, 3% O_2, 15% CO_2 and the balance N_2. Similar trends in exit sulfur oxide concentration are noticeable. At open-circuit there is significant sulfur dioxide absorption. The inlet gas stream contains 3000 ppm SO_2. With no applied current the exit concentration in pure $K_2S_2O_7$ is 2660 ppm. The open circuit SO_2 removal is slightly greater at higher sulfate concentrations which indicates that more SO_2 is adsorbed into molten sulfate than into pyrosulfate.

The gas analysis results examined to this point showed no reduction in the cathode SO_2 exit concentration when current is applied. Next the effect of adding V_2O_5 to the electrolyte will be reported. Table 7 shows the results for the following electrolyte compositions: pure $K_2S_2O_7$, 0.1% V_2O_5 in $K_2S_2O_7$, and 1% V_2O_5 in $K_2S_2O_7$. The working gas is 1% SO_2, 10% O_2 and the balance N_2, again the flow rate is 40 cc/minute, and the operating temperature is 340°C. At open circuit in pure $K_2S_2O_7$, 10% of the entering SO_2 is adsorbed, and the exit SO_2 concentration is 9000 ppm. As the percentage of V_2O_5 is increased the open circuit absorption of SO_2 is slightly enhanced. This is in agreement with other work in a V_2O_5 - $K_2S_2O_7$ melt [18]. Consistent with the data of Tables 5 and 6,

the cathode and anode exit SO_2 concentration in pure $K_2S_2O_7$ increases with higher currents. Again, at the anode pyrosulfate is being reduced to form SO_2.

A significant difference at the cathode is observed when the electrolyte is 1% V_2O_5 in $K_2S_2O_7$. The exit SO_2 concentration is measured at 8770, 8580, 8000, 7940, and 7940 ppm at 0, 5, 10, 20 and 30 mA respectively. A limit to the removal of sulfur dioxide with application of current is observed. This limit is equal to 9.5% removal and may either be due to mass transfer limitations or the kinetic limitations of some reaction step in the overall scheme. First, calculations will be made to determine the rate of SO_2 removal which can occur from the flue gas bubbles. The diameter of the bubbles is given by:

$$d_p = \left(\frac{6d_o\sigma g_c}{g\Delta\rho}\right)^{1/3} \tag{15}$$

Substituting $d_o = 4.76 \times 10^{-3}$ m, $\sigma = = 0.1$ N/m, $\Delta\rho = 2.5$ g/cm^3 yields

$$d_p = 4.9 \text{ mm} \tag{16}$$

The diffusivity of SO_2 in flue gas is estimated as:

$$D_G = 0.45 \text{ cm}^2/\text{sec} \tag{17}$$

Table 6. Effluent Analysis. 0.3 SO_2, 3% O_2, 15% CO_2, Balance N_2 to Cell.

I (mA)	[Pure $K_2S_2O_7$] Cathode Exit	[Pure $K_2S_2O_7$] Anode Exit	[25% K_2SO_4, 75% $K_2S_2O_7$] Cathode Exit	[25% K_2SO_4, 75% $K_2S_2O_7$] Anode Exit	[40% K_2SO_4, 60% $K_2S_2O_7$] Cathode Exit	[40% K_2SO_4, 60% $K_2S_2O_7$] Anode Exit
0	2400 (2660)	2400 (2660)	2200 (2500)	2300 (2570)	1700 (2410)	1500 (2330)
5			4500 (3620)	2900 (2850)	1400 (2260)	3100 (3290)
10	15800 (7040)	6400 (4400)	8900 (5260)	3400 (3120)	3800 (3300)	5300 (4000)
20	35100 (15210)	8700 (5090)	25600 (11800)	9500 (5470)		

Table 7. Effluent Analysis. 1% SO_2, 10% O_2, 89% N_2 to Cell.

I (mA)	[Pure $K_2S_2O_7$] Cathode Exit	[Pure $K_2S_2O_7$] Anode Exit	[0.1% V_2O_5, 99.9% $K_2S_2O_7$] Cathode Exit	[0.1% V_2O_5, 99.9% $K_2S_2O_7$] Anode Exit	[1% V_2O_5, 99% $K_2S_2O_7$] Cathode Exit	[1% V_2O_5, 99% $K_2S_2O_7$] Anode Exit
0	22800 (9020)	22600 (8980)	22600 (8980)	22700 (9000)	21900 (8770)	22000 (8790)
5			23500 (9400)		21100 (8580)	22500 (8960)
10	32000 (14000)	27400 (11290)	24700 (9810)		19200 (8000)	24300 (9820)
20	39100 (17100)	29100 (12400)	28500 (11930)		19000 (7940)	25900 (10440)
30	44100 (19170)	32400 (14500)			19000 (7940)	

Using Newman's correlation for unsteady state diffusion from a sphere it is found that the gas-phase resistance is negligible. This simply means that the concentration of SO_2 in the sphere is not a function of the radial position in the sphere.

The liquid phase mass transfer coefficient is calculated by:

$$k_\ell = \frac{D_\ell}{d_p} \times 0.42 \left(\frac{\mu_\ell}{\rho_\ell D_\ell}\right) \left(\frac{d_p^3 \rho_\ell \Delta\rho g}{\mu_\ell^2}\right) \qquad (18)$$

The value of D_ℓ is 2×10^{-5} cm^2/sec [17], $\mu_\ell = 0.1$ g/cm sec [18], and ρ_ℓ experimentally measured to be 2.5 g/cm^3. This results in $k_\ell = 3.6 \times 10^{-6}$ cm/sec.

The initial number of moles present in each bubble containing 1% SO_2 gas can be estimated using the ideal gas law to be 1.38×10^{-8} mole SO_2.

The final number of moles of SO_2 in the bubble is calculated to be 1.11×10^{-8} moles SO_2. This represents a percentage removal of

$$\frac{1.38 \times 10^{-8} - 1.11 \times 10^{-8}}{1.38 \times 10^{-8}} \times 100 = 19.6\% \qquad (19)$$

A simple error analysis based on the accuracy to which the parameters used in these calculations are known reveals that this figure is subject to a relative error of 45%. Thus the mass transfer limit of SO_2 removal should be reported as 20 ± 9%.

Since cathodic SO_2 removal is only seen when the electrolyte is 1% V_2O_5 - 99% $K_2S_2O_7$, and it is known that V_2O_5 is a catalyst in the oxidation of SO_2 to SO_3, it is logical to assume that SO_2 removal might also be limited by the conversion rate of SO_2 to SO_3:

$$SO_2 + \frac{1}{2} O_2 \underset{k_2}{\overset{k_1}{\rightleftharpoons}} SO_3 \qquad (20)$$

Numerous studies of this catalyzed reaction have been studied [19-25]. Thodos [25] investigated the reaction-rate kinetics over V_2O_5 and found that the kinetic data are well represented by a rate expression of the form:

$$r_m = k P_{SO_2}^n P_O^m \qquad (21)$$

where (at 340°C)

$$k = 8.944 \times 10^{-4} \qquad (22)$$

$$m = 0.500 \qquad (23)$$

$$n = 0.871 \qquad (24)$$

and r_m is expressed in gmoles/sec-g of catalyst.

The feed to the cathode has the following composition (mole%).

$$SO_2 = 1\% \qquad (25)$$

$$O_2 = 3\% \qquad (26)$$

$$N_2 = 96\% \qquad (27)$$

The total pressure is 1 atmosphere so that the partial pressures of the various species are numerically equal to their mole fractions. The partial pressures can then be expressed in terms of the degree of conversion, f. The power law rate expression then becomes.

$$r_m = 8.944 \times 10^{-6}\left(\frac{1-f}{100-0.5f}\right)^{0.871}\left(\frac{3-0.5f}{100-0.5f}\right)^{0.50} \qquad (28)$$

By assuming that the gas bubbles contact a column of liquid electrolyte, a mass of catalyst involved in the reaction may be estimated. This figure, in conjunction with the experimentally determined contact time, allows a conversion of 12 ± 3%, in good agreement with the observed results. Thus, the removal of SO_2 may be limited either by mass transfer or the oxidation kinetics. Either of these limitations can be overcome by improving the cell design.

A closer look at the effluent analysis results will help to develop a better understanding of the reaction mechanism. The reactions which are introduced will be further substantiated in subsequent section within the Free Electrolyte Results section.

Figure (17) shows the cathode-effluent sulfur oxide concentration (compared to open-circuit values) in a pure potassium pyrosulfate melt. The inlet gas contains 3000 ppm SO_2, 3% O_2, and balance N_2. The trend is clear; increasing the current lead to increased SO_2 evolution. This is in agreement with work by Fang and Rapp [26] who propose a cathodic reaction scheme resulting in SO_2 production. Their study was in a sulfate melt at 900°C, but pyrosulfate was identified as the active species.

Figure (17) also shows dashed lines comparing theoretical SO_2 generation at 1 mole/Faraday and 2 mole/Faraday. The results indicate that at low currents the generation most closely follows one mole faraday. As the current density is increased there is a gradual shift in the mechanism toward two moles of SO_2 generated per faraday. Under conditions of low overpotential the pyrosulfate reduction mechanism is described by:

$$2S_2O_7^{2-} + 2e^- \rightarrow 2SO_2 + 2SO_4^{2-} + O_2^{2-} \qquad (29)$$

with some of the evolved SO_2 reacting as:

$$SO_2 + O_2^{2-} \rightarrow SO_4^{2-} \qquad (30)$$

under conditions of high overpotential, the mechanism is postulated to be:

$$2S_2O_7^{2-} + e^- \rightarrow 2SO_2 + 2SO_4^{2-} + O_2^- \qquad (31)$$

with some SO_2 reacting as:

$$SO_2 + O_2^- + e^- \rightarrow SO_2^{2-} \qquad (32)$$

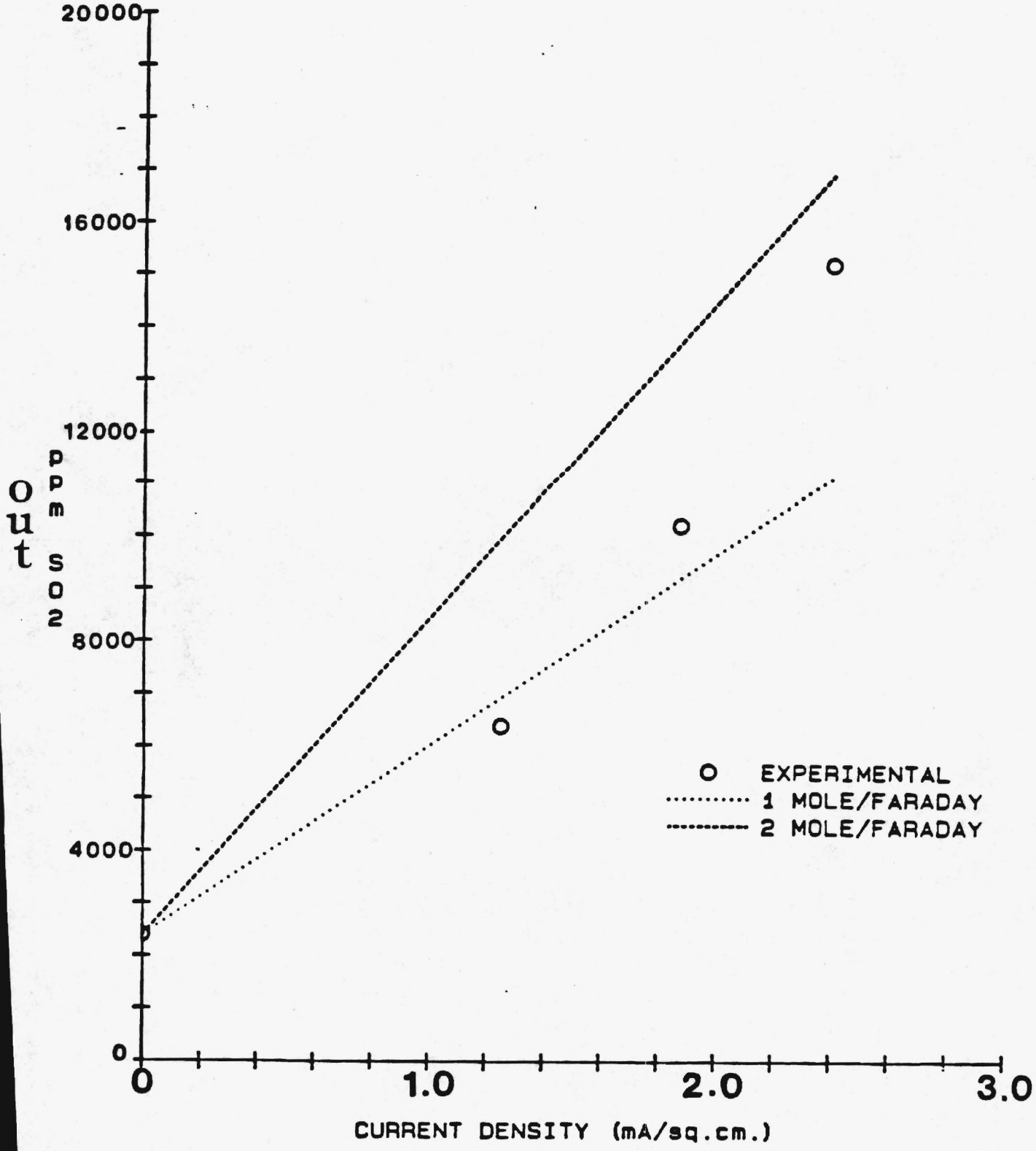

Figure 17. EFFLUENT SO_2 CONCENTRATION IN PURE $K_2S_2O_7$

Durand [27] examined the electrochemistry of both $K_2S_2O_7$ and $K_2S_2O_7/K_2SO_4$ electrolytes in contact with a pure SO_2 atmosphere at 430°C. He found the cathodic reaction under these conditions was:

$$2S_2O_7^{2-} + 2e^- = 3SO_4^{2-} + SO_2 \qquad (33)$$

for both non-sulfate containing electrolytes. Although the mechanism is not clear, this result is in agreement with the results presented above. Since Durand utilized a pure SO_2 gas environment, the electrolyte was always near its saturation limit in SO_2 [27]. In this case, reaction (30) and (32) apparently proceed rapidly, to completion with respect to the oxyanions. Reaction (29) and (30), and (31) and (32) could then be added to yield overall cathodic reactions for low and high overpotentials respectively. Both cases result in an overall cathodic reaction equal to reaction (33). Thus, Durand was unable to distinguish the mechanistic steps observed in our lab because of the pure SO_2 atmosphere.

From the reactions written above, one can see that "pure" $K_2S_2O_7$ with no K_2SO_4, is truly a misnomer. Passage of faradaic current produces sulfate as the reactions above show; however, the quantity generated in this fashion is quite small. For example, under our experimental conditions a 10 mA current would need to be applied to the effluent-analysis cell for over 50 hours to produce a 1.0% sulfate electrolyte. Sulfate also forms from the natural dissociation of pyrosulfate according to the equilibrium:

$$K_2S_2O_7 = K_2SO_4 + SO_3 \qquad (34)$$

The maximum amount of sulfate at equilibrium can be calculated from thermodynamic data [28-30]. The equilibrium constant is approximately 2×10^{-6} so that less than 0.2% of the pyrosulfate dissociates in the temperature range of interest. This was calculated assuming no K_2SO_4 or SO_3 are initially present. If either or both are initially in the system even less pyrosulfate will dissociate. Thus, although some sulfate will be present in $K_2S_2O_7$ electrolytes, the quantity is usually insignificant relative to electrolytes preloaded with K_2SO_4.

Earlier it was shown that the electrolytes containing K_2SO_4 promoted removal of SO_2. This can be explained as follows: Added sulfate reduced the acidity of the melt and helps neutralize the SO_2, possibly through the formation of dithionate:

$$SO_2 + SO_4^{2-} \rightarrow S_2O_6^{2-} \qquad (35)$$

which can disproportiae to

$$S_2O_6^{2-} \rightarrow SO_3 + SO_3^{2-} \qquad (36)$$

with the SO_3 quickly neutralized by any available SO_4^{2-}:

$$SO_3 + SO_4^{2-} \rightarrow S_2O_7^{2-} \qquad (37)$$

and the SO_3^{2-} oxidized by dissolved oxygen:

$$SO_3^{2-} + 1/2O_2 \rightarrow SO_4^{2-} \qquad (38)$$

Summing the equations yields an overall removal mechanism of:

$$SO_2 + 1/2O_2 + SO_4^{2-} \rightarrow S_2O_7^{2-} \qquad (39)$$

Although added sulfate enhances SO_2 removal the major cathodic reaction is still the reduction of pyrosulfate as given by equations (29-33).

Figure 18 shows graphically the results of effluent analysis experiments utilizing electrolytes containing vanadia. The figure shows increased SO_2 removal as the current is increased, and also increased removal with increasing sulfate concentration. The major cathodic reaction in these systems is still the reduction of pyrosulfate as before. Under steady conditions the cathodic reaction would be (no build up of the oxyanions in equations (30, 32)):

$$2S_2O_7^{2-} + 2e^- \rightarrow 3SO_4^{2-} + SO_2 \qquad (40)$$

In vanadia containing electrolytes the oxidation of SO_2 becomes an important reaction:

$$2SO_2 + O_2 \rightarrow 2SO_3 \qquad (41)$$

And in gases containing SO_3, the SO_3 will readily react with available sulfate:

$$2SO_3 + 2SO_4^{2-} \rightarrow 2S_2O_7^{2-} \qquad (42)$$

Adding equations (40), (41) and (42) yields an overall cathodic reaction of:

$$SO_2 + O_2 + 2e^- \rightarrow SO_4^{2-} \qquad (43)$$

Thus, there is net removal of SO_2 in electrolytes containing V_2O_5, and the removal increases with increased currents. The removal was found to be limited by either mass transfer or the rate at which SO_2 could be oxidized. Either of these limitations can be overcome by improved cell design.

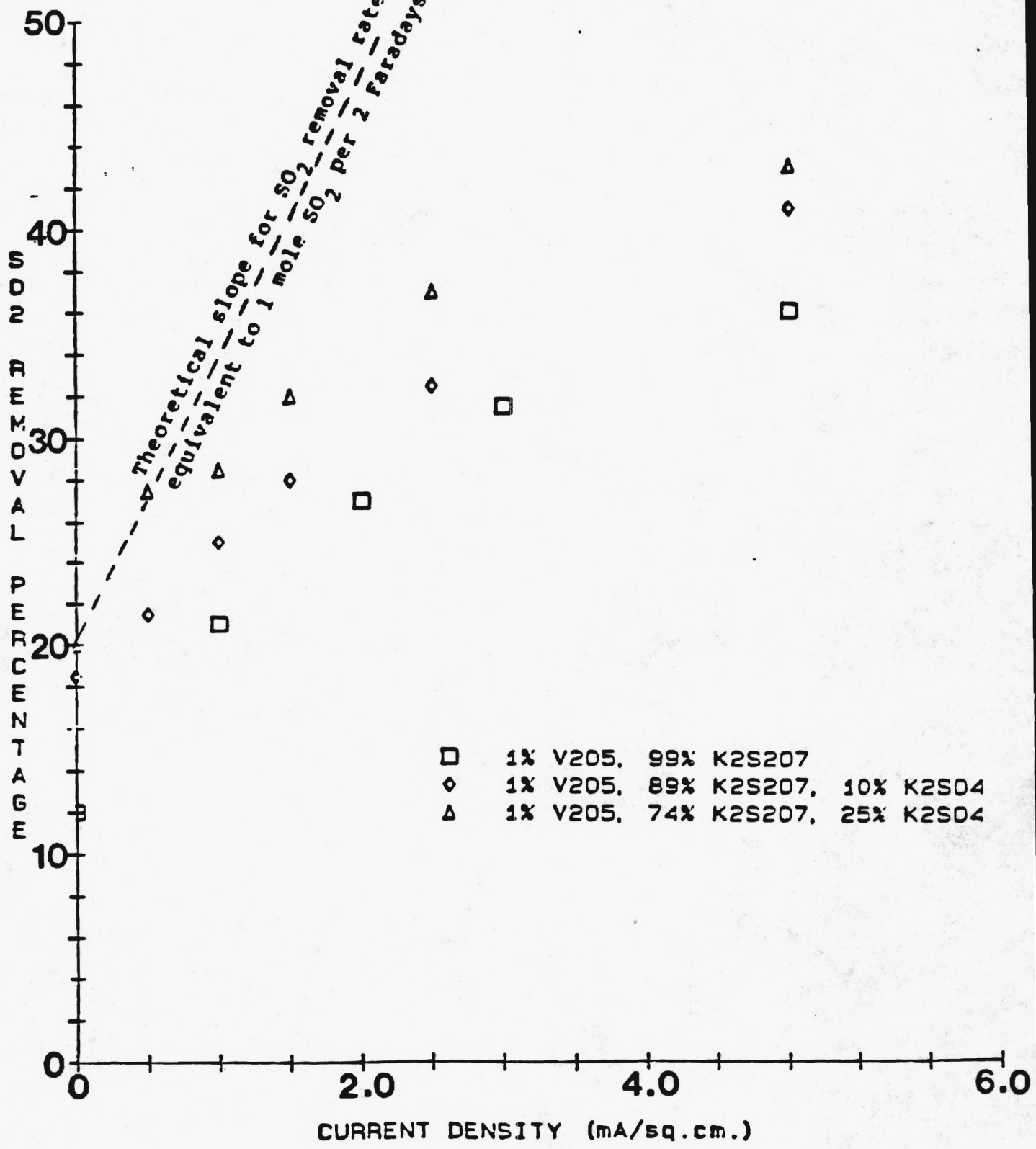

FIGURE 18. SO_2 REMOVAL IN $K_2S_2O_7$ MELTS CONTAINING V_2O_5 AND K_2SO_4

e. X-ray Diffraction

The composition of $K_2S_2O_7/K_2SO_4/V_2O_5$ electrolytes under $N_2/SO_2/O_2$ gas environments was studied by x-ray diffraction. Initial electrolytes ranged from zero to ten weight percent K_2SO_4 and one to ten weight percent V_2O_5. Four different gas environments were utilized 1) N_2, 2) air, 3) 1.0% SO_2 in N_2, and 4) 1.0% SO_2, 10% O_2 in N_2. The results indicate three major species exist in the electrolyte under all conditions. The species are $K_2S_2O_7$ K_2SO_4, and $[K_2O-V_2O_5-2SO_3]$ was identified. These results are consistent with those reported by Bazarova [31], who used I.R. spectra to identify electrolyte components. Bazarova's results also indicate $[K_2O-V_2O_5-4SO_3]$ may also exist in the molten electrolyte.

f. Cyclic Voltammetry

Cyclic voltammograms for $K_2S_2O_7/K_2SO_4/V_2O_5$ electrolytes under $N_2/SO_2/O_2$ gas environments were generated to study the electrochemistry of the system. Electrolyte compositions ranged from zero to ten weight percent K_2SO_4 and zero to five weight percent V_2O_5. Four gas environments were examined; 1) N_2, 2) air, 3) 1.0% SO_2 in N_2, and 4) 1.0% SO_2, 10.0% O_2 in N_2.

Figure 20 shows a CV corresponding to the simplest system, pure $K_2S_2O_7$ under N_2. The CV is characterized by one reduction peak, I, and one oxidation peak, II. The reduction reaction has been indentified in preceeding sections as the reduction of pyrosulfate. The anodic peak is attributed to oxidation of the

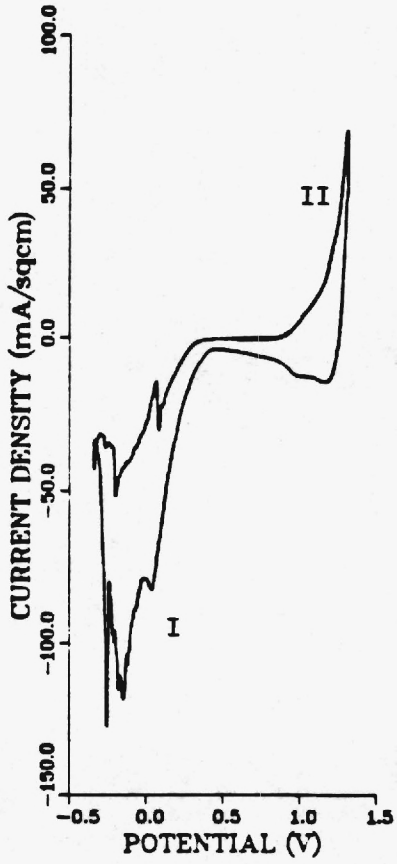

Fig. 20. Stabilized cyclic voltammogram of $K_2S_2O_7$ under a N_2 environment, 400 C, 100 mV/s

gold electrode. Durand et.al. [27] also observed gold oxidation in this potential region under similar conditions. Experimentally, if the potential of the working electrode was pushed anodically past 1.6 volts versus the Ag/Ag^+ reference, oxidation was severe and electrode replacement was required.

Figure 21 displays a CV corresponding to $K_2S_2O_7$ under an air atmosphere. This CV is virtually identical to that shown in figure (20). Thus, oxygen appears to play no direct role in the electrochemistry.

The CVs exhibited in figure (22) and (23) again correspond to pure $K_2S_2O_7$ with no initial additives, but under 1.0% SO_2 in N_2 and 1.0% SO_2, 10.0% O_2 in N_2 environments respectively. The two display the same features, further establishing the oxygen has no direct electrochemical role, but differ significantly from those without SO_2 in the gas. The effect of SO_2 on the CV is apparent in two ways. First, the pyrosulfate reduction peak has been reduced substantially and second, two new peaks, an oxidation, III, and a reduction, IV, have emerged.

The $K_2S_2O_7$ electrolytes in equilibrium with the gases containing SO_2 were analyzed by x-ray diffraction. The results show these electrolytes contain relatively high concentrations of sulfate, near the saturation limit of 4 weight percent [27]. Figure (24) exhibits four stabilized CVs, each corresponding to an initial electrolyte of $K_2S_2O_7$ saturated with K_2SO_4 but with four different gas environments. Each of the four CVs display the same features and are analogous to those in figures (22) and (23). Thus, SO_2 does not appear to have a direct role in the

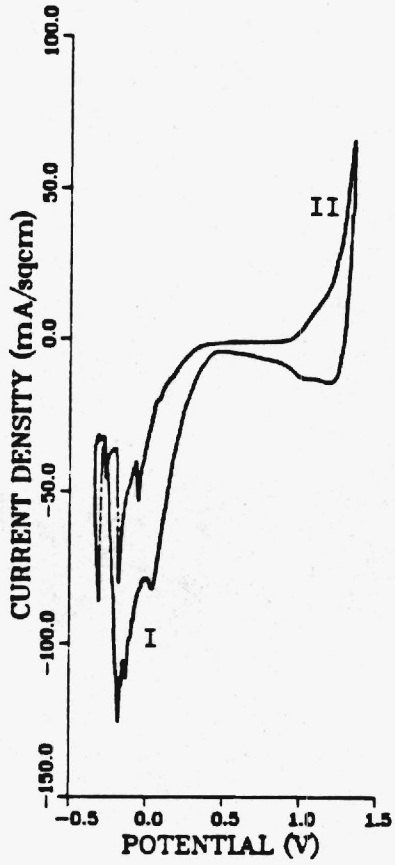

Fig. 21. Stabilized cyclic voltammogram of $K_2S_2O_7$ under an air environment, 400 C, 100 mV/s

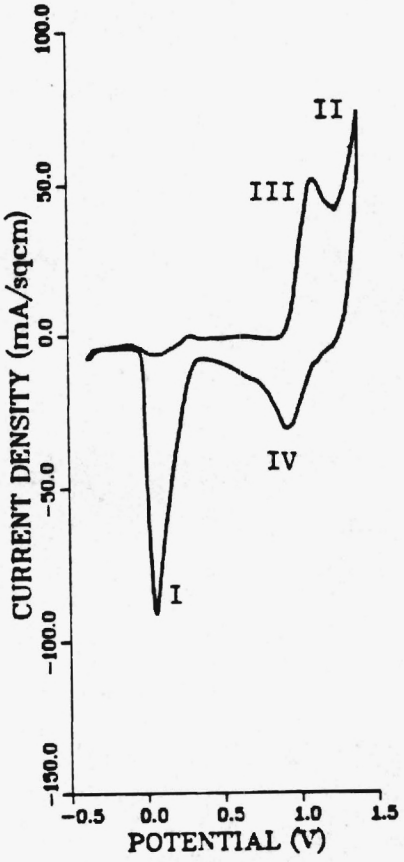

Fig. 22. Stabilized cyclic voltammogram of $K_2S_2O_7$ under a 1.0% SO_2 in N_2 gas environment, 400 C, 100 mV/s

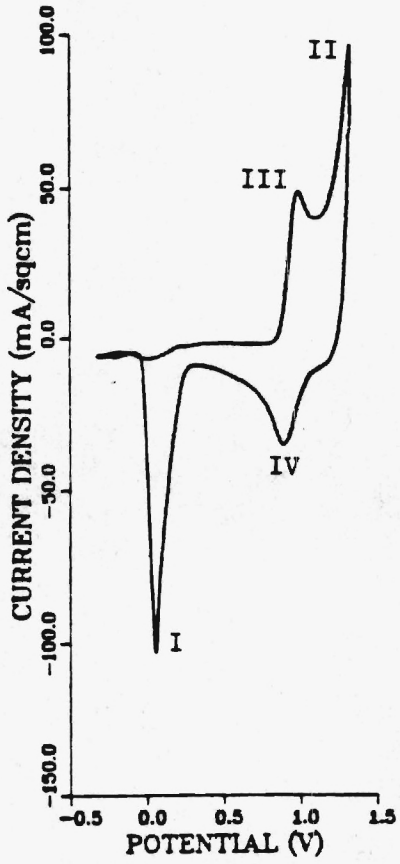

Fig. 23. Stabilized cyclic voltammogram of $K_2S_2O_7$ under a 1.0% SO_2, 10.0% O_2 in N_2 gas environment, 400 C, 100 mV/s

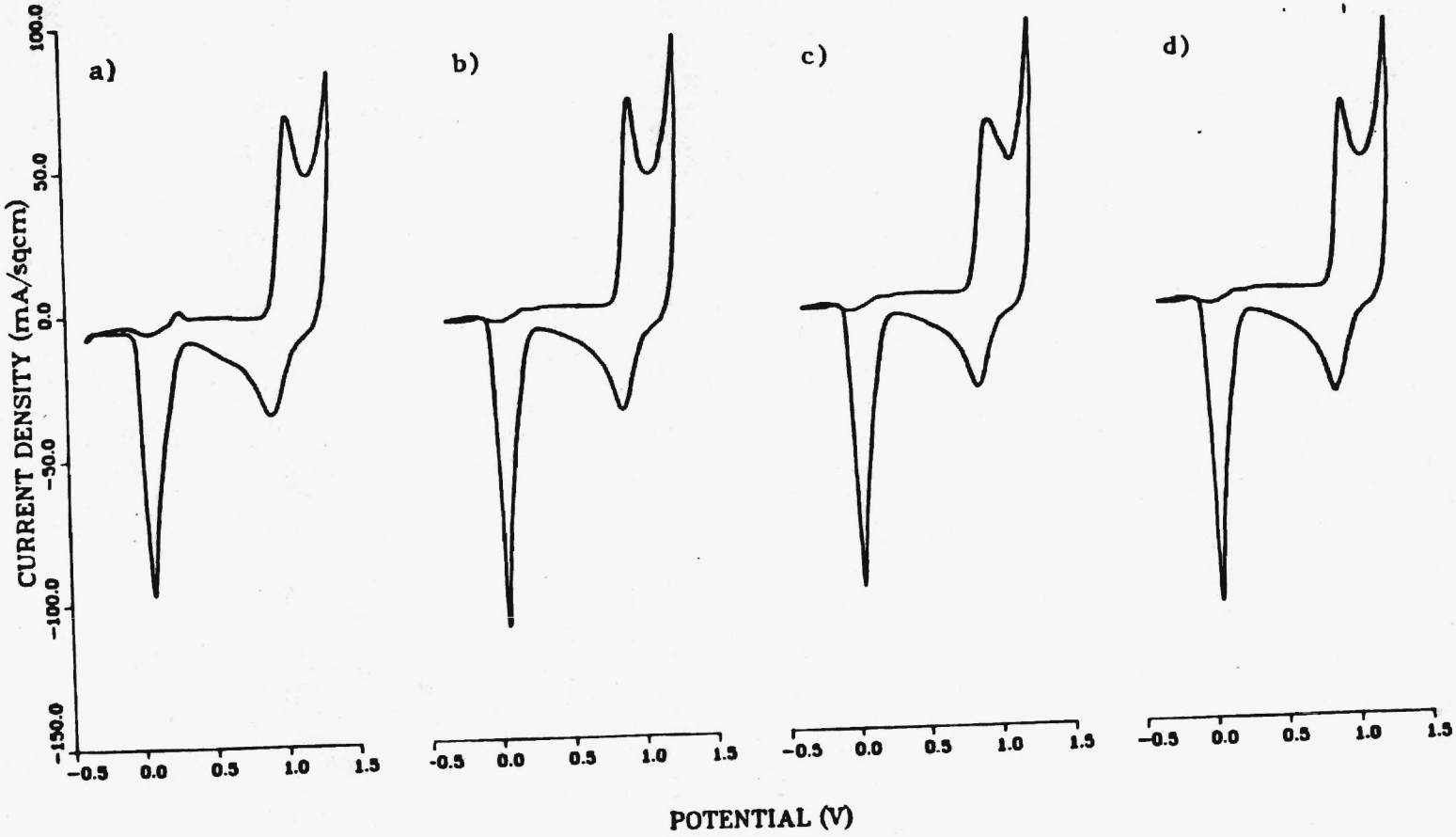

Fig. 24. Series of stabilized cyclic voltammograms of $K_2S_2O_7$ with 5.0% K_2SO_4 under various gas environments, 400 C, 100 mV/s a) N_2, b) air, c) 1.0% SO_2 in N_2, d) 1.0% SO_2 10.0% O_2 in N_2

electrochemistry but does have a strong influence on the concentration of sulfate in the electrolyte. This can be explained by considering the two equilibria:

$$SO_2 + 1/2\ O_2 = SO_3 \qquad K \sim 600 \qquad (44)$$

$$K_2S_2O_7 = K_2SO_4 + SO_3 \qquad K \sim 2x10^{-6} \qquad (45)$$

The first shows SO_2 oxidation is highly favored thermodynamically. However, the kinetics are extremely slow without a catalyst and virtually no SO_3 is formed through this path. The second equilibrium shifts to the right to form SO_2 and K_2SO_4 until a balance is reached between the two equilibria.

Peak III is attributed to the direct oxidation of sulfate:

$$SO_4^{2-} = SO_3 + 1/2O_2 + 2e^- \qquad (46)$$

Fang and Rapp [26] identified this reaction to occur in the same potential region as Peak III in sulfate melts. Peak IV appears to be a psudeo-reversible reduction of the oxidation products, likely [32, 8]:

$$SO_3 + 2e^- = SO_3^{2-} \qquad (47)$$

which can diffuse into solution and react further:

$$SO_3^{2-} + 1/2O_2 = SO_4^{2-} \qquad (48)$$

$$SO_3^{2-} + S_2O_7^{2-} = 2SO_4^{2-} + SO_2 \qquad (49)$$

Figure (25) illustrates how an increasing concentration of sulfate affect the resultant CV. As the sulfate concentration is raised, the pyrosulfate reduction is impeded while the sulfate redox peaks are enhanced. Figure (26) shows the relationship between the pyrosulfate reduction peak current and the scan rate for various sulfate concentrations. At higher concentrations, i.e., 3.0% and 5.0% sulfate by weight, a linear relationship, passing through the origin, is observed between the peak current and the square root of the scan rate. This behavior is characteristic of classical diffusion control [33]. The diffusivity of pyrosulfate under these conditions is calculated [33] to be 6×10^{-9} cm^2/s. This value is quite low even for viscous melts and indicates a thin layer of solid sulfate exists on the electrode surface during pyrosulfate reduction.*

Figure (27) displays the peak current functions, $i_p/V^{\frac{1}{2}}$, versus v, the scan rate, for various sulfate loadings. These curves indicate a shift from strictly diffusion control to a "catalytic" mechanism [34] with lower sulfate. When the electrolyte contains high concentrations of sulfate the mechanism appears to involve only the reduction of pyrosulfate, as given by equations (29-33). When the electrolyte contains little or no added sulfate, the mechanism involves pyrosulfate reduction followed by its production:

$$SO_4^{2-} + SO_3 = S_2O_7^{2-} \qquad (50)$$

* Under severe conditions (10 mA or more applied to high sulfate electrolytes for extended periods) a solid sulfate build-up has been visually observed.

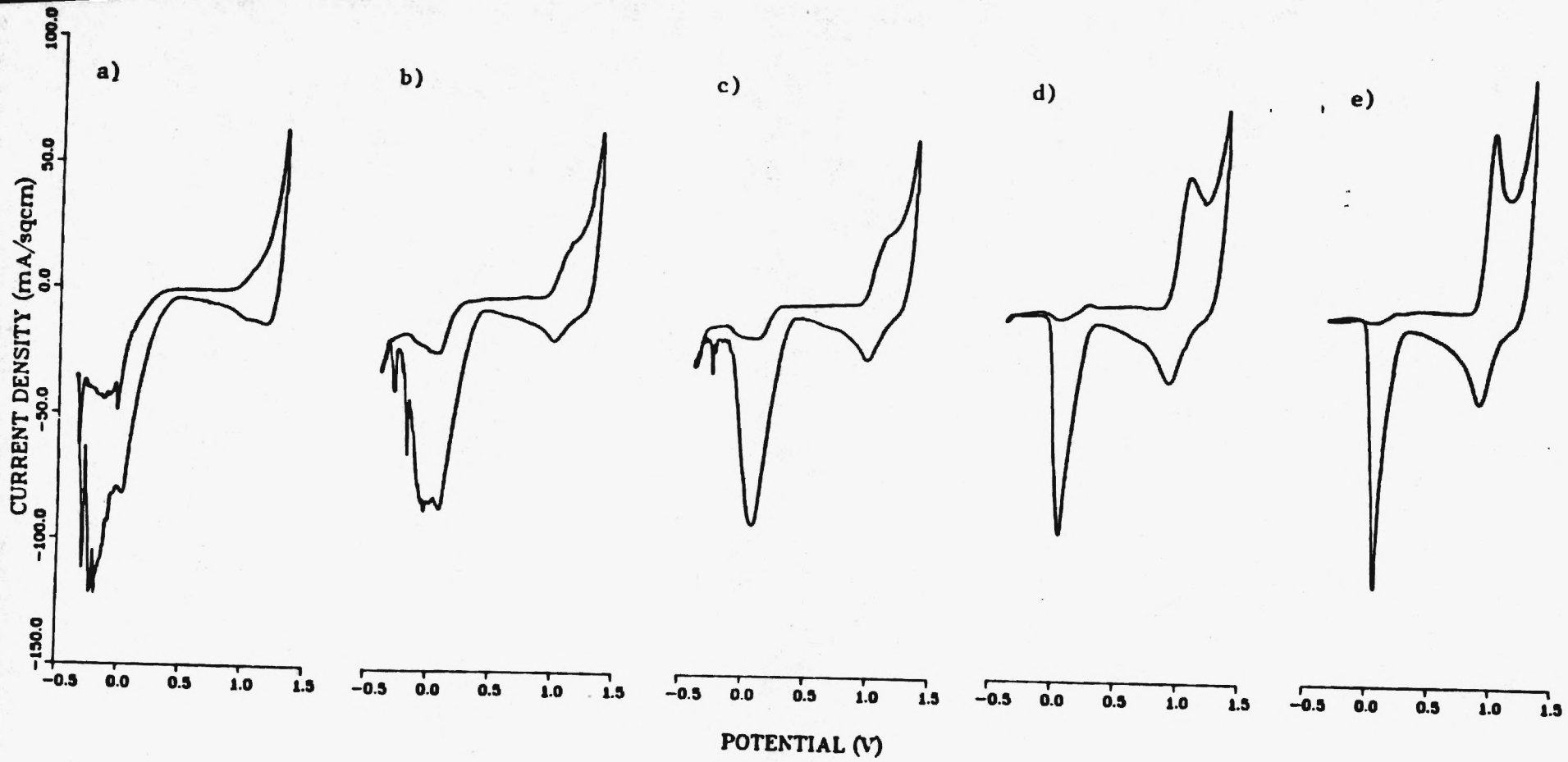

Fig. 25. Series of stabilized cyclic voltammograms of $K_2S_2O_7$ with various sulfate concentrations, air atmosphere, 400 C, 100 mV/s a) 0.0% K_2SO_4, b) 1.0% K_2SO_4, c) 2.0% K_2SO_4, d) 3.0% K_2SO_4, e) 5.0% K_2SO_4

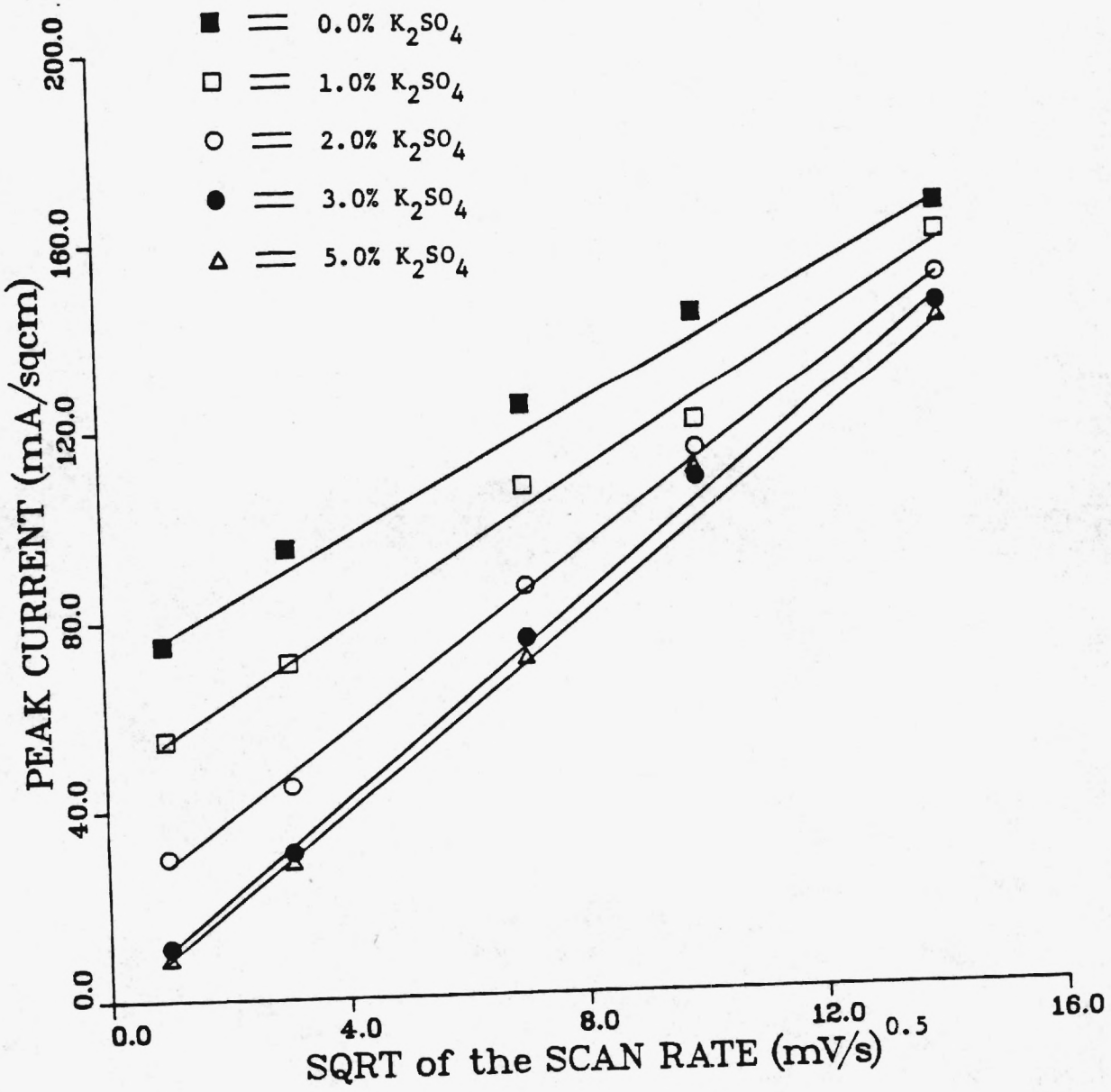

Fig. 26. Relationship between the peak current for pyrosulfate reduction and the scan rate for various sulfate concentrations, cathodic direction initially, 400 C, air environment

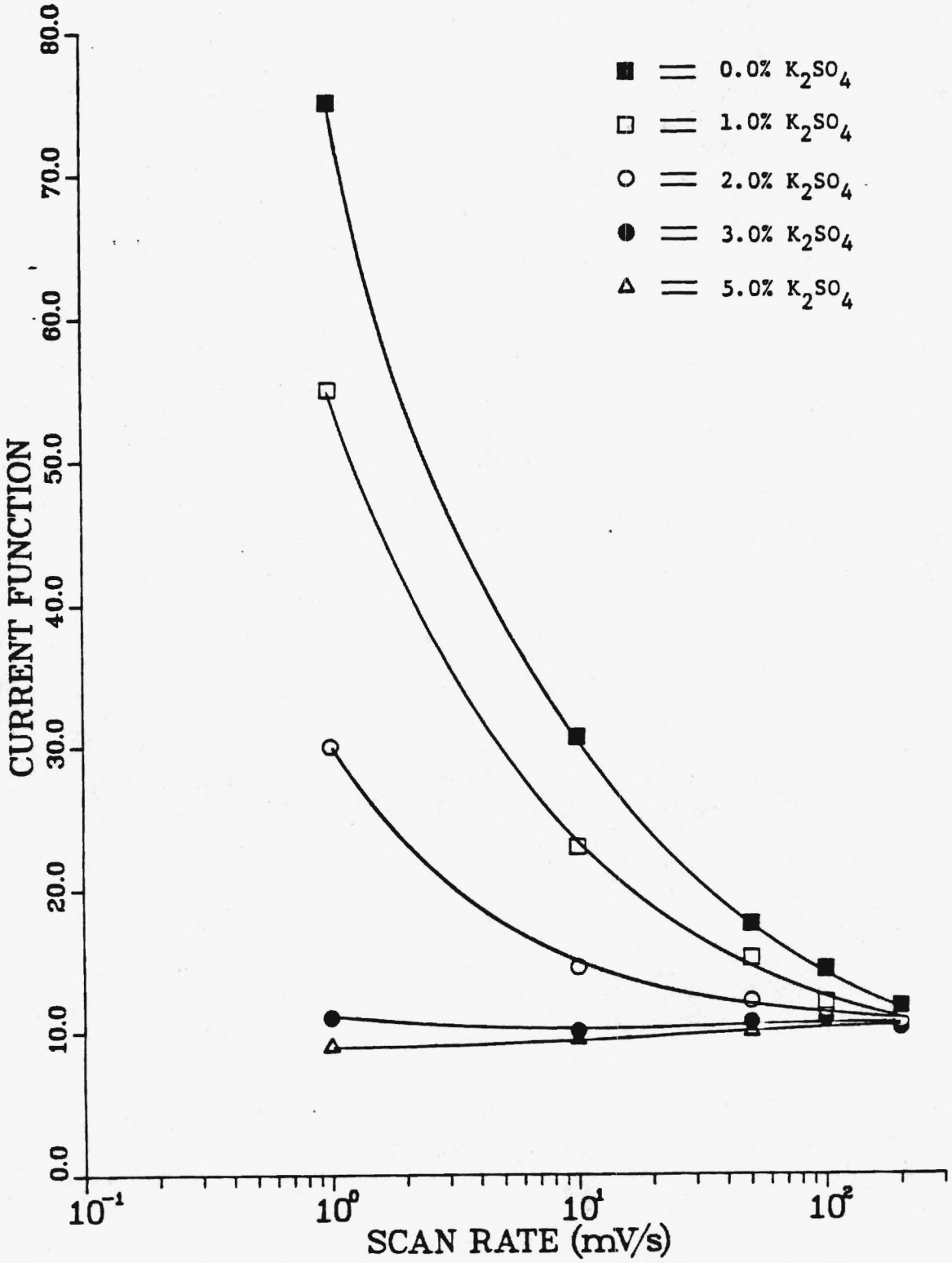

Fig. 27. Current function versus the scan rate for various sulfate concentrations. The current function is defined as the peak current divided by the square root of the scan rate [23]

The apparent shift in the mechanism is actually the result of a shift in the availability of SO_3. As the amount of sulfate added to the electrolyte decreases, more free SO_3 will be available to react with the generated sulfate as in equation (50). Thus, the current function of figure (27) indicates an increasing importance of the "catalytic" reaction as the sulfate concentration in the bulk decreases.

Figures (28) and (29) further substantiate the above premise. The electrolyte in these figures is pyrosulfate with sulfate. Figure (28) is a series of stabilized CVs where the cathodic switching potential is gradually moved to more positive values, thus decreasing the amount of pyrosulfate reduced and sulfate produced. The result is a decrease in the sulfate oxidation and reduction peaks. Similary, figure (29) is a series of stabilized CVs where the anodic switching potential is gradually moved to more negative values. As the switching potential becomes more negative less sulfate is oxidized and the interface is not being "cleansed" of the overabundance of sulfate. The result is a decrease in the peak current for pyrosulfate reduction.

Figure (30) exhibits a series of stabilized CVs generated from the initial electrolyte $K_2S_2O_7$ with 1.0% V_2O_5 under various environments. The figure shows vanadia is involved in a redox couple represented by peaks V and VI. Figures (31) and (32) exhibit the relationship between peak V current and potential and the scan rate. These indicate the peaks are a reversible redox couple limited by diffusional rates [33]. The diffusivity under these conditions is calculated to be $3x10^{-7}$ cm^2/s.

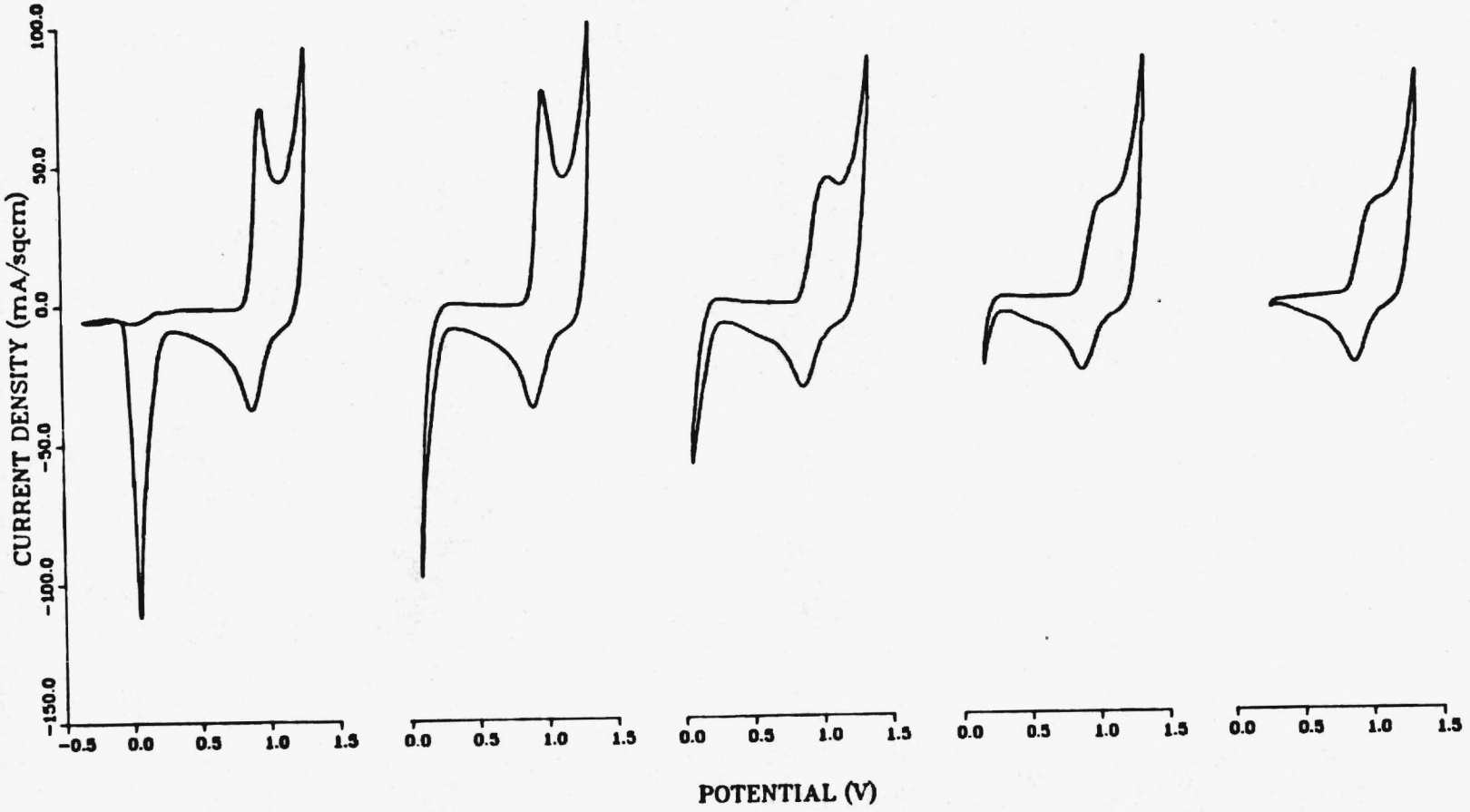

Fig. 28. Series of stabilized cyclic voltammograms for $K_2S_2O_7$ with 5.0% K_2SO_4 where the cathodic switching potential is gradually moved to more positive values, air environment, 400 C, 100 mV/s

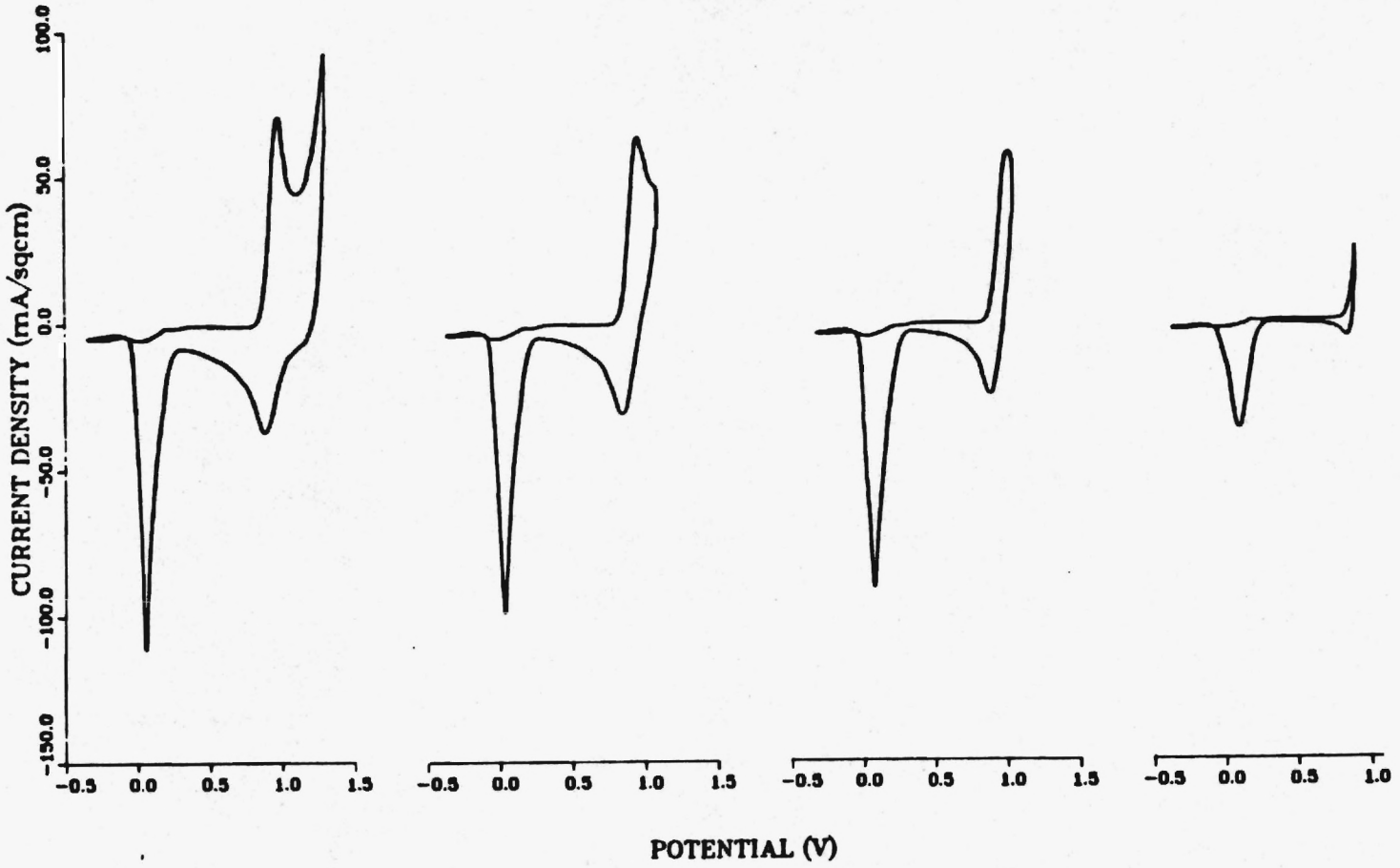

Fig. 29. Series of stabilized cyclic voltammograms for $K_2S_2O_7$ with 5.0% K_2SO_4 where the anodic switching potential is gradually moved to more negative values, air environment

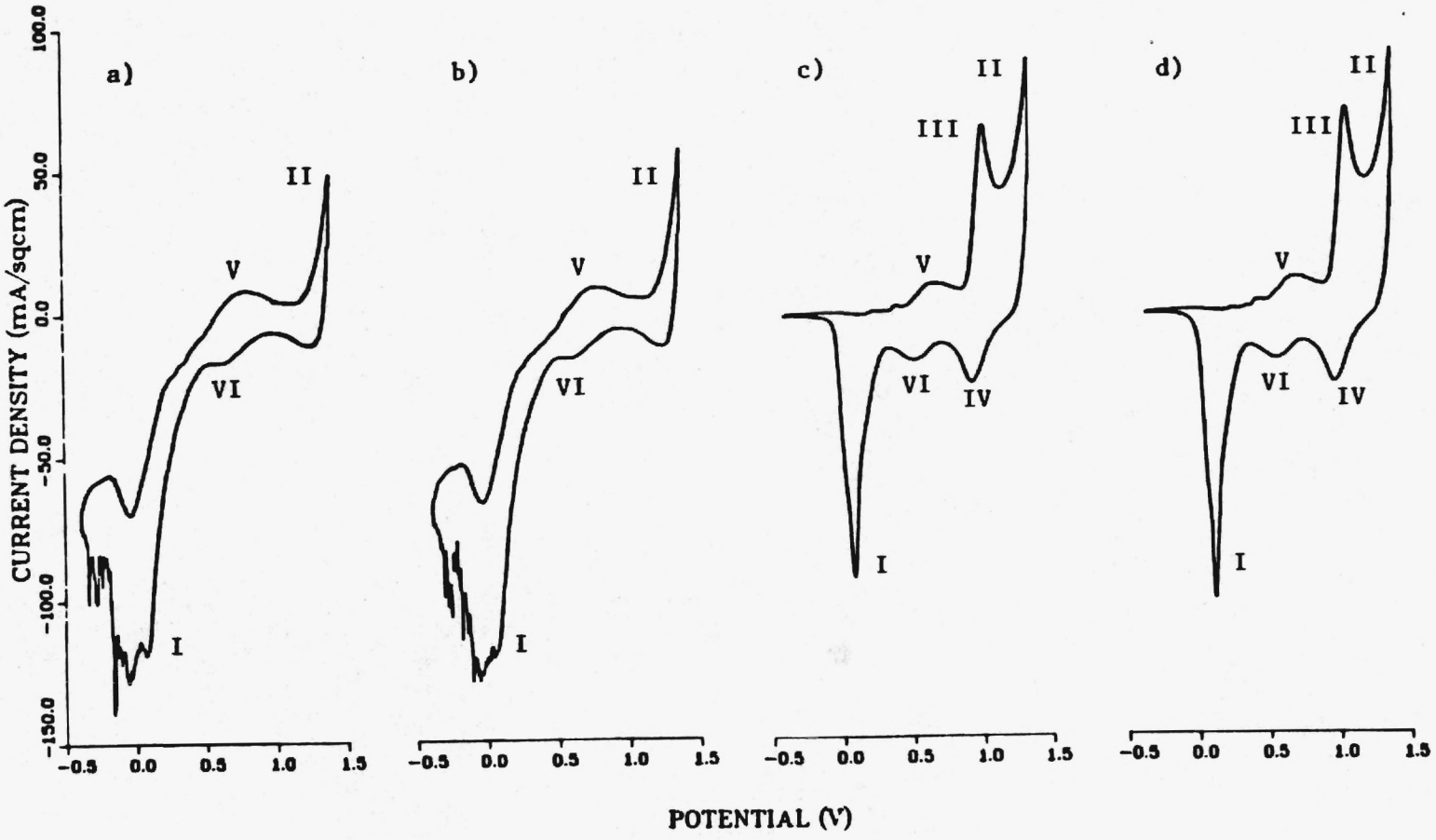

Fig. 30. Series of stabilized cyclic voltammograms for $K_2S_2O_7$ with 1.0% V_2O_5 under various gas environments, 400 C, 100 mV/s, a) N_2, b) air, c) 1.0% SO_2 in N_2, d) 1.0% SO_2, 10.0% SO_2 in N_2

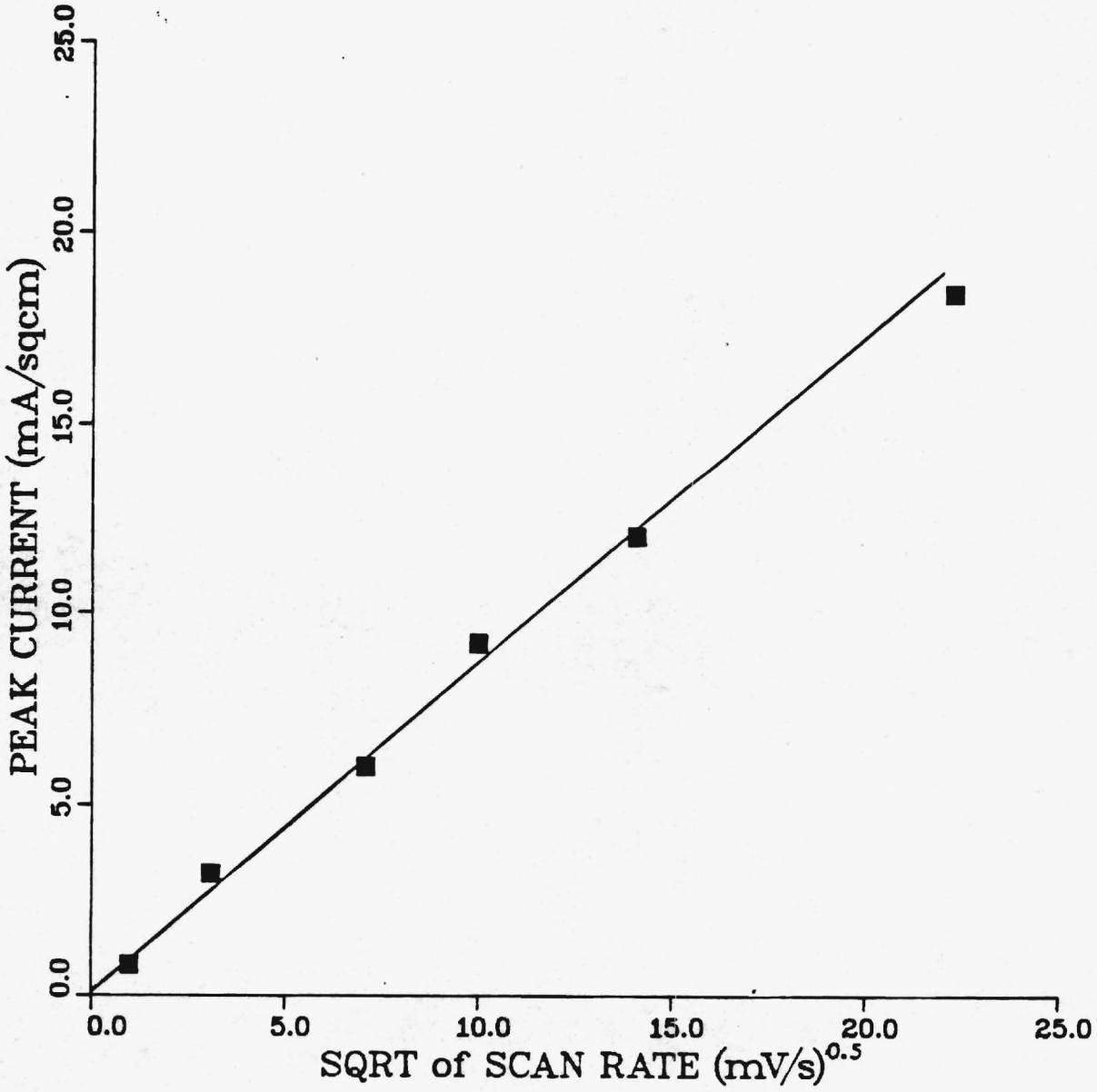

Fig. 31. Relationship between the peak current for the vanadia complex oxidation (peak V) and the scan rate, 370 C, air environment

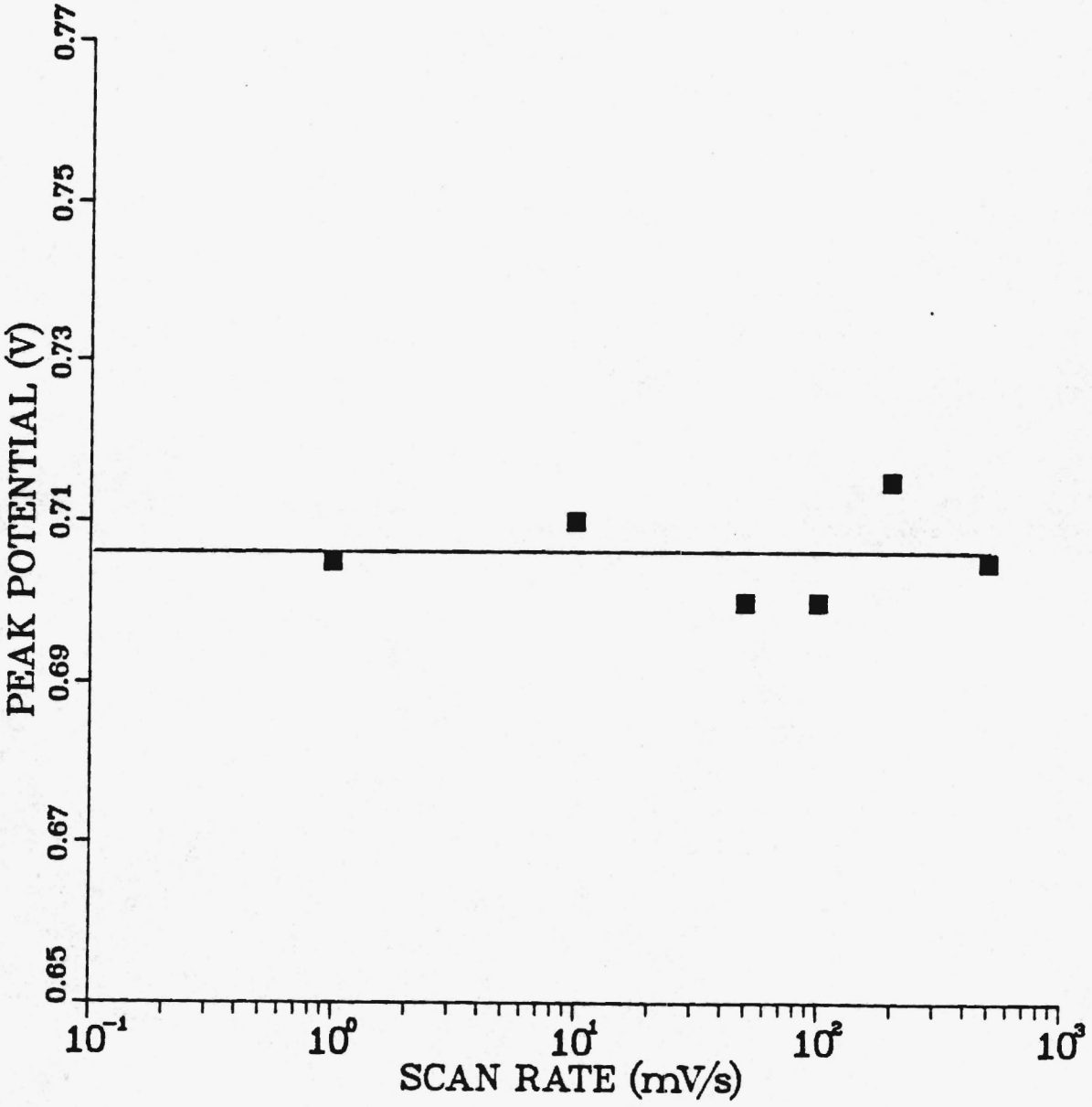

Fig. 32. Relationship between the peak potential for the vanadia complex oxidation (peak V) and the scan rate, 370 C, air environment

Diffusivities of this order have been reported elsewhere [35]. The redox reactions most likely involving the vanadia complexes identified in the x-ray diffraction section possibly:

$$[K_2O\text{-}V_2O_5\text{-}4SO_3] + 2e^- = [K_2O\text{-}V_2O_4\text{-}3SO_3] + SO_4^{2-} \qquad (51)$$

Figure (30) also shows the gas environment has little, if any effect on the stabilized vanadia peaks.

A comparison can be made between the four CVs shown in figure (30) and their counterparts without vanadia (figures 20-23). The vanadia appears to have essentially no influence on the pyrosulfate or sulfate redox processes.

g. Equilibrium Potentials

The equilibrium potential between the working and reference electrodes can be used to characterize the electrochemical processes. For $K_2S_2O_7$ and $K_2S_2O_7/K_2SO_4$ electrolytes, the electrode reaction has been established as:

$$K_2O_7^{2-} + 2e^- = SO_2^{2-} + SO_3^{2-} \qquad (52)$$

The overall reaction determining the equilibrium potential between the working and Ag/Ag^+ reference is:

$$2Ag_{(R)} + K_2S_2O_{7(W)} + 2KNO_{3(R)} = K_2SO_{4(W)} + K_2SO_{3(W)} + 2AgNO_{3(R)} \qquad (53)$$

Therefore, the equilibrium potential is given by:

$$E_e = E^o - \frac{RT}{2F} \ln\left[\frac{[K_2SO_4][K_2SO_3][AgNO_3]^2}{[K_2S_2O_7][Ag]^2[KNO_3]^2}\right] \quad (54)$$

where the activity of each species has been approximated by its concentration. The standard potential and Nernst terms may be calculated from thermodynamic data [28-30]. The concentrations of $K_2S_2O_7$, KNO_3, and $AgNO_3$ are known. The three equilibria:

$$SO_2 + 1/2O_2 = SO_3 \quad (55)$$

$$K_2S_2O_7 = K_2SO_4 + SO_3 \quad (56)$$

$$K_2S_2O_7 + SO_2 = K_2SO_3 + 2SO_3 \quad (57)$$

can be solved simultaneously to yield the concentrations for K_2SO_4 and K_2SO_3.

Calculated equilibrium potentials are compared to experimental data for a variety of electrolyte and gas composition in table 8. The results are reported on the basis of changes in the equilibrium potential relative to a base case of initially pure $K_2S_2O_7$ under an air atmosphere. These results show equation (54) accurately predicts changes in the equilibrium potential due to changes in the gas environment and electrolyte composition. The absolute value of the calculated potential differences are consistently 40 to 60 millivolts below the experimental values. This may be due to nonideal activities or errors in the free energies used in the calculations. These results reaffirm the validity of equation (52) being the redox reaction responsible for controlling the equilibrium potential.

For $K_2S_2O_7/K_2SO_4/V_2O_5$ a second redox reaction, proposed earlier, also influences the equilibrium potential:

$$[K_2O\text{-}V_2O_5\text{-}4SO_3] + 2e^- = [K_2O\text{-}V_2O_4 3SO_3] + SO_4^{2-} \qquad (58)$$

Figure (33) shows how equilibrium potential varies with the concentration of vanadia. The slope indicates the value of n is four which reflects a stoichiometric coefficient for vanadia of one. Thus, the pyrosulfate and vanadia redox reaction may be added to give an overall electrode reaction:

$$S_2O_7^{2-} + V^V_{complex} + 4e^- = 2SO_4^{2-} + V^{IV}complex + SO_3^{2-} \qquad (59)$$

Therefore, the equilibrium potential is given by:

$$E_e = E^o - \frac{RT}{4F}\ln\left[\frac{[V^{IV}_{complex}][K_2SO_4]^2[K_2SO_3][AgNO_3]^4}{[V^V_{complex}][K_2S_2O_7][KNO_3]^4[Ag]^4}\right] \qquad (60)$$

where the activities have again been approximated by the species concentrations. The lack of thermodynamic data available on the vanadia complex precludes a quantitative analysis. Qualitatively, experiments show the equilibrium potential increases with additions of V^V and decreases with additions of K_2SO_4, K_2SO_3 or V^{IV}. These results are consistent with equation (60).

Initial Electrolyte	Gas Environment	E calculated	E experimental
$K_2S_2O_7$	air	+0.940	+0.990
		Change in the Equilibrium Potential	
		Calculated	Experimental
$K_2S_2O_7$	air	0.000	0.000
$K_2S_2O_7$, 0.5% K_2SO_4	air	-0.060	-0.060
$K_2S_2O_7$, 1.0% K_2SO_4	air	-0.100	-0.090
$K_2S_2O_7$, 2.0% K_2SO_4	air	-0.140	-0.140
$K_2S_2O_7$, 4.0% K_2SO_4	air	-0.180	-0.170
$K_2S_2O_7$	N_2	-0.110	-0.120
$K_2S_2O_7$	1.0% SO_2 in N_2	-0.480	-0.470
$K_2S_2O_7$	1.0% SO_2, 10.0% O_2 in N_2	-0.120	-0.130
$K_2S_2O_7$, 4.0% K_2SO_4	N_2	-0.320	-0.300
$K_2S_2O_7$, 4.0% K_2SO_4	1.0% SO_2 in N_2	-0.520	-0.570
$K_2S_2O_7$, 4.0% K_2SO_4	1.0% SO_2, 10.0% O_2 in N_2	-0.180	-0.170

Table 8. Comparison of experimental and calculated equilibrium potentials for various gas environments and electrolyte compositions, 400 C, relative to Ag/Ag^+ reference. Results are reported on the basis of changes in the equilibrium potential relative to a base case of potassium pyrosulfate under an air environment.

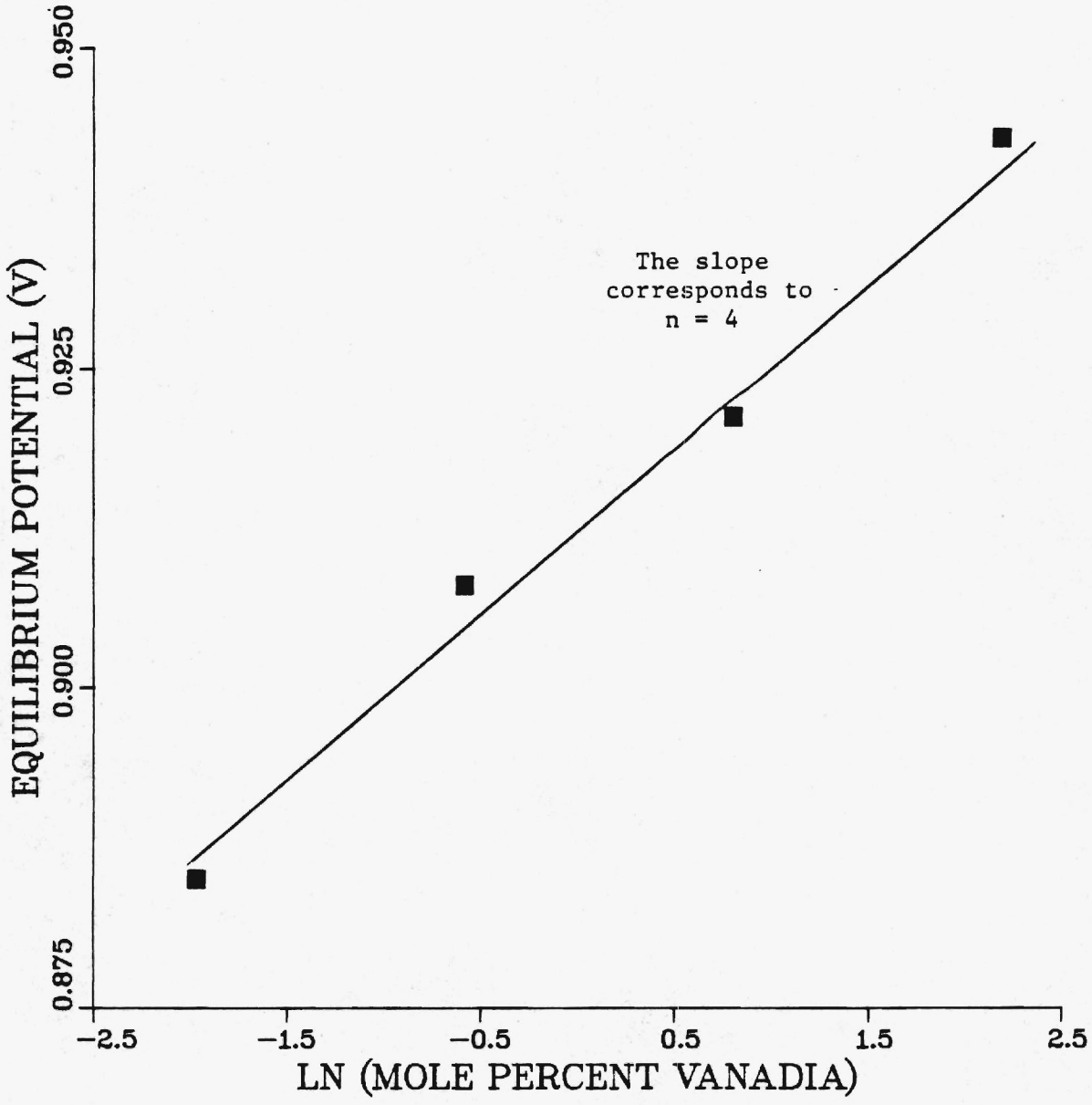

Fig. 33. Equilibrium potential of $K_2S_2O_7/V_2O_5$ electrolytes versus the natural log of the vanadia loading

The relative concentrations of the two vanadia complexes at equilibrium were a strong function of the gas environment. Three equilibria appeared to be important:

$$[K_2O\text{-}V_2O_5\text{-}2SO_3] + 2SO_3 = [K_2O\text{-}V_2O_5\text{-}4SO_3] \quad (61)$$

$$[K_2O\text{-}V_2O_5\text{-}2SO_3] + SO_2 = [K_2O\text{-}V_2O_4\text{-}3SO_3] \quad (62)$$

$$[K_2O\text{-}V_2O_4\text{-}3SO_3] + 1/2O_2 = [K_2O\text{-}V_2O_5\text{-}2SO_3] + SO_3 \quad (63)$$

The first equilibrium is a simple exchange of SO_3 molecules which is consistent with what Bazarova [31] reported. For electrolytes under 1.0% SO_2 in N_2 environments the second equilibrium was shifted strongly toward the right and the V^{IV} species dominated. In air environments the third equilibrium was shifted strongly toward the right and the V^{V} species dominated. When the electrolytes were under 1.0% SO_2, 10.0% in N_2 atmospheres the second and third equilibria balanced each other and resulted in a V^{IV}/V^{V} ratio of about 1/4.

TASK 2. ELECTRODES

a. Comparison to NiO

The standard cathode in molten carbonate fuel cells is porous NiO, formed from sintered Ni powder, reinforced with Ni screen, and oxidized in-situ. However, NiO is not a suitable electrode material for use in an electrochemical flue gas desulfurization device because it is not stable under operating conditions. At present the most attractive electrode material

for cell operation at 300°C appears to be the perovskite type compounds, $Ln_{1-x}M_xM'O_3$ (LN = lanthanoid element). These have been shown [36] to be satisfactory in both polarization characteristics and stability under working conditions as oxygen electrode materials. For a comparison of the kinetic performance of NiO and perovskite electrodes tests were run in a molten carbonate CO_2 concentrator cell and the results are described in this section.

Figure (34) shows an electron micrograph of a partially sintered $La_{0.8}Sr_{0.2}CoO_3$ electrode. For comparison a section of a NiO electrode is shown in Figure (35). BET specific surface area analysis indicated 0.9 ± 0.1 m^2/g for the perovskite and 0.5 ± 0.1 m^2/g for the NiO.

Polarization data were obtained under conditions appropriate to tests of the molten carbonate CO_2 concentrator for application to manned spacecraft [37,38]. The IR free polarizations are shown in Figures (36) and (37). The data in the low polarization region were used to estimate the exchange current density, i_o (superficial area basis), from

$$i_o = \frac{di}{d\eta} \frac{RT}{nF} \qquad (64)$$

Linear regression produced i_o values of 32 ma/cm^2 and 21 ma/cm^2 at 0.5 and 1.0% CO_2 respectively.

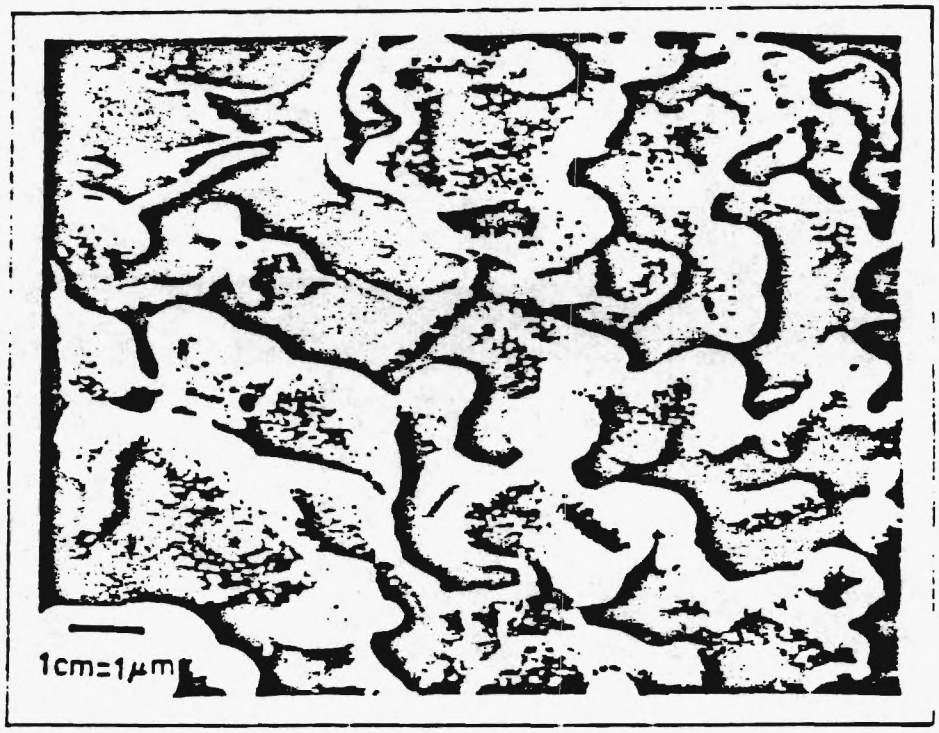

Figure 34. Electron Micrograph of Partially Sintered Perovskite Electrode

Figure 35 Electron Micrograph of NiO Electrode

The intermediate-range data were fit with the Butler-Volmer equation in the Allen-Hickling form:

$$\ln i/[\exp(nF\eta/RT)-1] = \ln i_o - \alpha \eta F/RT \qquad (65)$$

with i_o set with the low polarization values. The Allen-Hickling plots are shown in Figure (38). The transfer coefficients, α , obtained from linear regression are 0.59 and 0.73 for the 0.5 and 1.0% CO_2 gas mixtures respectively. The scatter in the data precludes any conclusion other than that they are consistent with an α of 0.6, as found in a more comprehensive study using NiO [39].

At high current densities at higher gas flow rates mass transfer effects become appreciable. Here in Figure (39), the perovskite is seen to be somewhat inferior to the NiO. Considering the relatively undeveloped fabrication techniques employed in making the perovskite electrodes, their performance compared to the NiO electrodes is quite good. Further development of these techniques should improve their performance.

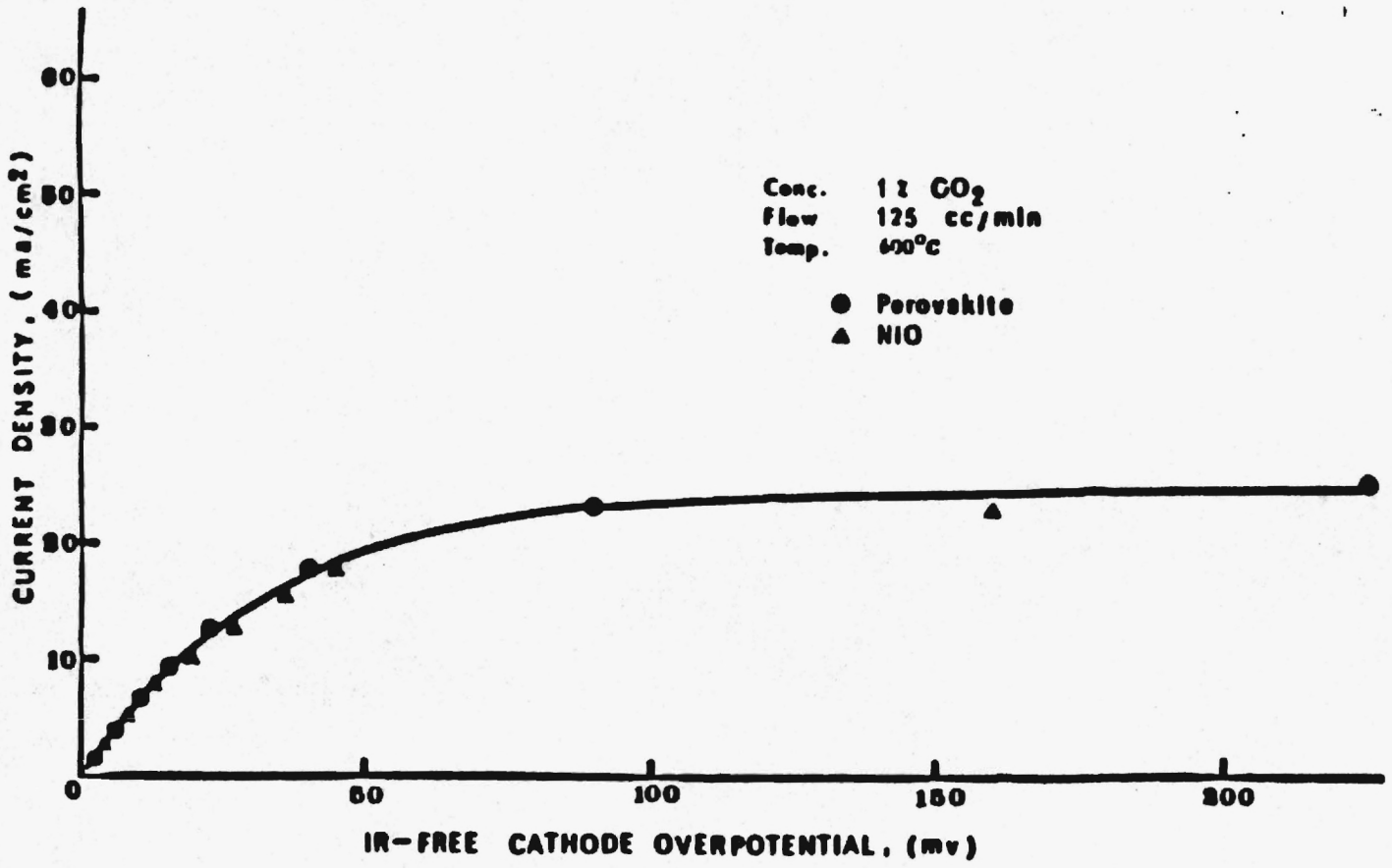

Figure 36. Comparison of Perovskite and NiO Polarization Data at Low Flow Rate

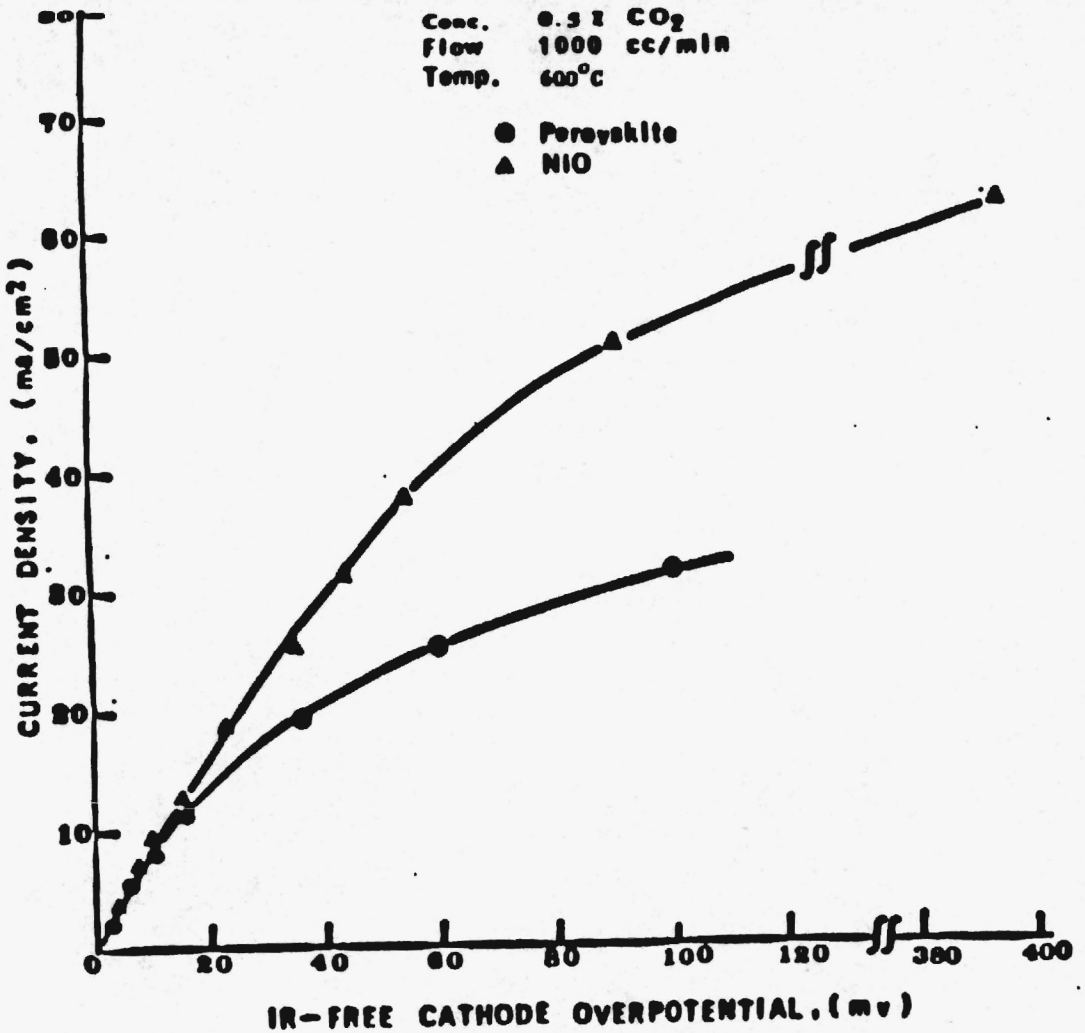

Figure 37. Comparison of Perovskite and NiO Polarization Data at High Flow Rate

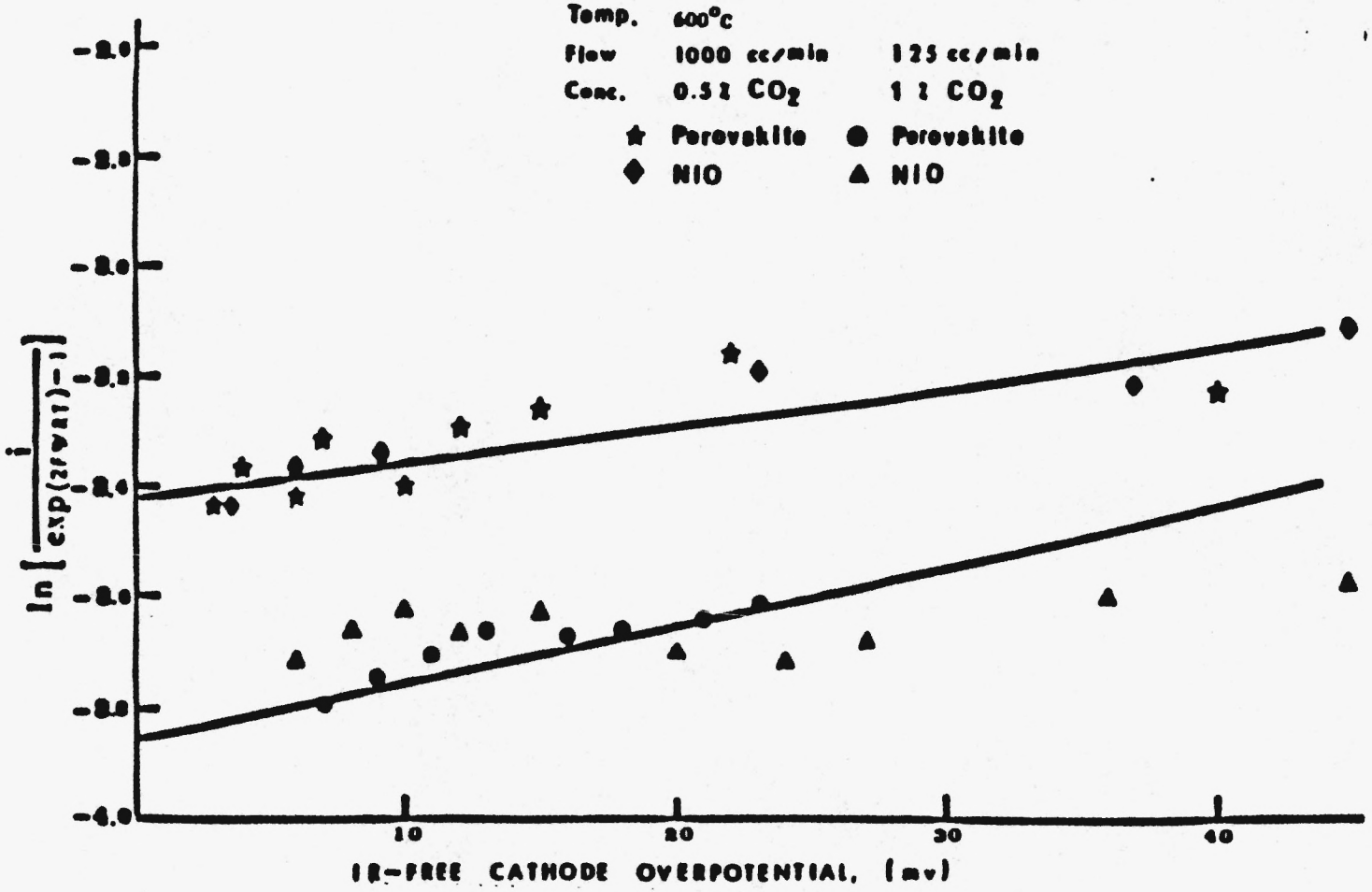

Figure 38. Allen-Hickling Plots for Obtaining Transfer Coefficients

Table 9 Limiting Currents From Polarization Data

Electrolyte	Gas Environment	i_l (a/cm^2)
$K_2S_2O_7$	Air	0.0048
$K_2S_2O_7$	Nitrogen	0.0059
1% V_2O_5- $K_2S_2O_7$	Air	0.0036
1% V_2O_5- $K_2S_2O_7$	Flue Gas	0.0044
1% V_2O_5- 10% K_2SO_4- 89% $K_2S_2O_7$	Air	0.0031
1% V_2O_5- 10% K_2SO_4- 89% $K_2S_2O_7$	Flue Gas	0.0035
1% V_2O_5- 25% K_2SO_4- 74% $K_2S_2O_7$	Air	0.0040
1% V_2O_5- 25% K_2SO_4- 74% $K_2S_2O_7$	Flue Gas	0.0043

* Flue Gas contains .3% SO_2, 3% O_2, 15% CO_2, bal N_2

b. Perovskite Polarizations

Perovskite electrodes were tested in free $K_2S_2O_7/K_2SO_4/V_2O_5$ electrolytes. These electrodes were sintered to obtain strong structures without regard to the resulting pore structure. Polarization data were taken for various electrolyte compositions under different gas environments using perovksite electrodes as both the anode and cathode. Table (9) lists the results of these polarizations while figure (39-47) display the data. The results show that the limiting current is not significantly affected by changes in the gas environment. This is consistent with the results of the thin film experiments where it was found that electroactive species were not supplied by the gas phase. In addition, sulfate and vanadia do not appreciably influence the limiting currents. This is consistent with the CV work earlier which showed the major cathodic reaction was the reduction of pyrosulfate regardless of the additives. On the average, the limiting currents were approximately 5 to 6 mA/cm^2. The relatively low values appear to be due to a thin layer of solid sulfate built up on the electrode surface. The limiting current would be significantly increased in an actual concentrator cell where SO_3 from the gas phase would react with sulfate at the electrode interface, thus "cleansing" surface.

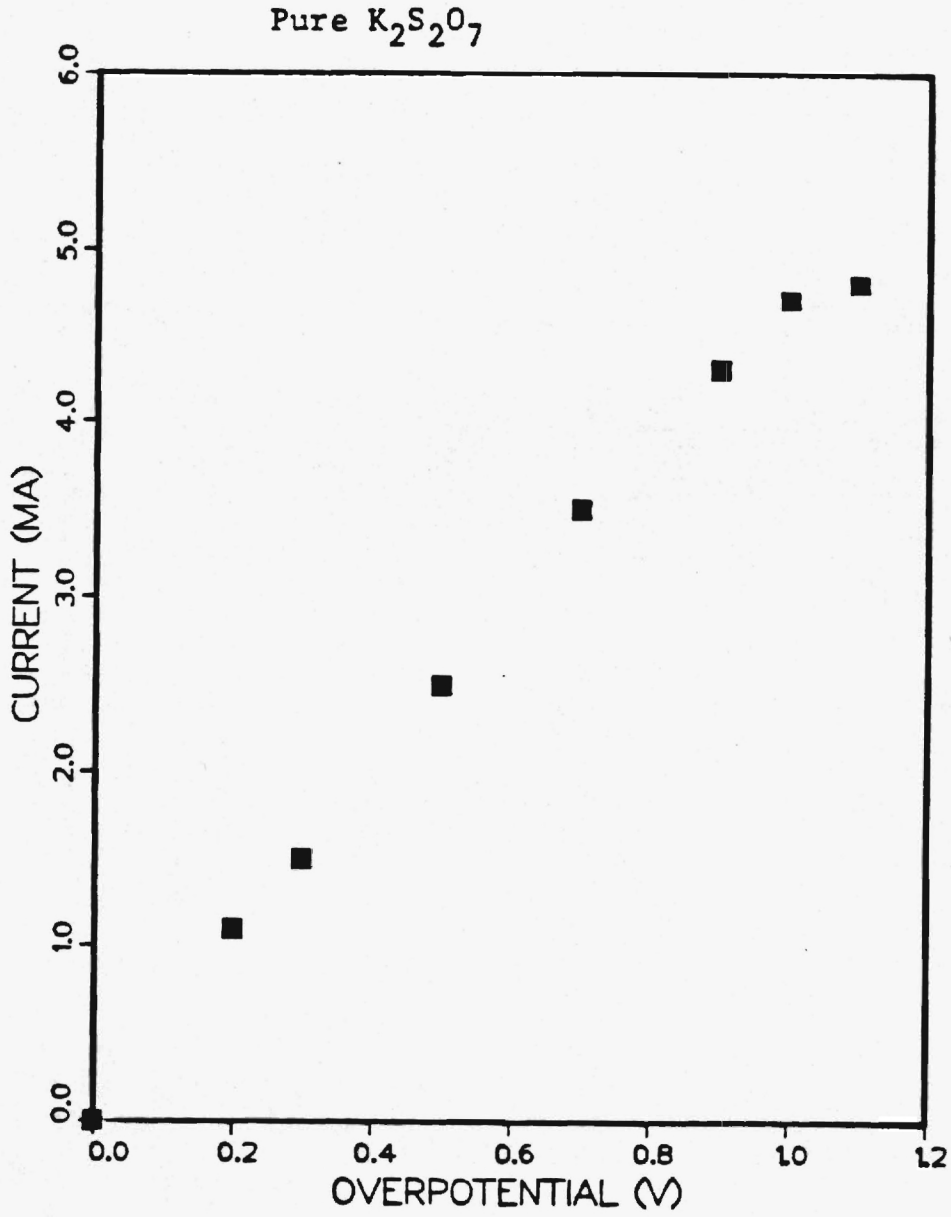

Figure 39. Polarization Data Under Air Environment

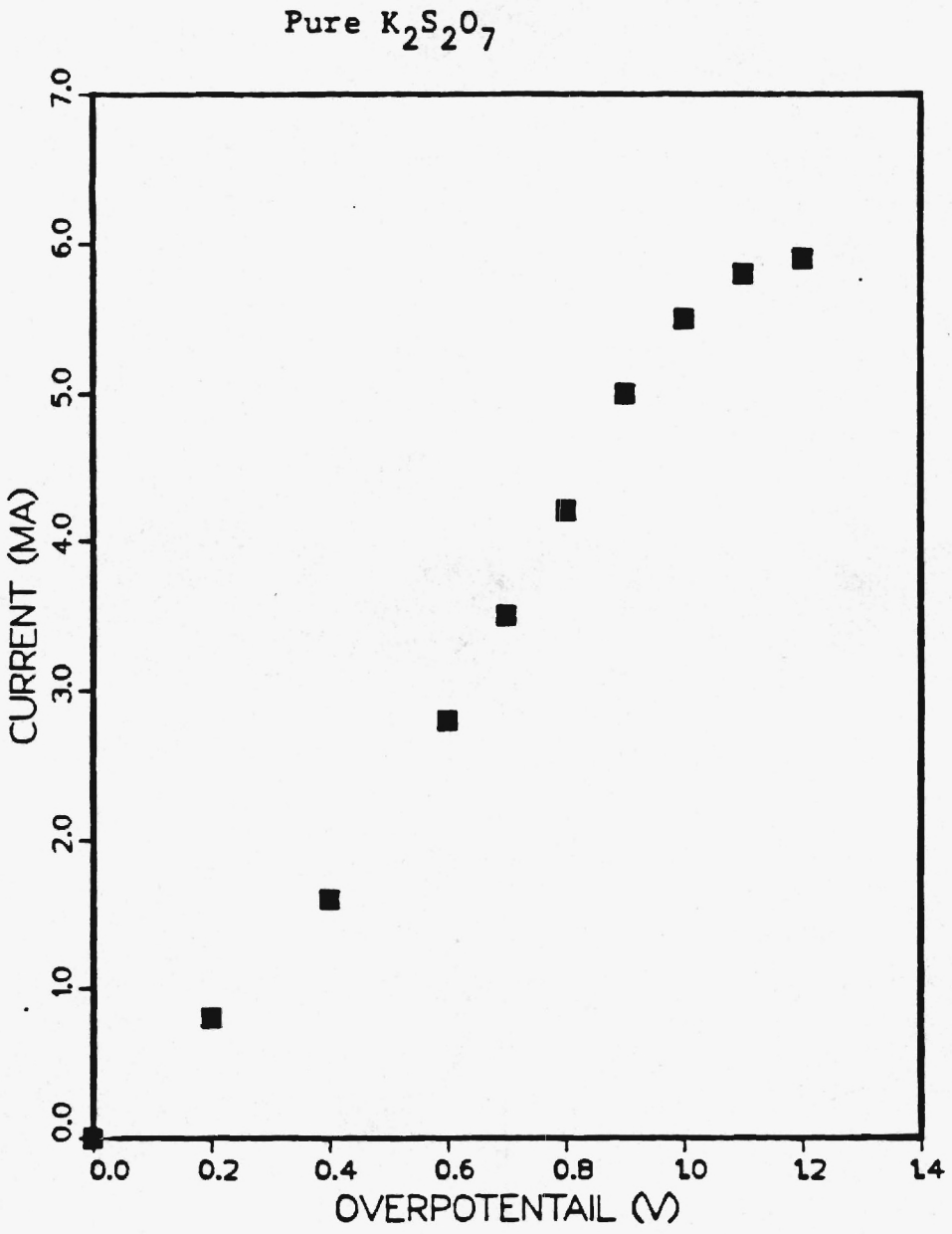

Figure 40. Polarization Data Under Nitrogen Environment

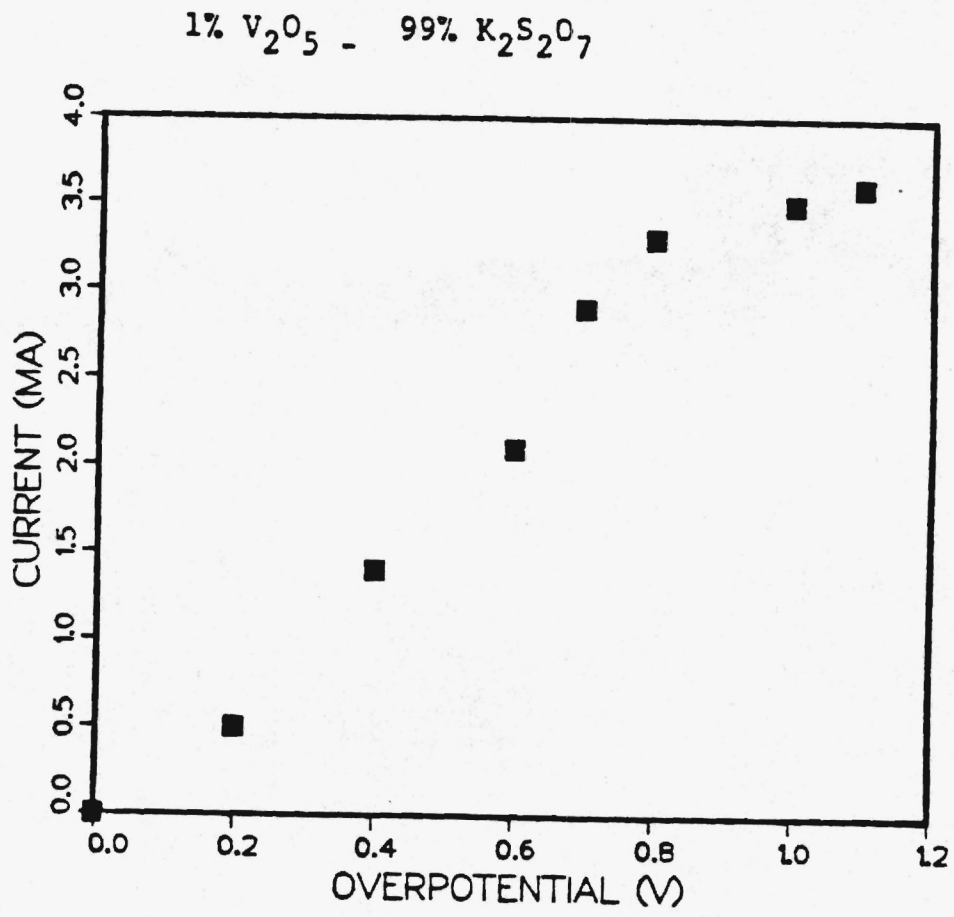

Figure 41. Polarization Data Under Air Environment

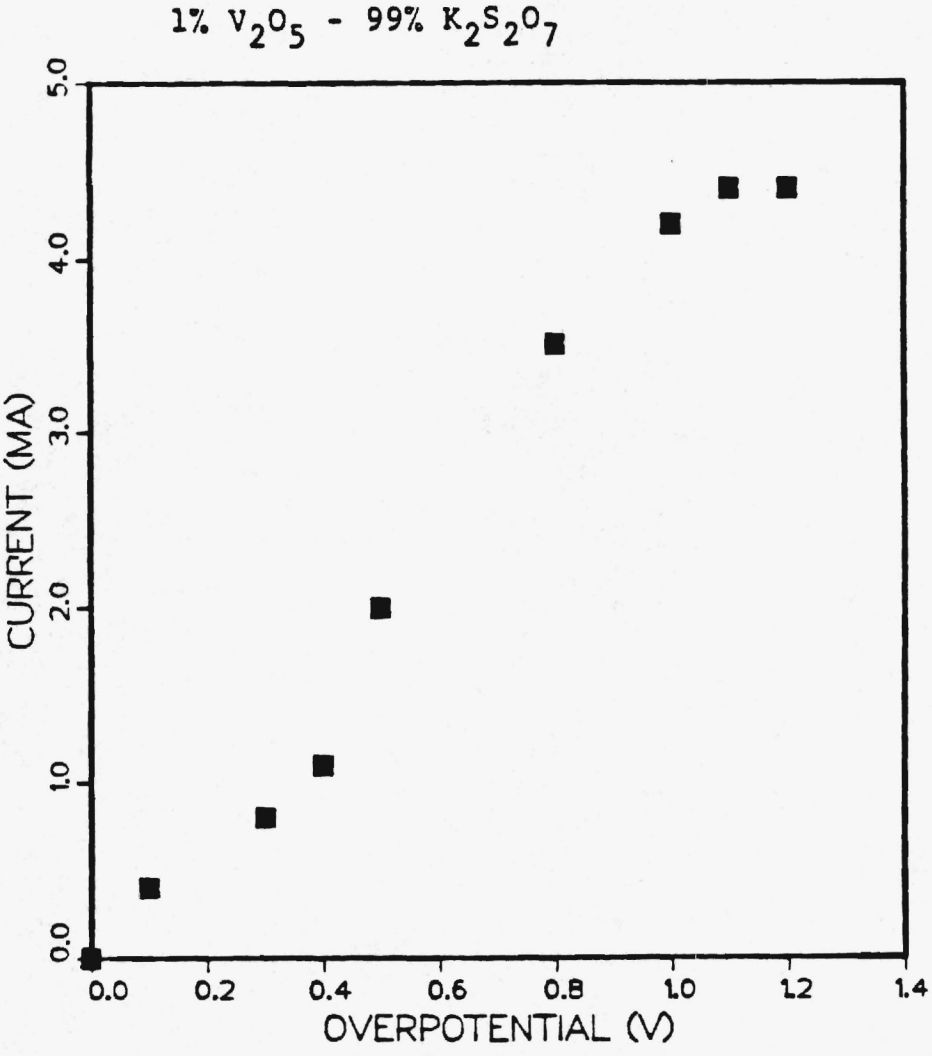

Figure 42. Polarization Data Under Flue Gas Environment

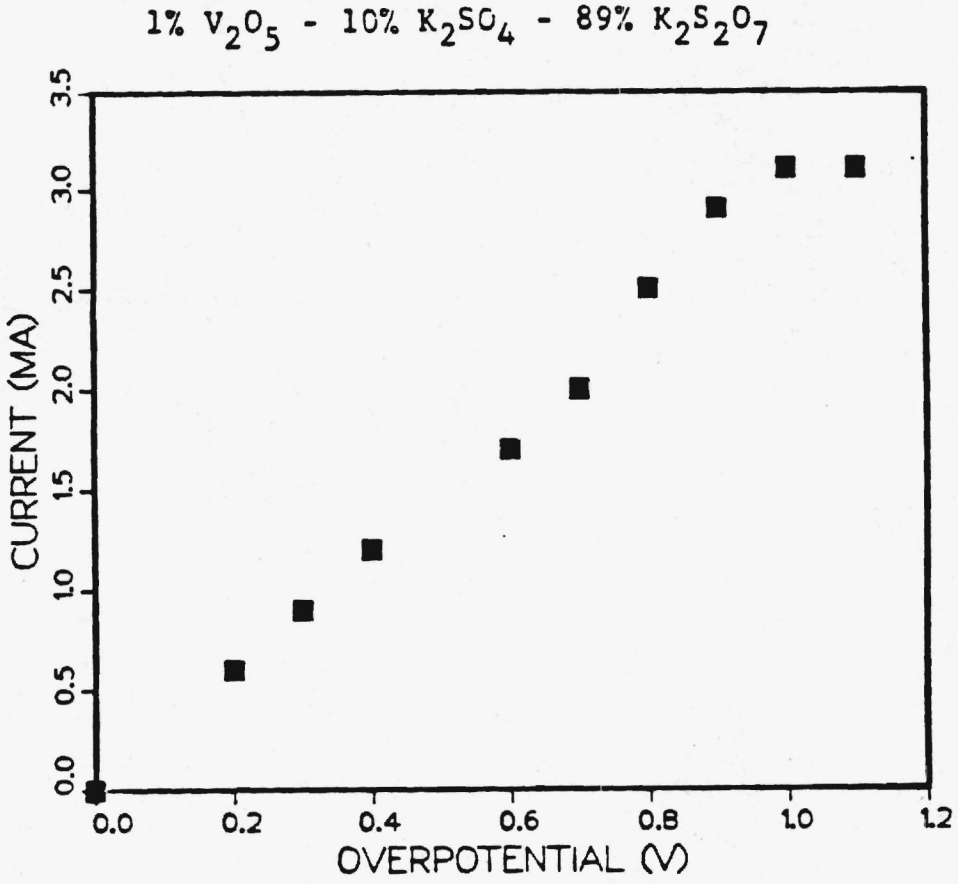

Figure 43. Polarization Data Under Flue Gas Environment

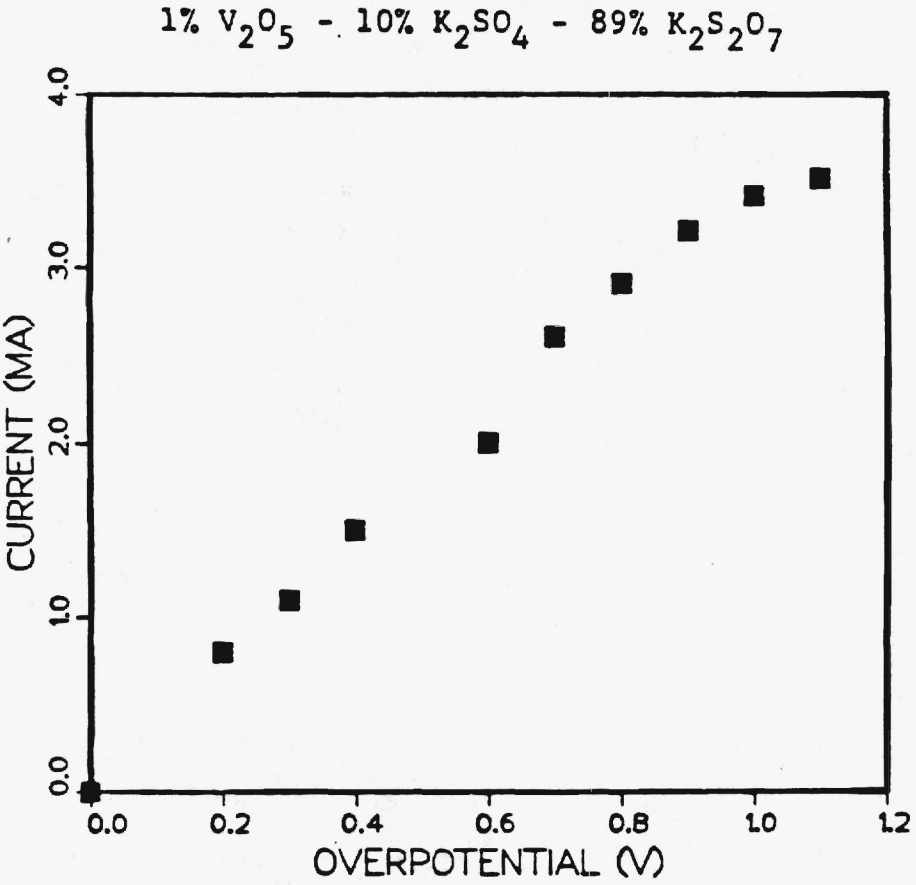

Figure 44. Polarization Data Under Air Environment

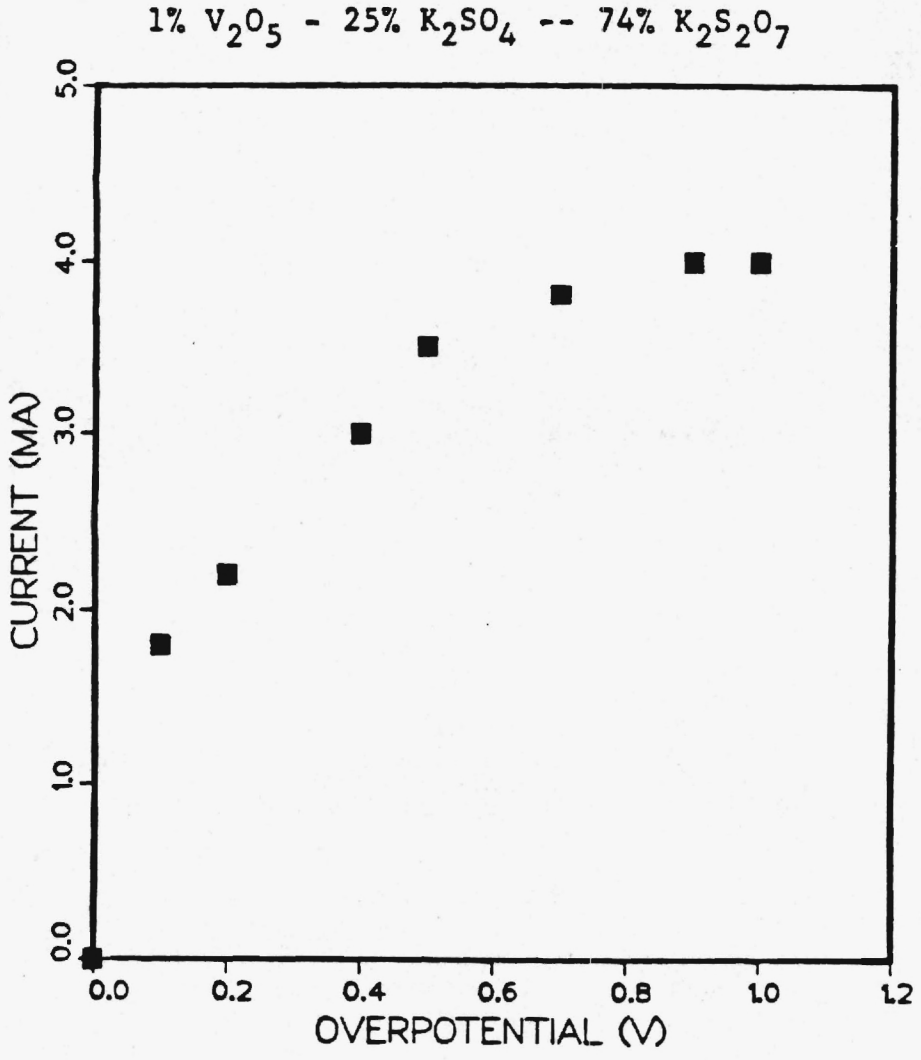

Figure 45. Polarization Data Under Air Environment

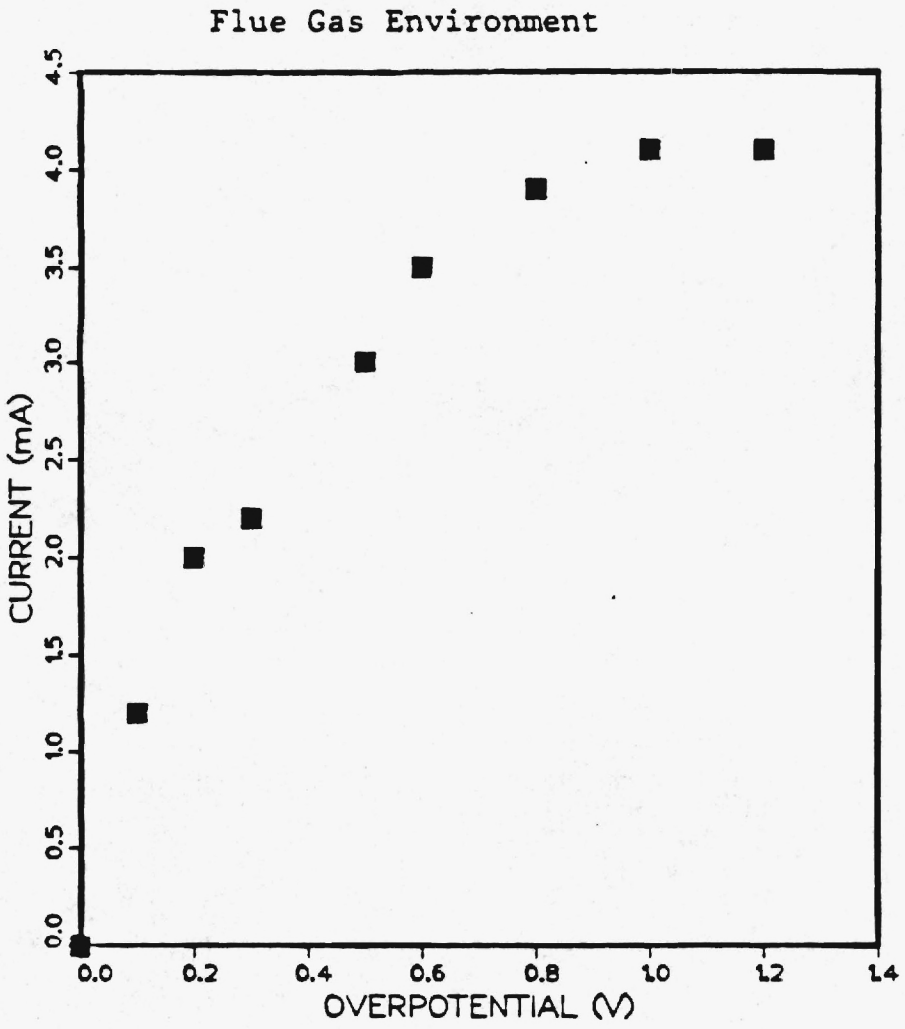

Figure 46. Polarization Data for 1% V_2O_5- 25% K_2SO_4- 74% $K_2S_2O_7$

TASK 3 CERAMIC MEMBRANE

The ceramic membrane is a homogeneous mixture of electrolyte and matrix materials. The matrix is an inert material which holds the electrolyte in place by capillary forces. Five materials, including zirconia felt, fritted pyrex, SiC, $SrTiO_3$, and MgO, were tested as matrices.

Membranes which employed zirconia felt and fritted pyrex were fabricated in accordance with the procedure outlined in the experimental section (a. Impregnation of commercial "matrices"). Although the zirconia felt displayed good chemical resistance to be corrosive electrolyte, the felt mesh was not fine enough, resulting in insufficient capillary forces to retain the electrolyte. Similar results were derived from membranes which employed fritted pyrex as the matrix. This structure comes as a porous pyrex disc, 5.0 cm in diameter by 0.4 cm thick, with a pore size of 4 to 5 microns (smallest pore size available), supplied by Corning. These structures also displayed good chemical resistance and were an improvement over the felt due to increased retention of the electrolyte. But electrolyte leakage continued to be a problem. Commercial membranes have nominal interstice size of 0.2 microns, over an order of magnitude smaller than that of the pyrex frits. These porous pyrex matrices appear to have potential for success, but the pore size must be reduced considerably to assure sufficient capillary forces.

The second type of membrane fabrication procedure was impregnating partially-sintered matrix structures (see Experimental section (3b)). Matrix materials tested were SiC, $SrTiO_3$, and MgO. The major problem encountered in this procedure was that the sintered matrix structures were very weak and tended to fall apart during electrolyte impregnation. Sintering the pressed ceramics was intended to strengthen the structure, but due to the very high melting points of these materials, and an upper limit of 1200°C on available furnaces, little sintering occured. This procedure was abandoned in favor of the method described below.

The final, and most successful, method for fabricating membranes was hot-pressing (see Experimental section (3c)). Two materials, $SrTiO_3$ and MgO, have proven to be good matrices.

X-ray diffraction was employed to determine whether the $SrTiO_3$ interacts chemically with the electrolyte. Figures (47) and (48) are the diffraction patterns of the pure materials and figure (49) is a mixture of the two. Figure (50) is again a mixture of the two, identical to figure (49), except that the mixture was pressed into a membrane and sintered at 325°C for three hours. Figure (50) shows distinct differences compared to figure (49), indicating the $SrTiO_3$ reacts with the electrolyte. The diffraction patterns give inconclusive information as to the identity of the reaction product, but it is likely some type of strontium or titanium sulfate complex.

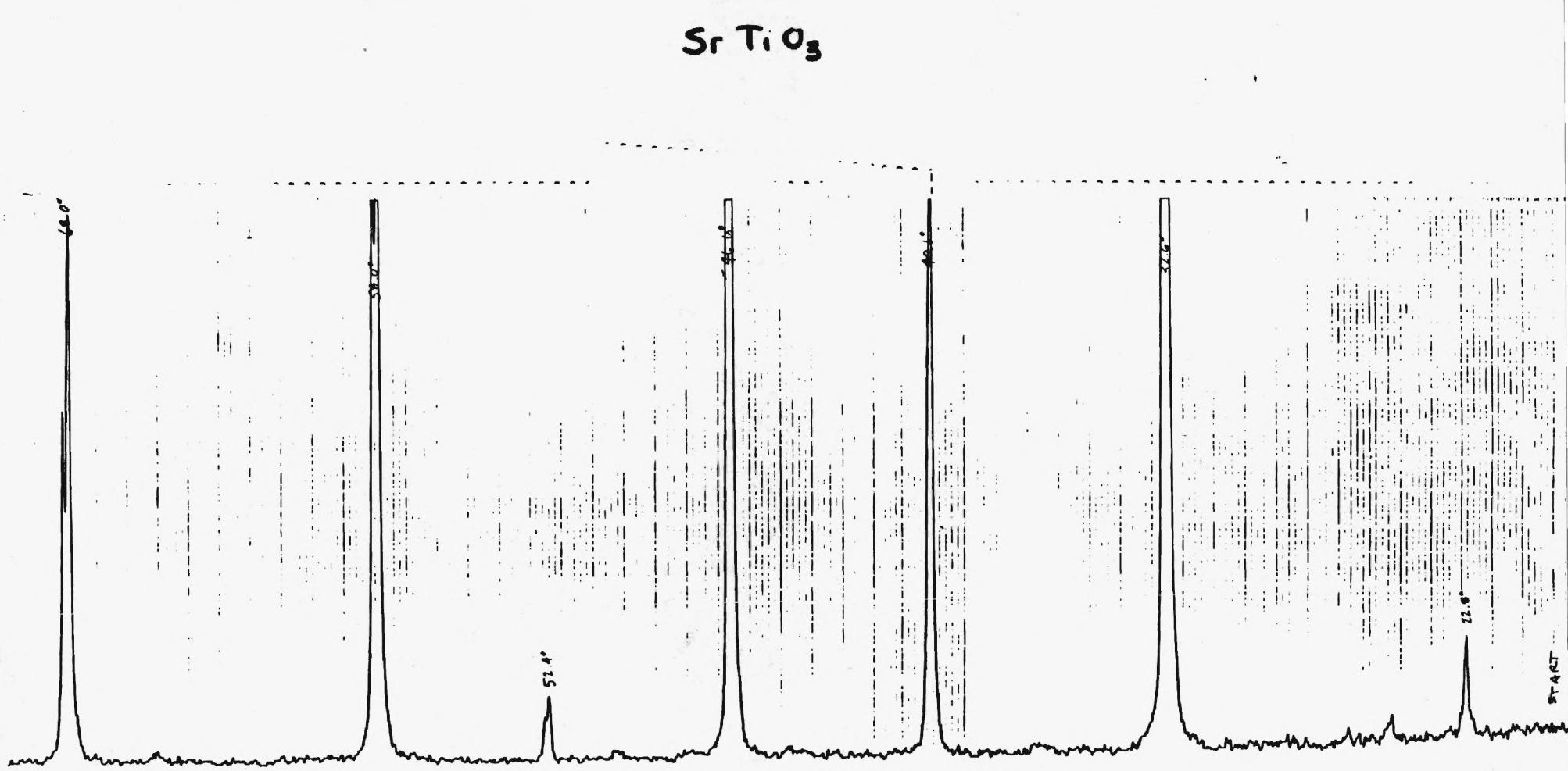

Fig. 47. Diffraction Pattern of $SrTiO_3$

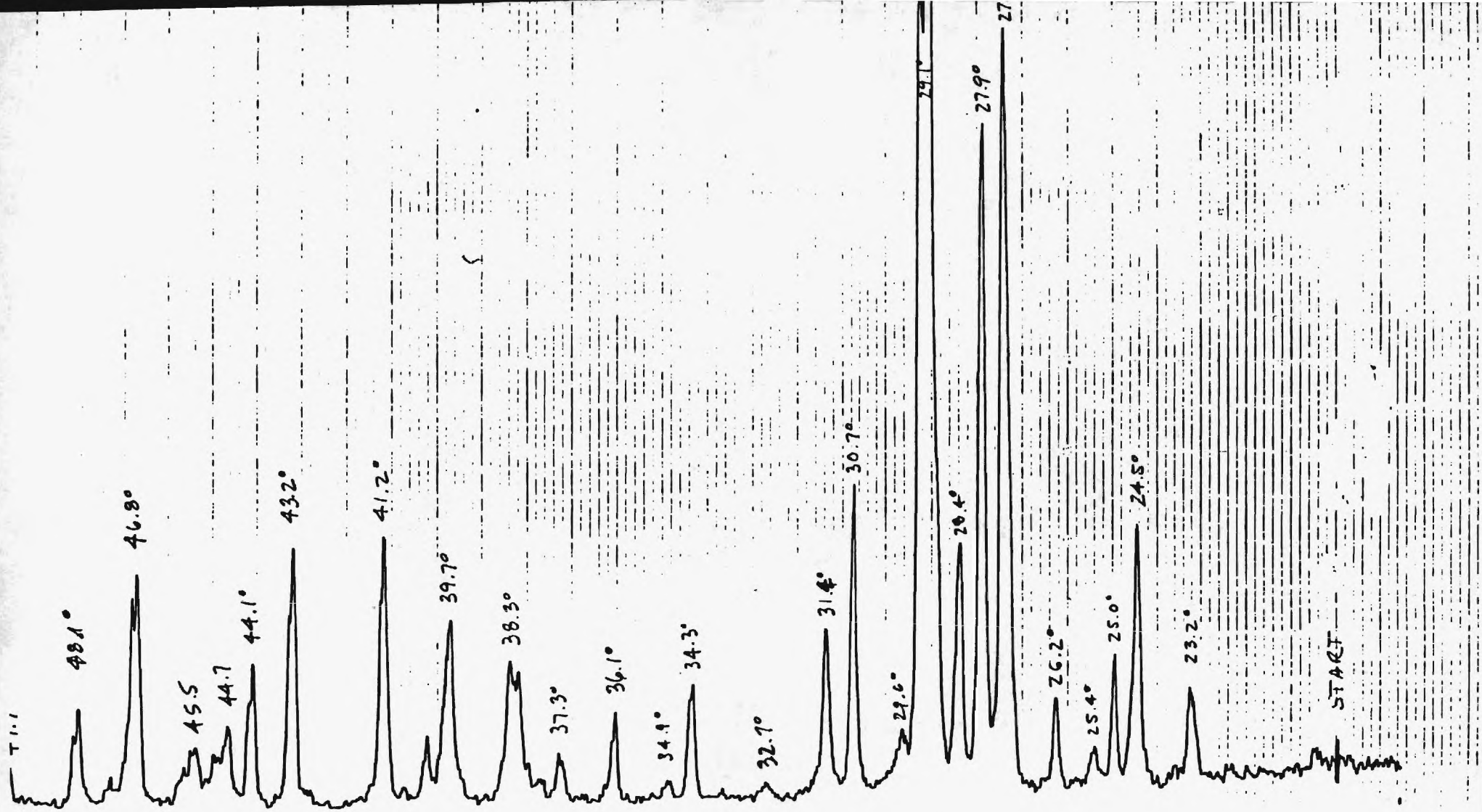

Fig. 48. Diffraction Pattern of $K_2S_2O_7$ with 1.0% V_2O_5

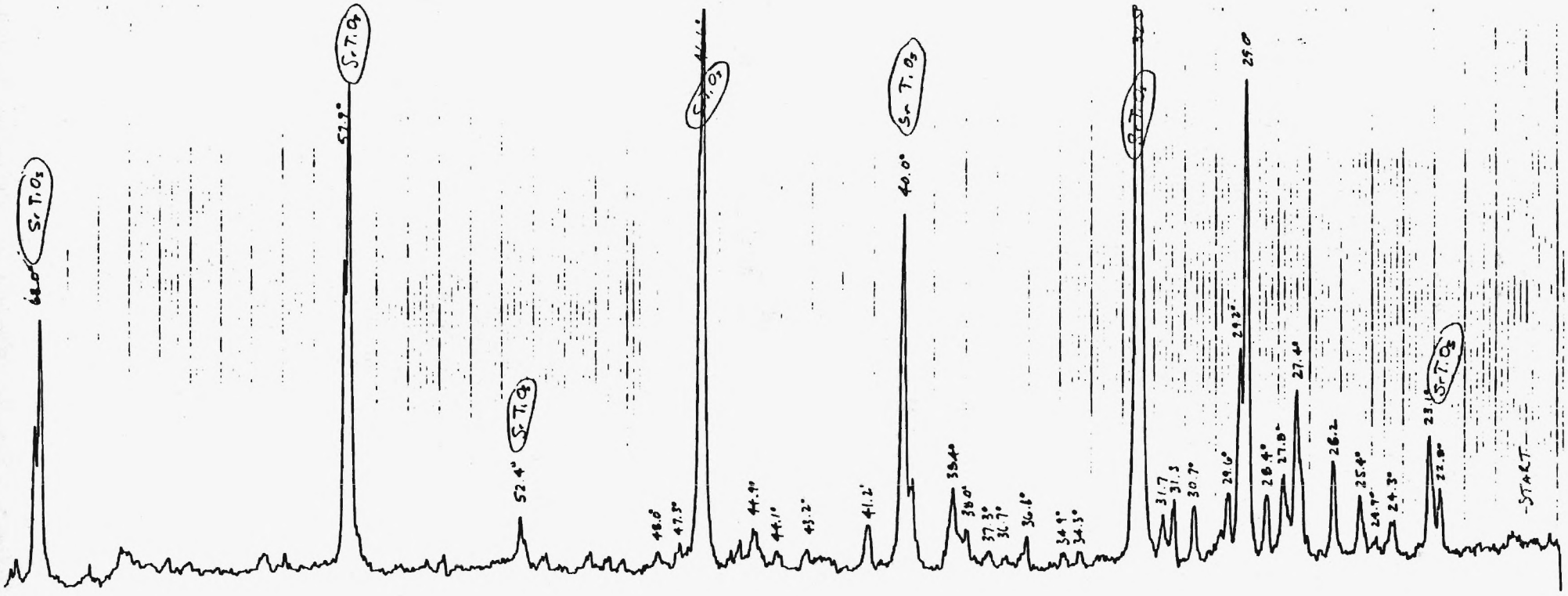

Fig. 49. Diffraction Pattern of 50% $SrTiO_3$, 50% $K_2S_2O_7/V_2O_5$

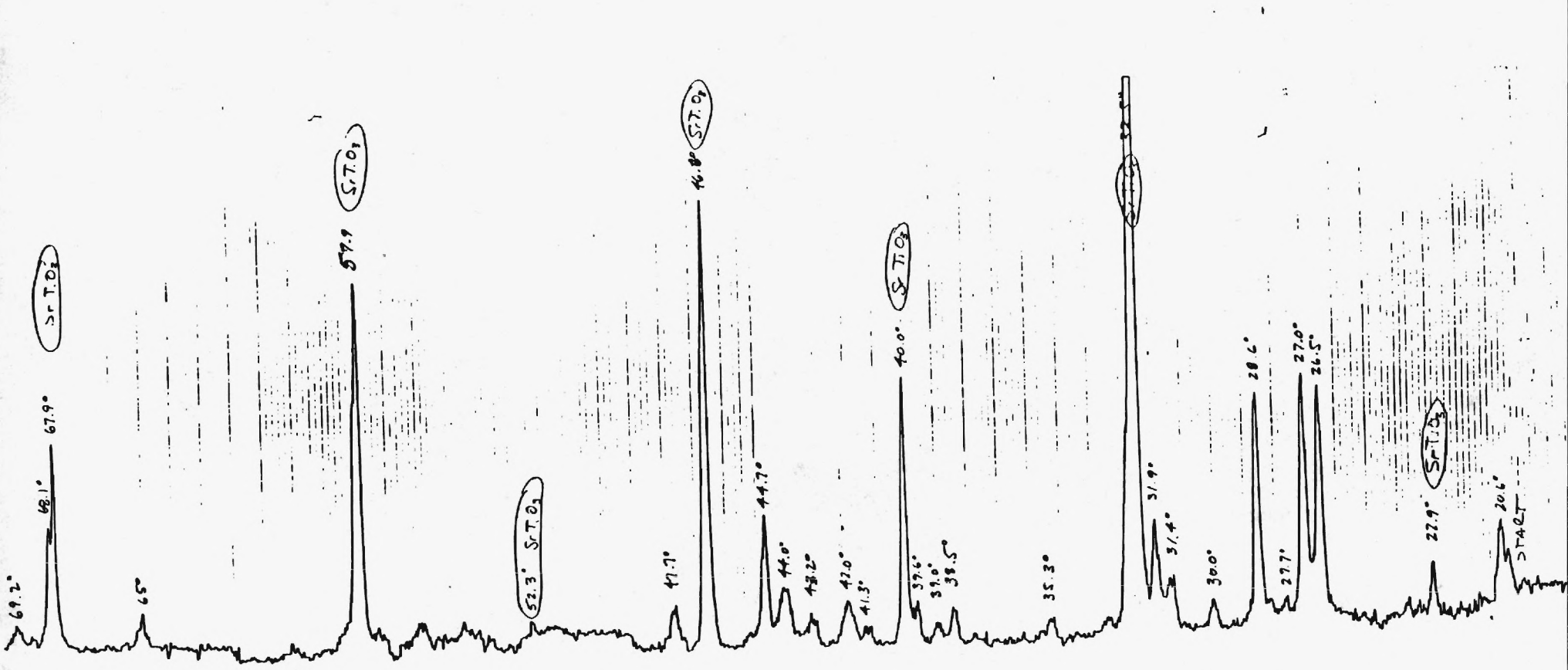

Fig. 50. Diffraction Pattern of 50% $SrTiO_3$, 50% $K_2S_2O_7/V_2O_5$ Sintered at 325°C for 3 Hours

Although the x-ray diffraction results may seem to indicate that $SrTiO_3$ is an inappropriate matrix material, commercial ceramic membranes have faced the same problem. In these cases a "new" matrix, the reaction product of the original matrix and the electrolyte, and possibly some left over original ceramic, is used as the matrix. This idea appears to be applicable to $SrTiO_3$ and our electrolyte system. Membranes of this nature have been fabricated which satisfy physical criteria, such as strength, density (>98% theoretical density), and conductivity (on the order of 1.0 ohm).

The other promising candidate as the ceramic material is MgO. Figure (51) is the x-ray diffraction pattern of a pressed mixture of MgO and electrolyte, sintered at 350°C overnight. Peaks corresponding to MgO, $K_2S_2O_7$ and SO_4 are identifiable but a new component has clearly been formed. The identify of the reaction product remains unclear, but appears to be a magnesium sulfate complex. Fabrication of membranes containing MgO is similar to $SrTiO_3$, where the reaction product is used as the matrix base. MgO containing membranes have been fabricated which meet required physical criteria (strength, density, and conductivity).

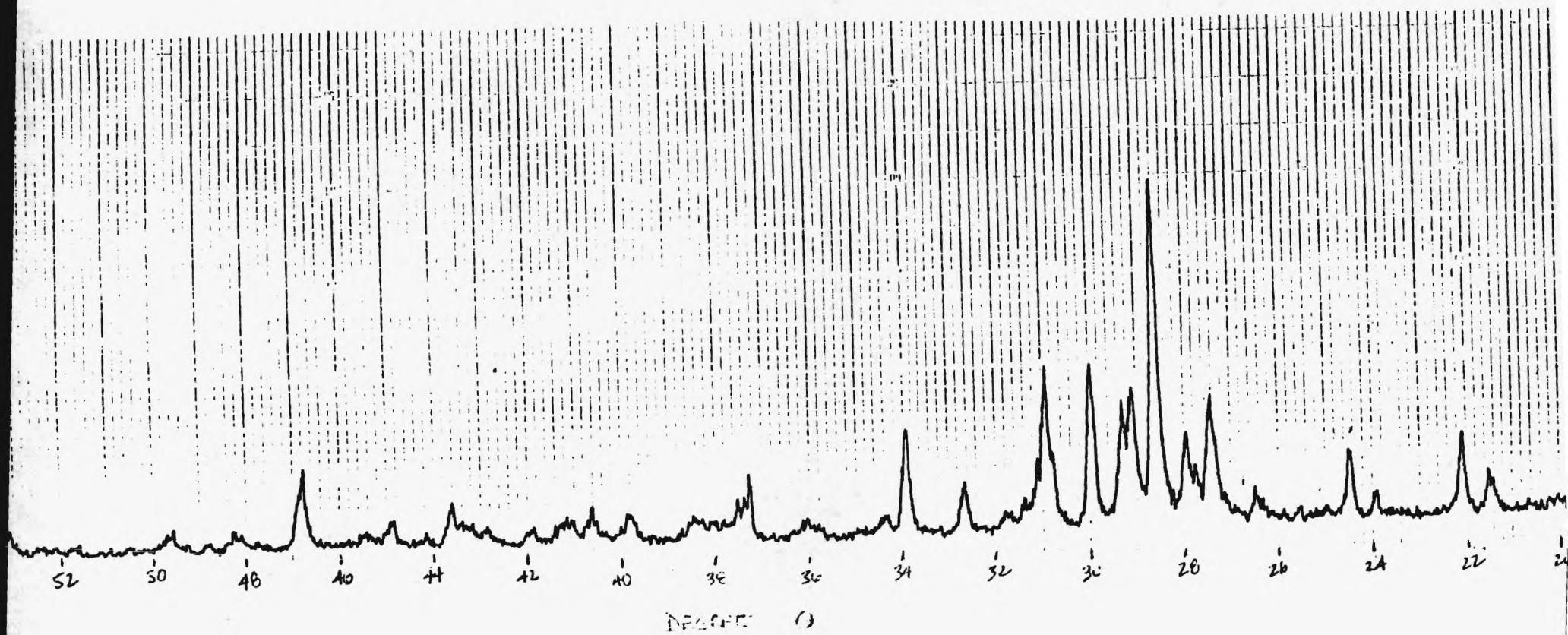

Fig 51. Diffraction Pattern of 83% $K_2S_2O_7$/1%V_2O_5, 8.5% K_2SO_4, 8.5% MgO. Sintered at 350°C overnight

TASK 4. NO_x REMOVAL

NO Removal

The removal of NO was examined in electrolytes containing vanadia. Initial tests were made in a 1% V_2O_5, 99% $K_2S_2O_7$ melt with NO removals ranging from 30 to 60%. This removal did not change with the application of current nor did the NO_x concentrations change during the course of the experimentation. The amount of removal did depend upon the flow rate of the working gas with the highest removals occuring at the lowest flow rates. The working gas in these experiments contained 900 ppm NO and the balance nitrogen.

More extensive studies were then conducted in the sulfate-containing electrolytes. Figure 52 shows the results of these experiments, detailing the dependence of NO removal with flow rates. At optimum flow rates of 30-40 cc/min, NO removals up to 50% were realized. The application of current did not change the removal rate in these electrolytes. The addition of sulfate, however, raised the NO removal values by an average of six to ten percent as compared to the removals seen in the vanadia-pyrosulfate melts. It is important to note that even at relatively high gas flow rates, a significant amount of NO was removed.

NO/SO_2 Removal

The passage of gases containing both SO_2 and NO through the test electrolytes revealed some additional insight into the contaminant gas removal process. Tests were conducted in the two sulfate-containing electrolytes with equi-volume and other volume concentrations of the separate working gases being used.

In these experiments, the amounts of NO removal were similar to the values obtained for the pure removal studies. The amounts of NO removal, ranging from 25 to 58%, were dependent on the total gas flow rate, not necessarily the flow rate of the NO_x gas mix. However, SO_2 removal versus applied current is ehanced as shown in Figure 53 for a 30 cc SO_2/10cc NO gas mixture. For this and other flow rates, the SO_2 removal efficiencies were on average five to ten percent higher than the corresponding values obtained in the pure SO_2 removal studies. As noted earlier the total amounts of SO_2 removal were again limited at values between 40 and 45%.

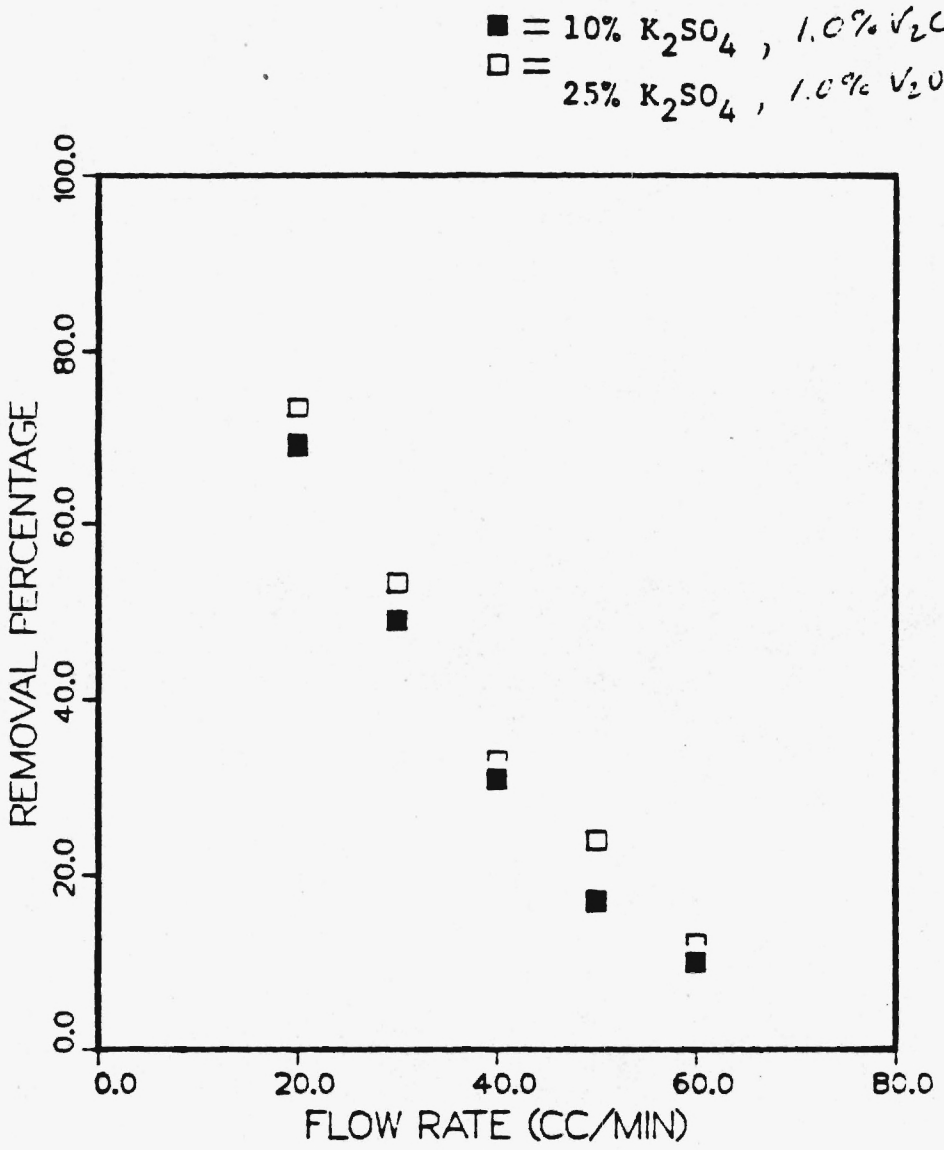

Figure 52. NO Removal Data

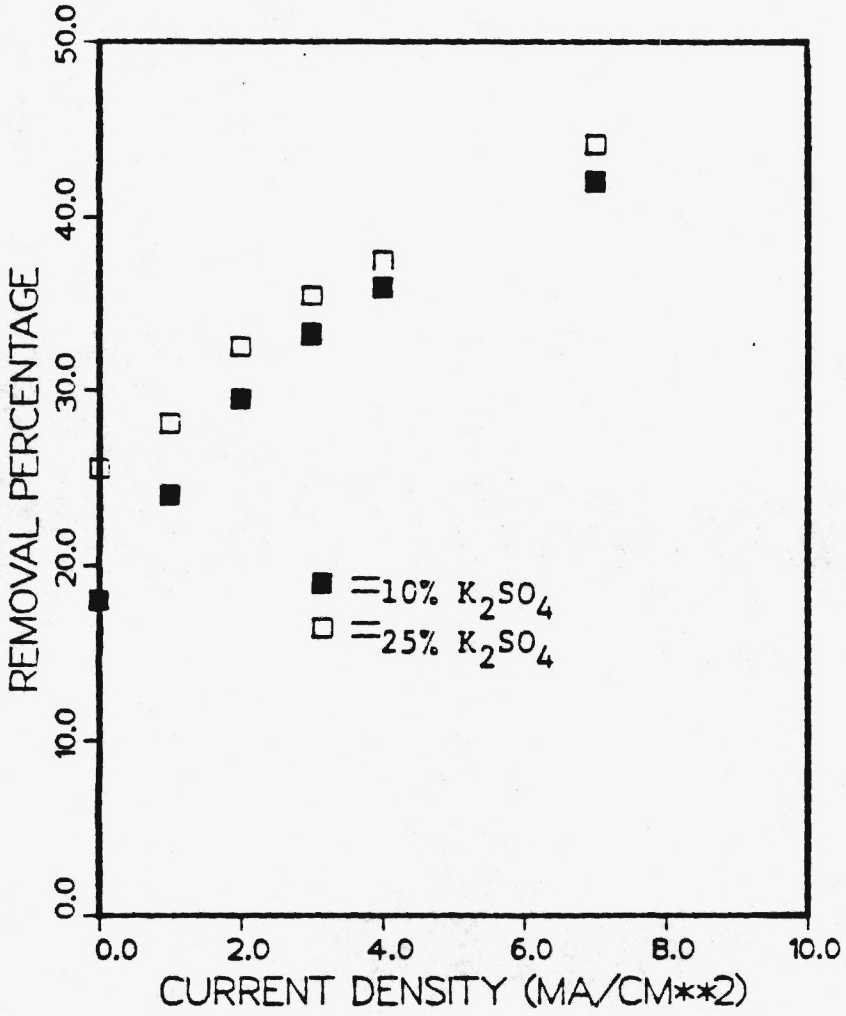

Figure 53. SO_2 Removal During NO/SO_2 Studies

TASK 5 FULL CELL TESTING

The bench scale electrochemical concentrator cell was described and diagrammed in the experimental chapter (section 5 and figure 6). Six full-cell runs are reported in the following pages. Each run is identified by a code of the form:

x-y-VaSb

where x identifies the electrode type and:

x = A - perovskite
B - gold screen
C - porous carbon
D - porous nickel

and y identifies the matrix material with:

y = 1 - zirconia felt
2 - pyrex frit
3 - $SrTiO_3$
4 - MgO

The last part of the code identifies the electrolyte composition, where V and S represent vanadia and sulfate and a and b are the weight fractions of vanadia and sulfate respectively. Thus, the code A-4-V1S1 would indicate the run utilized perovskite

electrodes, a MgO matrix, and the electrolyte was $K_2S_2O_7$ with 1.0% V_2O_5 and 1.0% K_2SO_4.

Each set of results is presented in chronological order and includes the cell temperature, cathode gas flow rate, concentration of SO_2 in the inlet and outlet streams, SO_2 removal, and electronic parameters (cell current, ohmic resistance, and electrode potentials ((c)-cathode, (A)-anode, (R)-reference)). Two types of removal are reported. The first is the actual removal, calculated from the inlet and outlet SO_2 concentrations. The second type, termed the ideal removal, is the theoretical amount of SO_2 which would be removed electrochemically, calculated on the basis of two faradays per mole of SO_2 removed.

The results of Run A-1-V1SO are shown in table 10. The removal results show the maximum removal was approximately 15%. This was achieved at open circuit, in the early stages of the run. During the course of the run the open circuit removal steadily declined to a final value of approximately 3%. A decrease in removal was also observed open passage of cell current. The reasons behind these trends are discussed in subsequent paragraphs.

TABLE 10 RUN A-1-V1S0

DATE	TIME	TEMP C	FLOW (cc/min)	SO_2 CONC (ppm) IN	SO_2 CONC (ppm) OUT	REMOVAL	IDEAL REMOVAL	CURRENT (mA)	RESISTANCE (ohms)	POTENTIALS (volts) C/R	POTENTIALS (volts) A/R
09/15/85	23:30	heating	20	10000	10000	0%	0%	0.0	-	-	-
09/16/85	9:00	320	20	10000	8500	15%	0%	0.0	9	+0.287	+0.480
	10:00	320	20	10000	8600	14%	0%	0.0	9	+0.280	+0.472
	10:30	320	20	10000	10000	0%	19%	5.0	-	+0.150	+0.770
	11:45	320	20	10000	9500	5%	19%	5.0	-	+0.010	+0.820
	13:00	320	20	10000	8500	15%	0%	0.0	11	+0.277	+0.471
	13:30	320	20	10000	9700	3%	38%	10.0	13	-0.380	+0.920
	14:15	320	20	10000	9500	5%	38%	10.0	-	-0.530	+0.980
	14:45	320	20	10000	9000	10%	0%	0.0	18	+0.269	+0.467
	16:00	320	20	10000	9200	8%	0%	0.0	21	+0.268	+0.464
	17:10	320	20	10000	9300	7%	19%	5.0	-	-0.045	+0.800
	18:20	320	20	10000	9300	7%	19%	5.0	-	-0.310	+1.035
	21:00	350	20	10000	9500	5%	0%	0.0	22	+0.249	+0.452
09/17/85	9:20	350	20	10000	9700	3%	0%	0.0	41	+0.192	+0.393
	9:45	350	20	10000	9700	3%	19%	5.0	-	UNSTABLE	
	12:00	350	20	10000	9700	3%	8%	2.0	_	-0.277	+0.690
	14:15	350	20	10000	9800	2%	0%	0.0	55	+0.188	+0.390
	16:00	400	20	10000	9700	3%	0%	0.0	53	+0.166	+0.367
	16:40	400	20	10000	9800	2%	19%	5.0	-	UNSTABLE	

The perovskite electrodes proved to be very stable in the cell environment. Unfortunately, the electrode pores were very small (1 to 5 microns, by SEM), thus exerting high capillary forces on the adjacent electrolyte. The result was pore flooding of the electrodes. This problem can be corrected by enlarging and optimizing the pore structure. Future work with perovskites will focus on optimizing fabrication techniques so that perovskite can be used successfully in full cell tests.

The zirconia felt was found to be a poor matrix. This was due to insufficient capillary forces exerted by the felt to retain the electrolyte within the membrane during operation. Examination of the cell showed electrolyte had leaked from the membrane onto the cell housings, into the flow channels and into the electrode pores.

The leakage of electrolyte from the membrane and into the electrode pores is the root of problems encountered in their run. During the run the electrode pores became increasingly filled with electrolyte. Upon passage of faradaic current, pyrosulfate is reduced to form sulfate. The sulfate is slow to diffuse out of the pores and accumulates, resulting in a solid sulfate build-up in the pores. This was confirmed by post-run analysis. Thus, during operation the electrode pores "clogged" with sulfate, blocking access to the membrane and decreasing SO_2 removal.

The electrical parameters in table 10 also show definite trends. The ohmic resistance (between the working (C) and counter (A) electrodes) continuously increased. This is due to

the electrolyte drainage from the membrane, which acts to decrease conductivity. In addition, the overpotential required for a given current steadily increased during the course of the run. For example, to drive 5 mA through the cell, the required cell potential (C/A) went from 0.6 volts at the start, to 1.35 volts eight hours later, to an unstable condition where the potential was out of control less than a day later. Lost membrane conductivity, electrode pore flooding, and solid sulfate build-up all contributed to this behavior.

The run was aborted after two days for two major reasons. First, the polarization behavior of the cell, described above, became intolerable. Secondly, essentially no SO_2 was removed, regardless of the cell current, after two days.

Table 11 gives the results of Run B-2-V1SO. Here the electrode and matrix have been switched to gold screen and a pyrex fritted disc respectively. The gold screen was chosen to eliminate the pore flooding problem encountered in the previous run. The fritted disc was expected to retain the electrolyte better.

Although the change in electrodes and matrix was expected to improve the cell operation, little change over the previous run was observed in performance. The same behavior was found for SO_2 removal. The highest removal was 5% at open circuit in the initial stages of the run. Open circuit removal decreased over the course of the run, to no removal at the end. Application of current was found to decrease removal, and in some cases resulted in a net increase of SO_2 (negative removal). This

removal is reminiscent of the effluent analysis results when the electrolyte did not contain vanadia. A proposed mechanism by which SO_2 is evolved upon passage of current was given by equations (29) through (33). Following addition of vanadia to the electrolyte, the effluent analysis results showed increased, and net SO_2 removal under all conditions. This behavior is attributed to additional reactions propogated by vanadia, summarized by equations (40) through (43). The role of vanadia is most important in equation (41), the oxidation of SO_2. Thus, the removal results of this run suggest vanadia may not adequately fulfill its oxidation role in the full-cell. This discussion is further developed in the next paragraph and in the appendix.

The absolute removal numbers are smaller in this run compared to the previous one. This is in part due to the higher cathode gas flow rate used in the present run (40 cc/min compared to 20 cc/min in run A-1-V1SO). This indicates mass transfer or SO_2 oxidation kinetics limit the removal rate. In the effluent analysis results it was seen that net SO_2 removal depended to a large extent on the oxidation of SO_2 to SO_3. Using the kinetic equations derived by Holroyd and Kenney [40] the conversion of SO_2 to SO_3 is calculated to be less than 0.5% for the conditions of this run and the cell geometry (see appendix). Thus, the removal rate may very well be limited by the oxidation rate.

TABLE 11 RUN B-2-V1S0

DATE	TIME	TEMP C	FLOW (cc/min)	SO_2 CONC (ppm) IN	SO_2 CONC (ppm) OUT	REMOVAL	IDEAL REMOVAL	CURRENT (mA)	RESISTANCE (ohms)	POTENTIALS (volts) C/R	POTENTIALS (volts) A/R
09/22/85	17:30	heating	40	10000	10000	0%	0%	0.0	-	-	-
	21:30	320	40	10000	-	-	-	0.0	2.3	+0.229	+0.350
	23:30	320	40	10000	-	-	0%	0.0	2.5	+0.233	+0.348
09/23/85	9:15	320	40	10000	9500	5%	0%	0.0	13.0	+0.278	+0.323
	10:00	320	40	10000	9900	1%	2%	1.0	-	+0.020	+0.526
	12:30	320	40	10000	10600	-6%	10%	5.0	12.0	-0.165	+1.165
	14:30	335	40	10000	10200	-2%	19%	10.0	15.0	-0.430	+2.040
	23:00	335	40	10000	10000	0%	0%	0.0	12.0	-	-
09/24/85	9:00	335	40	10000	10000	0%	0%	0.0	-	+0.130	+0.555
	9:30	335	40	10000	10600	-6%	19%	10.0	-	-0.410	+1.430
	10:10	335	40	10000	10200	-2%	19%	10.0	-	-1.580	+1.570
	10:40	335	40	10000	-	-	10%	5.0	-	-1.370	+1.270
	12:00	350	40	10000	-	-	10%	5.0	-	-1.440	+1.250
	13:00	350	40	10000	10000	0%	10%	5.0	28.0	-1.950	+1.310
	15:00	350	40	10000	10000	0%	0%	0.0	40.0	-	-

Although gold is highly conductive and quite stable in the cell environment, the screen is not well suited for full-cell tests. This is due to the low surface area of contact between the screen and the membrane. Relatively high current densities are required at these points of contact. Since the rate of sulfate generation in a given area is proportional to the current density, solid sulfate build-up at the electrolyte/electrode interface would be expected to worsen in this run. The effects of this are seen in the potentials listed in table 11. The required cell potential (C/R-C/A) for a given current is significantly higher in this run than in the previous run, even though the ohmic resistance is lower. This is most likely an artifact of the increased solid sulfate build-up at the interface, which acts as an additional impedance.

The pyrex fritted disk matrix had both good and bad features. The structure showed excellent stability in the cell environment. In addition, the conductivity was quite high in the initial stages of the run (~2 ohm). Although electrolyte leakage did occur, there was a substantial improvement over the zirconia felt. Still, leakage exceeded acceptable levels. A pyrex frit with a smaller pore size could prove to be an excellent matrix. Unfortunately, the frit utilized is the smallest pore size commercially available.

On the final day of the run cell performance was very poor. At open circuit there was no removal and applied current resulted in evolution of SO_2 In addition the polarization behavior was unacceptable. In excess of 3.0 volts was required to drive a 5 mA current. For these reasons the run was stopped.

Table 12 shows the results of Run C-3-V1SO, where the electrodes are commercially produced porous carbon and the membrane is a $SrTiO_3$ matrix (1.0 weight percent) with a 99% $K_2S_2O_7$, 1% V_2O_5 electrolyte. The membrane was produced by the hot-pressing procedure outlined in the Experimental chapter (section 3c).

The removal results of this run follow the same basic trends seen in the previous runs. The highest removal rates were achieved at open circuit (15%). Application of current resulted in decreased removal and a net production of SO_2. In this run the flow rate was held at 50 cc/min which translates to an approximate SO_2 to SO_3 conversion of 0.14% in the full-cell, see appendix. The very low conversion to SO_3 is likely a major reason for the poor removal results (see explanation for Run B-2-V1SO).

The carbon electrodes were employed because they were structurally appealing. First, these electrodes have a nominal pore diameter of 100 microns which is large enough to assure capillary forces on the electrolyte will be small and pore flooding should be minimal. Second, the surface area is large so that the ratio of current to current density is high, thus, the sulfate build-up at the interface should be relatively small. Some degradation of the electrodes during the run was evident in post-run analysis. Although the degradation was only slight and probably did not affect cell performance considerably, the carbon electrodes probably would not be effective for tests of long duration.

TABLE 12 RUN C-3-V1S0

DATE	TIME	TEMP C	FLOW (cc/min)	SO_2 CONC (ppm) IN	SO_2 CONC (ppm) OUT	REMOVAL	IDEAL REMOVAL	CURRENT (mA)	RESISTANCE (ohms)	POTENTIALS (volts) C/R	POTENTIALS (volts) A/R
10/22/85	16:00	heating	50	3000	3000	0%	0%	0.0	-	-	-
	19:30	300	50	3000	3600	-20%	35%	6.8	22.0	C/A = -1.000	
	22:00	300	50	3000	-	-	2%	0.4	-	C/A = -1.000	
	22:10	303	50	3000	-	-	21%	4.0	-	C/A = -1.000	
	22:15	306	50	3000	-	-	64%	12.5	-	C/A = -1.000	
	22:20	312	50	3000	-	-	77%	15.0	-	C/A = -1.000	
	22:25	315	50	3000	-	-	64%	12.5	-	C/A = -1.000	
	22:30	315	50	3000	-	-	46%	9.0	-	C/A = -1.000	
	22:50	315	50	3000	-	-	3%	0.5	-	C/A = -0.500	
	22:55	315	50	3000	-	-	5%	0.8	-	C/A = -0.500	
10/23/85	10:00	315	50	3000	-	-	1%	0.2	-	C/A = -0.500	
	10:50	330	50	3000	-	-	3%	0.5	-	C/A = -0.500	
	11:40	342	50	3000	-	-	11%	2.1	-	C/A = -0.500	
	14:00	355	50	3000	-	-	8%	1.5	-	C/A = -0.500	
	15:00	355	50	3000	-	-	6%	1.0	-	C/A = -0.500	
	15:30	358	50	3000	-	-	41%	8.0	-	C/A = -1.000	
	15:35	360	50	3000	-	-	67%	13.0	-	C/A = -1.000	
	18:00	360	50	3000	-	-	11%	2.2	40.0	C/A = -1.000	
	18:20	360	50	3000	3400	-14%	10%	2.0	-	C/A = -1.000	
	18:40	360	50	3000	3300	-11%	10%	1.9	-	C/A = -1.000	
10/24/85	9:45	360	50	3000	2600	15%	0%	0.0	-	C/A = 0.000	
	10:45	360	50	3000	3400	-14%	10%	2.0	53.0	C/A = -1.000	

The hot-pressed membrane was fabricated in the initial stages of developing this procedure. The density, 88% of theoretical, was considered good at the time but is far below what is recommended for membranes (>99%). In addition, a small amount of electrolyte was leaked during the run, further decreasing the density. The effect of the low density is shown in the high ohmic resistance across the membrane, ranging from 22 to 53 ohms. The low density of the membrane was due to the fabrication procedure followed. An important step in the hot pressing procedure is to heat the material in the die to 200°C to drive off any adsorbed H_2O on the matrix/electrolyte powder mixture. This step was omitted when the membrane was produced, simply because it had not yet been discovered as being important. X-ray diffraction patterns of the ceramic membrane before and after the run are shown in figures 54 and 55 respectively. The patterns show there was very little change, if any, in the membrane composition. Thus, $SrTiO_3$ has the potential to be a successful matrix, but fabrication procedures need to be refined before an operational membrane can be made.

There were two basic reasons for terminating the run. First, upon application of current there was no net SO_2 removal, only net production. Second, the polarization behavior of the cell was unacceptable, less than 2.0 mA was driven through the cell at an overpotential at -1.00 (C/A). This was in part due to the low density membrane and high ohmic resistance.

Table 13 displays the results of run C-3-V1S8. The conditions are nearly the same as the previous run except that the electrolyte contains 1% V_2O_5 and 8% K_2SO_4. Sulfate, as discussed in the effluent analysis results, enhances, SO_2 removal.

The removal results suggest sulfate in the electrolyte had little effect on the removal of SO_2. The highest removal rate, 16%, was achieved at open circuit shortly after commencement of the run. Application of current resulted in a decrease in removal and toward the end of the run at net increase in SO_2 concentration. These removal results are all consistent with that of the previous run, with no sulfate. During the first day of the run, net removal of SO_2 was accomplished after passage of cell current, although removal was less than that at open circuit. This was not observed in the previous run, so that the presence of sulfate may have enhanced removal in the early stages. The conversion of SO_2 to SO_3, calculated to be 0.13%, once again appears to be the factor responsible for the low overall removal.

Electrode performance in this run parallel the results reported for the previous run. Little pore flooding with electrolyte occured because of the large pore size of carbon electrodes. A slight degradation of the carbon was seen during analysis after the run.

The membrane was fabricated by hot pressing procedures (see experiment, section 3c). The density of the membrane was approximately 92% of the theoretical, an improvement over the previous membrane but still below recommended levels.

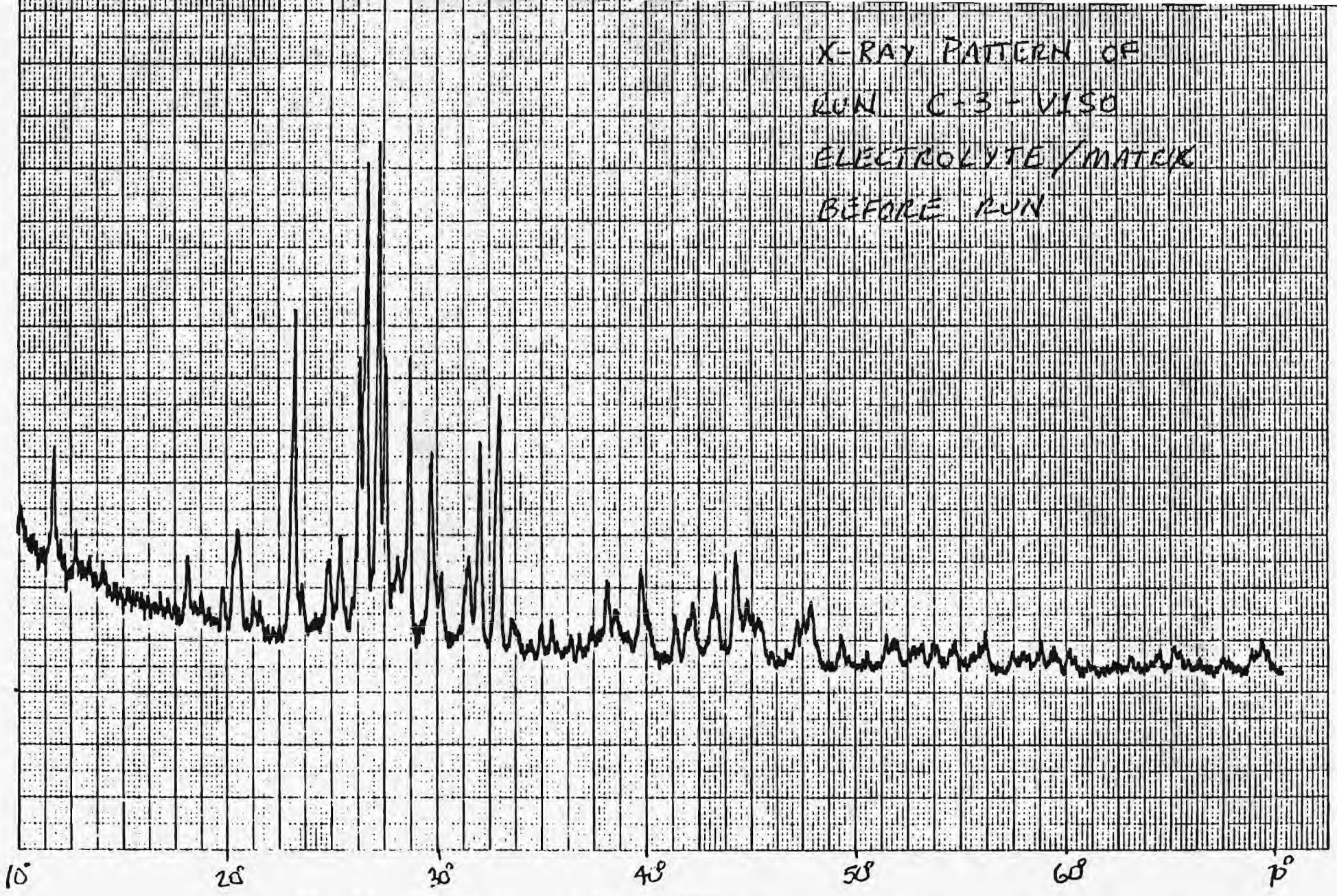

Fig. 54. X-ray Pattern of RUN C-3-V1SO Membrane (Before)

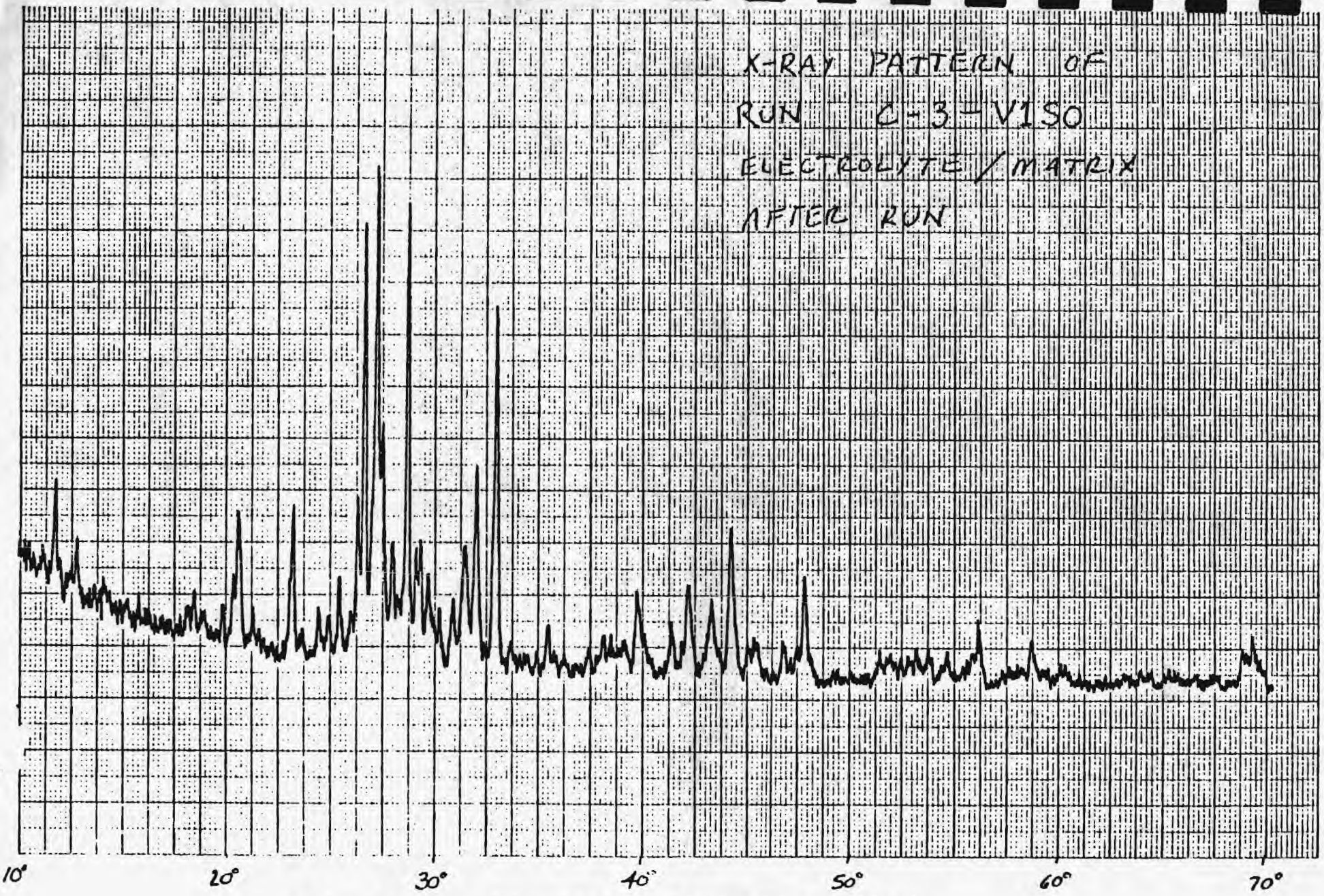

Figure 55. X-ray Pattern of RUN C-3-V1SO Membrane (After)

TABLE 13 RUN C-3-V1S10

DATE	TIME	TEMP C	FLOW (cc/min)	SO_2 CONC (ppm) IN	SO_2 CONC (ppm) OUT	REMOVAL	IDEAL REMOVAL	CURRENT (mA)	RESISTANCE (ohms)	POTENTIALS (volts) C/R	POTENTIALS (volts) A/R
11/21/85	1:00	heating	50	3000	3000	0%	0%	0.0	-	-	-
	9:00	330	50	3000	2500	16%	0%	0.0	6	C/A = 0.000	
	10:20	330	50	3000	-	-	51%	10.0	-	C/A = -0.500	
	10:21	330	50	3000	-	-	21%	4.0	-	C/A = -0.500	
	10:35	330	50	3000	-	-	17%	3.3	-	C/A = -0.500	
	10:50	330	50	3000	-	-	15%	3.0	-	C/A = -0.500	
	11:05	330	50	3000	-	-	15%	2.9	-	C/A = -0.500	
	11:20	330	50	3000	-	-	15%	2.9	-	C/A = -0.500	
	11:35	330	200	3000	-	-	15%	2.9	-	C/A = -0.500	
	11:50	330	10	3000	-	-	15%	2.9	-	C/A = -0.500	
	12:00	330	50	3000	2500	15%	15%	2.9	-	C/A = -0.500	
	14.00	330	50	3000	2700	10%	0%	0.0	-	C/A = -0.000	
11/22/85	8:00	330	50	3000	-	-	6%	1.1	-	C/A = -0.500	
	9:15	330	50	3000	3300	-10%	21%	4.0	-	-	-
	13:15	330	50	3000	-	-	21%	4.0	-	C/A = -0.505	
	14:00	330	50	3000	-	-	51%	10.0	-	UNSTABLE	
	15:00	330	50	3000	3050	-2%	0%	0.0	-	-	-
	15:20	330	50	3000	4600	-54%	46%	9.0	-	C/A = -1.000	
	15:25	330	50	3000	4600	-54%	31%	6.0	-	C/A = -1.000	
	15:30	330	50	3000	4100	-34%	22%	4.3	-	C/A = -1.000	
	15:35	330	50	3000	3500	-17%	19%	3.7	-	C/A = -1.000	
	15:45	330	50	3000	3200	-7%	12%	2.4	-	C/A = -1.000	
	17:00	330	50	3000	3000	0%	0%	0.0	32	C/A = 0.000	

One result of the improved density was the ohmic resistance was significantly decreased, enhancing the polarization characteristics of the cell. For example, comparing the previous run to this one, at 330°C, 50 cc/min and -0.500 V applied across the cell, the current increased from 0.5 to 2.9 mA. Future improvements in membrane fabrication methods will further enhance the cell polarization characteristics.

Although the ceramic membrane was improved over the previous run, and the added sulfate in the membrane enhanced removal slightly in the early stages of the run, performance was still unacceptable on the last day. Only net evolution was observed at that time, and the run was therefore aborted.

Run B-4-V1SO is summarized in table 14. Gold screen and MgO were employed as the electrodes and matrix respectively. Removal of SO_2 followed the same patterns seen in previous runs. The maximum removal was 10%, at open circuit and early in the run. Open circuit removal decreased slowly during the course of the run. Driving current through the cell resulted in a decrease in removal and a net increase in SO_2 concentration at the highest currents (10 mA). As in previous run, oxidation of SO_2 was restricted by cell geometry (0.14% conversion, see appendix) and appeared to be the limiting factor for SO_2 removal.

TABLE 14 RUN B-4-V1S0

DATE	TIME	TEMP C	FLOW (cc/min)	SO_2 CONC (ppm) IN	SO_2 CONC (ppm) OUT	REMOVAL	IDEAL REMOVAL	CURRENT (mA)	RESISTANCE (ohms)	POTENTIALS (volts) C/R	POTENTIALS (volts) A/R
12/04/85	16:15	heating	40	3000	3000	0%	0%	0.0	-	-	-
	21:40	360	40	3000	-	-	0%	0.0	3.2	+0.185	+0.269
	22:00	360	100	3000	-	-	0%	0.0	-	+0.179	+0.267
	22:30	360	10	3000	-	-	0%	0.0	-	+0.179	+0.265
	23:00	360	40	3000	2700	10%	0%	0.0	-	+0.180	+0.265
12/05/85	9:10	360	40	3000	-	-	0%	0.0	7.0	-	-
	9:45	360	40	3000	2900	3%	32%	5.0	-	-0.096	+0.835
	10:30	360	40	3000	2950	2%	64%	10.0	9.0	-0.333	+1.165
	12:00	360	40	3000	2800	7%	0%	0.0	8.5	+0.099	+0.412
	13:30	360	40	3000	3100	-3%	64%	10.0	-	C/A = -1.000	
	13:35	360	40	3000	3000	0%	38%	6.0	-	C/A = -1.000	
	13:40	360	40	3000	3000	0%	27%	4.5	-	C/A = -1.000	
	13:45	360	40	3000	2900	3%	21%	3.3	-	C/A = -1.000	
	14:00	360	40	3000	2900	3%	13%	2.0	-	C/A = -1.000	
	16:15	360	40	3000	2850	5%	0%	0.0	11.0	+0.081	+0.419
	19:45	380	40	3000	2800	7%	0%	0.0	11.0	+0.080	+0.402
	20:50	380	40	3000	3250	-8%	64%	10.0	-	-1.115	+1.765
	22:00	380	40	3000	2900	3%	0%	0.0	-	+0.044	+0.517
12/06/85	8:45	380	40	3000	-	-	0%	0.0	16.0	+0.029	+0.447
	9:45	380	40	3000	3100	-3%	64%	10.0	-	UNSTABLE	

The problems encountered in Run B-2-V1SO with the gold screen electrodes surfaced again in this run. The low surface area of these electrodes resulted in an increase in the sulfate build-up at the electrode interface (see discussion of Run B-2-V1SO), which in turn caused poor polarization behavior. Future full-cell tests will not utilize gold screen electrodes because of these drawbacks.

The ceramic membrane was produced by hot pressing (see experimental, section 3c). The membrane was 97% of the theoretical density, a vast improvement over previous runs, and approaching the quality of commercially produced membranes (99% or greater). The ohmic resistance was accordingly improved, varying between 3.2 and 16.0 ohms over the duration of the run. Some electrolyte leakage from the membrane occured, indicating the initial loading may have been to high, and explaining why the ohmic resistance slowly increased during the run.

The run was terminated for two major reasons. First, the polarization behavior of the cell, due primarily to the gold screen electrodes, was poor. Unreasonably large potentials were required to drive relatively small currents. Secondly, the cell was removing virtually no SO_2 at the runs end.

The results of Run D-4-V1S8 are summarized in table 15. Here, the electrode material has been switched to porous nickel (currently the electrode of choice in molten carbonate fuel cells), and the ceramic membrane contains 8.0% K_2SO_4.

The maximum overall removal of SO_2 through the cell was 25%. This was accomplished with an applied current of 1.0 mA and was significantly higher than the best open circuit removal (14%). Thus, electrochemical SO_2 removal was achieved in this cell. Unfortunately, electrochemical removal could not be maintained for extended periods of time. The reasons for this are discussed below.

The nickel electrodes were found to be unsuitable for use in the cell environment. The nickel was found to react with the electrolyte to form nickel sulfate, which is a non-conductive material. Conversion to the sulfate was not immediate, so that initial performance was not strongly affected. As the run proceeded through; there was less active electrode area and performance degraded. Nickel could not be used in runs of long duration. In addition, the pore size of the nickel ($\sim$ 5 microns) was small enough to exert appreciable capillary forces on the electrolyte to withdraw some from the membrane.

The ceramic membrane was fabricated by the hot pressing procedure and was 97.5% of the theoretical density. Two problems related to the membrane were encountered. First, as mentioned above, electrolyte was withdrawn from the membrane by the nickel electrodes. This decreased the conductivity of the membrane, deteriorating performance. Second, the sulfate loading in the membrane was to high to permit generated sulfate to diffuse away from the interface at an acceptable rate. Thus, solid sulfate build-up was a problem in this cell.

TABLE 15 RUN D-4-V1S8

DATE	TIME	TEMP C	FLOW (cc/min)	SO_2 CONC (ppm) IN	SO_2 CONC (ppm) OUT	REMOVAL	IDEAL REMOVAL	CURRENT (mA)	RESISTANCE (ohms)	POTENTIALS (volts) C/R	POTENTIALS (volts) A/R
1/28/86	12:50	225	10	3000	-	-	0%	0.0	450	-	-
	13:05	240	10	3000	-	-	0%	0.0	405	-	-
	13:20	260	10	3000	-	-	0%	0.0	295	-	-
	13:35	270	10	3000	-	-	0%	0.0	195	-	-
	13:50	280	10	3000	-	-	0%	0.0	115	-	-
	14:10	290	10	3000	-	-	0%	0.0	35	-	-
	14:30	300	10	3000	-	-	0%	0.0	18	-	-
	19:00	315	10	3000	-	-	0%	0.0	8	+0.075	-0.015
1/29/86	9:00	315	40	3000	-	-	0%	0.0	-	+0.186	-0.030
	12:00	315	40	3000	-	-	0%	0.0	-	+0.196	-0.030
	15:45	315	40	3000	2250	25%	6%	1.0	-	-0.180	+1.060
	17:15	315	40	3000	3000	0%	6%	1.0	-	-0.225	+1.160
	23:00	315	40	3000	-	-	0%	0.0	-	+0.250	-0.070
1/30/86	9:00	315	40	3000	2900	3%	0%	0.0	-	+0.235	-0.069
	12:00	330	120	3000	-	-	0%	0.0	-	+0.362	+0.034
	14:00	330	120	3000	-	-	0%	0.0	-	+0.340	+0.160
	16:00	330	120	3000	-	-	0%	0.0	-	+0.348	+0.150
	17:00	330	40	3000	-	-	0%	0.0	25	-	-
	18:00	330	40	3000	2570	14%	0%	0.0	-	+0.305	-0.128
	21:00	330	40	3000	2880	4%	0%	0.0	-	+0.305	-0.090
	23:00	330	40	3000	2900	3%	0%	0.0	-	+0.315	-0.085

The major reason for shutting down this run was the conversion of the nickel electrodes for a non-conductive nickel sulfate. This transformation resulted in poor polarization characteristics and poor removal performance.

CONCLUSIONS/RECOMMENDATIONS

The research conducted under DOE contract DE-FG22-84PC73226 has laid a solid foundation for the development of an electrochemical process to remove SO_x and NO_x from flue gas. Here, we point out the major developments and outline the direction future research will take to progress toward a novel, economic flue gas clean-up process.

The free electrolyte experiments have established that the main redox reaction is the reduction of pyrosulfate, and under steady conditions is:

$$2S_2O_7^{2-} + 2e^- \rightarrow 3SO_4^{2-} + SO_2 \qquad (66)$$

The role of vanadia is to oxidize SO_2 to SO_3:

$$2SO_2 + O_2 \rightarrow 2SO_3 \qquad (67)$$

When the electrolyte contains sulfate and the gas contains SO_3, another reaction becomes important:

$$2SO_3 + 2SO_4^{2-} \rightarrow 2S_2O_7^{2-} \qquad (68)$$

An overall cathodic reaction can be determined by adding equations 66-68 to yield:

$$SO_2 + O_2 + 2e^- \rightarrow SO_4^{2-} \quad (69)$$

The cyclic voltammetry results showed the anodic current originates from the oxidation of sulfate:

$$SO_4^{2-} \rightarrow SO_3 + 1/2O_2 + 2e^- \quad (70)$$

The cathodic and anodic reactions can be added to yield an overall cell reaction:

$$(SO_2 + O_2)_{cathode} \rightarrow (SO_3 + 1/2O_2)_{anode} \quad (71)$$

This result indicates that an electrochemical membrane concentrator utilizing a $K_2S_2O_7/K_2SO_4/V_2O_5$ electrolyte could be successfully applied to flue gas clean-up. Under steady conditions, an applied potential across the cell would result in a net electrolyte reaction of zero, but SO_2 would be removed at the cathode and evolved and concentrated as SO_3 at the anode.

The maximum amount of SO_2 removed from similated flue gas in the electrochemical cells was approximately 45%. The removal was restricted to this value because of a combination of mass transfer and SO_2 oxidation limitations. Both of these factors can be overcome by improved cell design. Future work will employ cells constructed to overcome these limiting factors.

Perovskite, $La_{0.8}Sr_{0.2}CoO_3$, proved to be an attractive electrode material. It was found to be stable and conductive in the cell environment, and displayed good polarization behavior in free electrolyte. Future work needs to focus on developing fabrication techniques which optimize the pore structure of perovskite electrodes so that they can be successfully employed in full-cell tests.

The best procedure for fabricating ceramic membranes was found to be hot pressing an intimate mixture of the electrolyte and matrix powders. Two materials were found to meet the requirements a matrix must satisfy, these are $SrTiO_3$ and MgO. Fabrication procedures have been advanced so that membranes of high strength and densities in excess of 97% of the theoretical can be routinely produced. Future work will concentrate on finding optimum membrane compositions, to minimize electrolyte leakage, and further developing the fabrication techniques so that membrane densities are atleast 99% of the theoretical density.

Favorable results were gained in the NO_x removal studies in free electrolyte. Removal rates of approximately 70% were achieved at low flow rates (20 cc/min). The removal was found to be limited solely by mass transfer rates. Thus, increased removal can be accomplished in cells designed for improved mass transfer. In addition, the presence of NO_x in the gas was found to enhance SO_2 removal rates by approximately 10%. Future research will focus on identifying the NO_x removal mechanism in free electrolyte and testing removal in full-cell tests.

The full-cell test were hindered by three factors. First, the cell configuration limited conversion of SO_2 to SO_3 to minimal amounts (less than 1.0%). This is an important step in the removal mechanism and was therefore the limiting factor on SO_2 removal. Second, the electrodes used in these tests were inadequate. The carbon and nickel electrodes were unstable in the cell environment, the gold screen had too small a surface area, and the perovskite had pores which were much to small. Lastly, the membranes were not able to retain electrolyte to the degree required, resulting in flooded electrode pores and low conductivity membranes. Future work will address each of these problems. The SO_2 will be oxidized in a pre-full-cell reactor. Fabrication procedures for perovskite electrodes will be refined to optimize the pore structure. Membrane fabrication procedures will also be optimized, to produce high density ceramic membranes which are able to retain the electrolyte within the structure.

REFERENCES

1. Langer, S.H. and R.C. Haldeman, J. Phys. Chem., 68, 962 (1964).

2. Winnick, J., et.al., Ind. Eng. Chem. Proc. Des. Dev., 13, 59 (1974).

3. Weaver, J. and J. Winnick, J. Electrochem. Soc., 130, 20 (1983).

4. Winnick, J., et.al., A.I.Ch.E. Jour., 28, 103 (1982).

5. Salzano, F.J. and L. Newman, J. of the Electrochem. Soc., 119, 1273 (1972).

6. Johnson, K.E. and H.A. Lastiner, J. of the Electrochem. Soc., 110, 314 (1963).

7. Liu, C.H., J.P. Chem., 66, 164 (1962).

8. Burrows, B.W. and G.J. Hills, Electrochem. Acta., 15, 495 (1970).

9. Wrench, D.M. and D. Inman, Electrochem. Acta., 12, 1601 (1967).

10. Wrench, D.M. and D. Inman, J. Electroanal. Chem., 17, 319 (1968).

11. Potter, P.J., "Power Plant Theory and Design", The Ronald Press Company, New York (1959).

12. Townley, D. and J. Winnick, Electrochim, Acta., 28, 389 (1983).

13. Cheng, A.Y., Masters Thesis, "The Electrochemical Kinetics of SO_2 Reactions in Molten Bisulfates", Georgia Tech (1983).

14. Spitsyn, V.J. and M.A. Meerov, J. of Gen. Chem. of U.S.S.R., 22, 963 (1952).

15. Shores, D.A. and Fang, W.C., J. Electrochem. Soc., 128, 346 (1981).

16. Barin, I. and O. Knache, "Thermochemical Properties of Inorganic Substances", Springer Verlag, Berlin (1973).

17. Sundheim, E., "Fused Salts", McGraw Hill (1964).

18. Jarz, G., "Molten Salt Handbook" (1964).

19. Bodenstein, M. and Fink, G.G., Z. Physik. Chem., 60, 1 (1907).

20. Lewis, W.K. and Ries, E.D., Ind. Eng. Chem., 19, 830 (1927).

21. Uyehara, O.A., and Watson, K.M., Ind. Eng. Chem., 35, 541 (1943).

22. Hougen, O.A., and Wilkie, C.R., Trans. Am. Inst. Chem. Engrs., 45, 445 (1945).

23. Calderbank, P.H., Chem. Eng. Prog., 49, 585 (1953).

24. Krichevskaya, E.L., J. Phys. Chem. (U.S.S.R.), 21, 287 (1947).

25. Davidson, B. and Thodos, G., A.I.Ch.E. J., 10, 568 (1964).

26. Fang, W.C., and Rapp, R.A., J. Electrochem, Soc., 130, 2335 (1983).

27. Durand, A., G. Picard and J. Vedel, J. Electroanal. Chem., 70, 55, (1976).

28. Barin, I. and O. Knacke, "Thermochemical Properties of Inorganic Substances", Springer Verlag, Berlin (1973).

29. Flood, H. and N.C. Boye, Zeitschrift fur Electrochimie, 66 (2), 184, (1962).

30. Flood, H. and T. Forland, Acta Chemica Scandiavica, 1, 781, (1947).

31. Bazarova, Z.G. et.al., Kinet, Catal. (USSR), 12, 845, (1971).

32. Dojcinovic, M., M. Susic and S. Mentus, J. Mol. Catal., 11, 275, (1981).

33. Bard, A.J. and L.R. Faulkner, "Electrochemical Methods", John Wiley and Sons Inc., New York, (1980).

34. Nicholson, R.S. and I. Shain, Analytical Chemistry, 36 (4), 707, (1964).

35. Bockris, J.O'M and A.K.N. Reddy, "Modern Electrochemistry 1", Plenum Press, New York, pg 548, (1970).

36. Kudo, T., Obayashi, H.and Yoshida, M., J. Electrochem. Soc., 124 321 (1977).

37. Winnick, J. et.al., I.E.C. Proc. Des, Dev., 13 59 (1974).

38. Winnick, J., Toghiani, H. and P. Quattrone, AIChE J., 28, 103 (1982).

39. Winnick, J. and Ross, P.N., J. Electrochem. Soc., 128, 991 (1981).

40. Holroyd, F.P.B., and C.N. Kenney, Chem. Eng. Sci., 26, 1963, (1971).

APPENDIX

Holroyd and Kenney [40] derived kinetic equations for the catalytic oxidation of SO_2 using a $K_2S_2O_7/V_2O_5$ molten salt catalyst. The rate equation they derived was:

$$R = K_o e^{-E/RT} (A)(P_{SO_2}{}^{1.00})(V_2O_5)^{0.69}$$

where $K_o e^{-E/RT}$ is the rate constant and:

$$K_o = .003 \frac{\text{mole}}{\text{cm}^2.\text{sec.atm}}$$
$$E = 46.2 \text{ KJ/mole}$$
$$R = 8.314 \text{ J/mole}^{\circ}\text{K}$$

A is the surface area of the molten catalyst exposed to the gas (cm^2), P_{SO_2} is the partial pressure of SO_2 in the gas phase (atm), and (V_2O_5) is the mole fraction of vanadia in the molten catalyst and R is the reaction rate in moles of SO_2 per second.

As an example calculation, typical full-cell testing conditions will be employed (T = 350°C, a cathode gas containing 0.3% SO_2, flowing at 50 cc/min, and a 1.0% V_2O_5 membrane). The temperature sets the rate constant at 1.34×10^{-7} gmole $SO_2/cm^2.sec.atm$. The area for the full-cell is estimated as approximately 4.0 cm^2 so that the reaction rate is estimated as $6.6 \times 10^{-11} \frac{\text{gmole } SO_2}{\text{sec}}$. The fractional conversion can be approximated by calculating the flow rate through the cell and comparing this to the reaction rate. Assuming an ideal gas, the

flow rate is calculated to be 4.9×10^{-8} gmole SO_2/sec. Thus, the conversion of SO_2 to SO_3 through the full-cell is estimated as 0.14% $\left(\frac{6.6 \times 10^{-11}}{4.9 \times 10^{-8}}\right)$.

In the full-cell experiments, the variables which effected the conversion was the temperature, partial pressure of SO_2, and the gas flow rate. None of the experimental conditions were drastically different from the example above and all calculated conversions ranged between 0.1% and 0.5%.